A CRITICAL STATE FRAMEWORK FOR UNSATURATED SOIL

by

VINAYAGAMOORTHY SIVAKUMAR. BSc, MSc, DIC.

UNIVERSITY OF SHEFFIELD

A thesis submitted to the University of Sheffield for the degree of Doctor of Philosophy

Department of Civil and Structural Engineering,

University of Sheffield

February 1993

ORIGINAL COPY TIGHTLY BOUND

CONTENTS

ACKNOWLEDGEMENT.

The critical state concepts for unsaturated soil developed in this thesis were first proposed by **Dr. S.J. Wheeler.** The experimental work was performed in the Department of Civil and Structural Engineering at Sheffield University. Financial support for the project was provided by the Science and Engineering Research Council.

My sincere thanks are due to **Dr.S.J.Wheeler** for his constructive and valuable suggestions and supervision throughout the period of the project.

Help from staff and technicians of the Department of Civil and Structural Engineering was always forthcoming. I am especially indebted to:

Mr. Paul Osborne and Mr. Mark Foster, who fabricated much of the equipment;

Mr. Tim Robinson, who wrote the logging and control software.

SUMMARY

A critical state framework for unsaturated compacted clay is proposed. Five state variables are included: mean net stress, deviator stress, suction, specific volume and water content. The proposed framework includes three equations to define isotropic normal compression states, three equations to define critical states and two equations to define a state boundary.

Support for the proposed critical state framework is provided by results from a series of controlled suction triaxial stress path tests on samples of unsaturated compacted kaolin. Unsaturated 50 mm diameter samples were produced by static compaction in 9 layers, prior to consolidation to virgin states at selected values of mean net stress and suction. Shear tests were conducted with a variety of different stress paths and drainage conditions, in a double-walled triaxial cell with independent computer control of cell pressure, pore air pressure and pore water pressure.

The experimental results indicated that all test paths originated on a unique isotropic normal compression hyper-line and terminated on a unique critical state hyper-line. To a first approximation all stress paths traversed a unique state boundary that could be defined by the expansion of a yield surface with elliptical cross-sections

at constant values of suction.

Possible applications of a critical state model for unsaturated soil include: providing a qualitative framework to aid understanding of unsaturated soil behaviour; guiding the choice of strength parameters to be used in conventional stability calculations; and providing a formalized mathematical stress-strain model for incorporation in a finite element program.

CHAPTER 1

INTRODUCTION

1.1 UNSATURATED SOILS

1.2 CATEGORIES OF UNSATURATED SOIL

1.3 HISTORICAL DEVELOPMENT OF UNSATURATED SOIL MECHANICS

1.4 AIM OF THE RESEARCH PROJECT

CHAPTER 1

INTRODUCTION

1.1 UNSATURATED SOILS

For constitutive modelling purposes soils can be divided into two major divisions: (1) saturated and dry soils; (2) unsaturated soils. In saturated and dry soils the pore spaces are filled with a single medium, either water or air. In unsaturated soils the pore spaces are filled with a mixture of two or more media, most commonly air and water.

Unsaturated soils are found all over the world. Unsaturated conditions exist:

(1) in natural soils, above the water table, particularly where the rainfall is less than the potential rate of evaporation,

(2) when soils are compacted for construction purposes as fill materials,

(3) when gas is generated within the soil by biological activity.

Since the early development of soil mechanics most effort has been directed to research into the behaviour of saturated and dry soils. Due to this extensive research, geotechnical engineers are now able to understand and predict saturated soil behaviour reasonably confidently in the field or laboratory. However the case of unsaturated soils is very different. The current practice for the prediction of unsaturated soil behaviour either ignores the unsaturated state of the soil or is based, at least partly, on empirical formulations.

Two major reasons can be identified for the relative lack of research on unsaturated soils. Firstly, natural soils in temperate regions (such as the UK) are generally saturated except for a shallow layer at the surface. Secondly, the stress systems and structural arrangements within unsaturated soils are more complex than in saturated soils and this made it difficult (or impossible) to identify a simple "effective stress" in unsaturated soil. In addition to the two reasons given above, laboratory testing of unsaturated soil is difficult and time-consuming. Despite these problems, many research projects on unsaturated soils have been undertaken during the last 4 decades, in an attempt to understand and model unsaturated soil behaviour. However the outcome of much of this research has been confusing and inconclusive.

1.2 CATEGORIES OF UNSATURATED SOIL

The structure of an unsaturated soil is greatly dependent on how the soil came to be unsaturated (eg drying of a natural soil or compaction of fill). The structure has a considerable influence on the behaviour of unsaturated soil in terms of compressibility and stiffness. For this reason, unsaturated soils produced by different processes tend to exhibit different forms of mechanical behaviour. In addition, even for soils formed by a given process the structure can vary considerably. This variation occurs particularly in compacted clay fills. The structure of unsaturated compacted clay fills changes dramatically with the method of compaction, the amount of compaction and the water content.

Wroth & Houlsby (1985) proposed three different categories of unsaturated soil on the basis of continuity of the fluid phases (Fig 1.1):

(1) Air phase discontinuous and water phase continuous(Fig 1.1a). This type of structure is found in unsaturated soils having a very high degree of saturation. In such soils the air occurs in the form of discrete bubbles. This situation probably occurs in a narrow transition zone in natural soil, above the saturated zone and below a zone with lower degree of saturation (Fig 1.2). This type of soil is

also found in the offshore environment, where relatively large gas bubbles form cavities within the soil structure (Wheeler, 1988a). The engineering behaviour of these offshore soils containing large gas bubbles differs considerably from the behaviour of land-based soils containing air bubbles that are small enough to fit within the normal void spaces (Sills et al.,1991)

(2) Air and water phases both continuous (Fig 1.1b). This type of unsaturated soil is found in soil having an intermediate degree of saturation. This range of degree of saturation occurs: (a) in a transition zone in a natural soil deposit, above the previously mentioned zone in category (1) and below a dryer surface layer(Fig 1.2); (b) in compacted fine-grained (silt and clay) fills used for construction purposes.

(3) Air phase continuous and water phase discontinuous (Fig 1.1c). This type of unsaturated soil is found in unsaturated soils having lower degree of saturation. This occurs: (a) in natural soils close to the surface (Fig 1.2) and (b) in some compacted coarse-grained (sand and gravel) fills. In natural soils, the depth of this category of unsaturated soil is greatest in arid and semi-arid regions.

The pore air pressure in unsaturated soils is always higher than the pore water pressure, because of curvature of the air-water interfaces. In land-based unsaturated soil containing a continuous air phase (categories (2) and (3) above) the pore air pressure will be zero (equal to atmospheric pressure), because the continuous air phase is open to the atmosphere, and the pore water pressure will be negative. In gassy offshore soils the gas pressure is dependent on the water pressure and the curvature of the gas bubble, and it is often considerably greater than atmospheric pressure.

The research described in this thesis focused particularly on unsaturated soils found in compacted fine-grained fills having continuous air and water phases. When a fine-grained soil is compacted for building dams and embankments or for back-filling behind retaining walls or beneath foundations, the compaction process typically leaves the soil at a degree of saturation between 75 and 85%, resulting in a soil falling within category (2).

Unsaturated compacted soils normally have high strength and low compressibility. However the designer must be aware of the possibility of the soil reaching a saturated state at some time during the life of the structure, due to inundation, climatic changes or post-construction loading. Unsaturated soil may lose some of its strength when it becomes saturated, and may also undergo large deformations

during the saturation process. The loss of strength could cause slips in dams or embankments. The failure of a railway embankment at Notch Hill, British Columbia, Canada (Krahn, Fredlund and Klassen, 1989) is a good example to show how unsaturated soil may lose some of it's strength during saturation.

If the soil is at it's weakest when it is saturated, it might be questioned why an understanding of unsaturated soil behaviour is important. There are two reasons why it is important to understand unsaturated soil behaviour. Firstly, the volume changes which occur in unsaturated soil can be predicted only if a proper framework is developed for unsaturated soil behaviour. In particular, the volume change which results from saturation of an unsaturated soil would be incorrectly predicted, sometimes in sign as well as magnitude , by a conventional saturated approach. Secondly, if the strength parameters (eg, undrained strength or drained strength) were evaluated when the soil was in an unsaturated state and these strength parameters were then used in a saturated analysis, this could lead to an over-estimation of the factor of safety, because of failing to take account of the loss of strength during saturation. Only within a proper unsaturated framework can this loss of strength be evaluated.

1.3 HISTORICAL DEVELOPMENT OF UNSATURATED SOIL MECHANICS

The development of unsaturated soil mechanics can be divided into three periods. In the first period, before about 1965, most of the research work carried out on unsaturated soil was to investigate the validity of the single effective stress concept for unsaturated soils (for example, Bishop, 1959 and Aitchison, 1960). During this period various forms of modified effective stress equation were examined in an attempt to analyse the behaviour of unsaturated soils.

In the second period, from 1965 to about 1987, most of the research was conducted to investigate the possibility of using two stress state variables instead of a single effective stress (for example, Matyas and Radhakrishna, 1968 and Fredlund, 1979).The "net stress" (total stress minus pore air pressure) and "suction" (pore air pressure minus pore water pressure) were treated as the two stress state variables. During this period simple independent frameworks were developed to model volume change and shear behaviour of unsaturated soils in terms of the two stress state variables. However the volume change and shear behaviour were treated completely separately

In the third period, since 1987, several researchers have been investigating unsaturated soil behaviour in terms of critical state concepts and attempting to investigate

yielding of unsaturated soils when the soil is loaded and unloaded (Alonso, Gens and Josa,1990). Until recently, the volume change and shear behaviour of unsaturated soil were treated completely separately. There was no generalised model (like the critical state model for saturated soils) linking these two central aspects of unsaturated soil behaviour. In recent years researchers have begun to link volume change and shear behaviour of unsaturated soil and to develop an elasto-plastic model. At the start of the current project, however, there was insufficient experimental data to validate such an elasto-plastic critical state model for unsaturated soil.

1.4 AIM OF THE RESEARCH PROJECT

Unsaturated compacted soils are commonly used as construction materials in building embankments and dams, and for back-filling beneath foundations or behind retaining structures. However the behaviour of unsaturated soil is less predictable than that of saturated soil. Although considerable research work has been done to understand unsaturated soil behaviour, there have been few attempts to model unsaturated soil behaviour in a generalised critical state framework.

The aim of the research reported in this thesis was to develop a generalised critical state model for unsaturated soil. A conceptual framework for an unsaturated critical

state model was first postulated, by extension from the conventional saturated critical state model (Chapter 3). A series of triaxial tests with a variety of different stress paths was then conducted on samples of compacted unsaturated kaolin, in an attempt to validate the proposed model (Chapters 4 to 7). Such a model should, ultimately, be capable of predicting volumetric strains, and changes of water content for any stress path and any drainage condition.

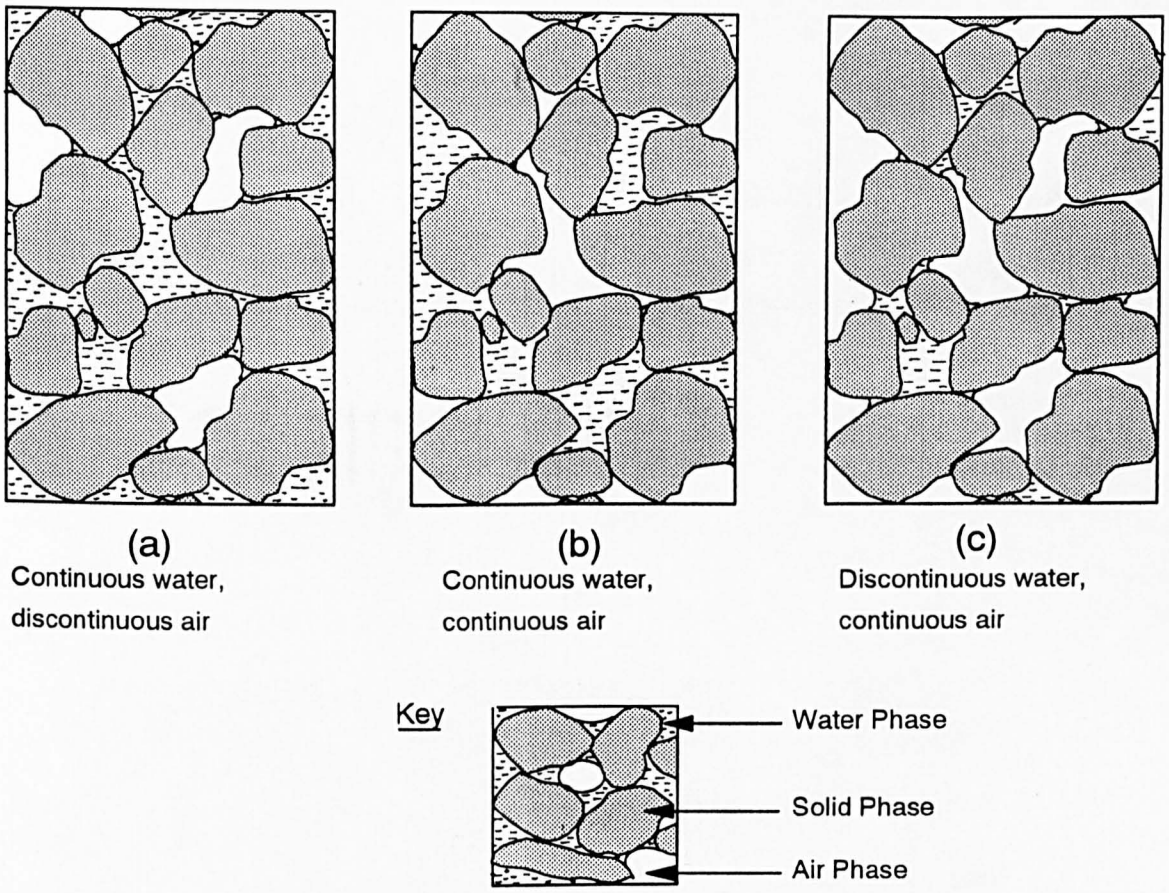

Fig (1.1). Structure of unsaturated soils.
(Wroth & Houlsby, 1985)

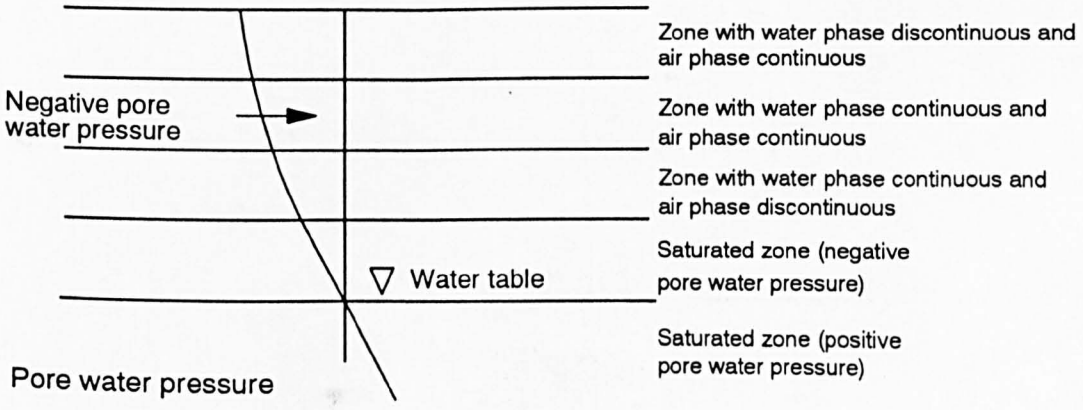

Fig(1.2) Continuous and discontinuous air and water phases in a soil stratum

CHAPTER 2

REVIEW OF STRESS-STRAIN BEHAVIOUR OF UNSATURATED SOILS

CHAPTER 2

REVIEW OF STRESS-STRAIN BEHAVIOUR OF UNSATURATED SOILS

This chapter is a literature review of previous research conducted on unsaturated soil behaviour.

2.1 SOIL SUCTION

The term "soil suction" was used by Schofield (1935) to represent the "pressure deficiency" in the pore water of any soil (saturated or unsaturated) that had the capacity to absorb water if additional water was supplied at atmospheric pressure.

2.1.1 Suction in unsaturated soils

Unsaturated soil is a three phase material containing soil particles, water and air. The mechanical behaviour of unsaturated soil is strongly influenced by both the pore air pressure and the pore water pressure. The value of pore air pressure is always higher than the pore water pressure, because the menisci separating air and water must be concave on the air side in order to achieve a contact angle of zero where the menisci come into contact with a wetted

soil particle.

The difference between the pore air pressure and the pore water pressure is defined as the "matrix suction". The value of this matrix suction is dependent on the surface tension and the radius of curvature of the menisci. As the degree of saturation falls the menisci withdraw into smaller and smaller pore spaces, the radious of curvature of the menisci reduces and, therefore, the matrix suction increases. Because of the smaller voids, far higher matrix suctions can develop in clay soils than in granular soils.

The flow of water through unsaturated soil is controlled by the gradient of total water potential. The total water potential can be expressed as the sum of three components: (a) gravitational potential, caused by the elevation of the soil water with respect to a reference level; (b) capillary or matrix potential, caused by the surface tension effects; (c) osmotic potential, caused by the concentration of dissolved ions in the soil water. For an unsaturated soil with the pore air at atmospheric pressure, the matrix potential is given by the matrix suction, defined above, multiplied by the unit weight of water (with a suitable change of sign). By anology the osmotic potential divided by the unit weight of water is termed the "osmotic suction" (again with a change of sign). The sum of matrix suction and osmotic suction is defined as the "total suction".

Experimental evidence suggests that the shear strength and volume change behaviour of unsaturated soils are dependent on the matrix suction rather than the total suction (Alonso, Gens and Hight, 1987). Therefore,the stress-strain behaviour is dependent on matrix suction whereas the flow of water is dependent on gradients of total suction (plus gravitational effects). This thesis is concerned solely with stress-strain behaviour, and therefore the term "suction " is used to refer to the matrix suction.

2.1.2 Measurement of suction

In unsaturated soils the pore water pressure in-situ is always less than atmospheric pressure. This negative pore water pressure may cause cavitation in any measuring system used in the field or in the laboratory, which makes it difficult to measure the magnitude of the pore water pressure.

A precise measurement of suction is important because any theoretical development in unsaturated soils mechanics can be put into practice in the field or laboratory only if the suction can be measured easily and confidently. Several methods have been developed in the past to measure the suction in the field and laboratory (Fredlund and Rahardjo, 1988). Some of the methods are briefly discussed in this section.

Hilf (1956) introduced the axis translation technique of using elevated values of total stress and pore air pressure in order to increase the pore water pressure above zero . This axis translation technique provided a method of measuring pore water pressure in the laboratory without altering the soil structure. Subsequently this method has been widely used to measure or control suction in unsaturated soils or to calibrate other types of measuring system. A fine porous stone, known as a high air entry filter, is used to prevent air getting into the pore water measuring system. By increasing the pore air pressure and the total stress the water pressure can be maintained at a desired positive value throughout the system. The difference between the pore air pressure and the pore water pressure will give the suction in the sample. However, the maximum value of suction that can be applied or measured is dependent on the air entry value of the porous stone. The disadvantage of the axis translation technique is that, by increasing the pore water pressure from a negative value to a positive value, the possibility of cavitation within the pore spaces of the soil is prevented (in addition to preventing cavitation within the measuring system), whereas cavitation of the pore water may be an important phenomenon in the behaviour of unsaturated soils under in-situ stress conditions. In addition, the axis translation technique cannot, of course, be used in in-situ devices for measuring soil suction.

Various other methods have also been used to measure suction in unsaturated soil samples without employing the axis translation technique. For example, the suction plate, pressure plate, pressure membrane, filter paper method, thermocouple psychrometer, thermal conductiviy sensor and the semi-permeable membrane.

In the suction plate technique, a sample of soil is placed in close contact with the flat upper surface of a sintered-glass disc of fine pore size (Croney and Coleman, 1960). Moisture equilibrium is established with water at a known negative pressure (relative to atmospheric) beneath the disc. By obtaining values of the equilibrium moisture content at various applied suctions, a suction versus moisture content relationship can be established. The technique is limited to suctions of less than 100 kPa.

In the pressure plate technique, a positive air pressure is applied above a sintered-glass porous disc (on which the soil sample is placed) and water beneath the disc is kept at atmospheric pressure. At equilibrium the applied air pressure is taken as the suction in the sample. The pressure membrane technique is the same as the pressure plate technique except that instead of using a sintered-glass porous disc a cellulose membrane is used.

The filter paper method for measuring suction in unsaturated soils, described by Chandler and Gutierrez

(1986), involves placing a piece of filter paper with the soil sample in a closed container. With time (at least 5 days) the suction in the filter paper and the soil sample will equilibrate. A careful measurement of the final water content of the filter paper can then be combined with a previously established calibration linking filter paper water content and the suction. The method gives a measure of the matrix suction in the sample when the filter paper is placed in direct contact with the sample, and a measure of the total suction in the soil sample if the filter paper is not in contact with the soil (in the former case transfer of water between the soil sample and the filter paper is mainly by flow of liquid, whereas in the later case it is solely by vapour transfer).

Thermocouple psychrometers have been used to measure the total suction in unsaturated soils (Edil and Motan, 1984). When a psychrometer is embedded in soil the relative humidity of the air in the psychrometer is a function of the total suction. A thermocouple is placed inside a protective chamber and this chamber is buried in the soil (Fig 2.1). A current is caused to flow through the thermocouple and the voltage developed between the thermocouple and the reference junction placed inside the chamber is measured. This voltage is related to the relative humidity of the air and therefore the total suction in the soil. The psychrometer method is restricted to suction values over 100 kPa and the device is capable

of measuring suctions up to 8000 kPa. The method is unsuitable for use in the field because of sensitivity to temperature variation.

Thermal conductivity sensors have been used by Wonk and Ho (1987) to measure the matrix suction in unsaturated soils. The sensor consists of a porous ceramic tip that contains a sensing unit that is used as a miniature heater and a temperature sensor (Fig 2.2). The operational principle of the sensor is that the rate of heat dissipation in the sensor unit and therefore the temperature change in a particular point in the sensor is related to the water content of the porous ceramic tip, which (under equilibrium conditions) is related to the matrix suction The sensor can be calibrated against a pressure plate (Fredlund and Wonk, 1989). The advantages of the thermal conductivity sensor are claimed to be that the device can be used over a wide range of suction values and that the response is unaffected by any salt in the pore fluid.

A semi-permeable membrane was used by Vicol (1990) to measure or control suction in the laboratory. The semi-permeable membrane allowed the passage of small molecules (such as water) but was impermeable to larger salt molecules. Fig (2.3) shows the arrangement for the measurement of suction. A supply of high concentration salt water at atmospheric pressure is applied to the bottom surface of the semi-permeable membrane. Under equilibrium

conditions (with no flow) the osmotic suction of the salt solution must equal the total suction within the soil sample. Therefore, by measuring the concentration of salt under equilibrium conditions the total suction is the soil can be evaluated from a calibration curve plotted against the concentration of salt.

2.2 FABRIC OF UNSATURATED SOILS

The fabric or structure of soils has a strong influence on their mechanical behaviour. This influence of fabric on soil behaviour is generally believed to be even more important for unsaturated soils than for saturated soils. The fabric of unsaturated soils is dependent on:

(a) The process by which the soil came to be unsaturated: for example, compaction, de-saturation due to evaporation from the ground surface or de-saturation due to gas generation within the soil.

(b) The degree of saturation. This is affected by factors such as water content (in compacted soils) or amount of evaporation or gas generation (in natural soils).

(c) Predominant soil particle size; for example: gravel, sand, silt or clay.

When describing the structure of unsaturated soils, it is useful to consider separately soils formed by the three different process outlined in (a) above. For each of the three processes there are a variety of different types of soil fabric, depending on the other factors (degree of saturation and predominant soil particle size).

2.2.1 Unsaturated natural soils

Natural soils are often unsaturated above the water table. If the rate of evaporation and transpiration exceeds the rate of rain-fall then the natural water table will fall. A fall in the water table causes negative pore water pressures above the water table and this causes de-saturation of the soil. However the amount of de-saturation is also dependent on the size of the soil particles. Fine-grained soils (clays and silts) will sustain greater values of negative pore water pressure before de-saturating than coarse-grained soils (sands and gravels).

The types of structure found in unsaturated soils can be put into three categories, depending on the air and water phase continuities. Fig (2.4a) shows the category of soil found in narrow transition zone, above the saturated soil and below surface zones with lower degrees of saturation. In the transition zone the air phase would exists in occluded form and the the water phase is continuous. As the water phase is continuous, the pore water pressure under

equilibrium conditions is given by $-\gamma_w z$, where z is the height above the water table. The measurement of pore air pressure in this type of soil is very difficult. Fig(2.4b) show the type of structure found in the next zone of soil, within which both air and water phases are continuous. In this zone the pore air pressure will be zero, as the continuous air phase is vented to the atmosphere, and the pore water pressure is still given by $-\gamma_w z$, because the water phase exists in continuous form. Fig (2.4c) show the structure of soil at the very low degrees of saturation commonly found in a top zone at the ground surface. In this case the water phase is discontinuous and and the measurement of pore water pressure is very difficult.

2.2.2 Unsaturated compacted soils

Unsaturated soils formed by compaction are very heterogeneous, with groups of soil particles joined together to form packets or lumps. The small intra-packet voids within these packets are normally completely filled with water, so that each individual packet consists of saturated soil (Brackley, 1975). The larger inter-packet voids are , however, filled with air or a mixture of air and water, so that the soil is unsaturated on a macro-scale Fig (2.5). Brackley (1975) investigated compacted soil behaviour in terms of the"packet void ratio". The negative pore water pressure that developed in the packets during compaction prevents the packets from breaking down. In

fine- grained compacted soils a large force is needed to break these packets, due to high suction holding each packet together, while in coarse-grained compacted soils the relatively low suction means that the packets can be destroyed relatively easily.

Fig(2.5a) shows the structure of unsaturated compacted soils at high degrees of saturation. The water phase is continuous whereas the air phase is discontinuous. This type of structure normally exists in compacted clayey soils. Fig (2.5b) show the structure of unsaturated compacted fine-grained soils, at slightly lower degree of saturation where the air and water phases are often continuous. The water phase is normally discontinuous in compacted coarse-grained soils (see Fig 2.5c), because of low placement water content, and there may also be individual soil grains as well as grains grouped together in packets (Brackley, 1975).

The factors affecting the fabric of compacted fine-grained soils have been studied by many research workers in the last 4 decades. Seed and Chan (1959) observed that unsaturated compacted soil exhibits a flocculated structure when the soil is compacted at a moisture content dry of optimum and a dispersed structure when the soil is compacted at a moisture content wet of optimum (Fig 2.6). Further, Seed and Chan observed that the axial shrinkage which occurs on drying of soil compacted at moisture

contents dry of optimum is appreciably less than the shrinkage of soil compacted at moisture contents wet of optimum. Seed and Chan suggested that shrinkage of unsaturated compacted soil was a form of particle re-orientation.

Seed and Chan (1959) examined the stress-strain behaviour of unsaturated compacted soils compacted at moisture contents wet and dry of optimum. High stiffness was observed for soil compacted at moisture contents dry of optimum and lower stiffness for soil compacted wet of optimum moisture content. However the failure strength was found to be approximately equal in both cases. Seed and Chan suggested that the reason for equal strength was that structural changes during shearing resulted in similar structures at failure (in the failure zone) for samples compacted wet or dry of optimum. Seed and Chan (1959) also examined the influence of method of compaction. At moisture contents dry of optimum, statically and dynamically compacted samples exhibited similar stress-strain behaviour. However, at moisture contents wet of optimum, statically compacted samples exhibited significantly higher value of stiffness than dynamically compacted samples. This was attributed to the different fabrics produced by the two methods of compaction: static compaction producing a flocculated structure and dynamic compaction a dispersed or flocculated structure depending on the water content. Seed and Chan suggested that the flocculated structure

caused by static compaction at moisture contents wet of optimum was the result of the smaller shear displacements caused in static compaction than in dynamic compaction.

Barden and Sides (1970) also examined the effect of structure on the behaviour of compacted unsaturated soils. Barden and Sides concluded that for soil compacted dry of optimum, the settlement during loading was small and the major construction problem was the collapse or swelling of soil during wetting. In soils compacted to moisture contents wet of optimum, settlement during loading was much more of a problem whereas collapse or swelling upon wetting was relatively unimportant.

Vaughan (1987) compared the behaviour of unsaturated compacted soil with that of saturated or dry sand. The behaviour of saturated clay is a unique function of the effective stress history, but the behaviour of saturated or dry sand is controlled by the initial density. Unsaturated compacted clay fills show behaviour similar to that of sand, in that the mechanical behaviour is dependent upon the initial density of the fill (at placement). This is because the placement conditions control the soil fabric, which in turn affects the subsequent soil behaviour.

Toll (1990a) defined the structure of unsaturated compacted soils by the degree of saturation, and the degree of

saturation was included as a variable in his analysis. A clear distinction was found between the behaviour of samples of Kiunyu gravel compacted to different values of moisture content. Toll (1990a) also claimed that the structure of unsaturated compacted soils was not destroyed even at high shear strain. This contradicted the conclusion of Seed and Chan (1959), who stated that soil samples with different structures ended up with identical structures at failure. Toll (1990a) explained the behaviour of compacted unsaturated soils in terms of a two level structure involving compression of the packing arrangement of different packets and swelling of each individual packet. These two different aspects of behaviour will cause different volume change or pore water pressure response and the overall behaviour is dependent on the relative contributions of each effect.

2.2.3 Unsaturated soils formed by gas generation

Fig (2.7) shows the fabric of gassy soils. This type of soil is commonly found in the offshore environment (Sills et. al , 1991) and when natural gases are generated below the water table in the onshore environment. The common feature is that both pore water pressure and pore gas pressures are positive. Fig (2.7a) shows the structure of gassy soil if the gas bubbles are smaller than the normal void spaces of the soil. Under equilibrium conditions, the size of all occluded bubbles at a particular level in a

soil stratum should be identical. The excess of the gas pressure in the bubbles over the pore water pressure is inversely proportional to the radius of curvature of the bubbles. Therefore smaller bubbles will be at higher pressure than larger bubbles. This pressure difference between bubbles causes potential diffusion of dissolved gas from small bubbles to larger bubbles, leading to growth of the larger bubbles and shrinkage of the smaller bubbles (Wheeler, 1988a). Eventually the smaller bubbles will disappear from the soil.

Wheeler (1988a) proposed a continuum model for soil containing gas bubbles significantly larger than the normal void spaces (Fig 2.7b). This type of soil is often found in the offshore environment. The large bubbles form cavities within an otherwise unsaturated soil. Nageswaran (1983), Wheeler (1986), Thomas (1987) and Gardner (1988) examined the effect of large gas bubbles on the consolidation behaviour, shear strength and acoustic response of fine-grained offshore sediments.

2.3 LABORATORY TESTING OF UNSATURATED SOILS

The intention in this section is to describe some of the special problems which have to be overcome during laboratory testing of unsaturated soils. The section also includes discussion of the apparatus and procedures developed by previous workers to solve these problems.

Laboratory tests on unsaturated soils have normally been conducted in an oedometer apparatus, a triaxial cell or a direct shear apparatus. Until recently, the tests have usually consisted of one or more of the following:

(1) In a triaxial apparatus:

(a) Inundation tests, where the sample is saturated by reducing the suction to zero under isotropic stress conditions

(b) Isotropic consolidation at constant suction (including loading and unloading)

(c) Shearing at constant water content (water phase undrained, air phase drained)

(d) Fully drained shearing (both air and water phases drained)

(2) In an oedometer apparatus:

(a) Inundation tests, where the sample is saturated by reducing the suction to zero under one-dimensional conditions

(b) One dimensional consolidation at constant suction (including loading and unloading).

(3) In a direct shear apparatus:

(a) Fully drained shearing (both air and water phases drained)

2.3.1 Triaxial testing

Good quality triaxial testing of unsaturated soils is considerably more difficult than testing saturated samples. A test conducted under undrained conditions is no longer a constant volume test and the sample volume change in a drained test cannot be measured simply by the flow of water from the sample. There is also the practical problem of air diffusing through the membrane under supposedly undrained conditions. Bishop and Donald (1961) observed a reduction in the pore air pressure due to air diffusion through the membrane of 28.8% over a period of 7 days. To solve this problem, Bishop and Donald used greased aluminium foil between two layers of rubber membrane and used mercury as the cell fluid. The reduction in the pore air pressure was then only 1.2% over the same period.

Two kinds of volume change need to be measured in triaxial testing of unsaturated soils. These are the overall sample volume change and the water volume change. The water volume change can be measured in the usual manner with a burette or automatic volume change device connected to the drainage line from the sample. The overall sample volume change, due

to changes in both air and water volume, can be measured in two ways: by measuring the flow of cell fluid into the cell or by measuring axial and lateral strains of the sample and hence calculating volumetric strain.

Bishop and Donald (1961) developed a modified triaxial cell to test unsaturated soil at Imperial College (Fig 2.8). The modified apparatus consisted of a double-walled cell, with an acrylic jacket forming an inner cell wall. Mercury was used as the cell fluid in the lower part of the inner cell. A hole was made in the upper part of the inner cell wall to keep equal pressures in both inner and outer cells, so preventing expansion of the inner cell with changes of cell pressure. A stainless steel ball floated on the mercury in the inner cell to monitor the movement of the inner cell fluid during the test. The movement of the stainless steel ball was monitored with a cathetometer and this reading was then converted to volume change of the sample. The main disadvantages of this apparatus were: (a) that the sample could not be seen during the test, (b) the stress variation over the height of the sample due to the weight of the mercury and (c) the safety consideration of working with a large volume of mercury. The design of the triaxial cell developed by Bishop and Donald (1961) was also successfully used by Matyas and Radhakrishna (1968) to conduct isotropic consolidation tests on undrained compacted kaolin.

Wheeler (1986) developed a double-walled triaxial cell to

test unsaturated soils in the laboratory (Fig 2.9). The basic idea of the double-walled triaxial cell was that volume change of the sample could be measured by measuring the flow of water into or out of the inner cell. Equal cell pressures had to be applied to inner and outer cells to avoid any volume change of the inner cell that would be caused by expansion of the inner acrylic cylinder. A rolling diaphragm seal on the loading ram was used to prevent water leaking from the inner cell. The double-walled cell still had to be calibrated for any apparent volume change caused by cell pressure application (due to compression of cell fluid, slight flexure of the top plate and expansion of the connecting tubes), water absorption by the acrylic cell wall and ram displacement

The axis translation technique has been used in most laboratory research involving triaxial testing of unsaturated soil. Elevated values of pore air pressure are applied to one part of the sample boundary via a low air entry filter and lower (but still positive) values of pore water pressure are applied or measured on a different part of the sample boundary via a high air entry filter. This use of high air entry filters does not however completely solve the difficulty of air getting into the water drainage line. Dissolved air within the pore water can still penetrate through the porous stone by diffusion, and this air may then come out of solution in the drainage line beneath the porous stone. Bishop and Donald (1961) and

Fredlund (1975) developed methods to remove and measure the amount of diffused air collected beneath a high air entry filter. The diffused air was flushed from the system using a device such as a bubble pump and the air was then collected and the volume measured in a suitable calibrated chamber.

2.3.2 Oedometer testing

In oedometer testing the soil sample is lateraly confined and therefore any movement of the sample takes place vertically, making it easier to measure volume change of an unsaturated soil sample than in a triaxial apparatus. Barden and Sides (1970) developed a modified Rowe cell (Fig 2.10) to conduct controlled suction one-dimensional consolidation tests on unsaturated compacted soil. The suction was measured or controlled by using the axis translation technique. Subsequently this type of apparatus was sucessfully used by many other research workers, including Fredlund and Morgenstern (1977) and Escario and Juca (1989). Vicol (1990), instead of using the axis translation technique, used a semi-permeable membrane to control or measure suction in the soil (see Section 2.1.2).

2.3.3 Direct shear testing

In the direct shear test a soil sample is sheared on a pre-determined shear plane, normally under constant normal

stress. This apparatus has been used for testing saturated and unsaturated soils for many years.

Escario (1980) developed a direct shear apparatus (Fig 2.11) to test unsaturated soil samples under controlled suction. The axis translation technique was employed, with an elevated value of pore air pressure applied to a container surrounding the entire apparatus. Pore water pressure was then applied or measured via high air entry filter at the sample base. The main advantage of the direct shear apparatus over the triaxial apparatus was the much faster rate of testing that could be used, because of the shorter drainage path length. The time required for testing is a big problem in unsaturated fine-grained soils, as the time taken for full consolidation may be several weeks.

2.4 EFFECTIVE STRESS CONCEPT FOR UNSATURATED SOILS

Soil mechanics research falls within the following categories (Bishop, 1959):

(1) Laboratory methods to measure the relevant soil properties

(2) Theories and empirical methods to relate laboratory measurements to full scale field problems

(3) Field measurements to compare the predicted and

actual performance

In all these categories the behaviour of saturated or dry soils is controlled by changes in the effective stress . The effective stress is defined in such a way that any volume changes, shear deformation or changes of shear strength occur only due to effective stress changes.

In saturated or dry soil the effective stress is found to be equal to the total stress minus the pore fluid pressure:

$$\sigma' = \sigma - u \qquad (2.1)$$

Where σ' is the effective stress, σ is the total stress and u is the pore pressure. For example, the shear strength τ of saturated or dry soil is related to the normal effective stress σ' by the Mohr-Coulomb relationship:

$$\tau = c' + \sigma' \tan\phi' \qquad (2.2)$$

where c' is the cohesion and Φ' is the angle of internal friction. Bishop (1959) explained the concept of effective stress with practical examples:

(1) "Continuing settlement of a foundation as the excess pore water pressure dissipates to hydrostatic pressure resulting in an increase of effective stress with the time"

(2) "No changes in strength of a soil sample tested at different cell pressures under undrained conditions. This process will bring no absolute changes in the effective

stress and therefore no changes in strength".

Early researchers examined the possibility that the concept of a single effective stress could also be applied to unsaturated soils. If the concept of a single effective stress were applicable to unsaturated soil, then the analysis of unsaturated soil behaviour would be greatly simplified.

Bishop (1959) proposed a modified effective stress equation for use with unsaturated soils:

$$\sigma' = \sigma - u_a + \chi(u_a - u_w) \qquad (2.3)$$

u_a was the pore air pressure, u_w was the pore water pressure and χ was a parameter which was unity for saturated soils and decreased as the degree of saturation fell, reaching zero for dry soils. The difference between pore air pressure and pore water pressure can be defined as the suction s:

$$s = u_a - u_w \qquad (2.4)$$

In 1960 many researchers considered the possibility of a single effective stress equation for unsaturated soils. Among these researchers was Aitchison (1960), who proposed an equation for effective stress which was based on a capillary model

$$\sigma' = \sigma + \Psi s \qquad (2.5)$$

s was the suction $u_a - u_w$, ψ was a parameter varying from 1 to zero depending on degree of saturation, σ was total stress

and the component ψs was the effective stress due to suction. Equation 2.5 was basically a re-statement of Bishop's Equation 2.3, with χ replaced by ψ, because Aitchison implicitly assumed that u_a was zero. Aitchison (1960) calculated the component of effective stress due to suction based on an idealised capillary model.

$$\sigma'' = \psi s = S_r s - \sum_{0}^{S_r} 0.3 s \Delta S r \qquad (2.6)$$

σ'' was the component of the effective stress due to suction, s was suction and S_r was degree of saturation.

Bishop (1960) reviewed the concept of effective stress for unsaturated soils given by Equation 2.3, while Jennings (1960) proposed another equation to calculate effective stress in unsaturated soils.

$$\sigma' = \sigma + \beta s \qquad (2.7)$$

s was suction, σ was total stress and β was a parameter which must be estimated or measured experimentally. This parameter represented, for a "wavy plane" passing through the void spaces and inter-particle contact points, the proportion of the projected area of the plane that intersected water rather than air.

Donald (1960) examined Equations 2.5 and 2.6 proposed by Aitchison (1960). Donald assumed 6 possible moisture characteristic curves of s/s_d versus degree of saturation S_r (Fig2.12a), where s_d was the suction required to get air

into the soil (the air entry value of the soil). Values of effective stress were worked out based on each type of moisture characteristic curve and, surprisingly, the plots of χ versus S_r almost merged into a single unique line (Fig2.12b). This line gave a close fit with experimental data presented by Bishop (1960).

Bishop and Donald (1961) conducted a series of triaxial tests to validate the effective stress concept given by Equation 2.3. Unsaturated compacted Braehead silt samples were consolidated to given values of suction s and mean net stress $p-u_a$. Then each sample was sheared under fully drained conditions. During the shearing, the cell pressure σ_3, pore air pressure u_a and pore water pressure u_w were varied in such a way as to keep (σ_3-u_a) and suction (u_a-u_w) constant (Fig 2.13). During this process the stress-strain behaviour of soil was unaffected. Bishop and Donald took this behaviour as evidence to validate the effective stress concept of Equation 2.3. Bishop and Donald (1961) also calculated the magnitude of χ from the test results. The values were plotted against degree of saturation and no marked difference was found between the values obtained from consolidation and shearing (Fig 2.14).

Jennings and Burland (1962) analysed the factors affecting the use of Bishop's effective stress Equation 2.3 for unsaturated soils. Oedometer and triaxial inundation tests were conducted on three different soils (silt, silty clay

and sand). In each test an unsaturated sample was loaded to a given value of $\sigma-u_a$ and then soaked at constant total stress. Each sample showed an additional compression during soaking and, surprisingly, the final void ratio of the wetted soil fell on the virgin consolidation line for saturated soil. Jennings and Burland pointed out that, if the single effective stress concept were valid, swelling of soil samples would be expected during wetting due to the reduction in the effective stress as defined by Equation 2.3. The reduction in soil volume observed during wetting was, therefore, exactly the reverse of the behaviour predicted by Equation 2.3 and this cast serious doubt on the single effective stress concept as applied to volume change

Jennings and Burland (1962) back-calculated values of χ (from volume change behaviour) for a variety of different soils and plotted χ against degree of saturation S_r (Fig 2.15). The values of χ obtained by Jennings and Burland differed widely from previous results and from the theoretical values obtained by Donald (1960). Jennings and Burland (1962) suggested a two-way mechanism to explain collapse behaviour on wetting of unsaturated soils. First bonding between the saturated soil packets will be removed, resulting in collapse of the packet structure into the air-filled inter-packet voids: second, each saturated packet takes in water and swells (ie collapse of the "macro-structure", but swelling of the "micro-structure" of each

packet). The overall volume changes are dependent on the void ratio within the packet and the strength of each packet available to prevent breakdown. Escario and Saez (1973), Sridharan (1972), Booth(1975) and Maswoswe (1985) also examined the collapse behaviour of unsaturated soils. Maswoswe concluded that the collapse nature of unsaturated soils during wetting was not due to overall shear failure, but was due to insufficient shear strength at the inter-granular contacts to carry the mean stress.

Bishop and Blight (1963) made a further attempt to validate the effective stress concept given by Equation 2.3. They conducted consolidation and shearing tests on various types of soils, adopting a variety of different stress paths. Bishop and Blight concluded from their experimental results that a single effective stress, as defined by Equation 2.3, could not be used for the volume change behaviour of unsaturated soil, but it could be used to predict the shear strength of unsaturated soils.

Bishop and Blight (1963) suggested a modified effective stress equation, in which the effective stress was function of $\sigma-u_a$ and u_a-u_w:

$$\sigma' = \sigma - u_a + f(u_a - u_w) \qquad (2.8)$$

Bishop and Blight also qualitatively represented the volume change and shear strength behaviour of unsaturated soil in three dimensional plots of void ratio e and shear strength τ plotted against $\sigma-u_a$ and u_a-u_w, (Fig 2.16).

Burland (1964) rearranged the experimental results of Bishop and Blight (1963) to demonstrate that the single effective stress concept was invalid for volume change behaviour of unsaturated soils. However Burland (1964) did use the experimental results of Bishop and Blight (1963) to show a unique relationship between deviator stress and void ratio at failure for unsaturated soils, as shown in Fig (2.17). The relationship obtained was a unique line for both saturated and unsaturated specimens. Burland suggested that this unique line might not be applicable at lower degrees of saturation.

In the continuation of research into the behaviour of unsaturated soils, the volume change behaviour and shear strength were related to the two stress state variables $\sigma-u_a$ and u_a-u_w, as postulated by Bishop and Blight (1963).

2.5 VOLUME CHANGE BEHAVIOUR OF UNSATURATED SOILS

Matyas and Radhakrishna (1968) were amongst the first researchers to consider the "net stress" $\sigma-u_a$ and "suction" u_a-u_w as two independent stress state variables. For the axisymetric conditions of the triaxial test, Matyas and Radhakishna defined three stress parameters as follows,

$$p' = \frac{1}{3}(\sigma_1+2\sigma_3) - u_a \qquad (2.9)$$

$$q = \sigma_1 - \sigma_3 \qquad (2.10)$$

$$s=u_a-u_w \qquad (2.11)$$

p' was the mean net stress, q was deviator stress and s was suction. Matyas and Radhakrishna suggested that the state of unsaturated soils could be defined by the three stress state variables, the void ratio e, the degree of saturation S_r and a factor Ω describing the soil structure.

Matyas and Radhakrishna(1968) conducted a series of isotropic consolidation and K_o consolidation tests on kaolin-flint to examine the viability of the two stress state variables suggested by Bishop and Blight (1963). All samples were prepared by static compaction at the same initial condition in order to obtain the same initial structure for every sample and to avoid the influence of the structural state variable Ω.

In the first set of experiments the samples were consolidated isotropically at various values of suction. In the second set of experiments the samples were consolidated under K_o conditions at various values of suction. In each set a few tests were conducted in which the sample was consolidated at constant volume by reducing the suction from the initial value to a selected final value. For each set of tests, Matyas and Radhakrishna plotted the void ratio e against suction u_a-u_w and mean net stress $p-u_a$. The points from each test series produced a warped surface in e, u_a-u_w, $p-u_a$ space (Fig 2.18). The results also showed the possibility of either swelling or

collapse during wetting (reduction of suction to zero) depending on the value of $p-u_a$. These results provided strong support for the concept of two stress state variables, as first proposed by Bishop and Blight (1963). Matyas and Radhakrishna also noticed that the void ratio of unsaturated samples fell inside the warped surface for test paths involving de-saturation (increasing suction).

The effect of initial structure on the volume change behaviour of unsaturated compacted soil was apparent from the two sets of experimental results (the K_o consolidated samples shown in Fig 2.18b were compacted to different initial conditions to the isotropically consolidated samples shown in Fig2.18a). The K_o consolidation line would normally be expected to stay below the isotropic consolidation line for a given suction at least for saturated conditions. However the results showed that the K_o line lay above the isotropic line and this suggested considerable influence from the initial structure of unsaturated compacted soils.

Matyas and Radhakrishna (1968) also plotted degree of saturation S_r against mean net stress and suction. The plots produced a curved surface in S_r, u_a-u_w, $p-u_a$ space, and the degree of saturation S_r approached 100 % as suction reached zero.

Barden, Madedor and Sides (1969) examined the Bishop and

Blight concept of two stress state variables by conducting a series of isotropic consolidation tests on Westwater clay. Compacted unsaturated samples were consolidated at a given suction and mean net stress and then samples were taken through different stress paths involving wetting and consolidation. Fig 2.19 shows the stress paths adopted in the research and the results of one series of tests. Several series of tests were conducted to explore the influence of moulding water content, stress increment ratio and clay content. Barden at al (1969) concluded that de-saturation following saturation was a major cause for stress path dependency. The size of the stress increment was also a hidden factor causing extensive compression and therefore large stress increments led to apparent stress path dependency. The effect of large stress increments was more apparent at low values of suction than at higher values of suction. Barden et al found that high clay content caused swelling behaviour at low mean net stress. Also the affect of large stress increment ratios was more apparent at high clay contents.

Barden et al suggested that large stress increments caused high values of air pressure within occluded air bubbles, disruption of the soil structure and greater mobility of soil particles at high water contents. Both these effects led to high compression. Also it was possible that excess pore water pressure in the sample during the application of external pressure led to saturation and then de-

saturation in some parts of the soil sample, because the excess pore air pressure caused by the application of external stress quickly dissipated to the back pressure value whereas the excess pore water pressure took considerably greater time to dissipate to the relevant back pressure value. The sample therefore underwent a saturation and de-saturation process in those parts well away from the boundary at which water drainage occurred.

Fredlund and Morgenstern (1976) analysed unsaturated soil behaviour by considering unsaturated soil as a four phase material. The contractile skin formed by the air-water interface was considered as the fourth phase in the analysis. Fredlund and Morgenstern suggested that any two of the three parameters $\sigma - u_a$, $\sigma - u_w$ and $u_a - u_w$ could be used as stress state variables. In practice the stress state variables normally chosen are the net stress $\sigma - u_a$ and the suction $u_a - u_w$.

Fredlund and Morgenstern (1976) examined the uniqueness of the surfaces of void ratio e plotted against net stress $\sigma - u_a$ and suction $u_a - u_w$, with a series of isotropic and K_o consolidation tests on three different soils. Values of the deformation moduli with respect to changes of $\sigma - u_a$ and $u_a - u_w$ were calculated using the deformation from small increments of stress along two different stress paths. The calculated deformation moduli were then used to compare with the anticipated deformation along a third stress path.

Some samples showed a good correlation between measured and calculated deformation while others showed poor correlation. Fredlund and Morgenstern (1976) attributed this poor correlation to the non-linear nature of the constitutive surface and hysteresis of the soil behaviour. Fredlund and Morgenstern then correlated measured and calculated deformation assuming a non-linear constitutive surface (the surface was linear when void ratio was plotted against logarithms of net stress and suction). This action produced considerable improvement in the correlation between measured and predicted deformation. However poor correlation was still found for those tests where the sample was unloaded (net stress reduced) or suction was increased.

Fredlund and Morgenstern (1976) also checked the uniqueness of the constitutive surface of water phase volume plotted against $\sigma-u_a$ and u_a-u_w. They found that the correlation was not as good as that of total sample volume change. This poor correlation was attributed to inaccuracy in the measurements of very small water volume changes.

In an attempt to validate the use of the two stress state variables, Fredlund and Morgenstern (1977) conducted a series of null tests on unsaturated soil. Samples were isotropically consolidated to given values of $\sigma-u_a$ and u_a-u_w and then equal increments of σ, u_a and u_w were applied. No volume change was observed and Fredlund concluded

therefore that the two stress state variables $\sigma-u_a$ and u_a-u_w could be used to analyse unsaturated soil behaviour.

Fredlund and Morgenstern (1977) proposed sets of constitutive equations to relate the volume change of unsaturated soils to the two stress state variables:

$$e=e_o-D_t\ln\left[\frac{(\sigma-u_a)_f}{(\sigma-u_a)_o}\right]-C_t\ln\left[\frac{(u_a-u_w)_f}{(u_a-u_w)_o}\right] \qquad (2.12)$$

$$w=w_o-D_w\ln\left[\frac{(\sigma-u_a)_f}{(\sigma-u_a)_o}\right]-C_w\ln\left[\frac{(u_a-u_w)_f}{(u_a-u_w)_o}\right] \qquad (2.13)$$

e was void ratio, w was the water content, C_t, C_w, D_t and D_w were constants and the subscripts o and f meant "initial" and "final" respectively. Equations 2.12 and 2.13 can be used only over a limited range of suction values as they do not satisfy saturated conditions when the suction approaches zero. Equation 2.12 is also unable to describe the type of warped surface that is required to model swelling behaviour on wetting at low value of net stress and collapse on wetting at higher values of net stress.

Lloret and Alonso (1985) examined a number of possible constitutive relationships for the volume change behaviour of unsaturated soils using a wide range of experimental data. Lloret and Alonso (1985) finally proposed semi-empirical equations to relate the volume change of unsaturated soils to the two stress state variables:

$$e=a+b\ln(p-u_a)+c\ln(u_a-u_w)+d\ln(p-u_a)\ln(u_a-u_w) \quad (2.14)$$

or alternatively;

$$e=a+b\ln(p-u_a)+c\ln(u_a-u_w)+d(p-u_a)(u_a-u_w) \quad (2.15)$$

e was void ratio and a,b,c,and d were constants. Equation 2.14 was best at high stress levels and Equation 2.15 was best at low stress levels. Again the constitutive Equations 2.14 and 2.15 do not satisfy saturated conditions when the suction approaches zero. They do, however, describe surfaces capable of representing both swelling and collapse on wetting

Toll and Hight (1990) attempted to investigate the processes of saturation and desaturation. The investigation mainly concentrated on initially saturated normally consolidated soils. Toll and Hight qualitatively explained the behaviour when the soil is desaturated and then re-saturated. Toll postulated a possible virgin de-saturation line when the soil was subject to drying and a saturation line for the wetting process. Toll also postulated the possibility of soil in an overconsolidated state falling beneath the de-saturation line (Fig 2.20). Toll validated these concepts with limited experimental data.

2.6 SHEAR STRENGTH OF UNSATURATED SOILS

Another important contribution to the development of a constitutive model for unsaturated soil behaviour was made by Fredlund, Morgenstern and Widger (1978), who suggested

a relationship between the shear strength τ of unsaturated soil and the two stress state variables $\sigma - u_a$ and $u_a - u_w$.

$$\tau = c' + (\sigma - u_a)\tan\phi' + (u_a - u_w)\tan\phi^b \qquad (2.16)$$

Here c' and ϕ' were the cohesion and friction angle (with respect to effective stress) at a saturated condition and ϕ^b was the angle of internal friction with respect to suction. Fredlund , Morgenstern and Widger (1978) showed experimentally that the ϕ' value was equal for saturated and unsaturated conditions by conducting triaxial tests on compacted shale at constant water content. All the failure points were plotted in τ, $u_a - u_w$, $(\sigma_1+\sigma_2)/2 - u_a$ space (Fig (2.21). The failure points produced a planar surface. Approximate values for ϕ', ϕ^b and c' were calculated from the results and these were used to define Equation 2.16.

Gulhati and Satija (1983) also examined the shear strength of unsaturated soil by conducting triaxial shear tests under fully drained and constant water content conditions. Gulhati and Satija correlated failure strength to net stress and suction by introducing two frictional factors. They were able to plot the failure points on a surface defined by q, $\sigma - u_a$ and $u_a - u_w$ and concluded that the strength of unsaturated soils could be defined in terms of two stress state variables $\sigma - u_a$ and $u_a - u_w$.

Escario and Saez (1986) presented results which suggested a need to modify Equation 2.16 slightly. Escario and Saez

(1986) conducted drained direct shear tests on compacted Guadalix red clay, Madrid grey clay and Madrid clayey sand at different values of controlled suction. The failure strength was plotted against suction u_a-u_w and net normal stress σ- u_a for each soil type. Fig (2.22) shows the result for one of the soil types used by Escario and Saez. The results indicated that ϕ^b in Equation 2.16 was not a constant for a given soil type. The value of ϕ^b was approximately equal to ϕ' at low values of suction and then tended to decrease as suction increased. However, a stable value of ϕ^b could be found at higher suction. The suction at which the value of ϕ^b dropped differed for each type of soil. Escario and Saez also concluded that the value of ϕ' was unaffected by changes of the suction.

The non-linearity of shear strength with suction was again observed by Gan, Fredlund and Rahardjo (1988) in triaxial tests conducted on a glacial till. Each shear test was conducted at a controlled values of suction. At low values of suction the value of ϕ^b was approximately equal to ϕ' and then ϕ^b started to fall as suction increased (Fig 2.23). The value of suction at which the value of ϕ^b drops from ϕ' to a lower value can be interpreted as the air entry value of the soil ie at suctions below this critical value the soil is still saturated and ϕ^b must be equal to ϕ' in Equation 2.16 if the conventional Mohr-Coulomb expression for saturated soil is to be recovered. The range of suction values over which the fall in ϕ^b occurs can be

interpreted as due to the range of pore sizes in the soil sample.

The non-linearity of shear strength with the suction was even more apparent in the direct shear tests conducted by Escario and Juca (1989). The shear strength of unsaturated soil was examined over a very wide range of suction values from 0 to 14 Mpa. Fig (2.24) shows the shear strength envelope plotted against suction for a series of tests on Guadalix clay at a constant value of net normal stress. The component of strength due to suction reached a maximum at a particular value of suction and then started to fall. Theoretically if the suction increases indefinitely the soil must ultimately reach a dry state and Equation 2.16 should reduce to the normal Mohr-Coulomb relationship for dry soil. To satisfy this condition ϕ^b must fall to zero at very high values of suction.

Krahn, Fredlund and Klassen (1989) analysed the effect of suction on slope stability. Krahn, Fredlund and Klassen conducted a series of multi-stage triaxial tests on Notchhill silt in connection with a recent slope failure in a railway embankment constructed at Notchhill in British Columbia, Canada. The analysis of Krahn et al, which assumed the shear strength relationship of Equation 2.16, showed a considerable reduction in the factor of safety due to a small reduction in suction. Krahn et al concluded that the suction must be considered when analysing slope

stability of compacted slopes and the main reason for the Notchhill railway embankment failure was the dissipation of negative pore water pressure which occurred as the soil became saturated in the long-term.

2.7 LINKING VOLUME CHANGE AND SHEAR STRENGTH

In recent years researchers have been attempting to analyse unsaturated soil behaviour in terms of constitutive relations linking volume change, shear deformation and strength in a single elasto-plastic model. The research has been applied to both naturally occurring unsaturated soil and compacted unsaturated soil. These two forms of unsaturated soils may require different forms of constitutive model, especially when defining a normal consolidation surface for volume change. Most of the studies in recent years have concentrated on unsaturated compacted soils.

Toll (1990) conducted a series of triaxial tests on compacted Kiunyu gravel. Although Toll's main aim was to develop a constitutive relationship, he also examined the effect of structure on unsaturated soil behaviour. Toll produced statically compacted samples at different moisture contents. The degree of saturation S_r was considered as an additional factor to take account of the effect of soil structure. Most of the tests were conducted by shearing at constant water content. In most of the tests true critical

states were not achieved and the sample continued to dilate even at large strain.

Toll (1990) proposed equations for deviator stress q and specific volume v at the critical state

$$q=M_a(p-u_a)+M_w(u_a-u_w) \qquad (2.17)$$

$$v=\Gamma_{aw}-\lambda_a \ln(p-u_a)-\lambda_w(u_a-u_w) \qquad (2.18)$$

M_a, M_w, λ_a, λ_w and Γ_{aw} were factors which changed with degree of saturation S_r. Equation 2.17 was equivalent to the shear strength relationship proposed by Fredlund, Morgenstern and Widger (1978) in Equation 2.16, with M_a related to ϕ' and M_w related to ϕ' and ϕ_b.

$$M_a=\frac{6\sin\phi'}{3-\sin\phi'} \qquad (2.19)$$

$$M_w=\frac{6\cos\phi'\tan\phi^b}{3-\sin\phi'} \qquad (2.20)$$

Toll (1990) back-calculated values of M_a, M_w, λ_a, and λ_w by conducting a regression analysis and assuming that each was a function of S_r only (Fig 2.25). The value of M_a increased from the saturated value M as the degree of saturation decreased. This behaviour can be perhaps be explained by the fact that ϕ' is not a constant for gravel soil and it changes with dry density. Further the strength parameters of a soil are not the same under wet and dry conditions (Skinner, 1975). The factor M_w decreased from the saturated value M as the degree of saturation

decreased. Inspection of Equation (2.20) showed that this decrease in M_w was consistent with the earlier conclusion that ϕ^b decreased. The values of λ_a increased and λ_w decreased with decreasing degree of saturation S_r. However the quality of these values may be poor because a poor quality of sample volume change measurements was adopted.

Fredlund,Rahardjo and Gan (1987) suggested that unique critical state relationships for q and v (in terms of $p-u_a$ and u_a-u_w) might be obtained if the initial structure were destroyed during shearing to produce similar structures at critical state. Fredlund, Rahardjo and Gan argued that if different initial structures were created in a number of different compacted soil samples then those samples should be considered as different soils. Fredlund et al (1987) suggested that samples with similar initial structures must be used when establishing any constitutive relationship, to avoid any influence of initial structure in the model.

Wheeler (1991) re-analysed some of the results obtained by Toll (1990). Wheeler described the difficulties involved in applying Equations (2.17) and (2.18). As Toll's equations depend on degree of saturation, it would be very difficult to predict the critical state value of q and v in a field problem or a laboratory test because there would be no way of predicting the variation of degree of saturation in advance.

Wheeler (1991) suggested an alternative form of critical state equation for deviator stress with degree of saturation S_r excluded from the analysis:

$$q=M(p-u_a)+f(u_a-u_w) \qquad (2.21)$$

Wheeler showed that the experimental results of Toll (1990) fitted Equation 2.21 with the function of suction given by a cubic equation. Equation 2.21 is independent of degree of saturation S_r and it predicted the strength more accurately than Equation 2.17 proposed by Toll (1990). Equation 2.21 is equivalent to Equation 2.16 with $(u_a-u_w)\tan\phi^b$ replaced by a non-linear function as suggested by Escario and Saez (1986). Equation 2.21 is therefore already well validated by a considerable body of data (not just the data of Toll, 1990).

Wheeler (1991) also defined a critical state volumetric relationship in terms of only mean net stress and suction.

$$v_w=\Gamma-\lambda\ln(p-u_a)+f(u_a-u_w) \qquad (2.22)$$

v_w was the "specific water volume" (the volume of water and solids in a volume of soil containing unit volume of particles), which is directly related to the water content w. Equation (2.22) was validated using Toll's experimental data. Wheeler pointed out that Equation (2.22) does not provide any information on the value of the specific volume v at the critical state and hence the overall volume change is not defined.

In recent years, a research group in Barcelona has conducted detailed studies of unsaturated soil behaviour with a view to developing an elasto-plastic critical state model for unsaturated soil. Josa, Alonso, Lloret and Gens (1987) conducted a series of isotropic consolidation tests to examine the elasto-plastic behaviour of unsaturated soil. Gens, Alonso and Josa (1989) and Alonso, Gens and Hight (1987) qualitatively expressed elasto-plastic behaviour of unsaturated soil. Alonso, Gens and Josa (1990) presented a mathematical formulation of an elasto-plastic model and attempted to validate the theoretical concept of elasto-plastic behaviour of unsaturated soil with available experimental data. Independently of the Barcelona group, Karube (1988) conducted a series of triaxial tests on unsaturated compacted kaolin to express a new concept for effective stress based on elasto-plastic behaviour of unsaturated soils.

Josa, Alonso, Lloret and Gens (1987) conducted a series of isotropic consolidation tests on identical statically compacted samples of kaolin. Each sample was taken through various stress paths involving loading and unloading (changing mean net stress) at constant suction s and wetting or drying (changing suction s) at constant mean net stress p' (Fig 2.26). The results were analysed in terms of a possible yield locus in the p', s plane and elastic and plastic components of volume change. The results showed plastic behaviour when the soil was wetted at high

mean net stress and elastic behaviour when the soil was wetted at low mean net stress. Josa, Alonso, Lloret and Gens concluded that there was evidence of a loading collapse (LC) yield curve as shown in Fig (2.27). Josa, Alonso, Lloret and Gens also concluded that there was a second section of yield locus, the suction increase (SI) yield curve (Fig 2.27). They expressed the possibility of coupling of the LC and SI yield loci.

In unsaturated compacted soil the initial position of the SI and LC yield loci are set by the compaction process. The initial positions of the yield loci are dependent on the compaction effort and initial moisture content.

The behaviour of unsaturated soil in the stress region enclosed by the LC and SI yield loci is apparently elastic whereas the behaviour is elasto-plastic when the stress state reaches one of the yield loci. A path involving loading or wetting or both may expand the LC yields locus from it's initial position in the p' s plane. For example , if an unsaturated sample is loaded along path ABC in Fig (2.27) the soil behaves elasticly until point B is reached and no irrecoverable volume change will occur. Plastic behaviour begins at B, and from B to C irrecoverable volume change occurs. Similarly if a sample is wetted along path ADE in Fig (2.27) the soil undergoes elastic swelling along AD and then plastic collapse along DE.

Alonso, Gens and Josa (1990) proposed mathematical equations to enable the amount of volume change to be evaluated . Under virgin loading conditions, at constant suction, the specific volume was assumed to vary linearly with $\ln(p-u_a)$ during expansion of the LC yield curve:

$$v=N(s)-\lambda(s)\ln(p-u_a) \qquad (2.23)$$

N(s) and $\lambda(s)$ were functions of suction. By considering the available experimental data, Alonso et. al. (1990) proposed an empirical equation relating $\lambda(s)$ to suction:

$$\lambda(s)=\lambda(o)[(1-r)\exp(-\beta s)+r] \qquad (2.24)$$

$\lambda(o)$ was the compression index at zero suction (saturated conditions), r was the ratio of the asymtotic value of $\lambda(s)$ at very high suction to the value $\lambda(o)$ at zero suction and β defined the rate at which the compression index reduced towards the asymtotic value with increasing suction.

To simplify the analysis Alonso, Gens and Josa assumed that the swelling gradient κ, for changes of $p-u_a$ inside the yield curve was unaffected by suction (Fig 2.28).

Similar expressions were adopted for relating specific volume to changes of suction. The specific volume was linearly correlated with $\ln(s + p_a)$ (where atmospheric pressure p_a was introduced to allow the model to be used down to zero suction), with a constant plastic compression index λ_s corresponding to expansion of the SI yield locus.

Elastic volumetric strains due to changes of suction inside the SI yield curve were also modelled by a linear variation with $\ln(s+p_a)$, using on elastic swelling index κ_s

By considering a soil sample on the LC yield curve (Fig 2.28), Alonso, Gens and Josa (1990) developed an equation linking mean net stress and suction to define the shape of the LC yield locus.

$$\frac{p_o'}{p_c'} = \left[\frac{p^{*'}_o}{p_c'}\right]^{\left[\frac{\lambda(o)-\kappa}{\lambda(s)-\kappa}\right]} \qquad (2.25)$$

p_o' was the preconsolidation stress (at zero deviator stress) corresponding to a particular value of suction, $p_c'$was a reference stress (a soil constant) and p^*_o' was the preconsolidation stress at zero suction (the intercept of the yield curve with the axis s=0). As the LC yield curve expands it become more inclined (Fig 2.29). The soil constant p_c' is the value of $p_o^{*'}$ at which the LC yield curve is vertical in a plot of s against p'(see Fig 2.29).

Alonso, Gens and Hight (1987) extended the LC yield locus to anisotropic stress states to form a yield surface in q, p', s space (Fig 2.30). This required an assumption on the relationship between deviator stress q, mean net stress p and suction s at critical states. Alonso et al (1990) assumed that the strength was linearly related to suction and mean net stress.

$$q=Mp'+Mks \qquad (2.26)$$

M was the slope of the critical state line for saturated soil and Mk was the slope of the critical state line on a plane with p' constant. Equation 2.26 is therefore directly equivalent to Equation 2.16. Although it is now a well established fact that the influence of suction on shear strength is non-linear, the assumption of linear relationship (Equation 2.26) was considered by Alonso et.al. to be appropriate as a first approximation in modelling unsaturated soil behaviour.

Alonso et. al. (1990) assumed that constant suction sections of the yield surface would be elliptical in shape with a constant aspect ratio M (consistent with the modified Cam clay model for saturated soil). Combining this assumption with the shape of the LC yield curve in the q=0 plane and the critical state relationship of Equation 2.27 gave the shape for the LC yield surface (see Fig 2.30).

By using Equations 2.26 and 2.23, Wheeler (in press) showed that the model of Alonso, Gens and Josa (1990) implied a relationship between specific volume v, mean net stress p' and suction s at critical states

$$v=N(s)-(\lambda(s)-\kappa)\ln\left(2+\frac{ks}{p'}\right)-\lambda(s)\ln p' \qquad (2.27)$$

In the model of Alonso, Gens and Josa (1990), the critical states are therefore defined by Equations 2.26 and 2.27.

Alonso et. al. presented no experimental data to support or disprove the existence of Equation (2.27) (which they did not explicitly state).

Alonso at al. presented data from a number of tests which provided support for many features of their model. Comparisons were made between the model predictions and the results of several suction controlled tests on kaolin (Josa, 1988 and Karube, 1986) and sandy clay (Maswoswe, 1985).

Many features of the elasto-plastic model proposed by Alonso, Gens and Josa were still unproven at the start of the current project (indeed the Alonso et. al model had not yet been published at that time). Also the model was not entirely complete, as it provided no equations relating water content w to the stress state variables (such as the critical state equations for v_w proposed by Wheeler (1991) in Equation 2.22). This means that the model of Alonso et. al. cannot be used to predict soil behaviour under undrained conditions of the water phase (see next Chapter). The model does, however, represent a major advance in constitutive modelling of unsaturated soil behaviour.

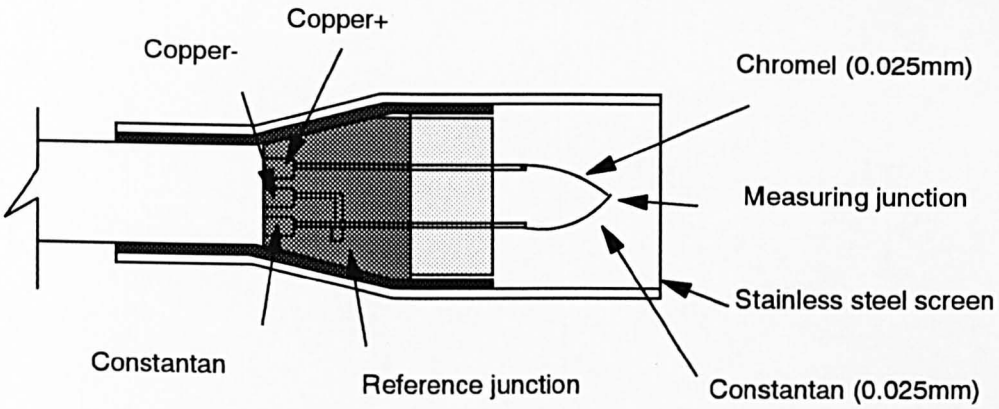

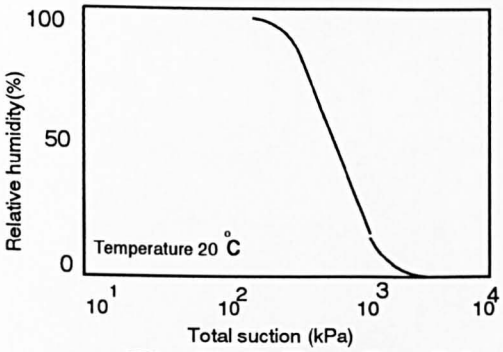

Calibration curve for thermocouple psychrometer

Fig (2.1) Details of thermocouple psychrometer
(Edil and Motan, 1984)

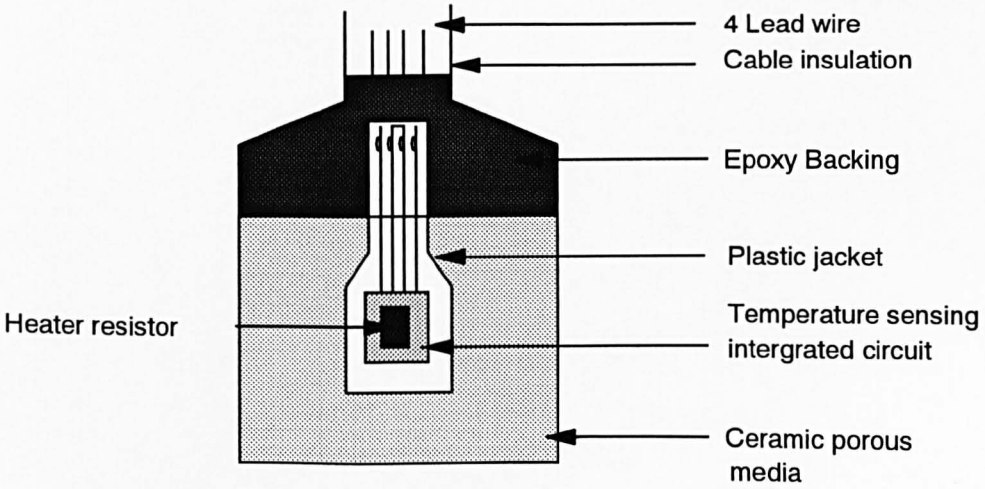

Fig (2.2) Thermal conductivity sensor.
(Wonk & Ho, 1987)

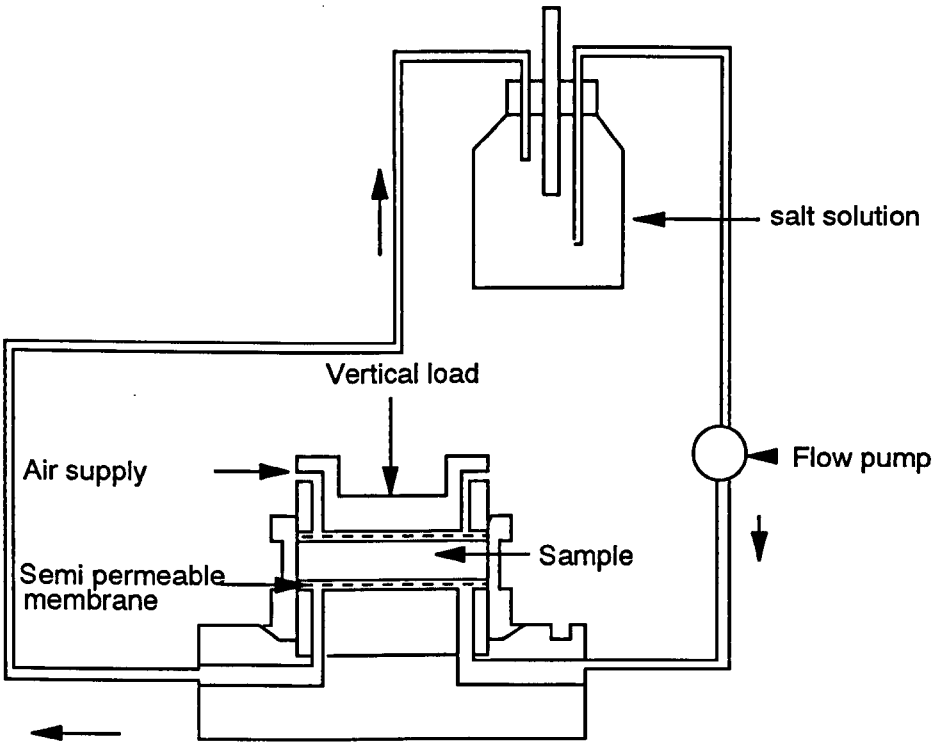

Fig (2.3) Measurement of suction by semi-permeable membrane

(Vicol, 1990)

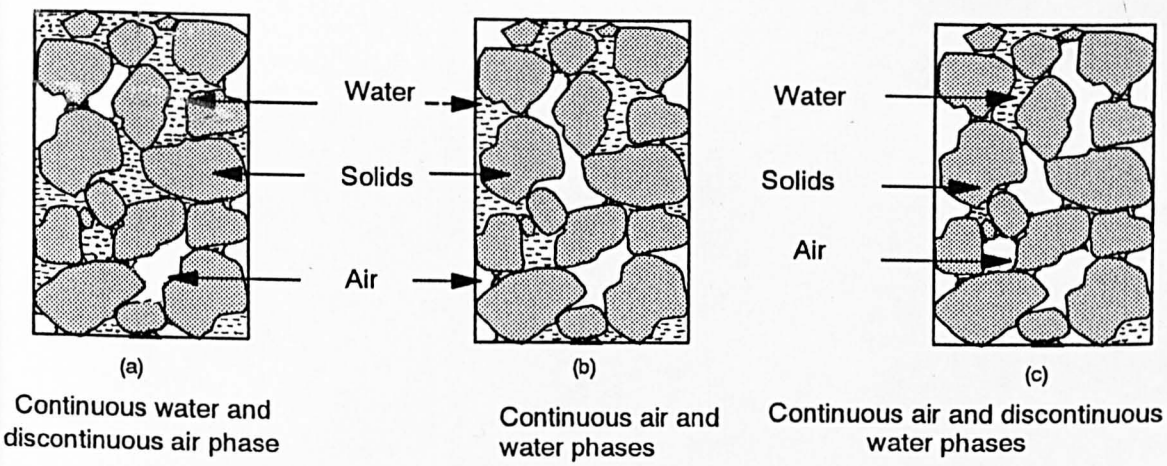

Fig (2.4) Structure of unsaturated natural soils.

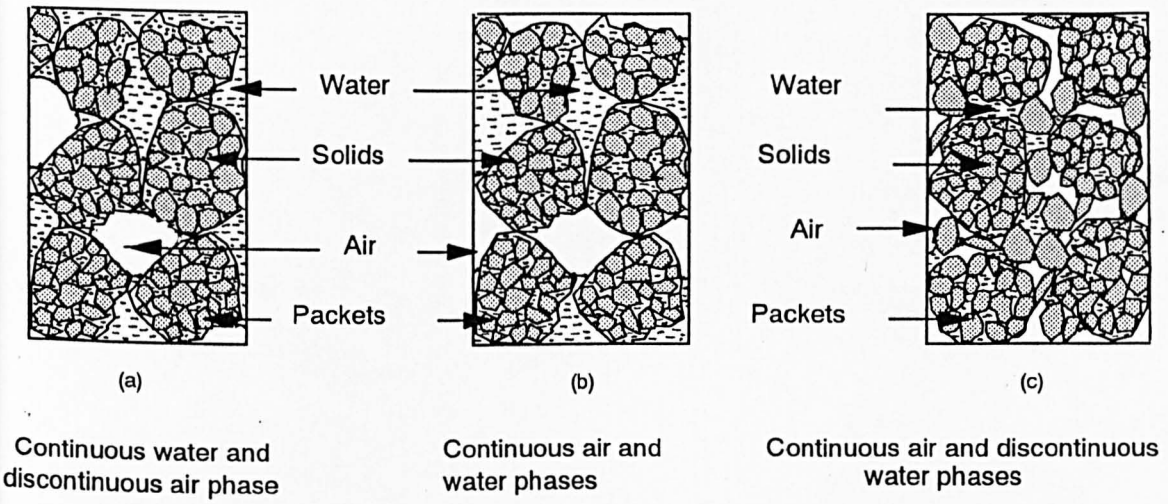

Fig (2.5) Structure of unsaturated compacted soils.

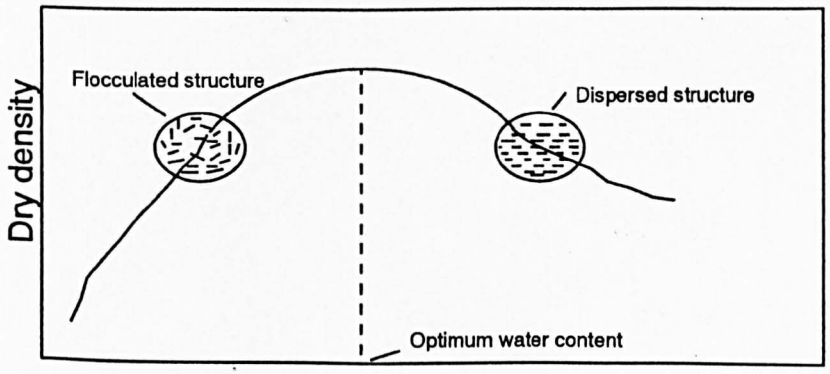

Fig (2.6) The effect of water content on compacted soil structure

(Seed and Chan, 1959, after Lambe, 1958)

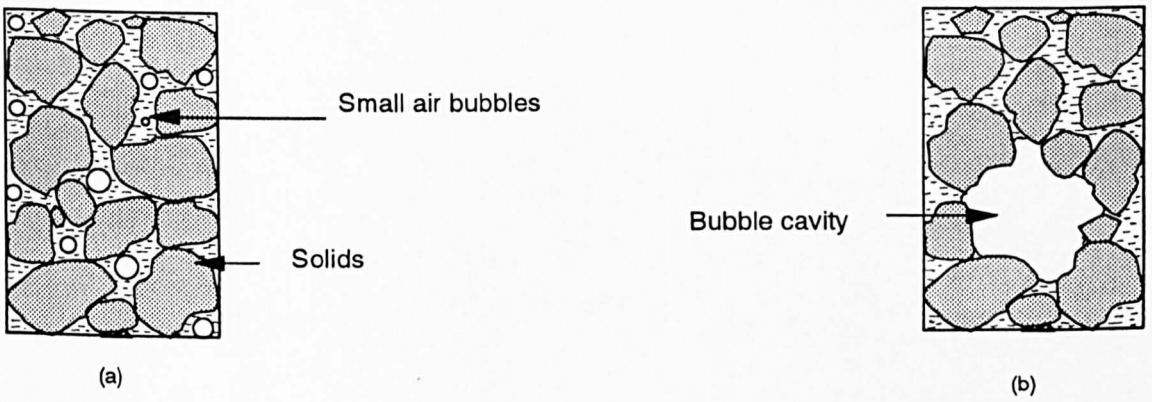

Fig (2.7) Structure of gassy soils.

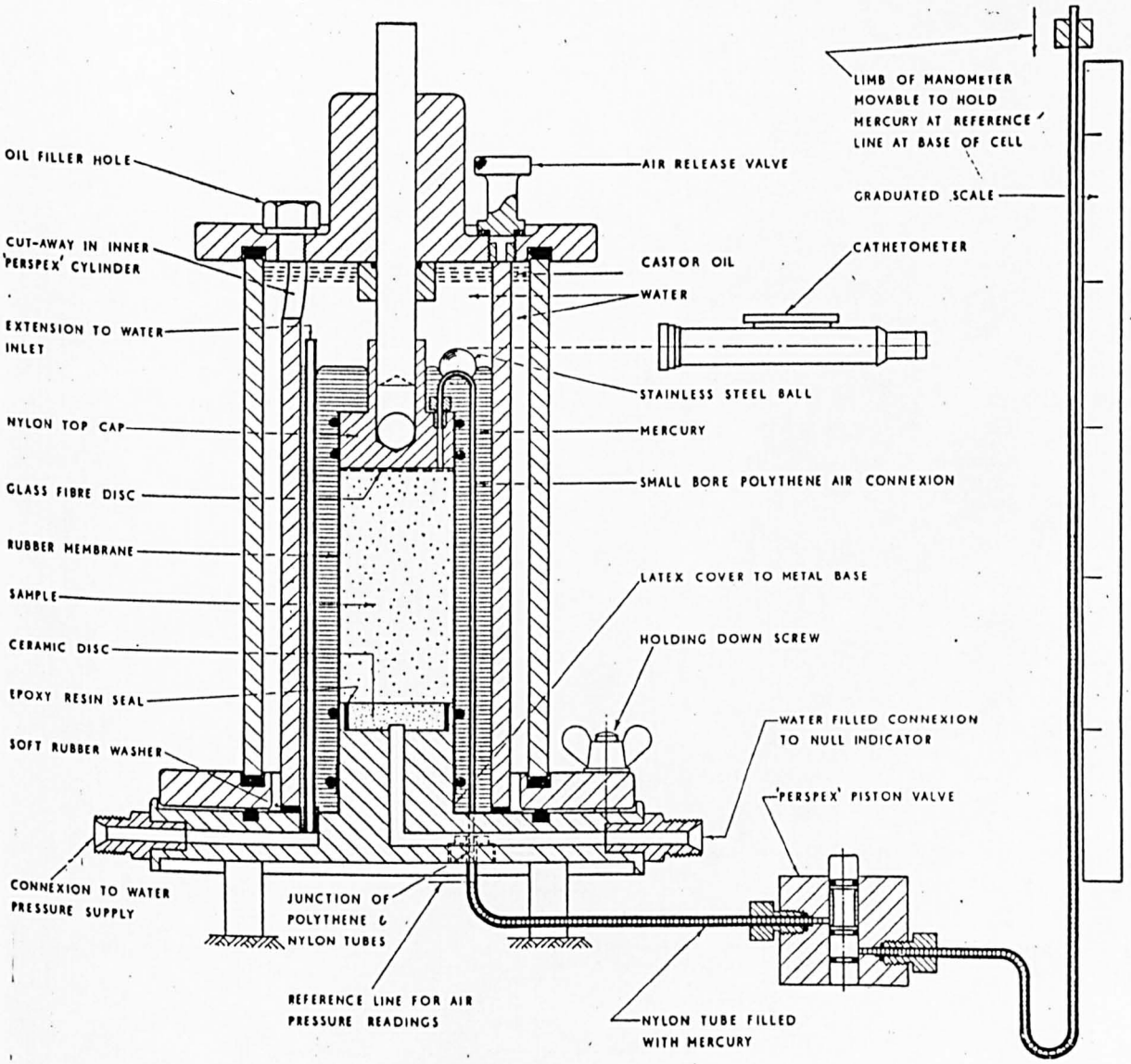

Fig (2.8) Modified triaxial cell to test unsaturated soils

(Bishop and Donald, 1961)

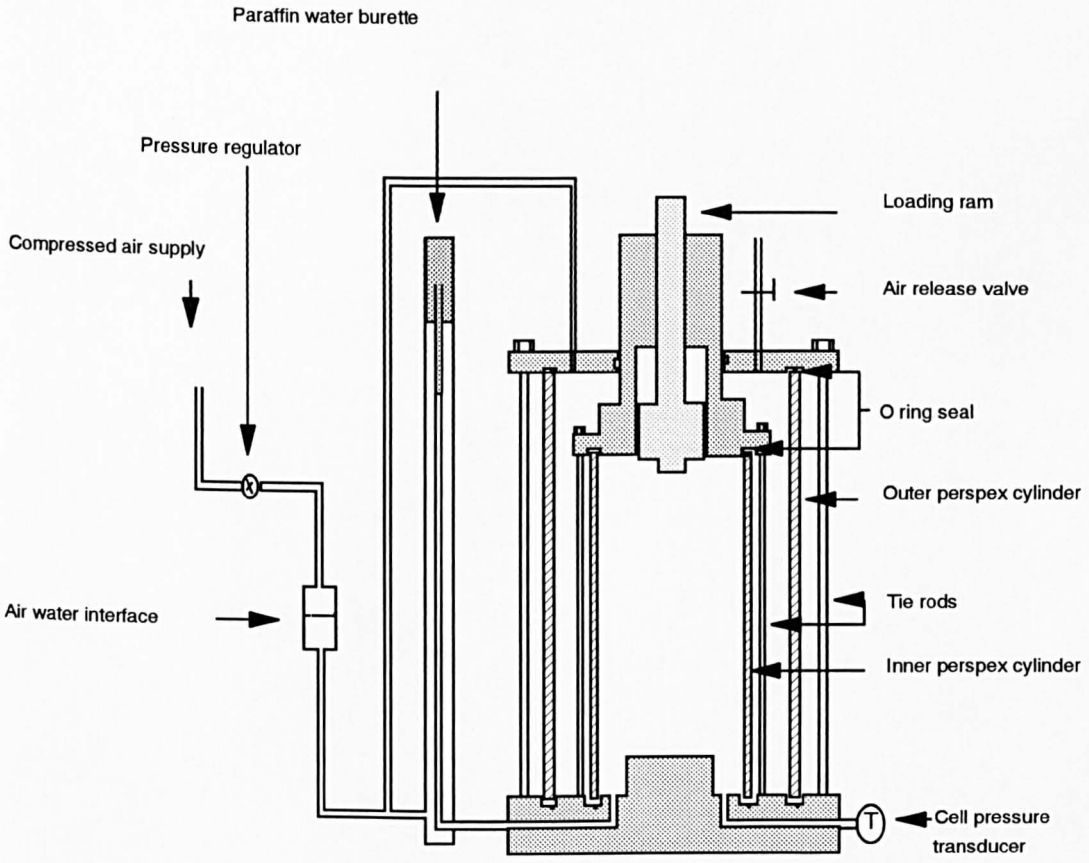

FIG (2.9) Double-walled triaxial cell

(Wheeler, 1986)

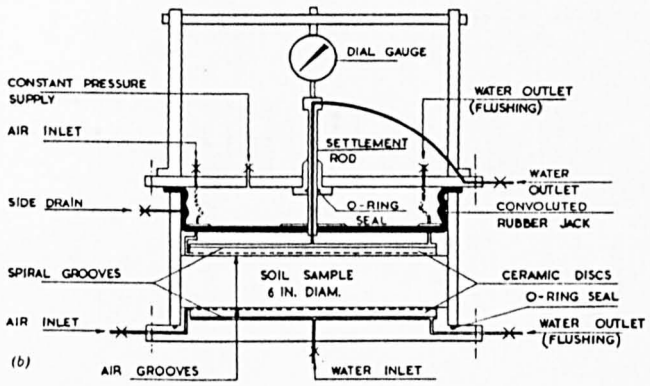

Fig (2.10) Modified Rowe cell

(Barden and Sides, 1970)

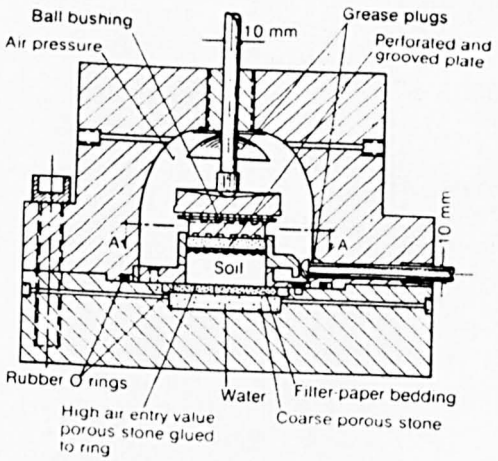

Fig (2.11) Modified direct shear apparatus

(Escario, 1980)

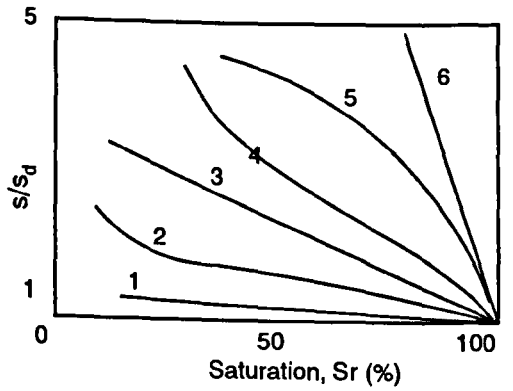

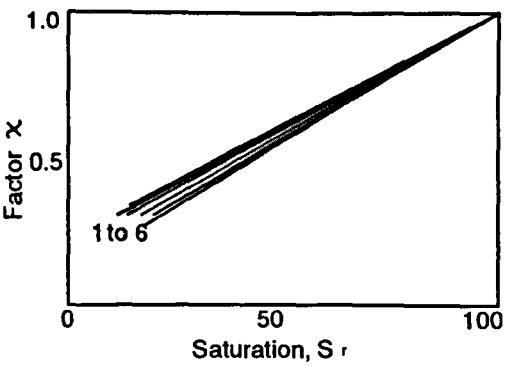

s Pressure deficiency (suction)

s_d Value at incipient drainage

(a) (b)

Fig (2.12) Theoretical relationship between χ and degree of saturation S_r (Donald, 1960)

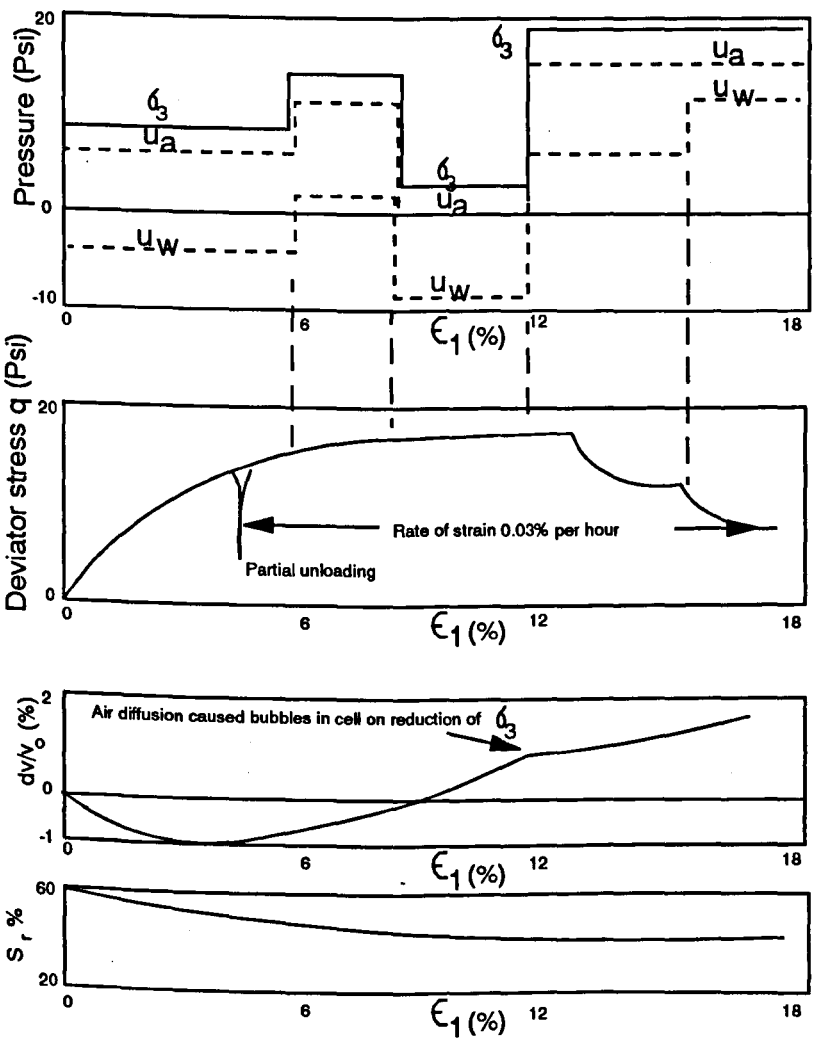

Fig (2.13) Drained test on unsaturated loose silt, in which u_a, u_w and σ_3 were varied so as to keep $\sigma_3 - u_a$ and $u_a - u_w$ constant. (Bishop and Donald, 1961)

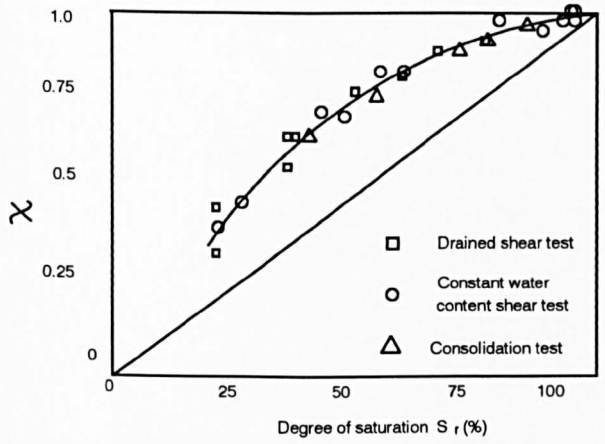

Fig (2.14) Experimental values of χ for Braehead silt
(Bishop and Donald, 1961)

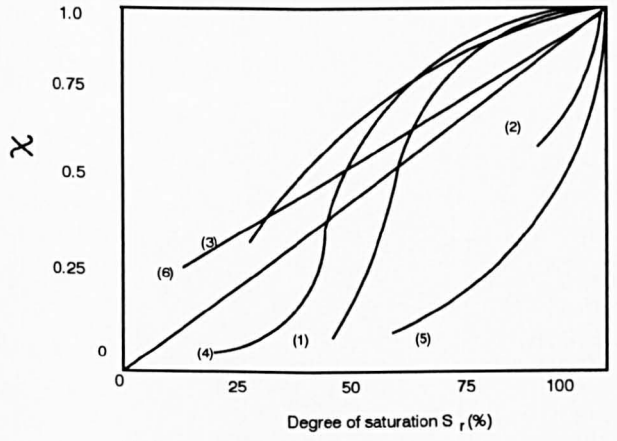

(1) Compacted boulder clay (4) Silt
(2) Compacted shale (5) Silty clay
(3) Braehead silt (6) Theoretical (Donald, 1960)

Fig (2.15) Curves of parameter against degree of saturation
(Jennings and Burland, 1962)

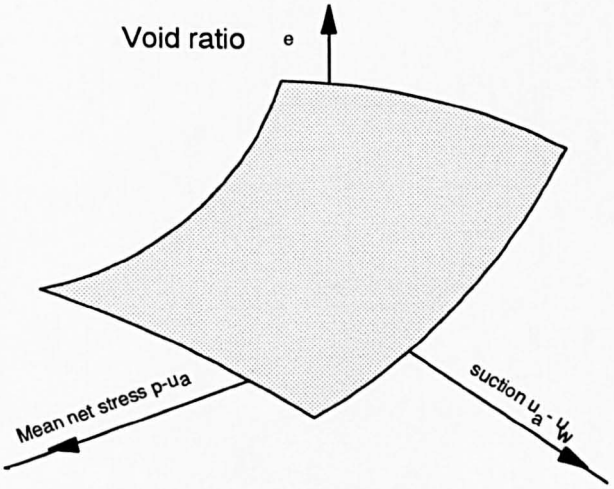

Fig (2.16) Proposed state surface for void ratio for unsaturated soils
(Bishop and Blight, 1963)

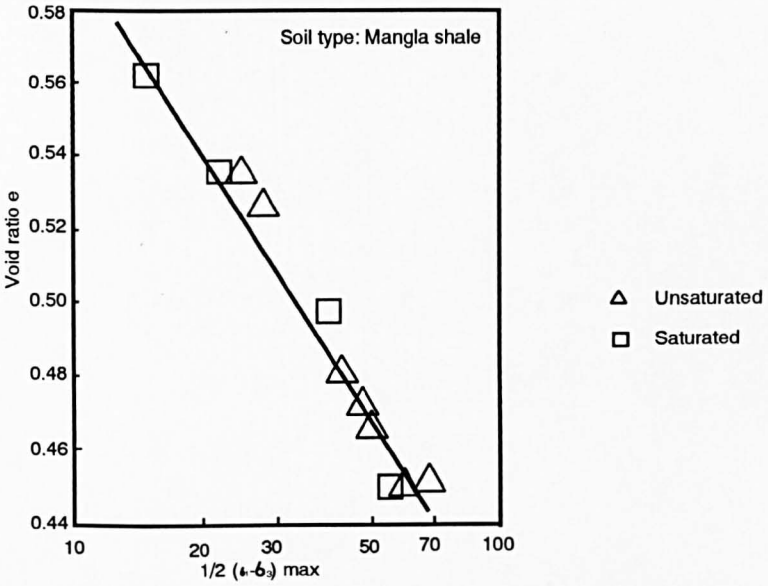

Fig (2.17) Relationship between void ratio and shear strength at failure
(Burland, 1964)

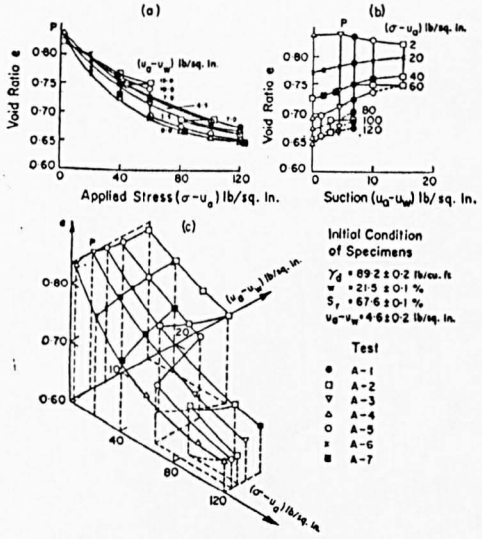

Fig (2.18 a) Isotropic compression tests on unsaturated compacted soil
(Matyas and Radhakrishna, 1968)

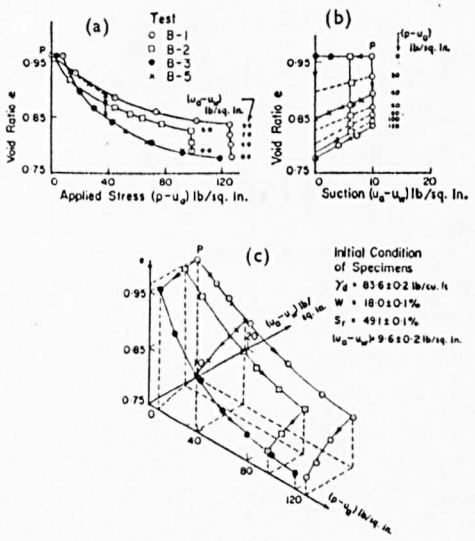

Fig (2.18b) K_o compression tests on unsaturated compacted soil.
(Matyas and Radhakrishna, 1968)

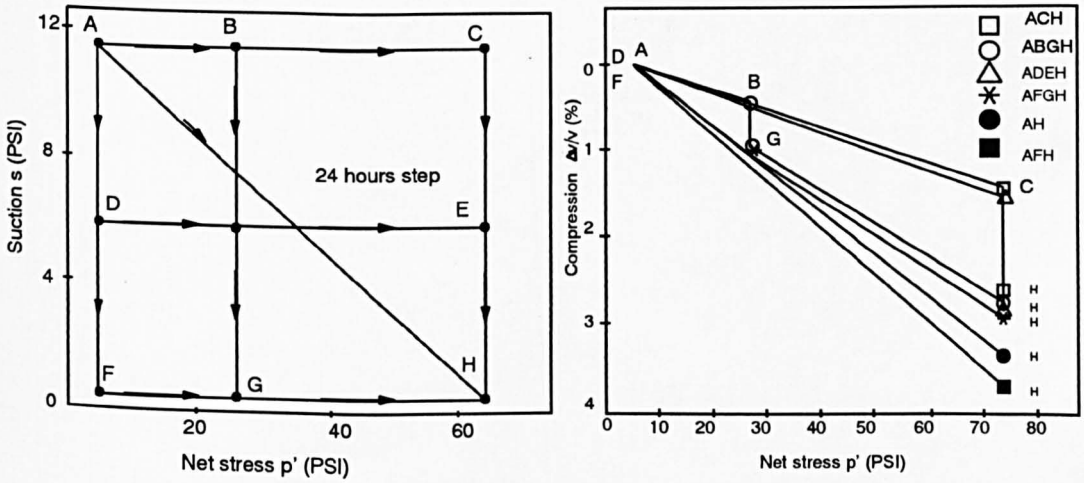

Fig (2.19) Volume change of clay
(Barden, Madedor and Sides, 1969)

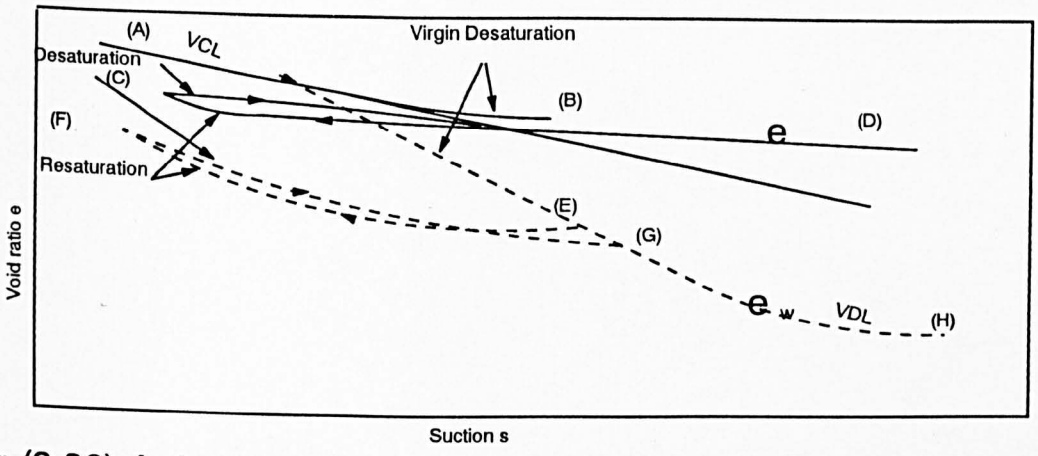

Fig (2.20) A drying and wetting cycle for a normally consolidated soil
(Toll and Hight, 1990)

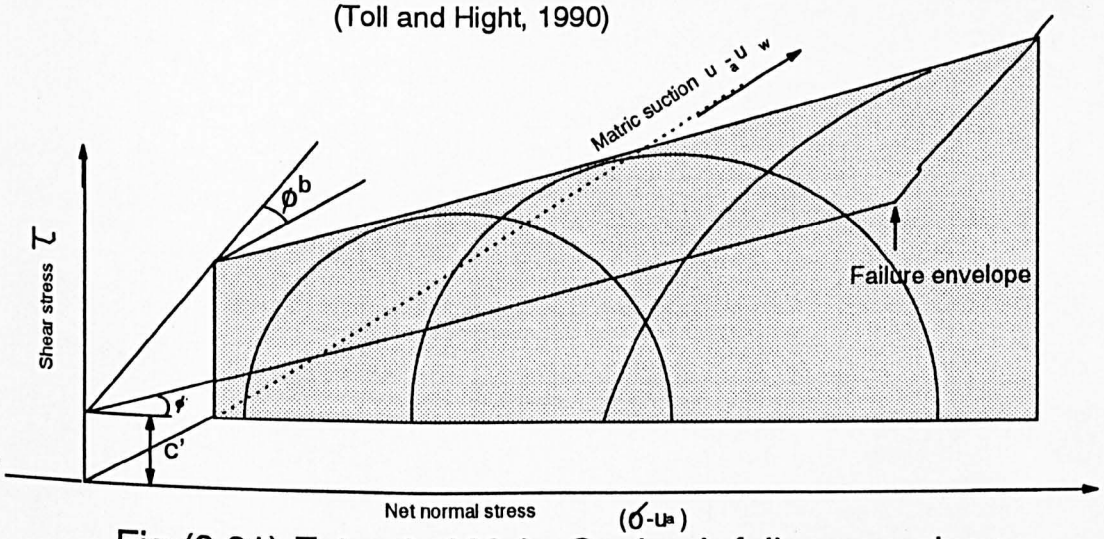

Fig (2.21) Extended Mohr-Coulomb failure envelope
(Fredlund, Morgenstern and Widger, 1978)

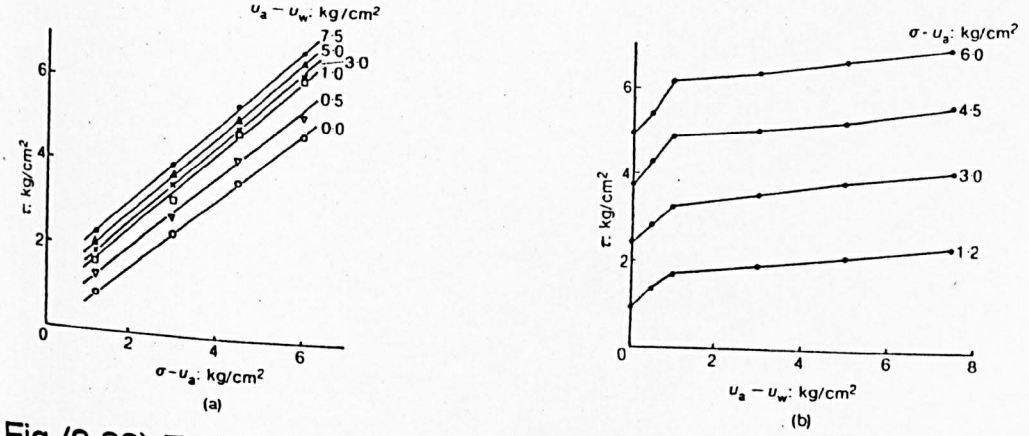

Fig (2.22) Failure strength plotted against suction and net normal stress
For Madrid clayey sand (Escario and Saez, 1986)

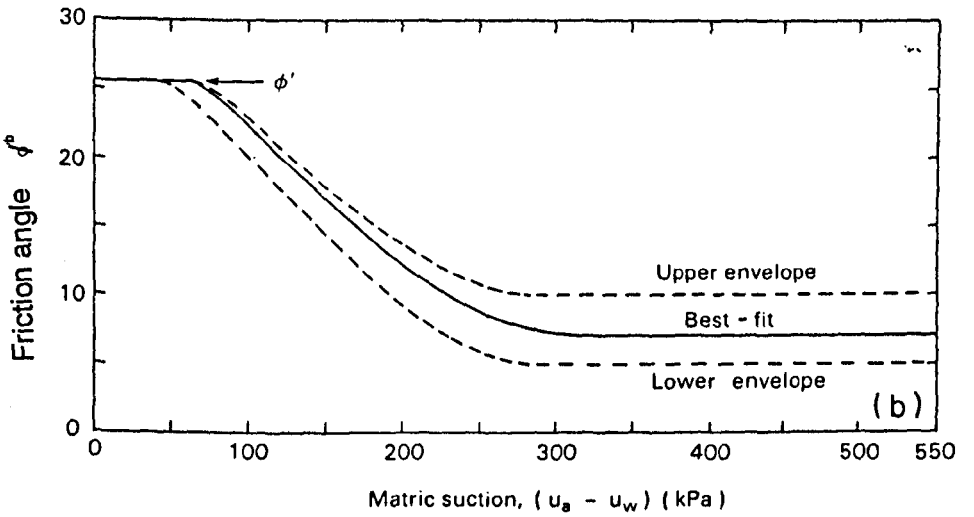

Fig (2.23) Value of ϕ^b plotted against suction
(Gan, Fredlund and Rahardjo, 1988).

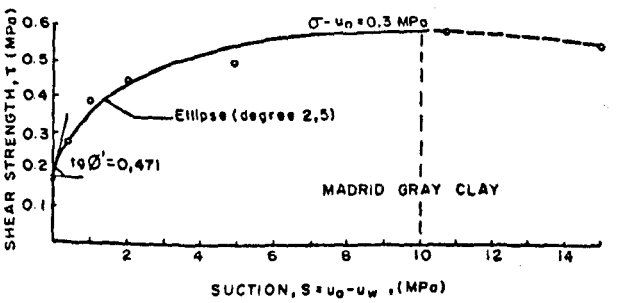

Fig (2.24) Shear strength envelope plotted over large range of suction
(Escario and Juca, 1989)

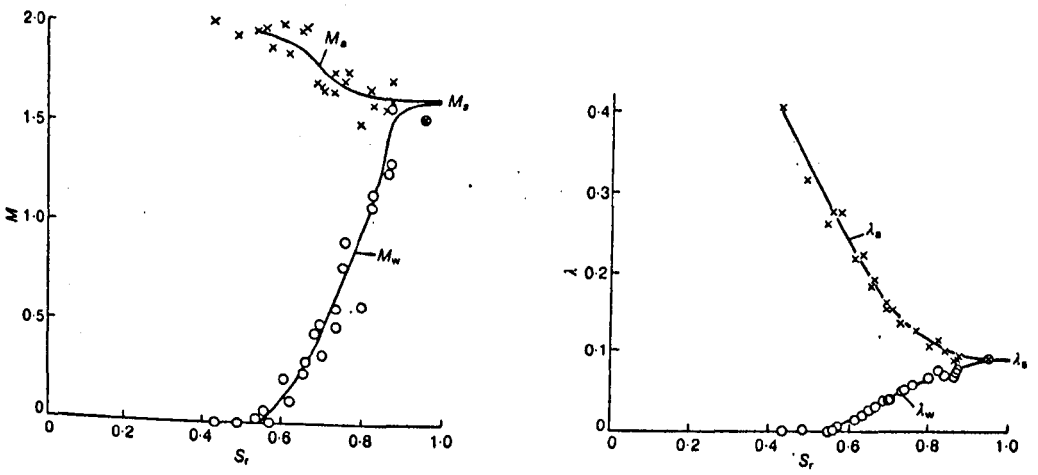

Fig (2.25) Variation of Toll's critical state parameters with degree of saturation for Kiunyu gravel

(Toll, 1990a)

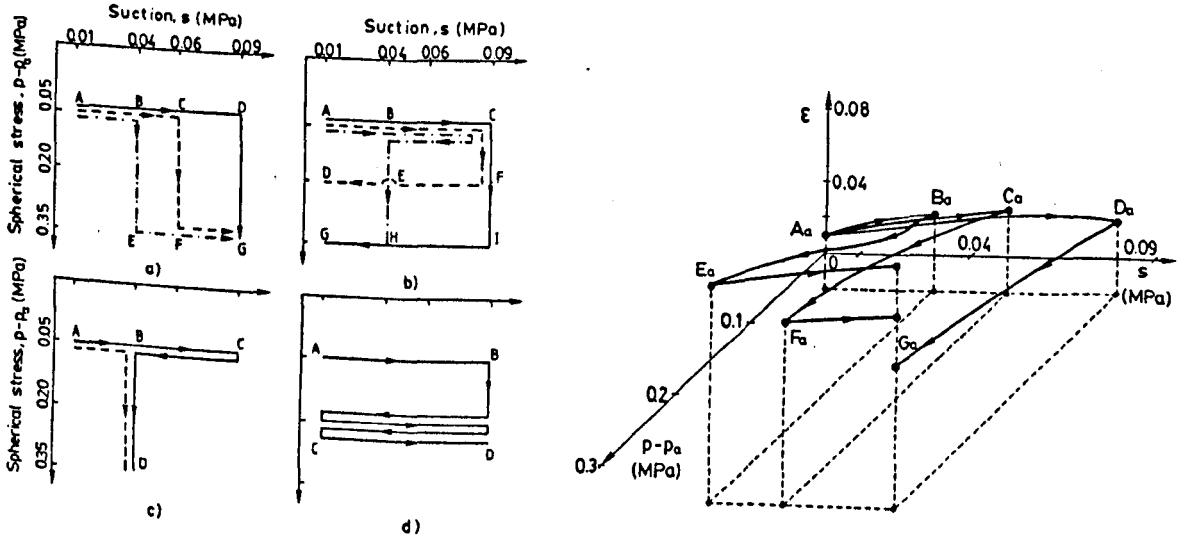

Fig (2.26) Isotropic compression tests on unsaturated compacted kaolin

(Josa, Alonso, Lloret and Gens, 1987)

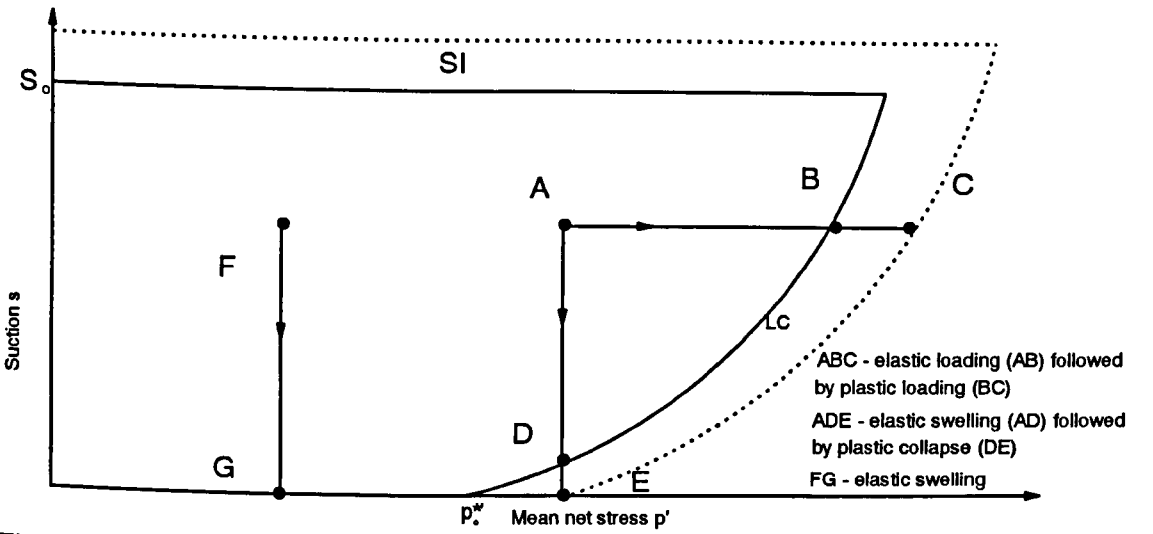

Fig (2.27) Yield curves for unsaturated soil under isotropic stress states
(Josa, Alonso, Lloret and Gens, 1987)

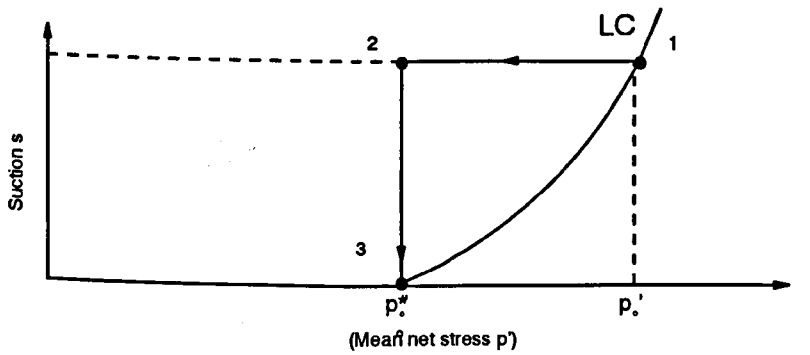

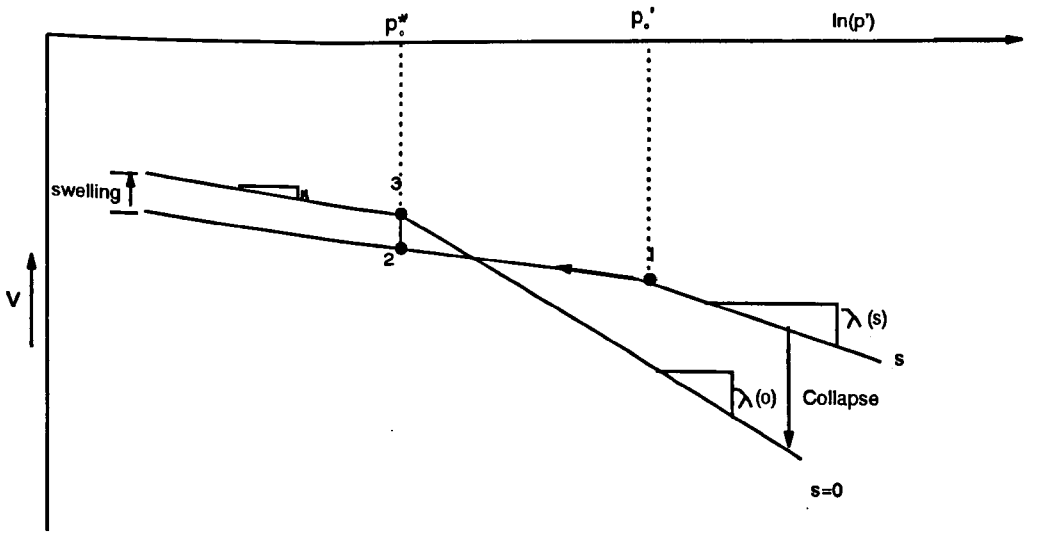

Fig (2.28) Compression behaviour of unsaturated soils

(Alonso, Gens and Josa, 1990)

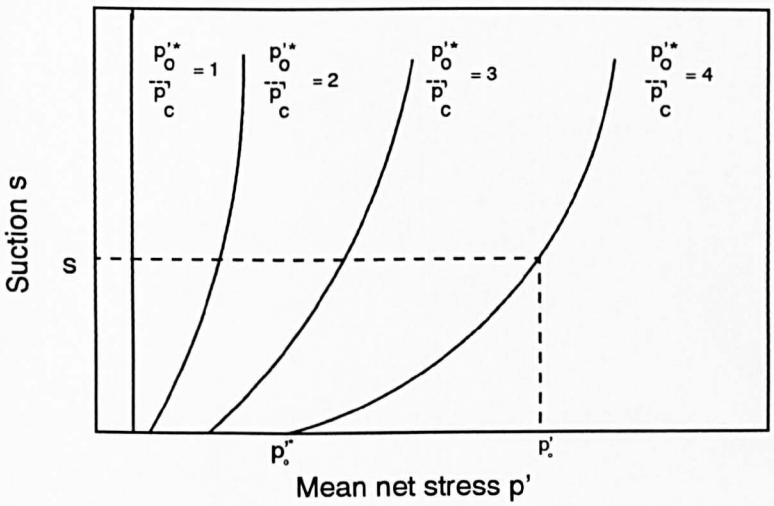

Fig (2.29) Expansion of the LC yield Curve

(Alonso, Gens and Josa, 1990)

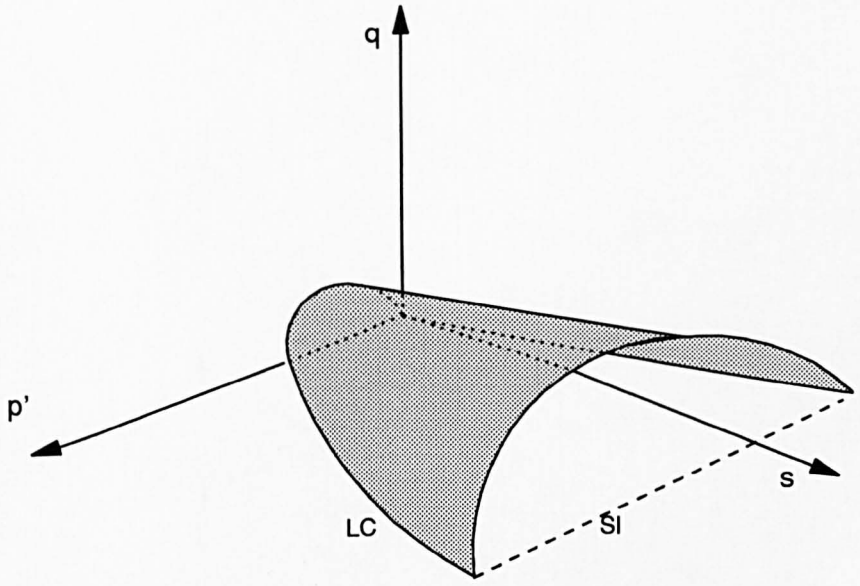

Fig (2.30) Yield surface for unsaturated soils in q, p' s space

(Gens, Alonso and Josa, 1989)

CHAPTER 3

CRITICAL STATE CONCEPTS FOR UNSATURATED SOIL

CHAPTER 3

CRITICAL STATE CONCEPTS FOR UNSATURATED SOIL

The main features of a proposed critical state framework for unsaturated soils are presented in this chapter.

3.1 SUMMARY OF GENERALISED CRITICAL STATE MODEL FOR SATURATED SOILS

Before describing a proposed set of critical state concepts for unsaturated soil, it is useful to see how critical state concepts work for saturated soil.

The critical state model developed for saturated soils is defined in terms of three state variables, mean effective stress p', deviator stress q and specific volume v (Schofield and Wroth, 1968). For the simplified conditions of the triaxial test ($\sigma_2=\sigma_3$), these state variables are defined as follows;

$$p'=\frac{1}{3}(\sigma_1+2\sigma_3)-u \qquad (3.1)$$

$$q=\sigma_1-\sigma_3 \tag{3.2}$$

$$v=1+e \tag{3.3}$$

If a saturated soil is sheared, it will ultimately reach a critical state where shear strain can continue without any further change in deviator stress q, mean effective stress p' or specific volume v. At a critical state the soil behaves like a frictional fluid (Schofield and Wroth, 1968).

Casagrande (1936) identified a critical state density at which soil continues to deform at constant shear strength. Rendulic (1936) identified that for a given soil at given conditions of initial stress and stress history, there was unique relationship between void ratio and changes in stress. Rendulic supported this concept by conducting undrained and drained tests on saturated soils and found that constant void ratio contours plotted from drained test data on axes of q and p' coincided with the contours plotted from undrained test data.

The specific volume v of soil at an isotropic normally consolidated state is linearly related to the logarithm of mean effective stress (Fig 3.1). It is obvious that the deviator stress q will be zero when the soil is under isotropic stress conditions. Therefore, the isotropic

normal compression line is defined by 2 equations.

$$q=0 \tag{3.4}$$

$$v=N-\lambda \ln p' \tag{3.5}$$

N is the specific volume of the soil when p' is 1 kPa and λ is the compression index.

When soil is sheared it will ultimately reach a critical state. These critical states were found to lie on a unique line in q, p',v space: the critical state line. This is defined by the following 2 equations:

$$q=Mp' \tag{3.6}$$

$$v=\Gamma-\lambda \ln p' \tag{3.7}$$

M and Γ are additional soil constants. The projection of the critical state line on the v, p' plane was found to be parallel to the isotropic normal consolidation line (Fig 3.1).

Roscoe and Poorooshasb (1963) examined saturated soil behaviour in a generalised elasto-plastic model. Undrained and drained tests were performed on isotropically normally compressed saturated soils. The results were plotted in p',q,v space. All undrained paths were found to be similar in shape (Fig 3.2). The contours of constant v from the undrained tests produced a surface in q,p',v space (Fig

3.3), which was known as the state boundary surface or Roscoe surface (a surface connecting the normal compression line to the critical state line). By using the equivalent pressure p'_e (the value of p' required to produce the same void ratio if the soil were on the normal consolidation line, see Fig 3.1), undrained and drained stress paths were normalised and all stress paths were found to reduce into a single curve (Fig 3.4), independent of what stress path was adopted.

When the soil state lies inside the state boundary surface, it behaves elastically. The elastic volume change behaviour can be modelled by an "elastic wall" having the following equation:

$$v=v_\kappa-\kappa \ln p' \qquad (3.8)$$

κ is a soil constant, the elastic swelling index, which is smaller in value than the compression index λ. v_κ is the specific volume when the soil is swelled to p'= 1 kpa. v_κ is not a constant and defines the particular elastic wall ie it varies with the preconsolidation pressure.

The behaviour of the soil on the state boundary surface is elasto-plastic, with the intersection of the relevant elastic wall and the state boundary surface defining a yield curve. Yielding of the soil causes plastic volume changes and the yield curve expands outwards (Fig 3.5). The amount of expansion of the yield curve is dependent on the

plastic volume change which has taken place during the application of the load.

If a soil is sheared under undrained conditions from an initial state A (Fig 3.6), the stress path will be vertical until the soil reaches the state boundary surface at point B. From point B the soil behaves elasto-plastically and the stress path will continue on the state boundary surface until the critical state is reached at C. The path from A to B is on a curved plane called the elastic wall, connecting the swelling line to the state boundary surface. The intersection of the elastic wall with the state boundary surface will give the yield curve at the particular consolidation pressure (Fig 3.6).

3.2 PROPOSED CRITICAL STATE MODEL FOR UNSATURATED SOIL

Unsaturated soil is a three phase material containing air, water and solid particles. Because of the presence of the additional phase (air) in the soil, an extra stress variable (such as suction s) and an additional volumetric variable (such as water content w) are required to fully define the state of the unsaturated soil. Therefore the proposed model for unsaturated soil consists of 5 state variables; mean net stress p', deviator stress q, suction s, specific volume v and water content w. The new state variables, mean net stress p' (in place of mean effective stress), suction s and water content w, are defined as

follows:

$$p'=\frac{1}{3}(\sigma_1+2\sigma_3)-u_a \tag{3.9}$$

$$s=u_a-u_w \tag{3.10}$$

$$w=\frac{S_r e}{G_s} \tag{3.11}$$

Therefore the proposed critical state model envisaged for unsaturated soil can be defined as a 5-dimensional model in terms of the above state variables. Within the 5-dimensional model there should be equivalents of the normal compression line, critical state line and state boundary surface. Although there are two more variables involved in the model there will be only one more degree of freedom than for a saturated soil, because there is only one additional phase. For example, there will be two degrees of freedom (two independent variables) at either isotropic normal compression states or critical states (rather than the single degree of freedom for saturated soil).

In the light of the above comments, it is possible to argue that isotropic normal compression states and critical states will each be defined by a set of 3 equations relating the 5 state variables. Similarly, a state boundary will be defined by 2 equations. The term "hyper-line" will be used to describe an entity defined by 3 equations in 5-dimensional space (or 2 equations in 4-dimensional space)

and the term "hyper-surface" will be used to describe an entity defined by 2 equations in 5-dimensional space (or 1 equation in 4-dimensional space). Therefore, we will refer to the normal compression hyper-line, the critical state hyper-line and the state boundary hyper-surface. The conventional terms "line" and "surface" will be used only when referring to 3-dimensional space.

For virgin isotropic stress states, a normal compression hyper-line can be postulated as follows:

$$q=0 \tag{3.12}$$

$$v=f(p',s) \tag{3.13}$$

$$w=f(p',s) \tag{3.14}$$

Equation 3.12 is true by definition for isotropic stress states. Mean net stress p' and suction s have been selected as the two independent state variables in Equations 3.13 and 3.14 in order to achieve maximum consistency with previous work. It would however be equally possible to re-state Equations 3.13 and 3.14 with other choices for the two independent variables. The existence of relationships of the form given in Equations (3.13) and (3.14) has now been widely accepted in principle (see section 2.5 on the volume change behaviour of unsaturated soils), although a variety of different equations have been suggested by different research workers (see, for example, Equations

2.12, 2.13, 2.14 and 2.15). What is certain is that the compressibility (the slope of v versus p' at constant s) reduces as the suction is increased (Alonso, Gens and Josa, 1990 and Vicol, 1990).

If the soil is sheared, it is expected that the soil will ultimately reach a critical state where shear strain can continue to increase indefinitely without any further change in the 5 state variables p', q, s, v, or w. If such a condition exists, then a critical state hyper-line can be postulated as follows:

$$q=f(p',s) \tag{3.15}$$

$$v=f(p',s) \tag{3.16}$$

$$w=f(p's) \tag{3.17}$$

The existence of a relationship of the form shown in Equation (3.15) has been well established in the past by previous research workers, such as Fredlund, Morgenstern and Widger, (1978) (Equation 2.16), Escario and Saez (1986), Alonso, Gens and Josa (1990) (Equation 2.26) and Wheeler (1991) (Equation 2.21); see section 2.6 on the shear strength of unsaturated soil for further details. However at the start of the project, there was little or no evidence available to support or disprove the existence of relationships of the form shown in Equations (3.16) and (3.17).

By extending the elastic behaviour of saturated soils to unsaturated soils it may be possible to define the equivalent of an "elastic wall" in the following way:

$$v=f(p',s,v_\kappa) \tag{3.18}$$

$$w=f(p',s,w_\kappa) \tag{3.19}$$

Where v_κ, and w_κ define the particular elastic wall (hyper-surface) ie they are related to the preconsolidation pressure. Again there was little evidence available at the start of the project to support or disprove the existence of relationships of the form shown in Equations (3.18) and (3.19).

Linking the isotropic normal compression hyper-line and and the critical state hyper-line, a state boundary hyper-surface can be postulated, described by the following two equations:

$$v=f(p',s,q) \tag{3.20}$$

$$w=f(p',s,q) \tag{3.21}$$

At the start of the project there was no evidence to validate the existence of such relationships for unsaturated soils. However if the behaviour of unsaturated soil includes an isotropic normal compression hyper-line (defined by Equations 3.12 to 3.14) and a critical state hyper-line (defined by Equations 3.15 to 3.17), then the

existence of a state boundary hyper-surface is a distinct possibility.

By extending the elasto-plastic model for saturated soil to unsaturated soil it may be possible to define elastic and plastic volume changes and shear deformations with suction treated as an extra stress variable. The proposal is that the behaviour of unsaturated soils on the state boundary hyper-surface is elasto-plastic whereas the behaviour of unsaturated soils inside the state boundary hyper-surface is purely elastic. A yield surface can be defined in terms of p', q, and s and the yield surface will correspond to the intersection of the current elastic wall with the state boundary hyper-surface.

3.3 COMPARISON WITH MODEL OF ALONSO, GENS AND JOSA

The model proposed by Alonso, Gens and Josa (1990), described in Section 2.7, involved 4 state variables: mean net stress p', deviator stress q, suction s and specific volume v. However Alonso, Gens and Josa did not include the water content w as an additional variable in their analysis. The proposed volumetric relationship for unsaturated soils under isotropic stress conditions (Equation 3.13) and the critical state relationship for deviator stress (Equation 3.15) are included in the model proposed by Alonso, Gens and Josa (1990), (Equations 2.23 and 2.26). Although Alonso, Gens and Josa did not

explicitly suggest the existence of a critical state relationship for specific volume, such a relationship can be derived from their proposed model (see Equation 2.27). This critical state equation involves the same state variables as the proposed critical state relationship of Equation (3.16)

Alonso, Gens and Josa did not include the water content w in their model. This means that their model can be used for "drained" analyses, when the value of suction is known, but it cannot be used for "undrained" (constant water content) analyses when the value of suction is a result of the requirement that water content remains unchanged. The addition of expressions for water content (such as Equations 3.14 and 3.17) would mean that critical state conditions could be predicted for all loading and drainage conditions, including the two most relevant cases in the field:

(a) Shearing at constant water content (but with the air phase fully drained), corresponding to short term stability.

(b) Shearing under fully drained conditions (of both air and water phases), corresponding to long-term stability.

Alonso, Gens and Josa (1990) proposed a possible yield

surface in q,p',s space. They assumed that constant s cross-sections of the yield surface were elliptical, intersecting the p' axis at -ks and p_o' (where the magnitude of both ks and p_o' increased with increasing suction; see Section 2.7). Alonso, Gens and Josa proposed that the behaviour of unsaturated soil was elastic inside the state boundary and elasto-plastic on the state boundary. Therefore, apart from the lack of water content relationships, their model is qualitatively consistent with the proposals described in this thesis.

3.4 OBJECTIVES OF THE RESEARCH

The main objectives of the research programme were to support or disprove the existence of the following:

(1) Isotropic normal compression relationships of the form given in Equations (3.12) to (3.14)

(2) Critical state relationships of the form given by Equations (3.15) to (3.17)

(3) State boundary relationships of the form given in Equations (3.20) and (3.21).

If such relationships could be shown to exist, a further objective was to establish the precise nature of the various equations. If critical state relationships and

state boundary relationships could be defined, an attempt would then be made to define yield surfaces and model elastic and plastic behaviour of unsaturated soils.

3.5. PROPOSED METHODOLOGY

The proposed methodology was to conduct a series of triaxial tests on unsaturated samples of kaolin, all prepared by static compaction to the same initial state. The tests would be performed in a double-walled triaxial cell, with changes of sample volume measured by the flow of water into or out of the inner cell.

The intention was that each sample would be isotropically consolidated to a virgin state at a given value of suction s and mean net stress ($p-u_a$). Then the sample would be sheared until it reached a critical state. Different types of shearing would be conducted to see whether all samples reached the same critical state hyper-line and followed the same state boundary hyper-surface, independent of test path.

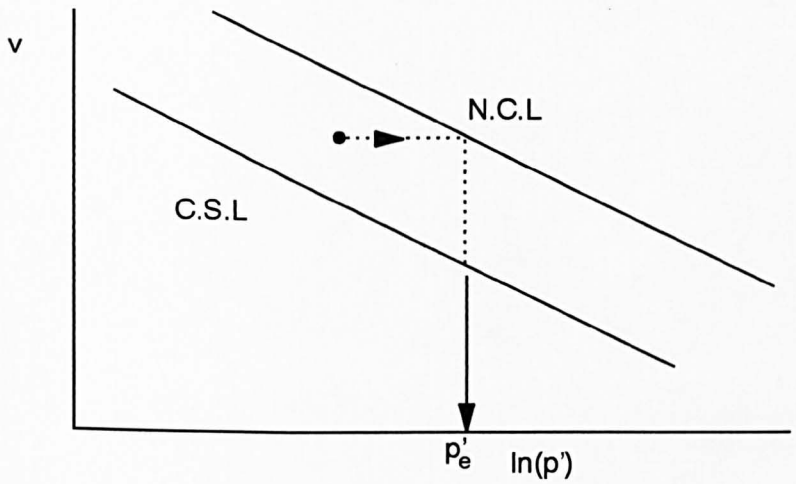

Fig (3.1) Normal compression and critical state lines for saturated soils

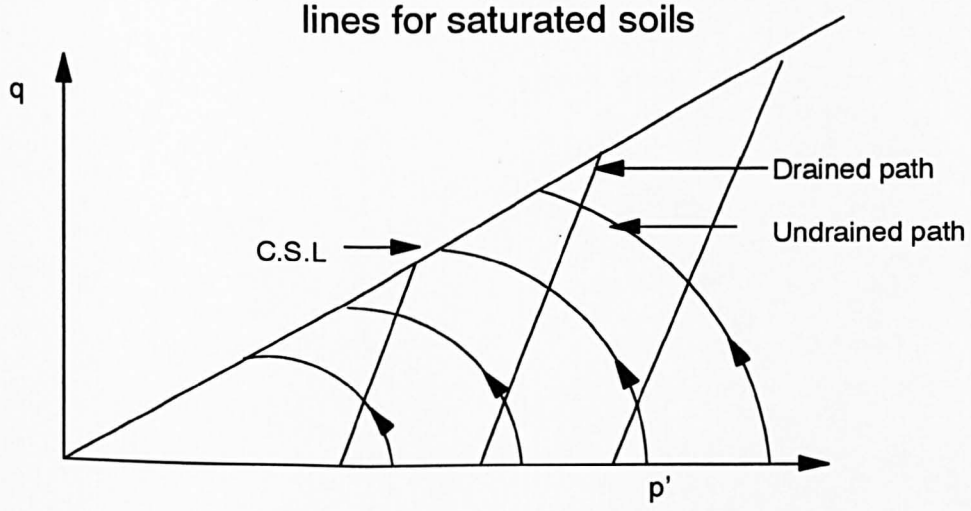

Fig (3.2) Drained and undrained stress paths

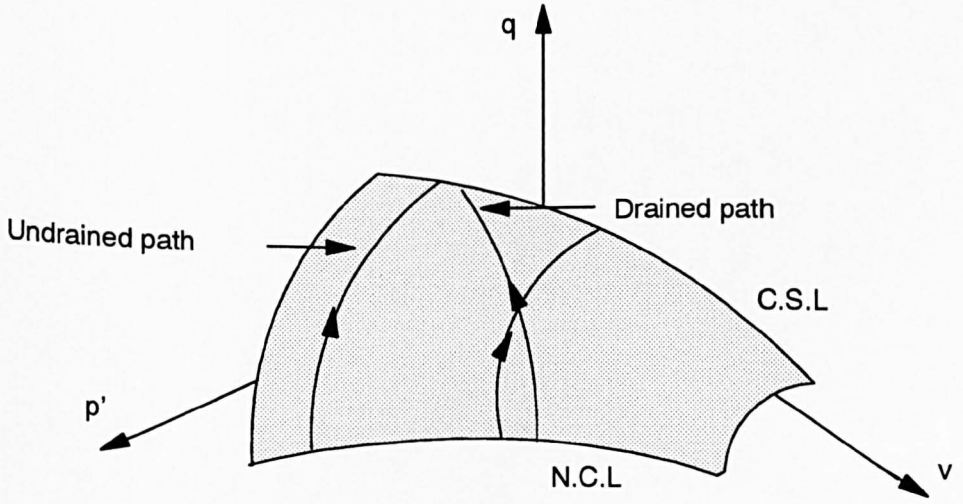

Fig (3.3) State boundary surface

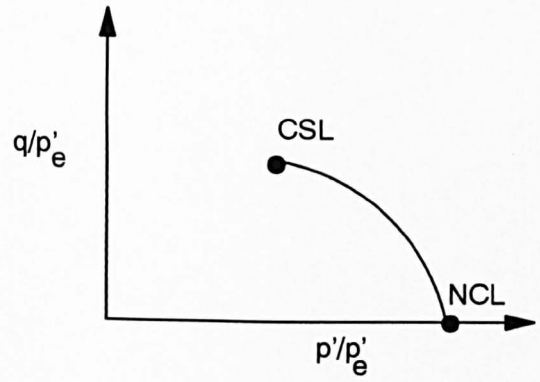

Fig (3.4) Normalised stress path

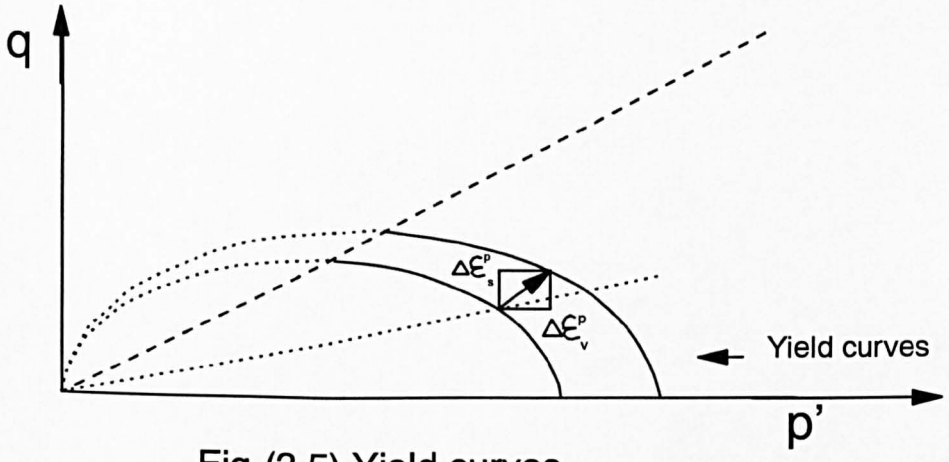

Fig (3.5) Yield curves

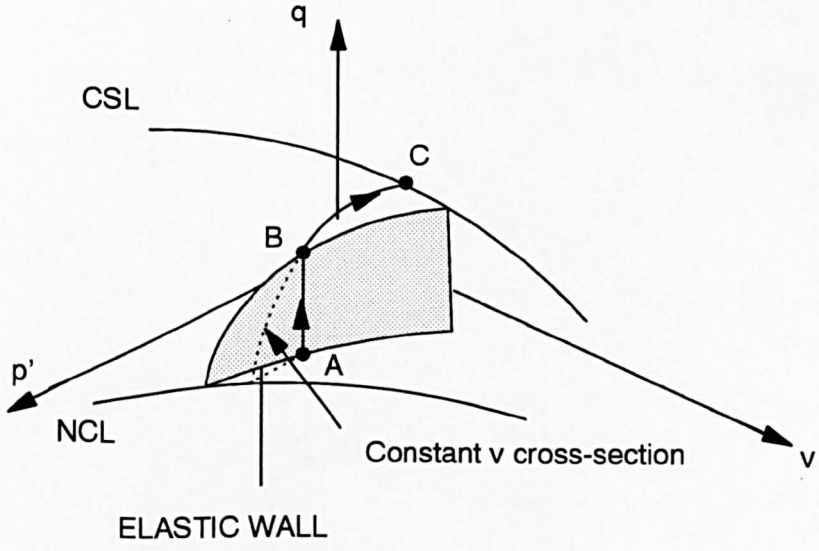

Fig (3.6) Elastic wall

CHAPTER 4

EXPERIMENTAL APPARATUS AND CALIBRATION TECHNIQUES

CHAPTER 4

EXPERIMENTAL APPARATUS AND CALIBRATION TECHNIQUES

The success of experimental research depends upon employing suitable equipment, adopting good instrumentation techniques and presenting the results in an appropriate way. Ideally the experimental system should consist of devices with good workability, durability and reliability of calibrations.

4.1 GENERAL LAY-OUT OF THE SYSTEMS

Two independent experimental systems were developed to conduct the testing programme. Fig 4.1 and Fig 4.2 show the lay-out of the two systems.

Each experimental system consisted of a double-walled triaxial cell, three pressure transducers, two volume change devices, a LVDT, a load cell and a compression frame.

The double-walled triaxial cell was used to measure the sample volume change. The design of the double-walled cell was originally developed at Oxford University by Wheeler

(1986) and the two cells used in the project were constructed for a previous project conducted at Queen's University of Belfast. The principle of the double-walled triaxial cell was the same as employed in the earlier cell developed by Bishop and Donald (1961) for the testing of unsaturated soil ie the sample volume change was measured by monitoring the flow of water into the surrounding cell.

The pressure transducers were used to measure the pore air pressure, pore water pressure and cell pressure. The first volume change device was used to measure the sample volume change by monitoring the flow of water in or out of the inner cell of the double-walled triaxial cell. The second volume change device was used to measure the flow of water draining from the sample. The LVDT was placed externally to the double-walled cell and used to measure the axial displacement of the sample during shearing. The load cell was used to measure the axial load that was applied to the sample.

An alternative method of measuring the sample volume change would have been to measure the axial and radial strains of the sample. This could have been done by using Hall effect transducers (Clayton and Khatrush, 1987), inclinometer gauges (Jardine, Symes and Burland, 1984), proximity transducers (Yung,1987) or LVDTs (Costa-Filho, 1985).

The reasons that internal measurements of axial and radial strains were not chosen were:

(a) Internal measurements of axial and radial strains would have provided accurate values of sample volume change at small strains but not at the large strains appropriate to critical states (which were of primary interest in the project) because of non-uniformity of the sample deformation

(b) The double-walled triaxial cells were already available in the department and , in the previous research of Wheeler (1986) and Sham (1989), had been shown to work very satisfactorily in the testing of unsaturated soils.

The two sets of experimental apparatus were almost identical except in the following arrangements:

(a) In System A the pore air pressure, pore water pressure and cell pressure were all automatically controlled by individual stepper motors, whereas in System B the pore air pressure and cell pressure were controlled by stepper motors but the pore water pressure was manually controlled by a regulator

(b) In System A each of the volume change devices consisted of a burette system connected to a

differential pressure transducer whereas in the System B Imperial College type volume change devices were employed.

The differences between the two sets of apparatus were the result of a need to save money in the second system. The lack of stepper motor control for the pore water pressure in System B meant that this system was less flexible than System A in the range of tests that could be conducted (see Chapter 6).

In Systems A and B the drainage and pressure connections were the same. The pore air pressure was applied to the top of the sample via a low air entry porous filter (less than 5 kPa air entry value). A flexible tube was used to connect the top of the sample with the regulated air pressure supply which was connected to an outlet in the cell base (see Figs 4.1 and 4.2). No attempt was made to measure the amount of air draining from the sample, because compression of air in the porous filter and connecting tube would have made this impossible.

The pore water pressure was applied or measured at the bottom of the sample. A high air entry filter (with an air entry value of 500 kPa) was used at the bottom of the sample to prevent air getting into the water drainage system. The suction in the sample was applied by means of elevating the pore air pressure at the top of the sample

and applying a lower (but still positive) pore water pressure at the base of the sample ie the axis translation technique was employed.

A Wykeham Farrance compression frame was used to give controlled axial displacement to the sample. Each frame had a capacity of 5 kN axial load and had facility to change manually the shearing speed from 0.0005 to 1.5 mm/min

There were a total of 7 transducers logged in each system. System A was logged via a PCL interface card and System B was logged via an IEEE card. Each transducer in the system was connected to an individual channel of the card.

The PCL card used in System A had an input range of 0-100 mV in 4 channels and 0-5 V in the other 4 channels. The output range of each pressure transducer was 0-100 mV, the output range of the LVDT and the load cell was 0-40 mV and the output range of each differential pressure transducer was 0-5 V. The output voltages of the differential pressure transducers and the pressure transducers were logged at the PCL card without amplification but the output voltages of the LVDT and the load cell were amplified to a range of 0-5 V by using individual external amplifiers (supplied by Fylde Electronics) before logging at the PCL card. The minimum resolution of the PCL card was 0.025% of the full range.

The IEEE card used in System B had a input range of 0-10 V in all channels. The output voltage of each pressure transducer was 0-100 mV, whereas the output voltages of the LVDT, load cell and Imperial College type volume change devices were 0-40mV. The output voltage of each transducer was amplified to 0-10 V by using individual external amplifiers (supplied by CIL electronics). The minimum resolution was 0.012% of full range for each channel.

4.2 VOLUME CHANGE MEASUREMENTS

The volume change of the sample was measured by monitoring the flow of water in or out of the inner cell with the first volume change device. The volume of water draining from the sample was measured by using the second volume change device on the drainage line leading from the base of the sample (see Fig (4.1) and Fig (4.2)). Automatic volume change devices were selected because each test lasted several weeks and also because the proposed testing programme involved the use of an automatic feedback system requiring an electrical read-out of volume change (see Chapter 6). In System A each volume change device consisted of a burette system connected to differential pressure transducer whereas in System B the volume change devices were of the Imperial College type.

4.2.1 Burette with differential pressure transducer

Fig (4.3) shows the details of the burette and differential pressure transducer type of volume change device used in System A . The volume change devices were made in the Department of Civil and Structural Engineering at Sheffield University. A glass burette was sealed inside an acrylic outer cylinder which allowed a back pressure to be applied to the system. The outer cylinder was partially filled with water to provide a reference pressure for the differential pressure transducer. The high pressure terminal of the differential pressure transducer was connected to the base of the burette while the low pressure terminal was connected to the base of the outer cylinder. The operational principle of the volume change units was that movement of the water column in the burette was detected by measuring the differential pressure between the base of the burette and the base of the outer cylinder (Pradhan, Tatsuoka and Molenkamp, 1986).

Thin layers of paraffin were floated on the water surfaces in the burette and the outer cylinder to avoid rapid evaporation of water. The paraffin also slowed down the rate of air diffusion into the water. The paraffin evaporated at a very slow rate compared to water and the evaporation did not significantly affect the differential pressure between the base of the burette and the outer cylinder, because the rate of evaporation was similar in

the burette and the outer cylinder.

The burette within each volume change device had a cross-sectional area of 1.75 cm^2 giving a capacity of 35 cm^3 for a 20 cm height of burette. A 20 cm column of water in the burette gave a differential pressure of approximately 2 kPa at the base of the burette. The differential pressure transducers were supplied by Sandhorst Scientific Ltd, U.K. The maximum range of the differential pressure transducers was 2 kPa and overall accuracy was 0.07% of the full scale. The line pressure on the transducer could go up to 2000 kPa.

Several practical problems were encountered in using the burette system in conjunction with differential pressure transducers:

(a) The water used in the burette tended to stick to the glass burette during movement of the water column in the burette. This problem was reduced by polishing the glass burette with car polish.

(b) The meniscus at the paraffin-water interface changed shape during the flow of water in or out of the burette. It was noticed that when water flowed into the burette the meniscus at the paraffin-water interface was convex upward whereas when the water flow out of the burette the meniscus shape changed

to convex downward. As the paraffin and the water were of different densities the changes in meniscus shape would cause an error of approximately 0.15 cm^3 in apparent volume. To solve this problem various fluids with approximately the same density as water (eg silicon oil and silicon fluid) were tried instead of paraffin. These alternative fluids gave even more problems than paraffin. Therefore paraffin was retained, but the errors due to changes of meniscus curvature were kept to a minimum by using the burette with flow in one direction only during each stage of a test. This meant that the probable direction of flow of water in the burette had to be predicted before commencing each stage of a test, so that the meniscus could be set up with the correct curvature prior to starting.

(c) Initially the high pressure terminal of the differential pressure transducer was connected to the fine bore tube carrying flow to the burette (Fig 4.3a). This meant that the reading of the transducer was affected by any pressure drop resulting from flow of water along the short length of connecting tube (Lade, 1988). To avoid this problem the high pressure terminal of the transducer was directly connected to the base of the burette (Fig 4.3). In this arrangement there was no head loss because there was no flow in the tube

connecting the transducer with the volume change device.

More teething problems were encountered during calibration of the volume change devices. Firstly, the output of one of the differential pressure transducers was found to be unstable. This instability was found to be due to a fault with the particular transducer, which was later rectified by the supplier. Secondly, the meniscus at the paraffin-water interface was found to change shape even with the flow maintained in only one direction. The variation in the shape of the meniscus was found to be dependent on the level of the water column in the burette. After setting the initial shape of the meniscus by applying a small flow in the required direction prior to use, the shape of the meniscus remained flat during flow into the burette until the water column reached a particular level, corresponding to a burette reading of approximately 30 cm^3. The shape of the meniscus then changed gradually to convex upwards. Although the reason for this pattern of behaviour was unclear, it was found to be entirely repeatable. The changes in meniscus shape during outward flow were minimal. Due to this difficulty, each volume change device was calibrated over a range of approximately 30 cm^3 (rather than the full range of 35 cm^3).

The calibration of each volume change unit was conducted by sending known amounts of water from a 10 cm^3 graduated

burette into the burette of the volume change unit and monitoring the output voltage of the differential pressure transducer. Fig (4.4) shows the lay-out of the calibration system. The same line pressure was applied to the 10 cm^3 graduated burette and the volume change device during calibration, with the flow between the two generated by a slight difference of level. Two air-water interfaces were used in the calibration, the higher one to supply water to the 10cm^3 burette and the lower one to drain water from the 10 cm^3 burette in order to set the meniscus in the 10 cm^3 burette at a precise level before sending water to the volume change unit. Before the calibration the differential pressure transducer and the connecting tubes were flushed with de-aired water to make sure there was no air trapped inside the system.

The first calibration was conducted at a line pressure of 200 kPa. Regression analysis showed that the output voltage of the differential pressure transducer could be linearly related to the amount of water that was sent into the volume change unit. Later it was found that the calibration factor of the differential pressure transducer was influenced by the line pressure. Therefore more calibrations were conducted at various values of line pressure. Fig(4.5a) and Fig(4.5b) show the changes in calibration factor with line pressure for each volume change device. A second order polynomial equation was used to relate the calibration factor to the line pressure.

The general form of linear calibration was therefore as follows:

$$V=\frac{x}{CF} \qquad (4.1)$$

$$CF=ap^2+bp+c \qquad (4.2)$$

Where V was the total volume of water in the volume change device, x was the output voltage, CF was the calibration factor at a given pressure and, a, b, and c were constants for each volume change device. Table 4.1 shows the relevant eqations and constants for the calibration of the differential pressure transducers.

An intercept of zero was used in Equation 4.1, because it was found that when the calibration curves were extrapolated to an output voltage of zero there was no influence of line pressure. This was demonstrated by holding a constant volume of water in the cell volume change unit and then increasing the line pressure from 0 to 600 kPa in steps of 100 kPa. The procedure was repeated with the water column in the volume change unit at 3 or 4 different levels, as shown in Fig 4.6. In each case the output voltage was noted and the change in output voltage due to the increase in line pressure was then calculated. By extrapolating from the results it was found that the output voltage would be independent of line pressure at an output voltage of zero (Fig 4.6).

Within the relevant operating range for each volume change

unit, the overall accuracy achieved was estimated to be ±0.10 cm^3.

4.2.2 Imperial College type volume change unit

The Imperial College type volume change device has been successfully used by many previous researchers. The operational principle of the device is that any volume flow in or out of a cylinder is detected by measuring the movement of a piston in the cylinder (Fig 4.7). The movement of the piston was monitored by a LVDT mounted on the cylinder.

There were some disadvantages of using the Imperial College type device:

(a) De-airation of the device was uncertain, because any air trapped inside the unit could not be seen. Air trapped inside the system was eliminated by flushing with freshly de-aired water and then pressuring the system for at least one day in order force any trapped air into solution. This procedure was repeated each time before starting any test.

(b) The weight of the piston and friction on the rolling diaphragm seal caused a pressure difference across the device. This was a particular problem when the direction of flow changed. It was found

that the changes in pressure caused by these effects were up to 4 kPa. To eliminate this error the pressures were adjusted whenever the direction of the flow in the volume change device was changed.

(c) The Imperial College type device did not work perfectly at zero pressure, because a small amount of pressure was required to keep the rolling diaphragms in the correct position. This meant that it was difficult to use the Imperial College type device in conjunction with the double-walled triaxial cell because it was necessary to start a test in the double-walled triaxial cell from zero pressure (see Chapter 6). To avoid this difficulty the output voltage of the volume change device was taken at a pressure of 25 kPa before opening the valve to the inner cell (ie, cell pressure was still zero). Then the pressure on the volume change unit was reduced to zero and the valves to the inner cell and outer cell were opened. After that the cell pressure was increased to the required value for the first stage of the test.

The calibration of the Imperial College type volume change devices was conducted in the same way as for the burette and differential pressure transducer type devices. The output voltage of the unit was linearly related to the amount of water that was transferred to the unit from a 10

cm^3 burette. Calibration was conducted at various line pressures and the calibration factor was found to be independent of the line pressure. The precision of the calibration was estimated to be $\pm 0.06 cm^3$ over the working range of 40 cm^3.

4.3 DOUBLE-WALLED TRIAXIAL CELL

The double-walled triaxial cells used in the research project were made at the Queen's University of Belfast, for triaxial testing of soils containing large discrete gas bubbles (Sham,1989). The original design was based on a sample diameter of 38 mm and slight modifications were made for this project in order to accommodate 50 mm diameter samples.

A detailed view of the double-walled triaxial cell is shown in Fig (4.8). The purpose of the double-walled construction was to prevent (or reduce) volume changes of the inner cell, by applying equal pressures to the inner and outer cells, so allowing the sample volume change to be measured by monitoring the flow of water in or out of the inner cell. The pressure to the inner cell was applied through the cell volume change unit while the pressure to the outer cell was applied through an air-water interface. An acrylic cylinder with fibreglass reinforcing bands was was used in order to increase the stiffness of the inner cell wall, because Wheeler (1986) had found that the

application of a step increase in pressure to a double-walled cell with a flexible inner cell could result in significant volume change of the inner cell (because of slight time delay between pressure application to the inner and outer cells and the hysteretic properties of acrylic).

The loading ram had a full stroke length of 70 mm. A rolling diaphragm seal around the loading ram prevented water leaking from the inner cell. The loading ram moved within two linear bearings held within a loading cylinder and these linear bearings reduced ram friction. The axial load was measured externally, on the assumption that any variation of ram friction was negligible. Unfortunately damage sometimes occurred to the linear bearings and the loading ram due to corrosion and this caused significant variation of ram friction. This was noted three times in the research programme and in each case the linear bearings were replaced and the loading ram was polished (see Chapter 7). In retrospect, use of an internal load cell for measurement of axial load would have avoided these problems.

4.3.1 Calibration for apparent volume change of cell

To enable the double-walled cell to be used to measure the sample volume change, it had to be calibrated for apparent volume change due to cell pressure application and ram displacement during shearing. Much of the volume change due

to pressure application was caused by slight flexure of the top plate of the inner cell (which was not completely surrounded by the outer cell), expansion of the connecting tubes and valves and compression of the water within the cell. Additional small volume changes took place with time due to absorption of water by the acrylic wall of the inner cell. Previous investigation (Wheeler, 1986) suggested that a period of about 9 months was required before the acrylic cell wall became saturated at a given pressure. If the cell pressure was changed, the process was repeated and it would take another 9 months to stabilise again. This rate of water absorption by the acrylic could be kept to a minimum by keeping the inner cell under water whenever the cell was not in use.

The double-walled cells were calibrated for the apparent volume change due to compression of the water, expansion of the connecting tubes, slight flexure of the top plate and the water absorption by the acrylic inner wall of the cell. Before the calibration various drainage connections in the cell base were flushed with freshly de-aired water to remove any trapped air. Then, to assemble the cell, a collar system was temporarily fixed to the base of the cell in order to perform the assembling of the inner cell under water (Photo 4.2). This assembly under water was necessary to ensure complete de-airing of the convolution of the rolling diaphragm. While the collar was filling with de-aired water, the top plate and loading cylinder assembly

was turned upside down and the convolution of the rolling diaphragm was filled with de-aired water using a small flexible tube connected to a syringe to displace any air trapped within the convolution (Photo 4.3). During this procedure a vacuum line was connected to the upper part of the loading cylinder (behind the rolling diaphragm) in order to keep the diaphragm properly inflated until the cell was assembled and cell pressure was applied. The loading ram was also clamped in position within the top plate assembly until the cell pressure was applied. The top plate and loading cylinder assembly (still held upside down) was brought into the collar system filled with water. Then the top plate was inverted under water and located in position on the inner cell wall. The valve to the inner cell was temporarily connected to a flexible water-filled tube, the other end of which was kept at an elevated position (above the level of the water in the collar). The valve to the inner cell was left opened until the three tie-bars used to enclose the inner cell were tightened. A spacer bar was used to check that all three tie-bars were tightened to equal displacement (otherwise the loading ram might not be aligned). Finally the collar system was removed from the base and the outer cell was assembled and filled with water in the usual way.

The calibration for apparent volume change of the inner cell was conducted by connecting the inner cell and the outer cell to a compressed air supply via an air-water

interface and a volume change unit. The cell pressure was then increased from 0 to 600 kPa in intervals of 200 kPa. Each pressure increment was maintained for at least 48 hours. The same procedure was repeated when the pressure was decreased from 600 kPa to zero in decrements of 200 kPa. Three complete calibration trials were conducted with the double-walled triaxial cell of System A during the 24 months of operation, whereas two trials were conducted with System B (which was in operation for only 14 months). In System B the cell was not calibrated at zero pressure, because the Imperial College type volume change unit could not work correctly at zero pressure (see Section 4.2.2).

Fig 4.9a and Fig 4.9b show the variation of apparent volume change with time for the cell in System A after a pressure increment from 200 to 400 kPa and for the cell in System B after a pressure increment from 400 to 600 kPa respectively. The total volume change was divided into: (1) "immediate" volume change due to the change of cell pressure, (2) a linear increase in volume change with time due to water absorption by the acrylic cell wall and (3) a cyclic volume change due to temperature fluctuation. The volume change due to temperature variation followed a cyclic variation with a period of 24 hours. The magnitude of this volume change due to temperature variation was approximately $\pm 0.03 cm^3$. This corresponded to temperature variation in the room of $\pm$ 0.5°C.

When the cyclic volume change due to temperature variation was eliminated from Fig(4.9a) and Fig(4.9b) the resulting steady volume change with time gave the rate of water absorption by the acrylic wall. This rate of absorption by the acrylic cell was dependent upon cell pressure. The average rate of absorption is plotted against cell pressure for two typical calibration trials in Fig(4.10a) and Fig(4.10b). The figure indicates that the water content of the acrylic was in equilibrium (zero rate of water absorption) with a water pressure of about 100 to 200 kPa in both Systems A and B.

Fig (4.11a) and Fig (4.11b) show the "immediate" volume changes of the cell during the application of cell pressure from zero to 600 kPa and then from 600 kPa to zero for Systems A and B respectively (in System B the pressure was not brought back to zero because of the use of the Imperial College type volume change unit). In both systems the volume change from 200 to 600 kPa was fairly linear and also reversible and repeatable. However a proportionaly greater volume change occurred with a pressure change from zero to 200 kPa, and this volume change was less reversible and repeatable. This irrecoverable volume change could have been due to slight slackness of the connectors and valves, and the possibility of trapped air in the systems. The calibration for "immediate" volume change of the cell due to the pressure application was in the form of a second order polynomial equation relating volume change to cell

pressure (see Fig 4.11). Table (4.1) shows the relevant equations and the constants for each calibration.

A further check was made to examine the influence of the cell pressure in the flexible air supply line providing the pore air pressure to the top of the sample. Various pressure differences were applied between the inner cell and the air supply line. The maximum volume change observed on the cell volume change unit was less than $0.03cm^3$. This volume change was considered to be insignificant and no calibration for the effect was included.

4.3.2 Calibration for movement of the loading ram

Some of the water in the inner cell was displaced from the inner cell during movement of the loading ram. The amount of water displaced from the inner cell by a given movement of the ram was dependent on the effective area of the loading ram.

To calibrate for the apparent volume change due to ram movement the cell was assembled in the usual way as explained in Section 4.3.1 The cell pressure was increased to the required value and the system allowed to stabilise for 24 hours. Controlled amounts of axial displacement were then applied to the loading ram and the volume of water displaced from the inner cell was measured. Many trials were conducted at various values of cell pressure and

these indicated linear, repeatable calibrations and no influence of cell pressure on the calibration factor for each cell.

The effective area of the loading ram was calculated to be 13.925 cm^2 for System A and 13.725 cm^2 for System B. The precision in the value of the effective area was approximately ±0.02 cm^2 for both cells. These corresponded to a precision in the volume change of ±0.07 cm^3 for a loading ram displacement of 35 mm (typical displacement for the triaxial shear tests described in Chapter 6).

4.3.3 Calibration for volume change of water drainage line

The changes of volume of water within the soil sample were measured by connecting the drainage line from the base of the sample to the second volume change unit. If the back pressure on the water drainage line changed during the test then the measured water volume change had to be corrected for the effect of expansion of the connecting tube and the connectors.

Fig(4.12) shows the calibrations for the volume change of the water drainage line with water back pressure for Systems A and B. The volume change appeared to be repeatable and recoverable to precision of ± 0.02 cm^3.

4.4 PRESSURE TRANSDUCERS

Diaphragm type pressure transducers were used to measure the cell pressure, the pore water pressure and the pore air pressure. The range of each pressure transducer was 0-700 kPa.

The pressure transducers were calibrated against a dead weight tester. Three trials were conducted with each pressure transducer. The output voltage of each transducer was linearly related to the applied pressure. The transducers showed negligible hysteresis and a linear calibration with an estimated precision of ± 0.5kPa.

A slight problem was noted with the cell pressure transducer in System A. The transducer showed significant drift (0-1.5 kPa) each time the transducer was de-pressurised after having been used for a test lasting 4-6 weeks. Initially this problem was thought to be due to a fault with the particular pressure transducer, but later it was found to be due to drift of the relevant channel of the logging system. At the start of each test this drift was adjusted by changing the zero shift of the pressure transducer. The gradient of the pressure transducer calibration remained unchanged and each time the transducer was checked against another pressure transducer before commencing any test.

4.5 LOAD CELL

In each system the axial load was measured by a load cell fitted external to the cell (there was insufficient space within the inner cell to use an internal load cell and the ram friction was considered to be relatively constant because of the use of the linear bearings). The capacity of each load cell was 5 kN.

The load cells were calibrated against the dead weight tester. The output voltage of each load cell was linearly related to the applied load. The calibration showed negligible hysteresis and an overall precision of ± 1.0 N, corresponding to a precision of ± 0.5 kPa in the deviator stress on a 50 mm diameter sample.

4.6 LVDT

The axial displacement of the loading ram was measured by an LVDT, with a range of 50 mm, fixed externally to the cell.

The LVDT was calibrated against a digital vernier. The precision of the digital vernier was 0.0001mm. The output voltage of the LVDT was linearly related to applied axial displacement. Three trials were conducted with each LVDT, showing excellent repeatability. The overall precision was ± 0.02mm for both LVDTs.

4.7 PRESSURE CONTROL

The pressure to Systems A and B was supplied by an air compressor with a maximum capacity of 1000 kPa. For each system, three regulators were used to reduce the pressure to the required levels for supplying cell pressure, pore air pressure and pore water pressure. In System A all three regulators were controlled by stepper motors, whereas in System B two were controlled by stepper motors and the final regulator (for pore water pressure) was manually controlled.

The regulators and stepper motors were supplied by Watson and Smith. The maximum capacity of the regulators was about 700 kPa. The total number of steps in the stepper motors was about 1600 and each step was equivalent to approximately 0.42 kPa. The stepper motors could be controlled either manually or by a computerised control system. A slight disadvantage of the stepper motors was slight "backlash" when the direction of pressure change was reversed. This was particularly noticeable when the stepper motor was under computer control.

To provide the cell pressure and pore water pressure, the air pressure was converted to water pressure by using a bladder type air-water interface. Bladder type air-water interfaces were used to avoid dissolution of air within the pressurised water system. This was particularly important

where the water was used to flush diffused air from beneath the high air entry filter (see Section 4.11.5) or to fill the volume change devices.

4.8 TEMPERATURE CONTROL

The temperature of all transducers had to be kept within the range specified by the manufacturers. Further, when using the double-walled cell to measure sample volume change it was very important to minimise any temperature fluctuations. Two temperature control units were installed in the research laboratory. The temperature variation was approximately ± 0.5°C, producing an apparent volume change of the double-walled cell of ± 0.03 cm^3 (see Sec 4.3.1).

4.9 RELIABILITY AND ACCURACY OF THE CALIBRATIONS

The long-term precision of each transducer was dependent on the precision achieved during each calibration and also any changes of calibration with time. To check for any variation of the calibrations of the various devices with time, each system was re-calibrated every year.

System A was calibrated three times during the testing programme. With the exception of the cell pressure transducer and the volume change device measuring water volume change, the calibration factors of all transducers remained unchanged (within the specified precision) during

the whole period. The drift of the logging channel for the cell pressure transducer has been described in Section 4.4. The calibration factor of the differential pressure transducer in the volume change device measuring water volume change shifted slightly during the period of 12 months between the two calibrations. The magnitude of the shift corresponded to an error of approximately ±0.15 cm^3 at full scale. The calibration factors were updated each time after full calibration.

System B was calibrated twice during a testing period of 12 months (at the beginning and end of the testing programme). The calibration factors of the pressure transducers and the load cell showed slight changes. However a significant change was noted in the calibration factor for the Imperial College type volume change units and the LVDT. The shift in the calibration factors caused errors of approximately ± 0.2 cm^3 at full scale for both Imperial College type volume change units and ± 0.15 mm at full scale for the LVDT.

The double-walled cells also were re-calibrated periodically to estimate the changes in the cell calibrations with time. Fig 4.13a shows the changes in the rate of absorption with time for the double-walled triaxial cell in System A. Apparently the rate of absorption at a cell pressure of 200 kPa decreased slightly between August 1989 and January 1992 (suggesting an increase in the water

content of the acrylic) whereas the rate of absorption at a cell pressure of 600 kPa showed an increase over the same period (suggesting a decrease in the water content of the acrylic). Therefore these changes in the rate of absorption over the period of testing could be simply a reflection of the precision of the estimation of the rate of absorption. The possible error caused by these apparent changes in the rate of absorption were aproximately ± 0.18 cm^3 over a period of one month (the typical period of a single test).

Fig 4.14a shows the "immediate" volume change of the cell during the application of cell pressure from zero to 600 kPa for three calibrations conducted with System A during the testing period of two years. The calibrations had changed approximately ± 0.12 cm^3 over the period.

The double-walled triaxial cell in System B was calibrated twice during the testing programme. Fig 4.13b shows the rate of absorption calculated at beginning and end of the testing programme. The changes in the rate of absorption could cause a the similar error to that calculated for for the cell in System A ie, approximately ± 0.18 cm^3 over the period of a single test with average time of one month. Fig (4.14b) shows the "immediate" volume change of the cell during the application of cell pressure from zero to 600 kPa at the beginning and end of the testing programme. The calibrations changed by approximately ± 0.20 cm^3 over the testing period with System B.

The overall accuracy of the sample volume change measurement was the cumulative accuracy of the volume change unit connected to the inner cell, the calibration for ram displacement, the accuracy of the ram displacement measurement, the calibration for "immediate" volume change of the inner cell with pressure and the rate of water absorption by the acrylic. In System A the overall accuracy of the sample volume change measurement was calculated as ± 0.60 cm^3 whereas an overall accuracy of ± 1.02 cm^3 was calculated for the sample volume change in system B. The maximum error of 1.02 cm^3 in System B was equivalent to approximately ± 0.011 in specific volume (the solids volume in each sample was approximately 90 cm^3).

The overall accuracy of the water volume change measurement was the sum of the errors in the calibration of water volume change unit and the variation in the calibration factor over the period of testing. The maximum overall error in the water volume change measurements was calculated to be approximately ± 0.12 cm^3 , which is equivalent to approximately ± 0.09% in water content.

4.10 TOP COLLAR

During setting up and subsequent consolidation of the soil sample it was unlikely that the sample would remain exactly vertical. Even a small amount of tilt would cause a bedding error during the shear stage of a test. To avoid this

problem, a specially designed collar was attached to the end of the loading ram (see Fig 4.15) to maintain sample alignment during consolidation. The internal diameter of the collar was approximately 0.5 mm greater than the diameter of the top cap placed on top of the sample. The loading ram was brought to just above the sample immediately after assembly of the cell, with the top cap locating within the alignment collar to ensure that the sample remained vertical during consolidation. The bedding error was successfully reduced by this arrangement. A cut-out was provided in the top collar for connection of the flexible tube carrying the pore air pressure supply to a fitting in the top cap.

4.11 FILTER ARRANGEMENTS

The suction u_a-u_w within the sample was maintained by applying elevated pore air pressure u_a at the top of the sample and measuring or applying a lower value of pore water pressure u_w at the bottom of the sample.

4.11.1 Low air entry filter

Pore air pressure was applied to the top of the sample via a low air entry porous filter with an air entry value of less than 5 kPa. The filter was cleaned (with an ultra-sonic cleaner) and dried before placing on the sample in each test.

4.11.2 High air entry filter

A high air entry filter was used to prevent air from the unsaturated sample entering the water drainage system. The filter used for this purpose was required to have the following characteristics (Bishop 1960):

(1) Adequate mechanical strength to support direct axial load when the sample was loaded.

(2) A high air entry value and uniform pore size. The smaller the pore size the higher the air entry value. Only if the air entry filter was fully saturated would it sustain the specified suction.

(3) High permeability. The rate of consolidation was dependent on the permeability of the soil. If the permeability of the high air entry filter was less than that of soil then the rate of consolidation was also significantly dependent on the permeability of the high air entry filter.

The high air entry filters used in Systems A and B were supplied by Soilmoisture Equipment Corp. Ltd (U.S.A). The filters were available with various air entry values, and filters with an air entry value of 500 kPa were selected. A disc of filter material, 30 mm in diameter and 8 mm thick, was cut from a larger sheet. This filter disc was

glued within an acrylic annulus having 31mm internal diameter, 50 mm external diameter and 8mm thickness. Araldite was used to glue the filter within the acrylic annulus. The surface was polished with ceramic cloth to give a smooth surface on either side. The filter disc and acrylic annulus arrangement was placed on top of the 50 mm diameter pedestal on the triaxial base and fixed with 4 screws located through the acrylic annulus. An "O" ring was placed between the pedestal and the acrylic annulus to avoid any leakage of cell fluid into the water drainage line. A circular groove was made on the top of the pedestal to flush any diffused air from beneath the filter.

Although the above filter arrangement worked satisfactorily there was slight uncertainty over whether the low permeability of the filter was slowing down the rate of consolidation. This uncertainty was accentuated by the fact that only a small percentage of the area of the lower surface of the filter was in contact with the circular groove leading to the drainage line (suggesting a very constricted flow pattern through the filter). To reduce this problem the filter arrangement was altered by placing a low air entry filter disc (air entry value less than 5kPa) with a thickness of 3 mm underneath the high air entry filter with a thickness of 6 mm (Fig 4.16). The thickness of the combined filter arrangement was 9 mm. A significant difference in the flow rate through the filter was observed between the two types of filter arrangement.

The combined filter arrangement showed a significant increase in the rate of consolidation compared to the single filter arrangement.

4.11.3. Saturation of filter

Complete saturation of the high air entry filter was necessary to achieve the specified air entry value. If the filter was not de-aired properly then the air would blow through the filter and get into the water drainage system.

The filter was de-aired by mounting the complete filter and pedestal arrangement on the base of a standard triaxial cell which was then filled with water and an elevated cell pressure was applied to force the air into solution. The double-walled cell was not used for this de-airing procedure, which took place while the previous test was still in progress in order to minimise the turn-round time between tests.

For the de-airing process the filter and pedestal arrangement was fixed to the base of the de-airing cell. The drainage line through the pedestal was flushed with freshly de-aired water. Then the cell was connected to a bladder type air/water interface to supply cell pressure to the de-airing cell. The cell pressure was increased to 600 kPa and left for two days with the valve on the drainage line closed. The drainage line valve was then

opened and water was allowed to drain through the high air entry filter for one day at a cell pressure of 600 kPa. The drainage line valve was closed and the system was left for another day at a pressure of 600 kPa. Then the cell pressure supply valve was closed and the drainage valve was opened, producing a gradual reduction of cell pressure. The full procedure was repeated within 2-3 days after changing the water in the cell and in the air/water interface.

The filter was re-saturated after each test. If the filter was kept under water after each test then it was sufficient to re-saturate the filter in 2-3 days. 4 spare pedestals were made to supply de-aired filters continuously and so avoid any gaps between tests.

Although the air entry value was specified by the manufacturer, the value was checked before using the filter. Air pressure was applied to the top of a saturated filter while the bottom was connected to the water volume change device. The double-walled cell was used for this purpose (with pressurised water in the outer cell) because of the danger of applying elevated air pressure to a single-walled cell. 350 kPa air pressure was applied to the top of the filter while 50 kPa water pressure was applied to the bottom of the filter, giving $u_a - u_w$ = 300 kPa. The water volume change was monitored for two days. Fig(4.17) shows the measured water volume change plotted

against time. Water flowed into the inner cell at a rate of about 0.05cm^3/day. This was probably due to water evaporation from the top surface of the filter. The air pressure was then increased to 450 kPa and subsequently to 500 kPa (u_a-u_w = 400 kPa and 450 kPa respectively) and no change in the water flow was observed. When the air pressure was increased to 550 kPa (u_a-u_w = 500 kPa) the air started to blow through the filter. This indicated that the filter had an air entry value of approximately 500 kPa (as specified by the manufacturer).

4.11.4 Fuse wire technique

There was a danger that the high air entry filter could de-saturate in the early stage of a test due to two possible causes. Firstly, if the filter were left exposed to the atmosphere for a significant time , there was a possibility of it drying out slightly. To avoid this problem a small amount of water was left on top of the filter during the setting up process and delays in the setting up process were kept to minimum. Secondly, de-saturation of the filter could occur once the sample was mounted on the filter, because there was a large value of negative pore water pressure in the unsaturated sample immediately after compaction and prior to application of the cell pressure. Direct contact between the sample and the filter at this stage could therefore result in cavitation of the water within the filter and the drainage line. This problem is

more serious with clay soils where the suction is normally high. To avoid this problem, two short length of fuse wire with a diameter of 0.36mm were placed between the sample and the filter. The wire was made into two semi-circles to allow easy expulsion of any water or air trapped between the filter and the sample. The fuse wire intruded into the sample when the cell pressure was applied, thus providing a direct contact between the filter and the sample. An estimate showed that a cell pressure of about 35 kPa was needed to push the wire into the sample.

The fuse wire arrangement was important when using the double-walled cell because assembling of the cell took about 2-3 hours. In a trial test conducted without fuse wire the pressure recorded by the pore water pressure transducer dropped to -100 kPa suggesting a serious danger of cavitation within the porous filter or the drainage line. When the fuse wire was employed the minimum pressure recorded by the pore water pressure transducer during setting up of the sample was -1 to -4 kPa.

Although the fuse wire arrangement avoided negative pressures in the drainage system during the assembling time, there were two practical difficulties in employing this method:

(1) Intrusion of the fuse wire into the sample resulted in an error in the measurement of sample

volume change during the first application of cell pressure. The volume displaced was estimated as $0.7cm^3$ (based on a fuse wire thickness of 0.36 mm and a sample area of 19.6 cm^2) and a correction of this magnitude was applied in all tests.

(2) The cell pressure required to make the contact was approximately 35 kPa. In one trial test the difference between the cell pressure and the pore air pressure was just under 35 kPa and no flow of water occurred until the pressure difference was raised above 35 kPa.

4.11.5 Flushing system

Although a high air entry filter was used to prevent air flowing into the water drainage system, air still diffused through the filter from the unsaturated soil sample in solution within the water (Fredlund, 1975). The diffused air then came out of the solution and collected underneath the filter. This affected the measurement of water volume change and possibly also the measurement of pore water pressure at the base of the sample (Nageswaran, 1983). The diffused air was periodically flushed from the base of the filter to eliminate the error. The flushed air was collected in an inverted 10 cm^3 burette (Fig 4.18), which meant that the volume of flushed air could be measured, Fredlund (1975).

The flushing was conducted by sending a flow of water from one air/water interface through the flushing groove in the pedestal to another air/water interface (within which was the inverted 10 cm^3 burette). The flushing flow was generated by a slight difference in level between the two air/water interfaces. A 4-way valve was used to reverse the direction of the flushing, which helped to flush air bubbles that tended to stick to the surface of the drainage line.

Flushing was conducted at the end of each stage of every test (see Chapter 6). After most stages no air was collected in the flushing system, which showed that no air diffused into the system during the test.

4.12 LOGGING AND CONTROL SYSTEM

Logging and control programs were written in Quick Basic for data acquisition and for control of the stepper motors to provide specified stress paths. These programs were written by Mr.Tim Robinson, electronics technician in the Department of Civil and Structural Engineering at Sheffield University, and they are described in Chapter 6.

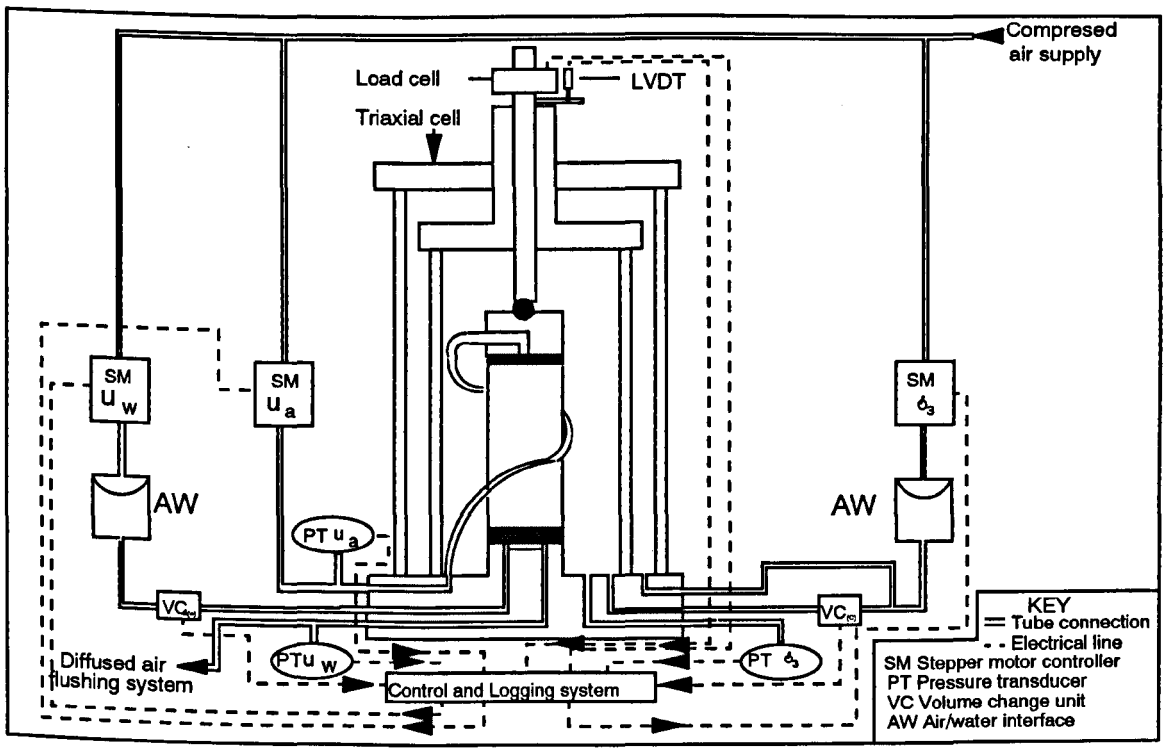

Fig (4.1) Experimental Apparatus (System A)

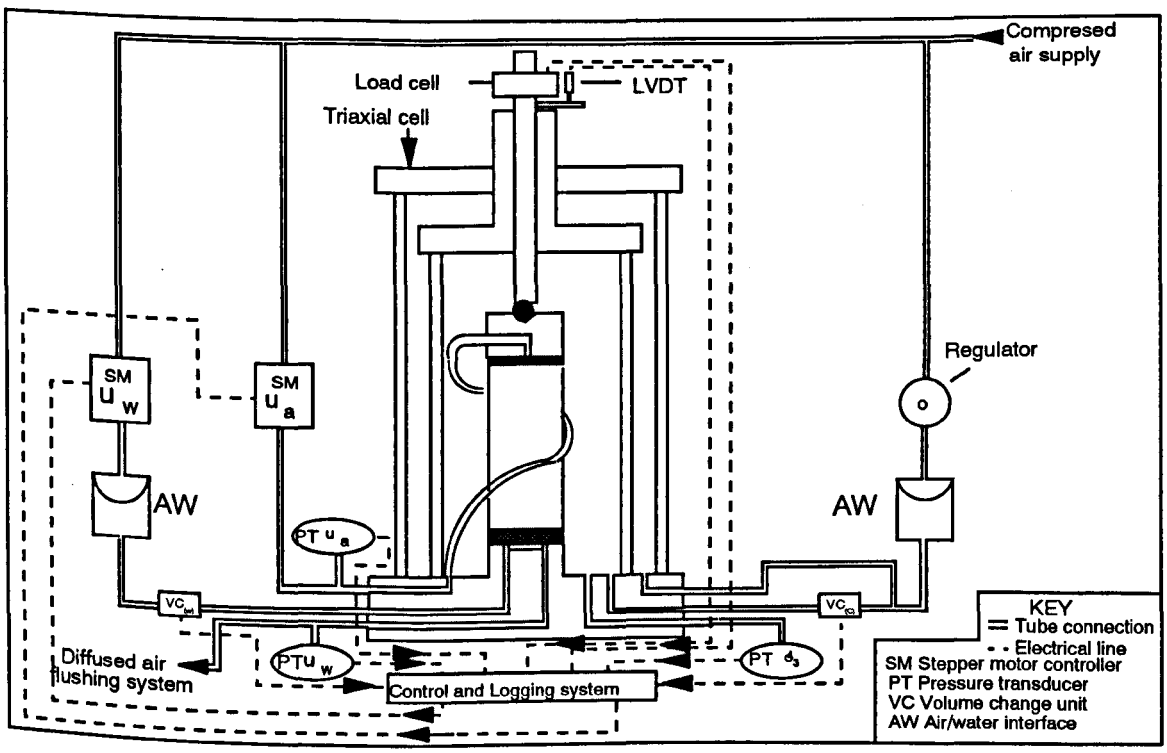

Fig (4.2) Experimental Apparatus (System B)

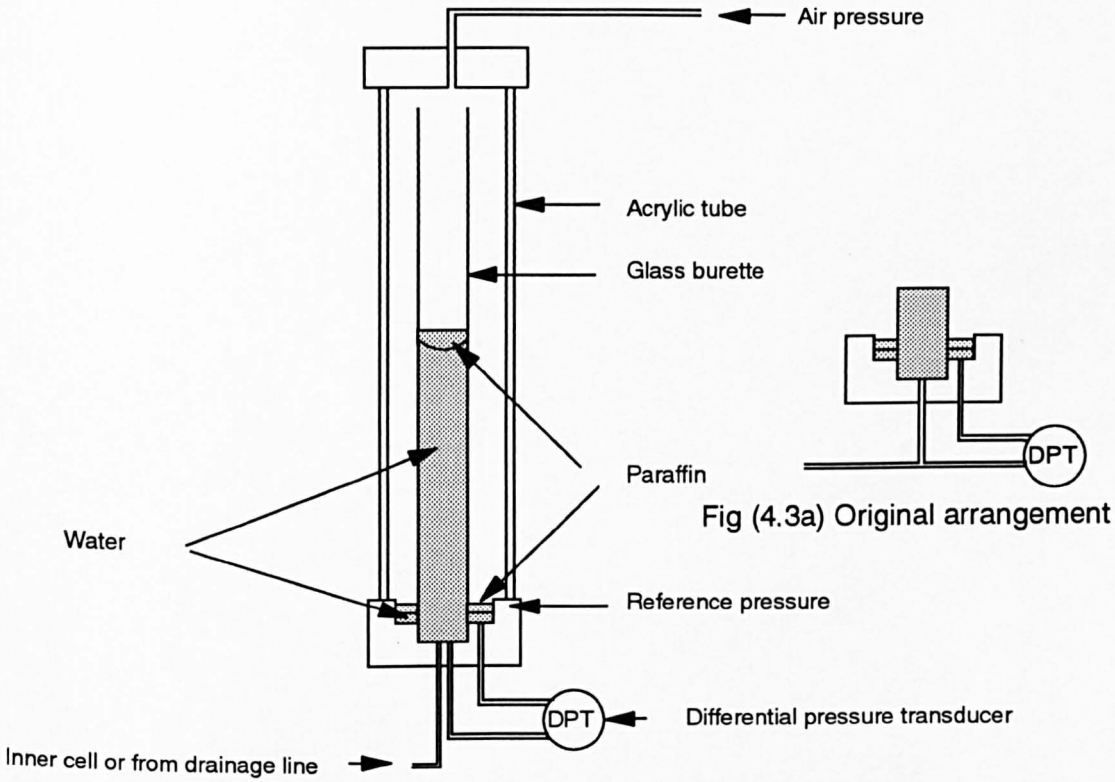

Fig (4.3a) Original arrangement

Fig (4.3) Volume change device

(Burette with differential pressure transducer)

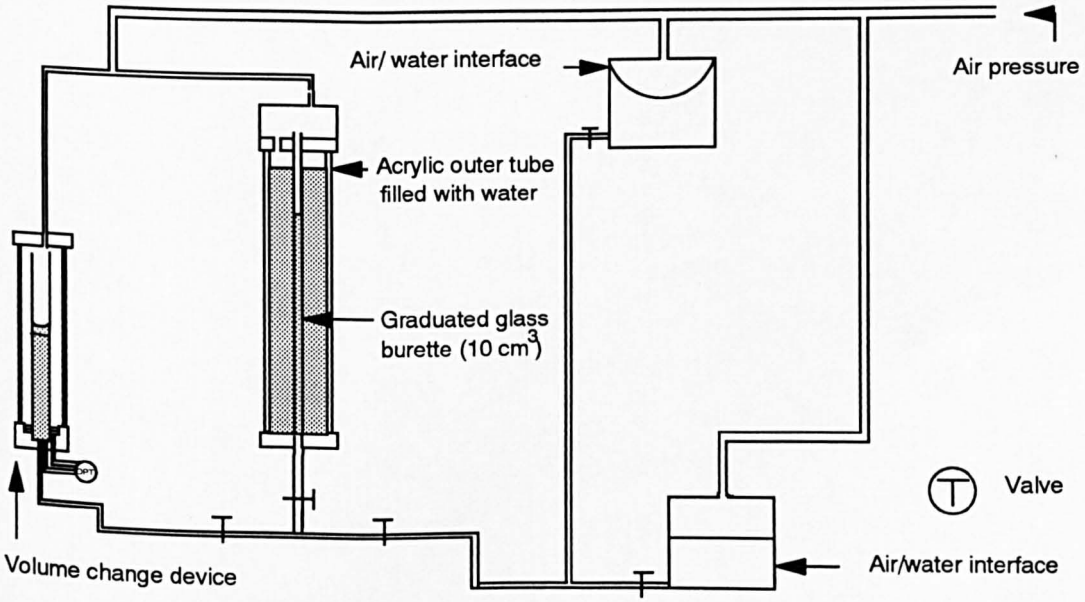

Fig (4.4) Calibration system for volume change devices

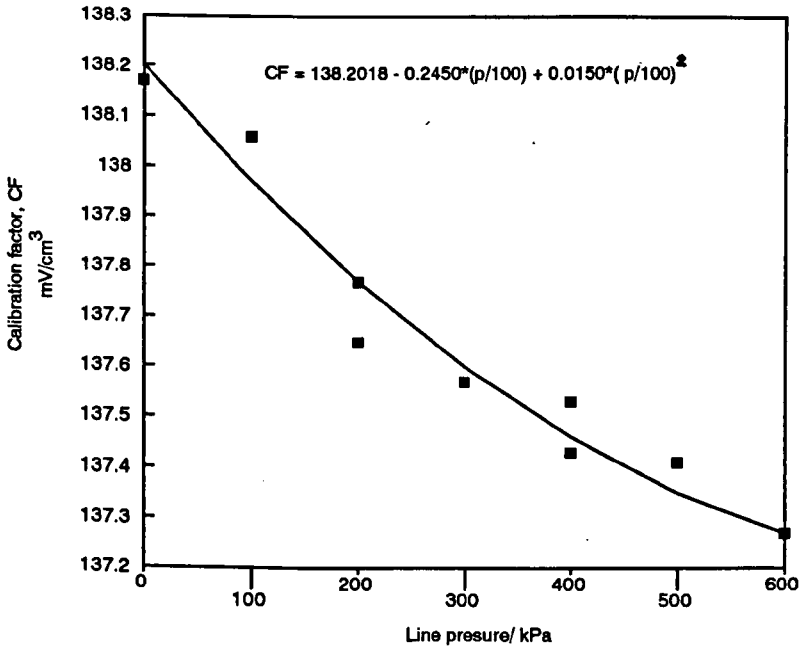

(a) Cell volume change device

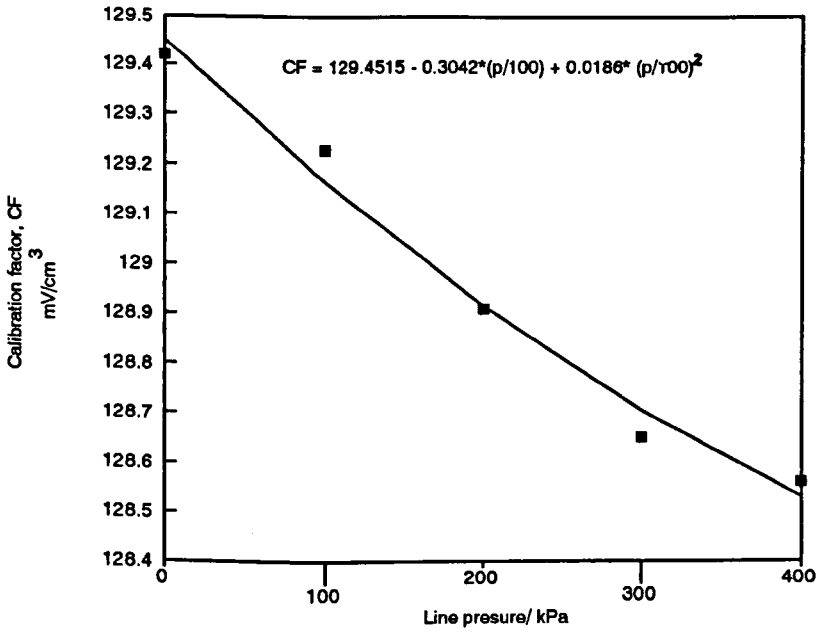

(b) Water volume change device

Fig (4.5) Calibration factor versus line pressure for volume change devices (differential pressure transducer type)

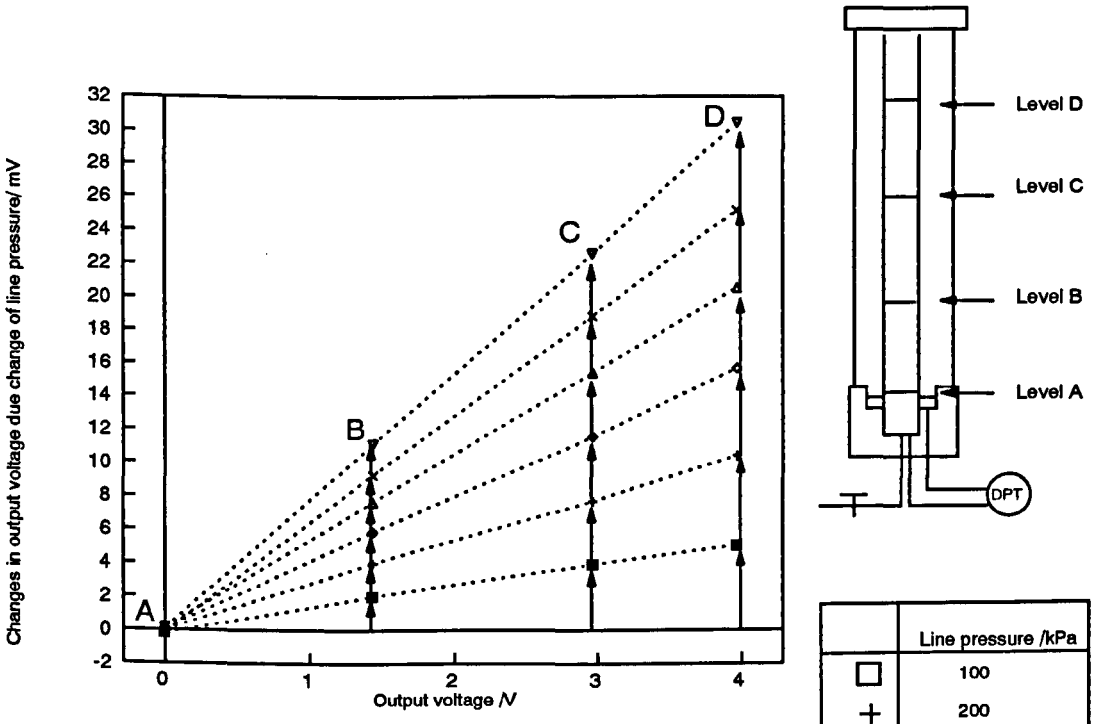

(a) Cell volume change unit

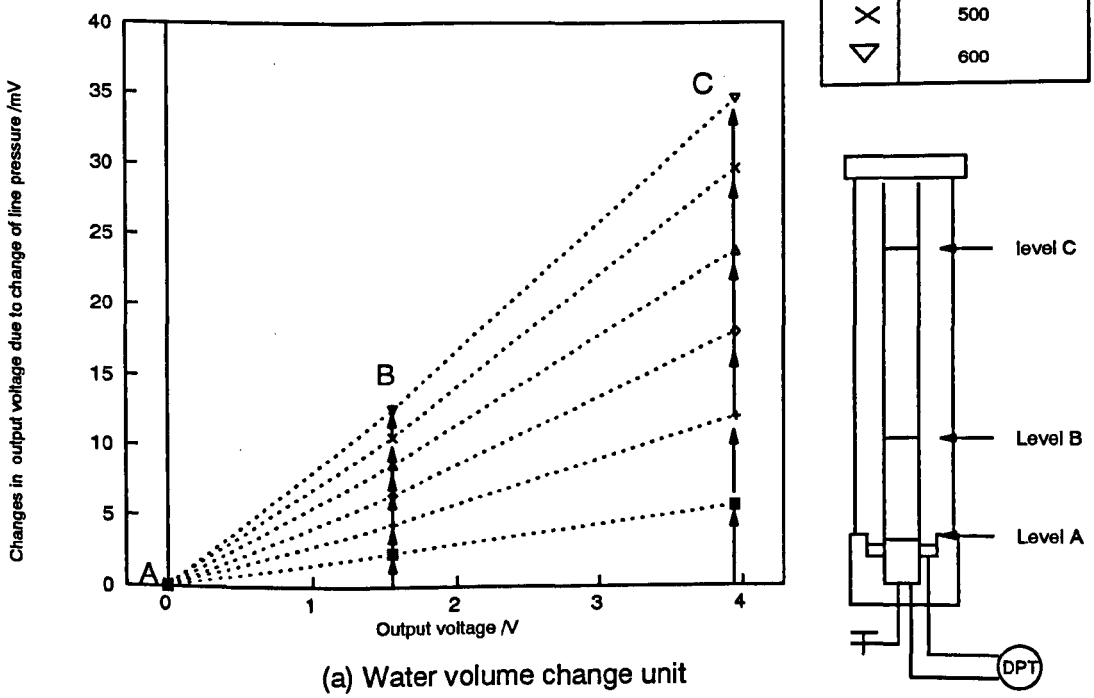

(a) Water volume change unit

Fig (4.6) Changes in output voltage of the volume change units due to changes in line pressure

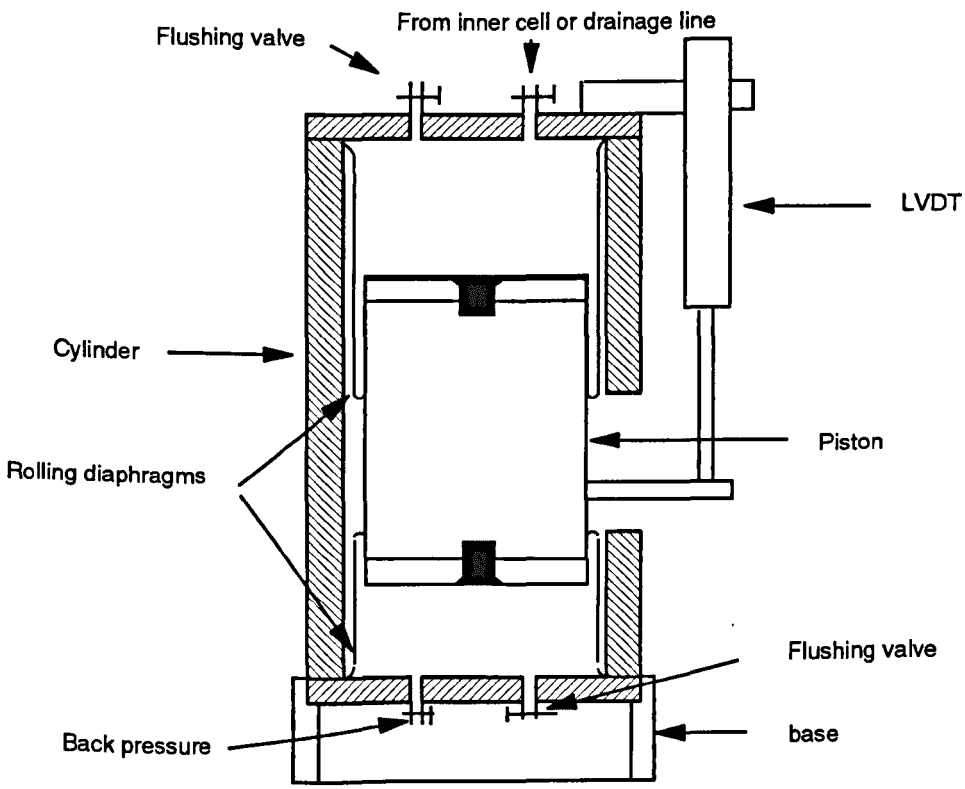

Fig (4.7) Imperial College type volume change unit

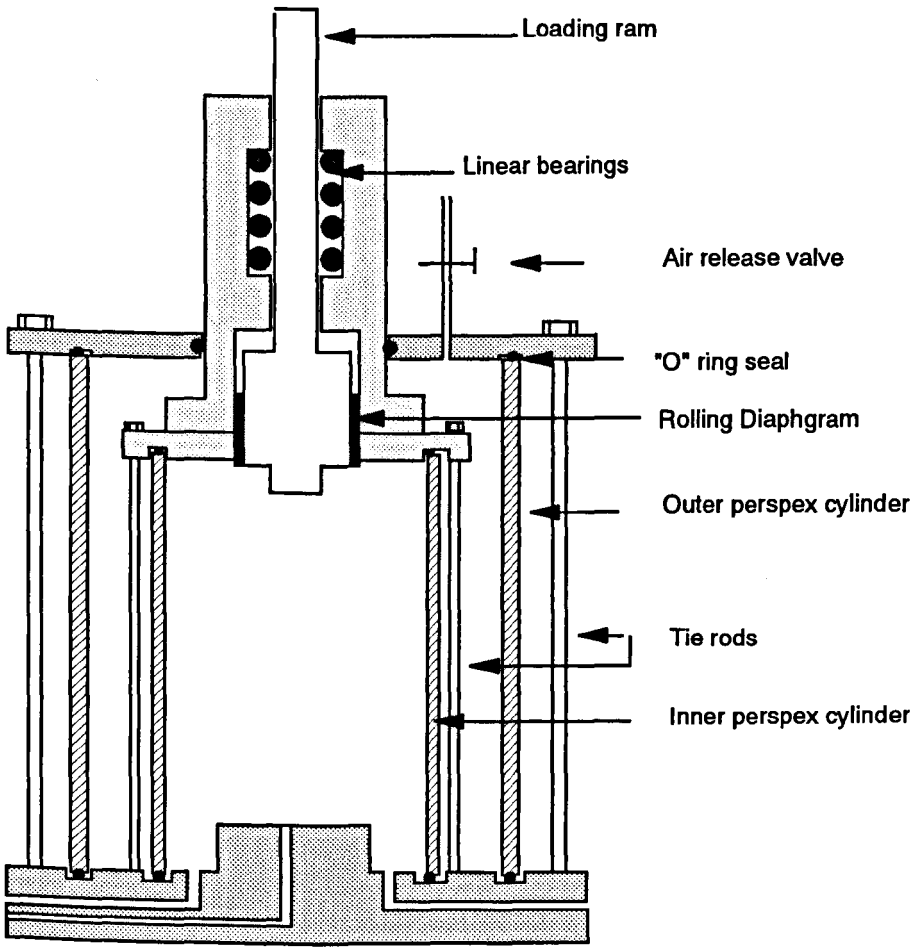

FIG (4.8) Double-walled triaxial cell

(Wheeler, 1986)

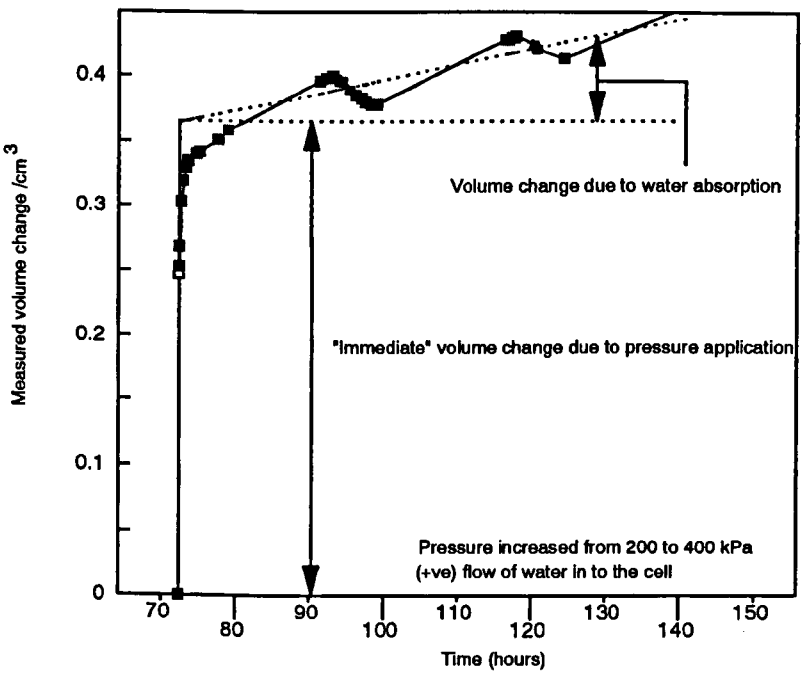

(a) System A

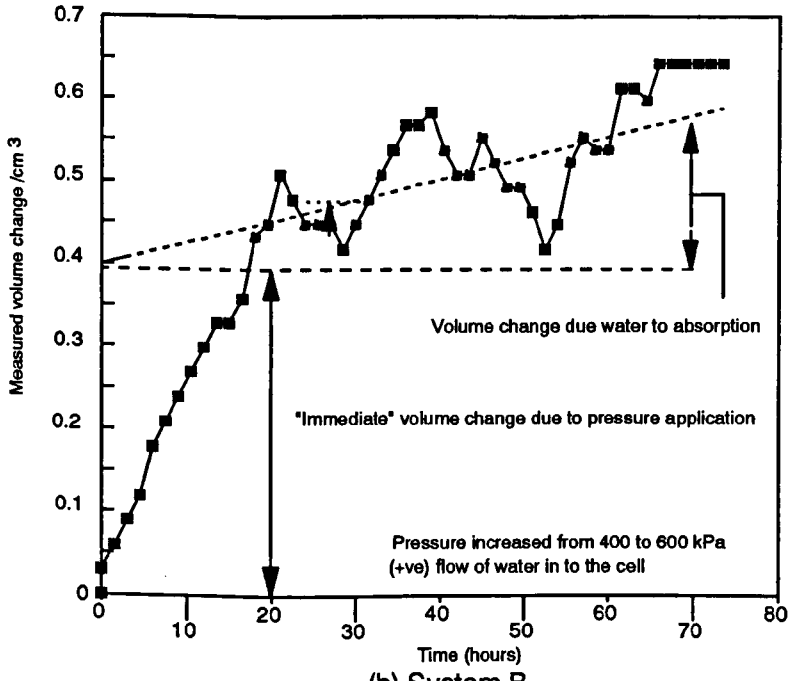

(b) System B

Fig (4.9) Cell volume change due to pressure application

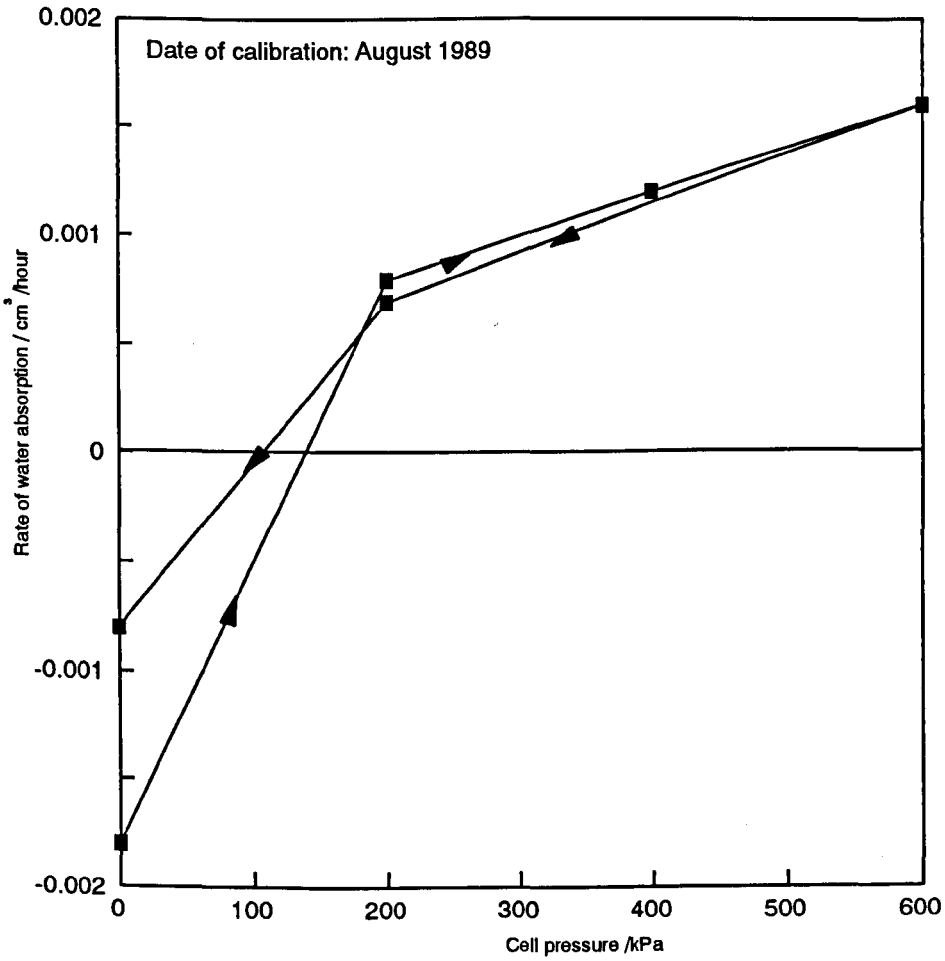

Fig (4.10a) System A

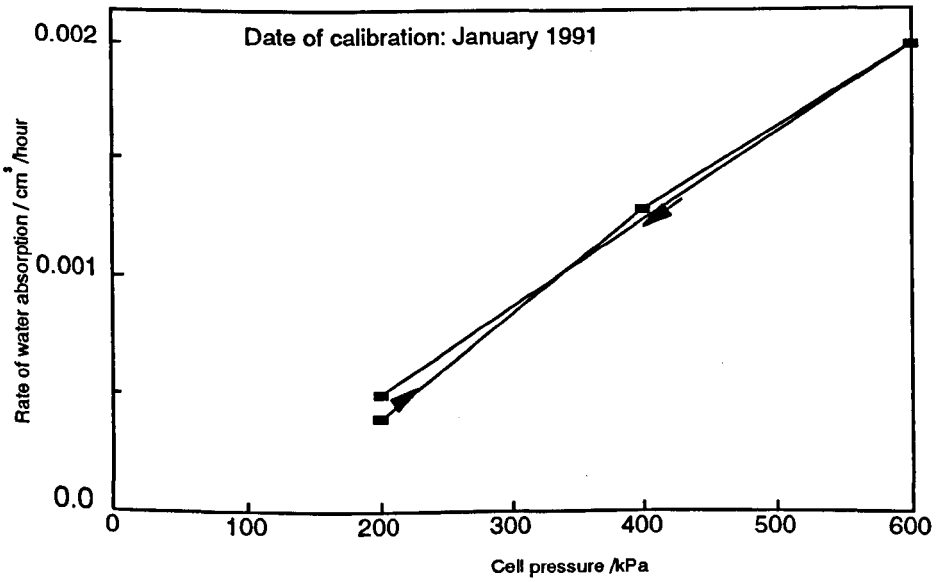

Fig (4.10b) System B

Fig (4.10) Variation of rate of water absorption with cell pressure

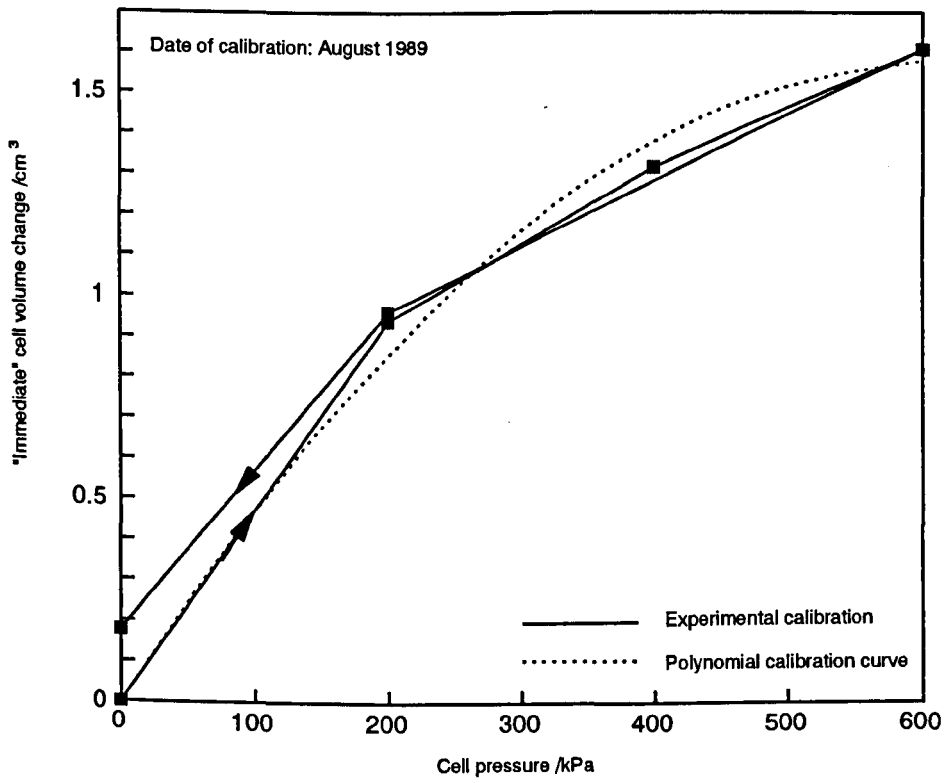

Fig (4.11a) System A

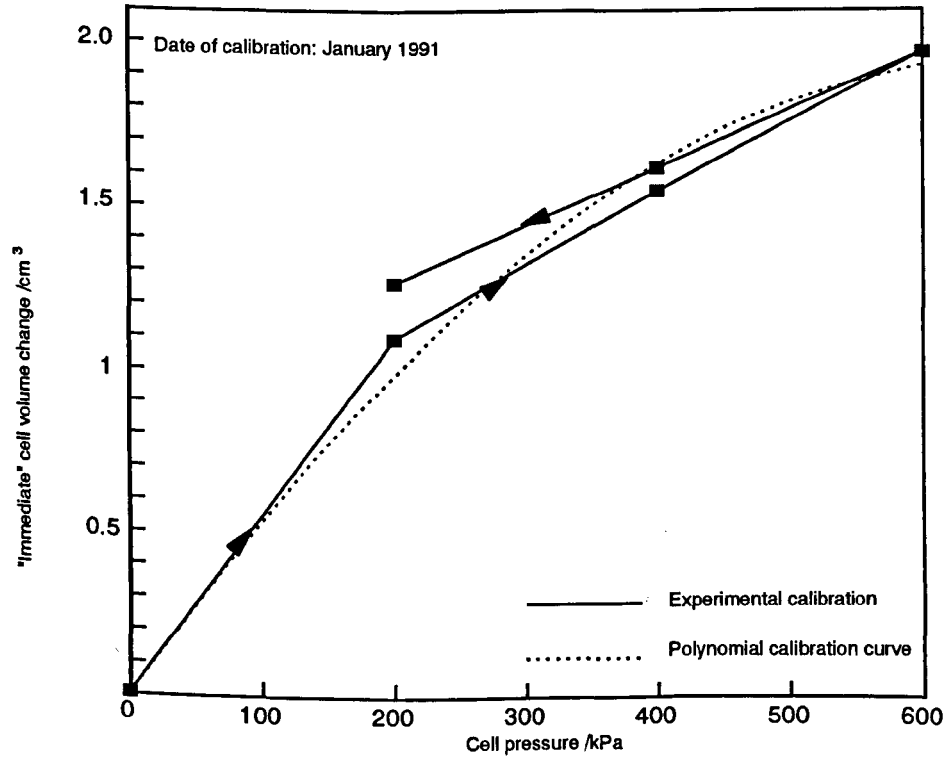

Fig (4.11b) System B

Fig (4.11) "Immediate" volume change of cell

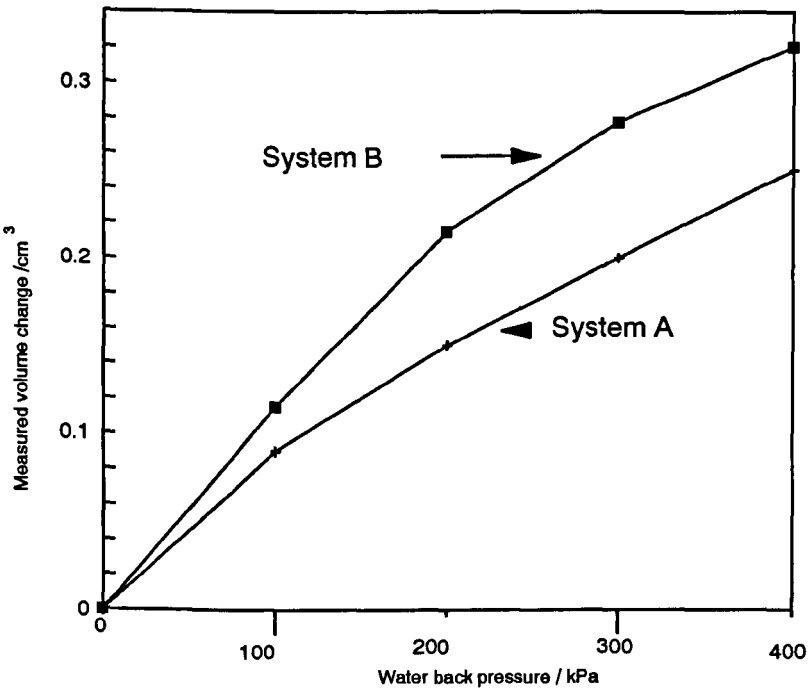

Fig (4.12) Calibration for volume change of water drainage line

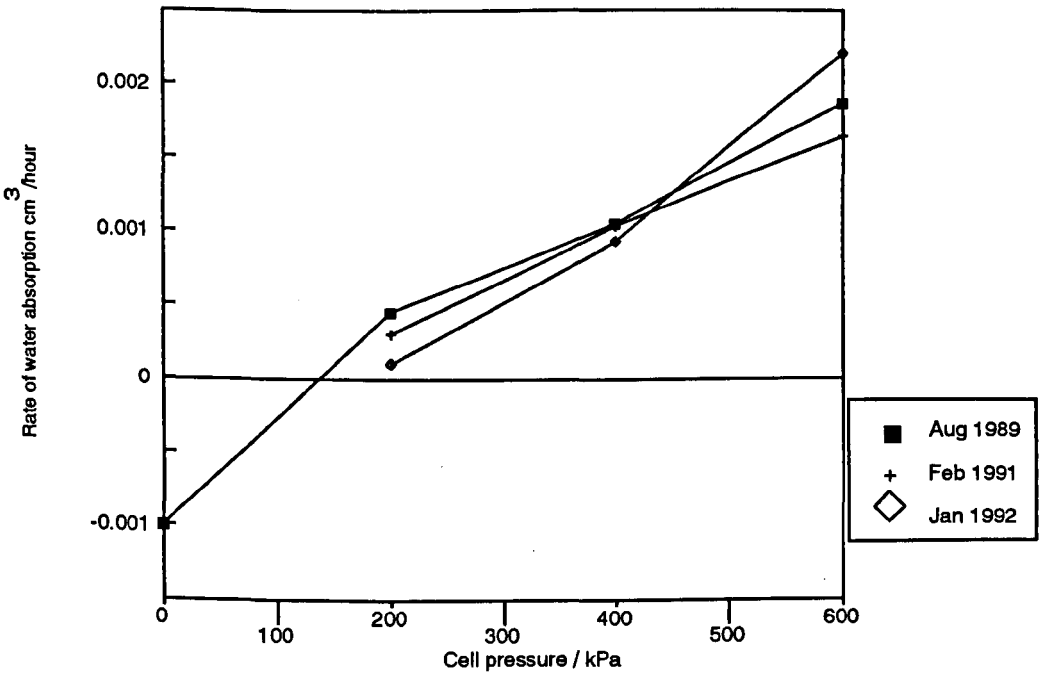

Fig (4.13a) System A

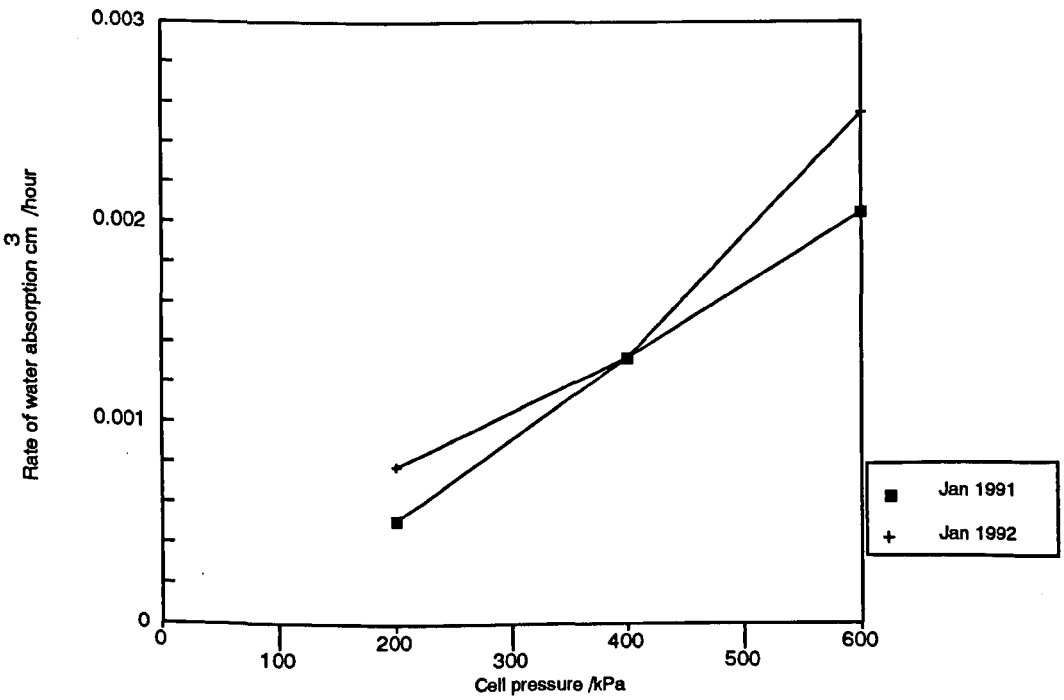

Fig (4.13b) System B

Fig (4.13) Rate of water absorption by acrylic cell wall

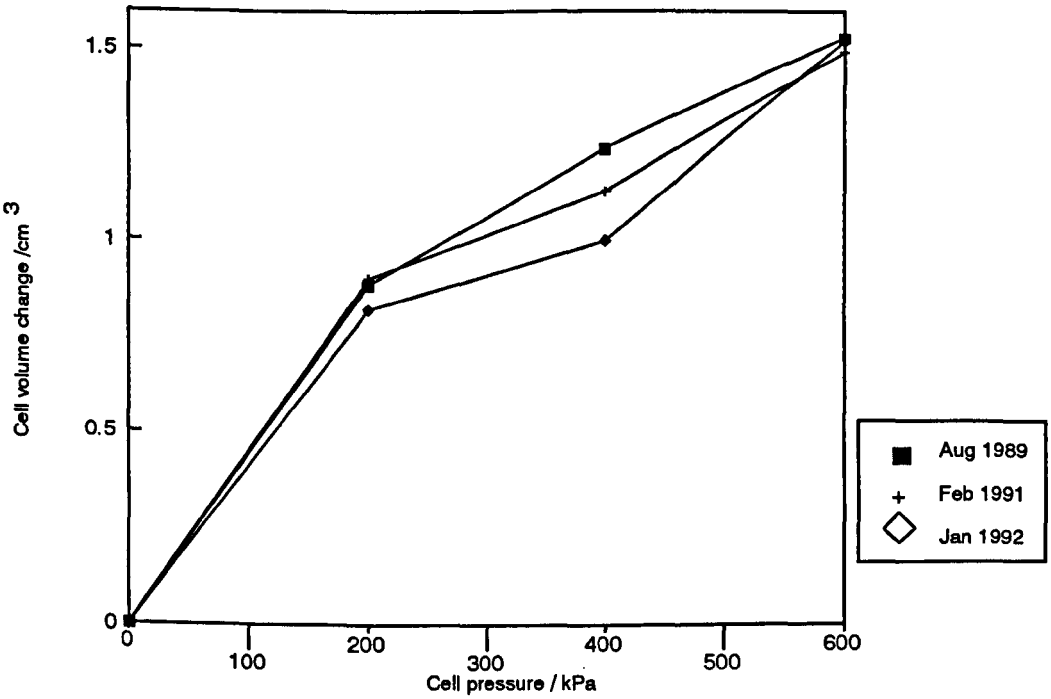

Fig (4.14a) System A

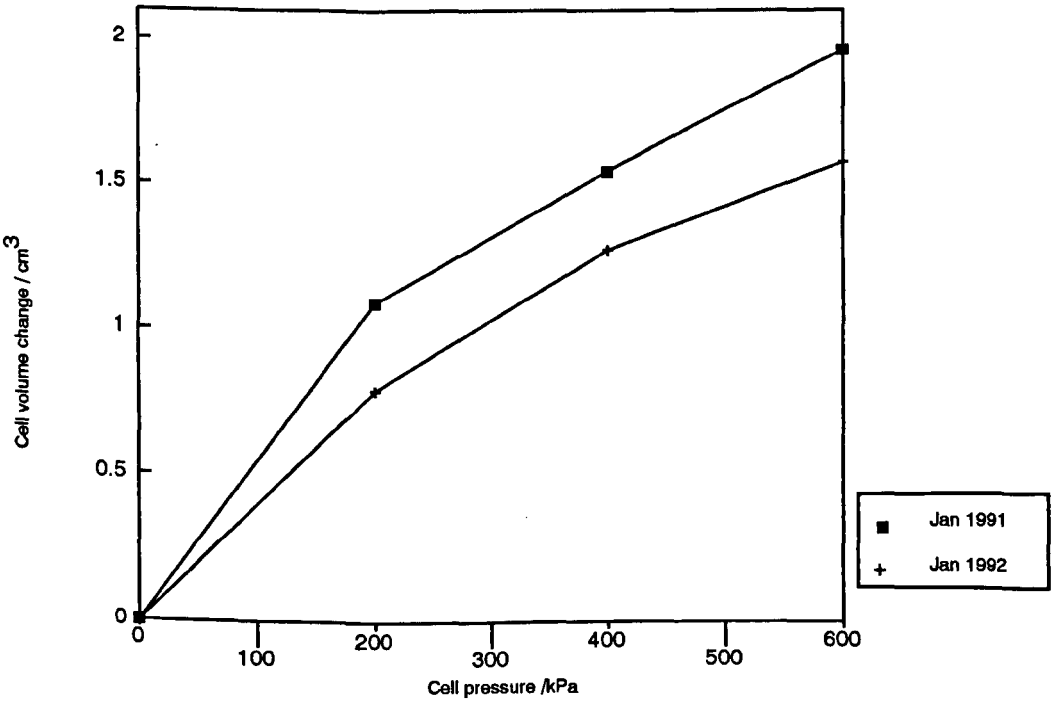

Fig (4.14b) System B

Fig (4.14) Calibration for immediate volume change of cell

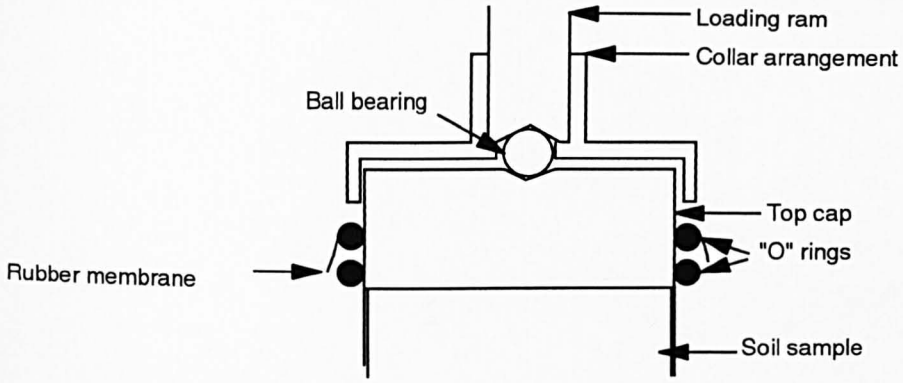

Fig (4.15) Top cap arrangement

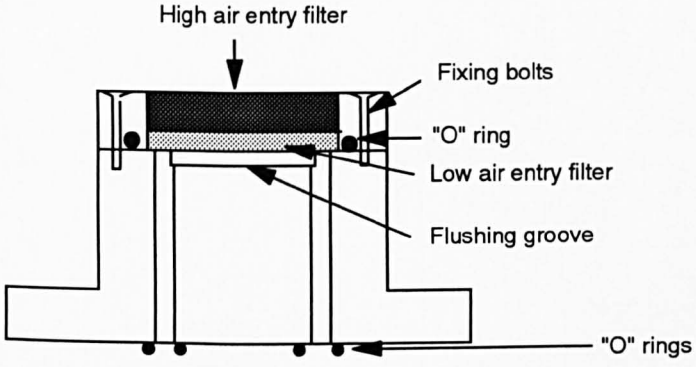

Fig (4.16) High air entry filter arrangement.

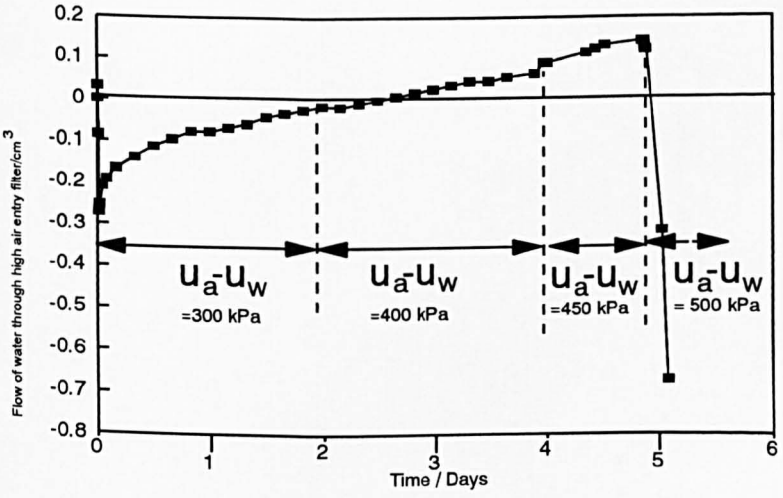

Fig (4.17) Check for air entry value of high air entry filter

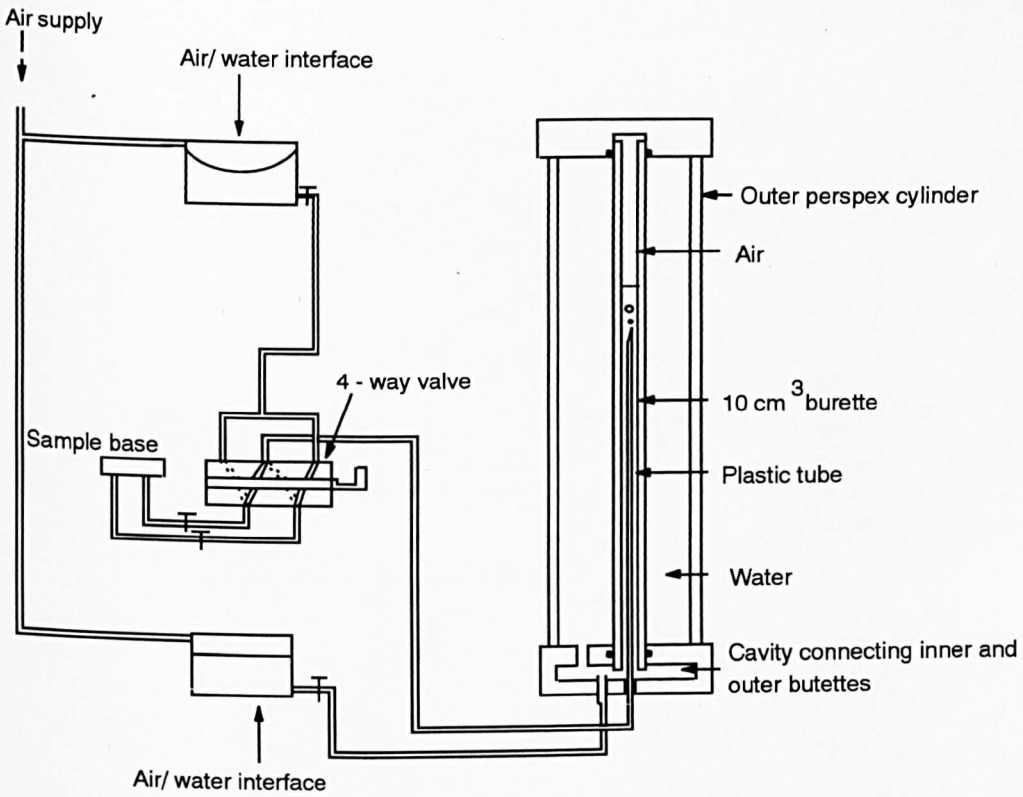

Fig (4.18) Flushing system

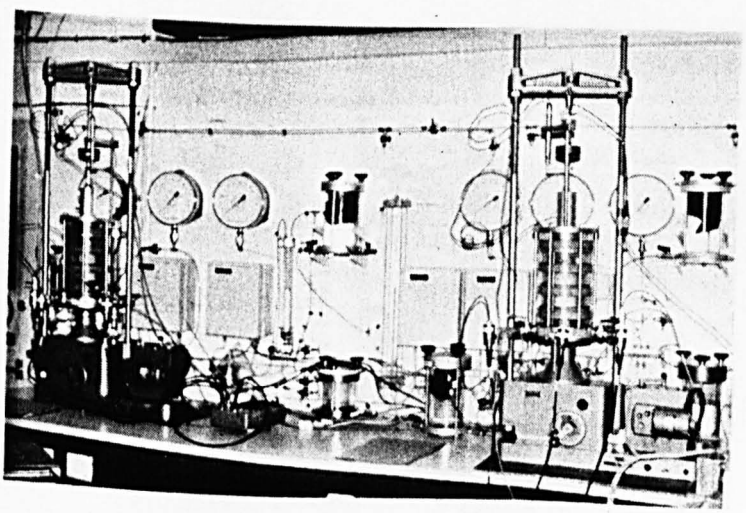

Photo (4.1) Experimental Systems A and B

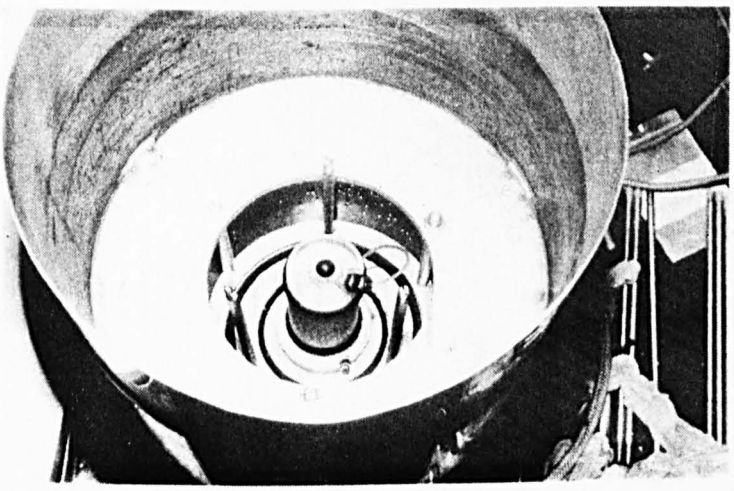

Photo (4.2) Collar arrangement used for the assembly of the inner cell under water

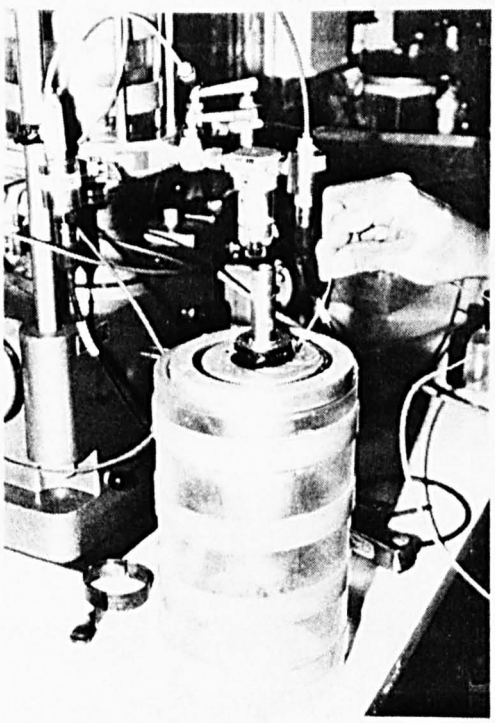

Photo (4.3) De-airation of rolling diaphragm

Type of calibration	Form of the equation	Aug 1989	Jan 1991	Jan 1992	Possible error due to drift
Air pressure transducer	ax+b	a=6.9989 kPa/mV b= -2.0 kPa	a=7.0169 kPa/mV b= -2.6 kPa	a=7.0022 kPa/mV b= -3.52 kPa	±1.0 kPa
Water pressure transducer	ax+b	a=7.0509 kPa/mV b= -2.6 kPa	a=7.0666 kPa/mV b= -5.5 kPa	a=7.0510 kPa/mV b= -9.7 kPa	±1.0 kPa
Cell pressure transducer	ax+b	a=7.0126 kPa/mV b=-11.1 kPa	a=6.9759 kPa/mV b=-14.78 kPa	a=6.9833 kPa/mV b=-38.6 kPa	±1.5 kPa
Cell volume change unit	x / ap2+bp+c	a=0.0121 cm³/mV/kPa² b= -0.2243 cm³/mV/kPa c= 138.2 cm³/mV	a=0.0121 cm³/mV/kPa² b= -0.2243 cm³/mV/kPa c= 138.2 cm³/mV	a=0.0121 cm³/mV/kPa² b= -0.2243 cm³/mV/kPa c= 137.96 cm³/mV	±0.03 cm³
Water volume change unit	x / ap2+bp+c	a=0.0185 cm³/mV/kPa² b= -0.3043 cm³/mV/kPa c= 129.45 cm³/mV	a=0.0185 cm³/mV/kPa² b= -0.3043 cm³/mV/kPa c= 130.34 cm³/mV	a=0.0185 cm³/mV/kPa² b= -0.3043 cm³/mV/kPa c= 130.18 cm³/mV	±0.15 cm³
Displacement transducer	ax	a= 0.010789 mm/mV	a= 0.010796 mm/mV	a= 0.010790 mm/mV	±0.01 mm
Load cell	ax	a= -0.4159 N/mV	a= -0.4160 N/mV	a= -0.4160 N/mV	±1.0 kPa
Cell volume change	ap2+bp+c	a= -0.0387 cm³/kPa² b=0.4832 cm³/kPa c=0	a= -0.0425 cm³/kPa² b=0.506 cm³/kPa c=0	a= -0.0219 cm³/kPa² b=0.3765 cm³/kPa c=0	± 0.12 cm³
Water absorption	ap+b	a= 0.00045 cm³/kPa /hour b= -0.00077 cm³/hour	a= 0.00033 cm³/kPa /hour b= -0.0003 cm³/hour	a= 0.00052 cm³/kPa /hour b= -0.0010 cm³/hour	± 0.18 cm³
Water drainage line	ap2+bp+c	a= -0.0143 cm³/kPa² b=0.1370 cm³/kPa c=0	a= -0.0143 cm³/kPa² b=0.1370 cm³/kPa c=0	a= -0.0121 cm³/kPa² b=0.1050 cm³/kPa c=0	± 0.03 cm³
Ram displacement (ram area / cm2)	a	a= 13.93 cm²	a= 13.89 cm²	a= 13.91 cm²	± 0.07 cm³

System A

Type of calibration	Form of the equation	Aug 1989	Jan 1991	Jan 1992	Possible error due to drift
Air pressure transducer	ax+b	*	a= -0.06063 kPa/mV b= -1.2 kPa	a=-0.06099 kPa/mV b= -3.5 kPa	±1.5 kPa
Water pressure transducer	ax+b	*	a= -0.06129 kPa/mV b= -0.9 kPa	a=-0.06165 kPa/mV b= -2.5 kPa	±1.5 kPa
Cell pressure transducer	ax+b	*	a= -0.06056 kPa/mV b= -14.78 kPa	a=-0.06082 kPa/mV b=-2.0 kPa	±1.5 kPa
Cell volume change unit	ax	*	a= -0.00478 cm³/mV	a= -0.00483 cm³/mV	±0.20 cm³
Water volume change unit	ax	*	a= -0.00531 cm³/mV	a= -0.00535 cm³/mV	±0.20 cm³
Displacement transducer	ax	*	a= -0.00518 mm/mV	a= -0.00515 mm/mV	±0.15 mm
Load cell	ax	*	a= 0.20549 N/mV	a= -0.20630 N/mV	±2.0 kPa
Cell volume change	ap2+bp+c	*	a= -0.0439 cm³/kPa² b= 0.5846 cm³/kPa c=0	a= -0.0191 cm³/kPa² b=0.3557 cm³/kPa c=0	±0.20 cm³
Water absorption	ap+b	*	a= 0.0003 cm³/kPa /hour b= -0.00024 cm³/hour	a= 0.00044 cm³/kPa /hour b= -0.0002 cm³/hour	±0.18 cm³
Water drainage line	ap2+bp+c	*	a= -0.0257 cm³/kPa² b=0.1734 cm³/kPa c=0	a= -0.0260 cm³/kPa² b=0.1534 cm³/kPa c=0	±0.02 cm³
Ram displacement (ram area / cm2)	a	*	a= 13.73 cm²	a= 13.75 cm²	±0.04 cm³

x Output voltage

p pressure (devided by 100)

* not conducted

System B

Table (4.1) Calibration factors.

CHAPTER 5

SAMPLE PREPARATION TECHNIQUE

CHAPTER 5

SAMPLE PREPARATION TECHNIQUE

This chapter describes the sample preparation technique used in the research programme.

5.1 SOIL TYPE

Kaolin was selected as a suitable material for the research project, because it is a soil type which obeys critical state concepts under saturated conditions. For a soil type where critical state concepts were inapplicable under saturated conditions there would have been little hope of it following critical state ideas under unsaturated conditions.

There were many other advantages in using kaolin to produce samples for the testing programme:

(1) With a 75% clay fraction, kaolin was representative of the fine-grained unsaturated soils that were of interest in the project.

(2) Kaolin was commercially available in a uniform, homogeneous form.

(3) Kaolin has a higher rate of consolidation than most other clay soils, thus reducing the time required for testing (this is particularly important for the testing of unsaturated samples, which is notoriously slow).

(4) Several previous researchers working in the field of unsaturated soil behaviour (Josa (1988) for example) tested kaolin samples, and the experimental data arising from the project would thus be complementary to existing data.

However the selection of kaolin as the soil type for the test programme did have the disadvantage that kaolin is an "ideal" material and any constitutive relationship developed would therefore be "ideal" and might not include some of the features required to describe unsaturated behaviour of less ideal soils.

5.2 SAMPLE SIZE

The following four factors were considered when deciding the dimensions of the sample:

(1) The sample size must be much larger than the dimensions of the structural elements forming the soil fabric (macrostructure), so that the sample is representative.

(2) The maximum size of sample that would fit in the existing cells was about 120 mm in height.

(3) The larger the size of the sample the greater the accuracy of the volumetric strain measurement in the double-walled cell.

(4) The larger the size of the sample the longer the time required for each test (because of the need for pore water pressure equalization throughout the sample) and therefore the smaller would be the number of the tests completed within the project period.

The sample size was selected as 50 mm in diameter and 100 mm in height. The maximum size of the macrostructural elements within the sample was less than 1.18 mm, because the material was sieved through a sieve with a size of 1.18 mm (see Section 5.3). With a sample height of 100 mm there was sufficient space at the top of the inner cell above the sample (this space was needed during assembly of the double-walled cell under water, see Section 4.3.1). The estimated error in the volume change measurement was approximately ±0.6 cm^3 in System A and ±0.1.02 cm^3 in System B (see Section 4.9) and the corresponding maximum error in the specific volume was ±0.01 for a 50 mm diameter sample. This error was considered to be within acceptable

limits and therefore it was not necessary to use larger samples.

5.3 SAMPLE PREPARATION TECHNIQUE

Unsaturated samples could have been prepared either by compaction or by de-saturation of initially saturated samples. Compaction was selected because the primary application of the research, in the U.K. environment at least, was considered to be unsaturated compacted clay fills.

Desirable features of the sample preparation technique were considered to be:

(a) Sample uniformity (including avoidance of any interfaces between layers in a sample compacted in several layers)

(2) Sample repeatability

(3) A sample structure which was representative of field conditions.

Various possible methods of compaction were available, including dynamic (impact) compaction, "static" compaction or kneading. Dynamic or static compaction methods were considered likely to give the best uniformity and

repeatability and these two methods were therefore examined in detail.

5.3.1 Dynamic compaction

A 50 mm split compaction mould was made together with a 22 mm diameter hammer for dynamic compaction (Photo 5.1). Collars were made to extend the mould at the top and bottom in order to prepare samples more than 100 mm in height which could then be trimmed to 100 mm. The height of fall of the hammer was approximately 30 cm and provision was made to vary the hammer weight in order to optimise the compaction effort. The hammer diameter of 22 mm in the 50 mm mould was roughly proportional to a 50 mm diameter hammer in a 102 mm diameter mould, as specified for the standard Proctor compaction process.

In order to prepare compacted samples, the required amount of powdered kaolin was first weighed in a mixing bowl. The required quantity of de-aired water, to achieve a desired moisture content, was then added slowly to the kaolin and mixed thoroughly in an electric food mixer. After 5 minutes of mixing, the soil was passed through a sieve with an aperture size of 1.18 mm (BS 1377). The reason for sieving was that the mixture prepared before sieving was extremely heterogeneous and the size of each lump varied greatly from tiny packets to lumps more than 5 mm in diameter. The material remaining on the sieve was broken up with a mortar

and pestle and sieved once more, with the whole process repeated until only a small amount of material remained on the sieve. The loss of moisture content during the process was found to be approximately 0.5%. The sieved mixture was placed in a plastic bag and sealed with adhesive tape. The sealed bag was kept in an air-tight container for 7 days to allow the water content to equalise throughout the material. No loss of water content occurred during this period even over 1 month.

The first aim of the sample preparation technique was to investigate the influence of compacting a sample in a number of layers and to identify the number of layers required to produce a reasonably uniform sample.

As a first attempt, the material was compacted in three layers, with 27 hammer blows for each layer. A variety of hammer weights were used. After the compaction a 100 mm sample was trimmed from the material in the mould. However, with the sample compacted in only 3 layers the bottom of each layer was found to be less compacted than the top of the layer. It was therefore decided to compact the soil sample in 9 layers, with 9 blows for each layer. A fixed amount of soil mixture was used for each layer. The bulk density variation along the sample was examined by measuring the wet weight of a known volume of compacted soil. Table 5.1 gives the maximum variation of bulk density along the sample for samples compacted in 3 layers and

samples compacted in 9 layers. The soil samples compacted in 9 layers (9 blows each) were much more uniform than sample compacted in 3 layers (27 blows each). In the former case, the percentage variation of bulk density was approximately 3.4 %.

A series of compaction tests were conducted to examine the hammer weight to simulate the standard Proctor compaction process, which takes place in a larger mould, with a diameter of 102 mm. The hammer weight required to produce a compaction curve almost identical to that produced by the Proctor compaction process was approximately 0.49 kg (see Fig 5.1). The hammer weight of 0.49 kg on the 22 mm diameter hammer used in the 50 mm mould corresponded to the same pressure as the 2.5 kg hammer of 50 mm diameter used in the standard compaction test.

The compaction curves were not extended beyond optimum moisture content because it was difficult to sieve soil mixture prepared at higher water content.

5.3.2 Static compaction

It was suspected that samples produced by the dynamic compaction process described above would be less repeatable than samples produced by static compaction. Therefore it was decided to examine the possibility of using a static compaction technique.

Various static compaction techniques were examined, using a compression frame (Photo 5.2) to provide "static" compression at a fixed displacement rate of 1.5 mm/min. Four steel plugs were made, all 49.75 mm in diameter with heights of 17.5 mm, 57.5 mm, 87.5 mm and 112.5 mm. The required amount of soil mixture was put into the mould and the plug was placed on top of soil mixture inside the mould. The compaction mould was then placed on the compression frame and a fixed rate of axial displacement was applied until a pre-defined axial load was reached. Once the load had been reached the plug was removed from the mould and the top surface of the layer was scarified before adding more soil mixture for the next layer. A fixed axial load was applied to each layer.

The following compaction techniques were examined:

(a) Compaction in a single layer.

(b) Compaction in a single layer, but compression from both ends in turn.

(c) Compaction in 4 layers.

(d) Compaction in 9 layers.

In cases (a), (b), and (c) considerable problems were encounted with sample non-uniformity or the presence of

marked interfaces between layers. However in case (d) (compaction in 9 layers) sample uniformity was greatly improved.

For samples compacted in 9 layers, each compaction stage was continued to a specified axial load or pressure (which was the same for all layers). The surface of each layer was scarified before adding the material for the next layer. The samples produced by this method were very uniform and interfaces between the layers were barely apparent. The repeatability of the technique was also found to be excellent. Table 5.1 shows the variation in bulk density along a sample produced by the various static compaction techniques, together with a qualitative indication of any problems with interfaces between layers.

Although one of the intentions of the sample preparation technique was to produce samples representing actual field conditions, a further intention was to produce samples with a low value of apparent pre-consolidation pressure, so that it was relatively easy subsequently to consolidate the samples to virgin states. The pre-consolidation pressure increases with compactive effort (Alonso, Gens and Hight, 1987). An initial test suggested that if samples were compacted to the standard Proctor compaction effort then the pre-consolidation pressure would be higher than the maximum cell pressure available in the laboratory, so that it would be impossible subsequently to consolidate the

samples to virgin states. Therefore it was necessary to use a lower compactive effort than the standard Proctor value.

Another feature noted in the static compaction process was that the compaction curve (dry density versus moulding water content) was distinctly different to the dynamic compaction curve. For static compaction the dry density continued to increase beyond the optimum water content estimated from dynamic compaction, suggesting that the optimum water content for static compaction was higher than for dynamic compaction (see Fig 5.2). A possible reason for this difference was that the shear displacements which caused dispersed soil structure on the wet side of optimum water content were considerably less in static compaction than in dynamic compaction.

The technique of producing samples by static compaction with 9 layers was finally identified as a suitable procedure. The moisture content of the soil was fixed as 25 %, which was 4% less than the optimum moisture content identified from the standard Proctor compaction process. Each layer was compressed at a fixed displacement rate of 1.5 mm/min to a pressure of approximately 400 kPa. This resulted in a dry density of 1.2Mg/m^3, a specific volume of 2.21 and a degree of saturation of about 54%.

5.4 INITIAL AND FINAL MEASUREMENTS OF SAMPLE VOLUME AND WEIGHT

To monitor the variation of specific volume during each test it was necessary to measure not only changes of sample volume during the test but also the sample volume at the beginning or end of the test. Similarly monitoring of the sample water content required not only measurement of water flowing in or out of the sample but also the volume of water within the sample at the beginning or end of the test.

The initial volume of the sample was easier to measure than the final volume because the sample was initially cylindrical, whereas it was severely deformed by end of the test. The initial volume was calculated by measuring the diameter and height of the sample, using a specially designed jig (see Photo 5.3). The jig consisted of a digital vernier (with a resolution of 0.001 mm) used to measure the diameter of the sample and a micrometer gauge (with a resolution of 0.0025 mm) used to measure the height of the sample. Measurements were taken with a dummy sample of known dimensions and with the soil sample. The dimensions of the soil sample were calculated from the differences in reading between the soil sample and the dummy sample.

A rigid target was fixed to the moving end of the

micrometer gauge and digital vernier (see Photo 5.3). A dial gauge was fixed on the frame holding the micrometer gauge. The dial gauge fixed on the holding frame indicated any movement of the frame carrying the micrometer gauge. When the target came into contact with the soil sample or dummy sample the first indication was movement of the dial gauge as the holding frame flexed slightly.

Repeated readings indicated that the measurements of sample height using the micrometer jig had a precision of ± 0.05mm. Measurements of sample height were taken 30 minutes after removal from the mould, to allow for any changes in height which occurred on removal from the mould. Unfortunately the measurements of sample diameter were unsatisfactory, because the target fixed at the end of the vernier did not make precise contact with the cylindrical surface of the sample. Therefore it was assumed instead that the sample diameter was equal to the mould diameter of 49.987 mm. This made no allowance for any lateral expansion of the sample on removal from the mould, but did ensure consistency between tests.

The accuracy of the measurement of initial sample volume based on measured sample height and assumed diameter was checked by measuring the sample volume in an alternative way by applying Archimedes principle after measuring the weight of the sample in air and then submerged in water. The accuracy of the measurement of sample volume by using

Archimedes principle was independently ratified by measuring the volume of a dummy sample (of known dimensions) in a similar way. 5 trials were conducted with the dummy sample. The method of measuring the sample volume by using Archimedes principle was found to be accurate to ± 0.025 cm^3 (the density of water was assumed to be 0.997 g/cm^3 rather than 1 g/cm^3, because a fixed difference was observed between the measured and calculated volumes). Four trials were conducted with unsaturated soil samples and the calculated volume (based on assumed diameter and measured height was always about 0.4 cm^3 less than the measured volume using Achimedes principle (with an assumed water density of 0.997 cm^3). This suggested that the assumption of sample diameter equal to the mould diameter was not correct and the diameter would be always higher than the mould diameter due to expansion of the sample after removal from the mould. However this error would be a fixed amount and would not change from one sample to another if the same compaction process was adopted for all tests.

The initial water content of the sample was calculated by measuring the initial wet weight of the sample (just before setting up in the triaxial cell) and the final dry weight of the sample at the end of the test. As a check, the final wet weight of the sample was measured in order to back-calculate the amount of the water at the start of the test (see Section 7.1). However the measurement of final wet weight involved many potential errors, due to transfer of

water to or from the sample during the process of removing the sample from the cell.

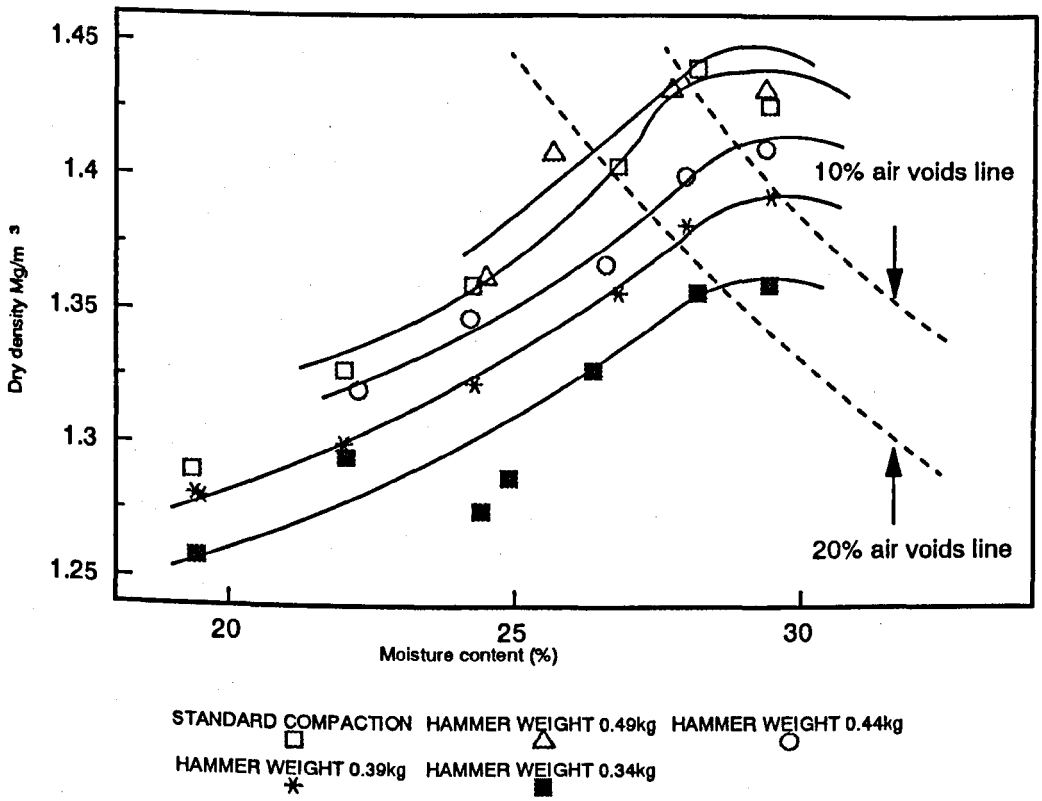

Fig (5.1) Dynamic compaction characteristics

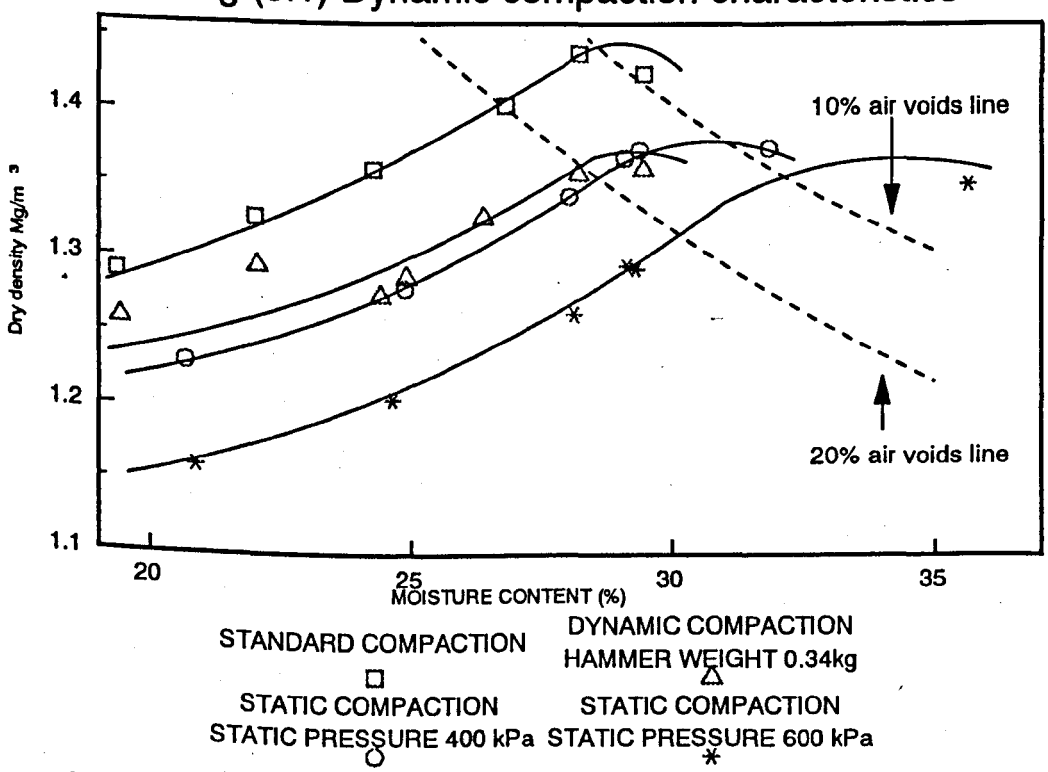

Fig (5.2) Static and dynamic compaction characteristics

	No of layers	One layer (compaction one side)	One layer (compaction both sides)	Three layers	Four layers	Nine layers
Dynamic compaction	Variability of bulk density	*	*	9.3%	*	3.4%
	Interface problems	*	*	Yes	*	No
Static compaction	Variability of bulk density	6.6%	6.2%	*	*	1.4%
	Interface problems	No	No	*	Yes	Minor

Note: Variability is defined as the difference between the maximum and minimum recorded values of bulk density within a single sample (expressed as percentage)

* Not examined

Table (5.1) Dynamic and static compaction procedures

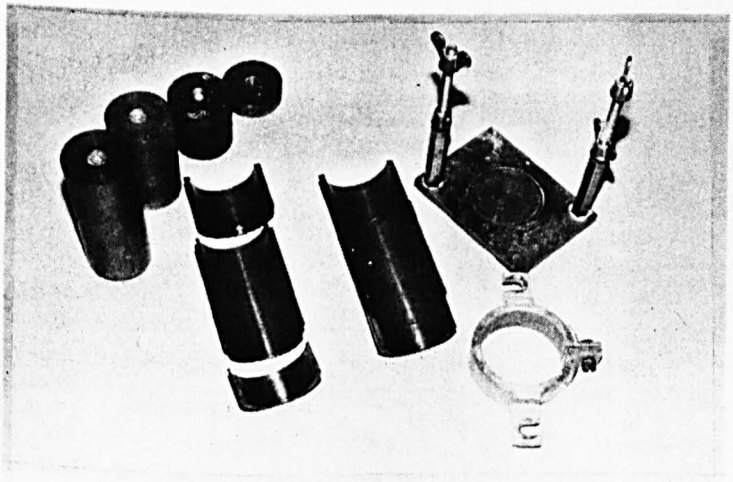

Photo (5.1) A modified 50 mm compaction split mould

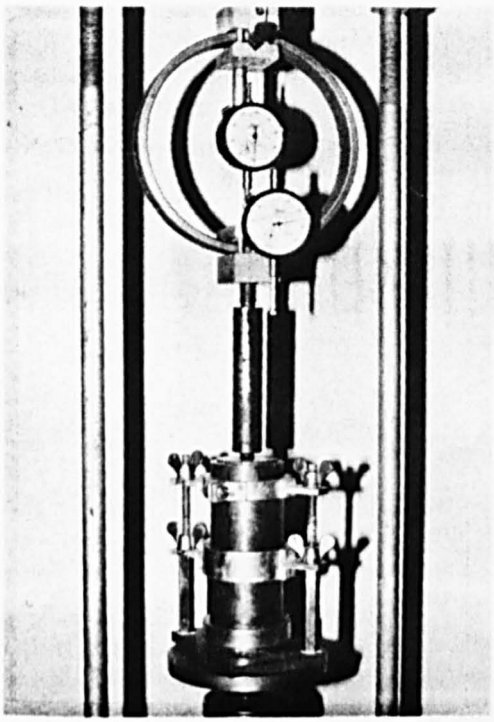

Photo (5.2) Compression frame used for static compaction

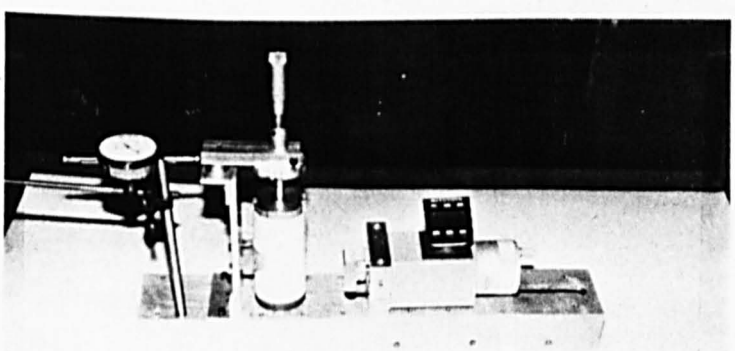

Photo (5.3) Jig used to measure sample diameter and height

CHAPTER 6

EXPERIMENTAL PROGRAMME

CHAPTER 6

EXPERIMENTAL PROCEDURE

This chapter describes the methods and procedures that were used to set up the soil samples in the double-walled triaxial cell, and then describes how the unsaturated soil samples were consolidated to virgin states and sheared in various ways to achieve critical states.

6.1 GENERAL METHODOLOGY

A series of triaxial tests was conducted on unsaturated samples of kaolin prepared by static compaction in 9 layers. Each sample was isotropically compressed to a virgin state at given values of suction s and mean net stress p'. The sample was then sheared until it reached a critical state. Different types of shearing were conducted to see whether all samples followed the same state boundary "hyper-surface" during shearing and ultimately reached a unique critical state "hyper-line" that was independent of the conditions of shearing (see Chapter 3).

6.1.1 Consolidation

Each soil sample was isotropically compressed to a virgin

state by increasing the mean net stress p' while holding suction s constant.

The most obvious way of increasing mean net stress while holding suction constant was to increase the cell pressure. Barden, Madedor and Sides (1969) examined the influence of the size of the stress increment ratio when adopting a step-loading approach and they concluded that a high stress increment ratio always caused greater compression than when the same total increment of load was applied in a larger number of smaller increments. This behaviour can be explained with the help of the yield locus proposed by Alonso, Gens and Josa (1990). Fig (6.1) shows the proposed shape of the yield curve for unsaturated soil and the movement of the yield curve during isotropic consolidation with the increase in cell pressure applied as a single step increment. As the increment of external load is applied to the sample, excess pore air pressure and excess pore water pressure will be generated within the sample. Any excess pore air pressure that is generated will dissipate very quickly to the air back pressure value (because of the relatively high value of air permeability k_a) and the mean net stress $p-u_a$ therefore rises almost immediately to its final value throughout the entire sample. However the excess pore water pressure will take considerable time to dissipate to the water back pressure value (due to the relatively low value of water permeability k_w) and this means that the suction u_a-u_w increases in the sample over

the period of consolidation.

Fig (6.1) shows the probable stress paths and corresponding movement of the yield curves for the top and bottom of a triaxial sample during the application of a step increment in cell pressure and during the subsequent consolidation period. At the bottom (water drained) face of the sample, the pore water pressure quickly dissipates to the water back pressure value and the soil reaches the final equilibrium point B on yield curve Y_b. At the top (water undrained) face of the sample, excess pore water pressures occur and the soil reaches a point C on yield curve Y_c at the time of loading. As excess pore water pressures dissipate during consolidation the state of the soil at the top of the sample moves to point B. It is obvious that the path from B to C will take the top of the sample into the elastic region and away from the virgin state. Greater expansion of the yield curve has taken place for the top of the sample than for the bottom of the sample. Therefore additional compression will take place along the path A-C-B at the top of the sample.

The amount of excess pore water pressure generated at the top of the sample could be minimised by applying the external load slowly enough to allow the excess pore water pressure at the top of the sample to dissipate during loading. This could be done by ramping the cell pressure at a rate at which the excess pore water pressure at the

top of the sample was within acceptable limits. In this way it should be possible for the whole sample to almost reach a virgin state on the normal compression hyper-line. The selected method of consolidation therefore involved ramping the cell pressure. An additional advantage of using ramped consolidation was that it gave a continuous plot of v versus p' at a given value of suction. This plot was used to identify the pre-consolidation pressure caused by the compaction process and to measure the slope of the subsequent normal compression line for the particular value of suction.

6.1.2. Shearing

Each soil sample was sheared once the sample was consolidated to a virgin state. The following six types of shear tests were adopted:

(A) Constant volume, constant suction shearing. In these tests the control system was used to increase or decrease the pore air pressure u_a and pore water pressure u_w by equal amounts (maintaining constant suction) in such a way as to keep the volume of the sample constant during shearing.

(B) Constant mean net stress, constant suction shearing. During shearing the control system was used to increase or decrease the pore air pressure

u_a and pore water pressure u_w by equal amounts (maintaining constant suction) in such a way as to keep the mean net stress p' constant.

(C) Fully drained, constant suction shearing. In these tests pore air pressure u_a and pore water pressure u_w were both maintained constant during shearing (giving constant suction). This type of test was similar to a drained test on a saturated sample.

(D) Constant water content, rising suction shearing. During shearing, the pore air pressure u_a was maintained constant, but the water phase was kept undrained, leading to a decrease in u_w and hence an increase in suction s.

(E) Constant volume, rising suction shearing. In this test the pore water pressure u_w was held constant while the pore air pressure u_a was increased (leading to an increase in suction) in such a way as to keep the sample volume constant.

(F) Constant mean net stress, falling suction shearing. In this test the pore air pressure u_a was increased in such a way as to keep the mean net stress p' constant while the pore water pressure u_w was increased at 1.5 times the rate of the increase

in pore air pressure (leading to a reduction in suction).

In all test types the cell pressure σ_3 was held constant during shearing. When using a double-walled cell it was important that the cell pressure was not reduced during a test, because there was the danger of air bubbles forming within the inner cell (resulting in error in the measurement of sample volume change). Therefore the various different stress paths were achieved by controlling the pore air pressure and pore water pressure rather than by controlling the cell pressure.

The majority of the tests were of types A, B, or C. In all three of these test types the suction s remained constant during shearing. Tests were conducted at four different values of suction: zero, 100, 200 and 300 kPa. The results were intended to provide constant suction cross-sections of the state boundary hyper-surface and the critical state hyper-line and to indicate whether the state boundary and critical state relationships for each value of suction were independent of the test path to the critical state.

In test types D, E and F the suction varied during each test and these tests were designed to show whether the critical state and state boundary relationships defined from the constant suction shear tests (types A, B and C) were also applicable to test paths where the suction

varied. Only if this were true could the critical state hyper-line and state boundary hyper-surface be described as truly unique (independent of test path).

6.2 LOGGING AND CONTROL SOFTWARE

System A was controlled by a PCL interface card and System B was controlled by an IEEE card. In each system there were 7 transducers and the details of each transducer and its voltage ranges were described in Chapter 4.

A logging program was written (by Mr T.Robinson, electronics/software technician) in Quick Basic to log the output voltage of each transducer every second and convert it to engineering units. Appropriate calibration factors for the conversion to engineering units (including the cell calibrations for pressure, water absorption and ram displacement) were inserted before starting the test. The converted engineering units were saved in the hard disc, in "Lotus 123" spreadsheet format, at a specified time interval. The time interval at which the data was logged in the spreadsheet was defined before starting a test and there was the option of changing the interval of logging to a higher or lower value later in the test. The data could be also copied to floppy disc without disturbing or stopping the test.

The values of the 5 state parameters (deviator stress q,

mean net stress p' suction s, specific volume v and water content w) were calculated by using the following equations.

$$q=\frac{F}{(V_o-\Delta V)}(H_o-\Delta H)-100\frac{\Delta H}{H}q_{(mem)} \qquad (3.1)$$

$$p'=(\sigma_3-u_a)+\frac{q}{3} \qquad (6.2)$$

$$s=u_a-u_w \qquad (6.3)$$

$$v=\frac{\rho_w G_s(V_o-\Delta V)}{W_d} \qquad (6.4)$$

$$w=\frac{(W_o-W_d+\Delta W)}{W_d} \qquad (6.5)$$

Where F was the deviator load, V_o was the sample volume at the start of the particular stage of the test, ΔV was the change of the sample volume during the stage, H_o was the sample height at the start of the stage, ΔH was the change of the sample height during the stage, ρ_w was the density of water, σ_3 was the cell pressure, G_s was the specific density of the soil particles, $q_{(mem)}$ was membrane correction for 1% axial strain, W_d was the dry weight of the sample (measured at the end of the test), W_o was the weight of the sample at the start of the stage and ΔW was the weight of water flowing into the sample during the stage.

Values of all 5 state parameters were calculated on the spreadsheet, but the suction s, deviator stress q and mean

net stress p′ were also calculated in the main logging program during shearing to enable s to be held constant during shearing (test types A, B, and C) or to enable p′ to be held constant during shearing (test types B and F). Values of specific volume v and the water content w were not calculated until the test was completed, because only then was the dry weight of the sample known.

6.2.1 Control logic for consolidation

A control programm written in Quick Basic by T.Robinson, was used to control the stepper motors in order to achieve the test conditions described in Section 6.1

Fig 6.2 shows the flow chart for the consolidation stage of the program. The main feature of this program was that the cell pressure σ_3, pore air pressure u_a and pore water pressure u_w could each be ramped at a given rate to achieve a given target pressure. The target pressure and the ramping rate for each stepper motor were defined before running the test. By defining a required accuracy of the pressures the cell pressure, air back pressure and water back pressure were maintained within a given accuracy as soon as the target pressures were achieved. It was also possible to switch OFF or ON the computer control to any of the stepper motors, in order to use the program with either System A (which included stepper motor control of σ_3, u_a and u_w) or System B (which included stepper motor

control of only σ_3 and u_a).

6.2.2 Control logic for shearing

Individual control programs were written to control each type of shearing.

Fig 6.3 shows the flow chart for constant volume, constant suction shearing (test type A). The volume change of the sample during shearing was checked every second and maintained within a given accuracy (± 0.03 cm^3, equivalent to ±0.0003 in specific volume) by sending equal signals to air and water pressure stepper motors to increase or decrease pressure by a single step if the volume differed from the target by more than the specified accuracy. Each step of the motor was equivalent to a pressure change of 0.42 kPa. Once a signal had been sent to the stepper motors by this "IF LOOP" the program waited for a specified period of time to allow the volume of the sample to respond to the pressure changes. This delay time (10 seconds was selected) was fed into the software before running the test. As there was no guarantee that the size of the step pressure increments for the air pressure stepper motor and water pressure stepper motor were absolutely identical, the value of the suction u_a-u_w was checked after each increment and, if necessary, the water pressure stepper motor was adjusted by a single step to bring the suction back to the required value (within a specified accuracy). Finally the

control program also maintained the cell pressure σ_3 and, if necessary, adjusted the cell pressure stepper motor by a single step to bring the pressure back to the required value (within a specified accuracy). The target values and required accuracy (normally ±0.5 kPa) for both suction and cell pressure were specified by the operator at the start of the shear stage.

The flow chart for the constant mean net stress, constant suction tests (test type B) was very similar to that for constant volume, constant suction shearing. Instead of checking the volume change , the mean net stress p′ was calculated every second and compared with a target value. If the measured value of p′ differed from the target by more than a specified accuracy (set at 0.5 kPa), equal signals were sent to air and water pressure stepper motors to change by one step in order to bring the value of p′ back to the target.

The flow chart for the fully drained, constant suction tests (test type C) was relatively simple as there was no check on either sample volume change or on changes of p′. The values of u_a, u_w and σ_3 were simply held at constant target values throughout the test.

The flow chart for the remaining 3 types of shear test (D,E and F) all employed a similar overall logic to that described above. One difference was that there was no loop

to maintain constant suction during the test because test, types D, E and F were all variable suction tests.

In all the stages of a test the data in the spreadsheet could be copied into a floppy disc while running a test without disrupting the control and logging process.

System A was capable of doing all six types of test (A to F) whereas System B was only capable of doing test types C, D and E, because System B did not have a stepper motor to control the pore water pressure.

6.3 TESTING PROCEDURE

6.3.1 Setting up

50 mm diameter samples of unsaturated compacted kaolin were prepared by static compaction in a mould at a water content of 25% (see Chapter 5). Each sample was left in the atmosphere for approximately 30 min, to allow any rapid swelling caused by equalization of pore air pressure, before the height of the sample was then measured. The initial height of the sample was measured by using a specially designed jig (see section 5.4).

While waiting the 30 minutes before measuring the sample height the pedestal containing the high air entry filter was removed from the de-airing cell and connected to the

base of the double-walled triaxial cell. The drainage lines were flushed with freshly de-aired water. Any excess water left on the high air entry filter was removed with a dry tissue, but a small amount of water was still left on the filter in order to avoid any de-saturation of the filter.

The initial wet weight of the sample was measured just before putting the sample on the pedestal. Two lengths of fuse wire, each arranged as a semi-circle, were positioned on the high air entry filter before putting the sample on the pedestal (see Section 4.11.4). After positioning the sample on the pedestal, a rubber membrane was placed on the sample by using a membrane stretcher. A low air entry filter was put on the top of the sample and then the top cap connected to the air supply line was placed on top of the low air entry filter (see Photo 6.1). The rubber membrane was sealed at top and bottom using two "O" rings that were positioned by using an "O" ring stretcher. The excess rubber membrane at top and bottom was cut off in order to avoid trapping any air within the membrane folds (this would have caused inaccuracies in the measurement of sample volume change using the double-walled cell technique).

The inner cell was assembled under water (see Section 4.3.1) to avoid trapping air in the rolling diaphragm of the double-walled cell (see Photos 4.2, 4.3 and 6.2). The outer cell was assembled in the usual way. During assembly

the pore water pressure transducer connected to the base pedestal was monitored to check that the fuse wire kept the sample and the high air entry filter separated, so that negative pore water pressure in the sample was not transmitted to the water drainage line (see Section 4.11.4). Finally, the assembled cell was placed in the compression frame.

In System A the meniscus shapes were set in the appropriate directions in the burettes of the cell volume change unit and water volume change unit before taking the initial output voltages of the two units (see section 4.2.1). In System B the volume change devices were pressurised to 25 kPa before taking the initial reading and the pressures were then brought back to zero before opening the valves to the cell (see Section 4.3.1).

6.3.2 Equalisation stage.

After setting up the sample in the triaxial cell and taking the initial readings from the volume change units with the computer, the valves to the inner cell, outer cell and water drainage line were opened to the cell volume change unit, air-water interface and water volume change unit respectively. At this stage the cell pressure, air back pressure and water back pressure were all zero. The cell pressure, air back pressure and water back pressure were then manually increased to 50 kPa, 25 kPa and 10 kPa

respectively. The loading ram was then brought close (1-2mm clearance) to the ball bearing placed on the top cap. This was done to locate the sample top cap within the alignment collar attached to the loading ram, so as to prevent any tilting of the sample during equalization and consolidation stages. The magnitude of the loading ram displacement during this operation was recorded for future use (see Section 6.3.4 below).

The controls on the stepper motors were set to auto, in order to accept any signal from the control software. The pressures were then ramped at a fast rate to achieve a mean net stress p' of 50 kPa and a suction of zero, 100, 200 or 300 kPa (see Fig 6.4). The pressures were ramped at a rate of 1.6 kPa/min with the target pressures set in the control program (the consolidation control program was used in this equalization stage). The water back pressure was set to 50 kPa during the equalization stage in all tests except Test 9D where the water back pressure was set to 100 kPa. The air back pressure in all tests was set at s + 50 kPa, where s was the required value of suction, and the cell pressure was set at s + 100 kPa (giving a mean net stress p' of 50 kPa).

The equalization stage took at least 7 days before the flow of water into the sample had almost ceased.Because of the practical difficulties of installing an additional high air entry filter within the top cap, no attempt was made to

measure the pore water pressure at the top of the sample to make sure that the pore water pressure had equalized to the water back pressure value throughout the sample. However a standard procedure was adopted that the equalization stage was terminated once the flow of water into the sample reduced to 0.1 cm^3 per day. This was equivalent to 0.04% change in the water content per day.

During the equalization stage the water always flowed into the sample, suggesting that the applied suction values of zero, 100, 200 and 300 kPa were all less than the high value of suction produced by the initial compaction process.

A slightly different procedure was adopted for the tests at zero suction. The air back pressure was set at 35 kPa (15 kPa lower than water back pressure) in order to accelerate the saturation rate. In Test 25C (the first test conducted under zero suction) the air back pressure was kept at 50 kPa (equal to the water back pressure) and the sample equalized at a degree of saturation of about 92%. However the tests at zero suction were intended to be on saturated samples. The air back pressure in Test 25C was therefore brought down to 35 kPa to bring the sample to a saturated state. A water extractor was connected on the air drainage line to the triaxial cell base in order to collect water coming out through the air drainage line.

A further difference in procedure in the tests conducted at zero suction was that the value of p' during equalization was 40 kPa, rather than the standard value of 50 kPa used in all other tests. The reason for choosing this lower value of p' was to try and ensure that the yield stress induced by the initial compaction process could be observed in the subsequent consolidation stage, bearing in mind that the yield stress would be lowest at zero suction because of the inclination of the LC yield curve (see Section 7.1 and 7.2).

The saturation of the samples to be tested at zero suction took approximately the same time as the equalization in all other tests, but the saturated samples were left under the equalization stage for a slightly longer time (2-3 days more) to ensure a degree of saturation very close to 100 %. The amount of water that was required to saturate the samples used in the zero suction tests was more than the capacity of the water volume change devices. Therefore the water volume change devices (for Systems A and B) were refilled whenever necessary and the amount of water used for refilling was monitored. In the meantime the water coming out of the sample into the air drainage line was also weighed each day (by closing the air drainage valve and measuring the amount of water collected in the extractor) to see whether the sample had reached an equalization state with the water outflow at the top of the sample equal to the water inflow at the bottom.

6.3.3 Consolidation stage

Once the sample was equalized at a given suction (zero, 100, 200 or 300 kPa) and a mean net stress p' of 50 kPa (or 40 kPa for the tests at zero suction), the sample was then isotropically consolidated at constant suction to a pre-selected value of mean net stress (normally 100, 150, 200, 250 or 300 kPa) (see Fig 6.4). While maintaining the suction constant (water and air pressure held constant) the cell pressure was ramped at a given rate to the required target value.

The process of ramped consolidation was used to limit the excess pore water pressure generated at the top (water undrained) face of the sample to an acceptably low value (see Section 6.1.1). Thomas (1987) presented the following equation to calculate the equilibrium value u_{eq} of excess pore water pressure produced at the undrained face of a saturated sample loaded by ramped consolidation with the total stress increasing with time at a constant rate A:

$$u_{eq}=\frac{Ah^2}{2c_v} \qquad (6.6)$$

c_v is the coefficient of consolidation, and h is the sample height. The appropriate value of c_v for unsaturated compacted kaolin was calculated from the results of step-loading isotropic consolidation tests conducted before the main test programme was conducted. Inserting $c_v = 7.1*10^{-8}$ m^2/sec and h= 100 mm into Equation 6.6 gives:

$u_{eq}=19.5A$ (6.7)

Where the rate of total stress increase A is expressed as a rate per hour. Equation 6.7 suggests that the excess pore water pressure that could be expected at the undrained face would be 12 kPa if A were set at 0.6 kPa/hour.

The method adopted to evaluate c_v and the use of Equation 6.6 are strictly valid only for saturated soils. With the cell pressure ramped at 0.6 kPa/ hour, the excess equilibrium value of pore water pressure might be considerably less than 12 kPa in an unsaturated sample, because excess pore water pressures generated by undrained loading of unsaturated soil tend to be much lower than in saturated soil. 12 kPa as a conservative estimate was considered to be an acceptably low value of excess pore water pressure during ramped consolidation and therefore the rate of increase of cell pressure was selected as 0.6 kPa/hour. With the cell pressure ramped at 0.6 kPa/ hour, the ramped consolidation stage normally took 5-18 days (depending upon the target value of p'). A time lapse of at least 24 hours was left between the end of ramping of cell pressure and the beginning of shearing, to allow full dissipation of excess pore water pressure throughout the sample.

Each sample was consolidated to a virgin state prior to shearing. The change in the curvature of the consolidation curve plotted during ramped consolidation provided a clear

indication that the mean net stress was increased above the pre-consolidation pressure caused by the compaction process (see Section 7.2).

6.3.4 Shearing stage

Fig (6.5) shows how the sample height was measured at the start of shearing (after consolidation). The distance "a" was the fixed distance between the top and bottom plates of the inner cell of the double-walled cell. Distance "b" was the fixed height of the top cap and porous stone placed on the sample. Distance "c" was the depth of the loading ram out of the top plate when the loading ram was at top of its stroke. Distance "d" was the depth of the pedestal. Distance "e" was the fixed distance between the top cap and the loading ram when the loading ram contacted the ball bearing placed on the top cap. The height of the sample "f" at the start of shearing was calculated by using these dimensions and the displacement of the loading ram required to bring the ram from the top of it's stroke into contact with the sample at the start of shearing. The precision of this measurement was calculated by repeatedly measuring a dummy sample in the double-walled cell and was estimated to be ±0.1mm.

Before starting the shearing stage, the appropriate gear was selected on the compression frame in order to give a suitable shearing speed. Once this had been done, the

required shearing stage was selected on the computer and relevant test conditions (eg target values of cell pressure and suction, logging interval, etc) were fed in. The loading ram was then manually brought into contact with the ball bearing on the top cap. After starting the compression machine, the initial voltages were taken and an external signal applied to start the test once the friction on the loading ram had mobilised.

All tests were strain-controlled at a constant rate of axial strain. This provided good quality data at failure or at the ultimate critical state but relatively poor quality data in the early stage of each test (when the deviator stress was rising very rapidly and equalization of pore water pressure was very poor). This was considered to be sensible strategy, because the primary objective of the test programme was to investigate the conditions at critical states.

The rate of shearing was calculated for 95% equalization at failure. The equation suggested by Bishop and Henkel (1982) for drained triaxial testing of saturated samples was used to calculate the required time t to failure:

$$t=\frac{20h^2}{0.75c_v} \qquad (6.8)$$

Here 2h was the sample height, c_v was the coefficient of consolidation and t was the time to failure. By substituting the value for c_v the time required for failure

was approximately 11 days under fully drained conditions.

In five of the six shear test types included in the testing programme the water phase was allowed to drain during shearing (test types A, B, C, E and F), whereas the water phase was undrained in test type D. However the shearing speed for all tests was calculated using Equation (6.8), so as to avoid the possibility of strain rate effects influencing the results.

For constant volume test types A and E the strain to failure was 8 to 12%, and an axial displacement rate of 0.0008mm/min was selected. For all other test types the strain to failure was 20 to 35%, and axial displacement rate of 0.0012mm/min was selected.

Shearing was terminated when the change in mean net stress p', deviator stress q, suction s, sample volume V and water content w almost ceased. In test types A, B, C, E and F the water content w continued to change very slowly, whereas in test type D the suction s continued to change very slowly.

6.3.5 Final measurements

All tests were terminated after the shearing stage. No swell-back stage was conducted. The pore air pressure and pore water pressure applied to the sample were first

reduced to zero. The cell pressure was then reduced to zero. The sample was dismantled from the pedestal and then the membrane was carefully removed. The final wet weight of the sample was taken immediately after removing the membrane from the sample. The final wet weight of the sample was only used as an extra check for the water content measurement of the sample during the test. The sample was then put in oven for 3 days before taking the final dry weight of the sample. This dry weight was used to evaluate the specific volume and water content changes during the test (see Section 6.2).

6.4 TEST PROGRAMME

Thirty tests were conducted in the main testing programme. Table 6.1 shows the type of test and the time spent on each test. Each test was assigned a test number followed by a letter (A to F) defining the test type. Of thirty tests, 26 were constant suction tests (type A, B, or C) whereas the remaining 4 tests were variable suction tests (D, E or F). Relatively large numbers of constant suction tests were conducted at suctions of zero and 200 kPa (so that the critical state hyper-line was well defined for at least 2 values of suction) and relatively small numbers of constant suction tests were conducted at suctions of 100 and 300 kPa.

6.4.1 Test series at zero suction

Eight constant suction shear tests (types A, B and C) were conducted at zero suction. The equalization stage of Test 24C was not conducted with a standard procedure (see Section (6.3.2). Tests 19A and 23B were slightly affected by a failure in the pressure supply system during the shearing stage (the consolidation stages were unaffected by the pressure drops). Of the 8 tests, two samples were sheared with v constant (type A), three samples were sheared with p' constant (type B) and three samples were sheared under fully drained conditions (type C).

6.4.2 Test series at suction of 100 kPa

Four constant suction shear tests were conducted at a suction of 100 kPa, including one sample sheared at constant v (type A) two samples sheared at constant p' (type B) and one sample sheared under fully drained conditions (type C).

6.4.3 Test series at suction of 200 kPa

Nine constant suction shear tests were conducted at a suction of 200 kPa. Among them four samples were sheared at constant volume (type A), two samples were sheared at constant p' (type B) and two samples were sheared under fully drained conditions (type C). One test (1A) was

terminated after the consolidation stage, because substantial friction on the loading ram was noticed at the beginning of shearing. In Test 6B shearing was discontinued at a later stage of the test because of a pressure drop in the system, but the data from this test was considered to be still valid because the results suggested that the sample had virtually reached a critical state (see Chapter 7).

6.4.4 Test series at suction of 300 kPa

Five constant suction shear tests were conducted at a suction of 300 kPa. Among them one sample was sheared at constant v (type A), one sample was sheared at constant p' (type B) and two samples were sheared under drained conditions (type C). One test was discontinued (14A) after finding that air had blown through the high air entry filter during the later stages of equalization. Test 16B was interrupted in the middle of shearing by a cell pressure increase of about 25 kPa, the cause of which was unknown, but the pressure drop was brought under control within a few minutes.

6.4.5 Test series with change in suction during shearing

Two samples were sheared at constant water content with rising suction (type D). The initial suction prior to the shearing was 100 kPa in Test 27D and 200 kPa in Test 28D.

No constant water content, rising suction shear tests were conducted with an initial suction of 300 kPa, because the suction at failure would have been considerably greater than 300 kPa and therefore well outside the region covered by the data from the constant suction shear tests.

One constant volume, rising suction shear test (type E) was conducted, together with one constant p', falling suction test (type F). The initial suctions in the two tests were 100 kPa and 200 kPa respectively, as shown in Table 6.1.

6.5 INITIAL STEP LOADING CONSOLIDATION TESTS

Before the control program was written, 3 step-loading tests were conducted on unsaturated samples produced by the same compaction procedure and equalization stage as used in the main test series. In the step-loading tests the mean net stress p' was then increased by reducing the pore air pressure while holding the cell pressure and pore water pressure constant. Fig (6.6) shows the probable stress paths and corresponding movement of the yield curves for the top and bottom of a sample during the application of an increment of p' by a step-reduction in the air pressure and during the subsequent consolidation period. At the bottom of the sample, excess pore air pressure and pore water pressures dissipate quickly and reach an equilibrium state at point E on yield curve Y_e. At the top of the sample, the pore air pressure reaches its final value

quickly but a negative excess pore water pressure is set up and the soil reaches a point F on yield locus Y_f at the time of loading (at a higher value of suction than the final equilibrium value). Over the period of consolidation, suction falls to its final value and the soil at the top of the sample reaches point E on the same yield locus Y_e as the bottom of the sample. Therefore the process of reducing air pressure increases the mean net stress while taking the whole sample to a virgin state.

Three tests were conducted with this step loading method. In Test S1 the sample was brought to equilibrium at a mean net stress p' of 100 kPa and a suction value of 200 kPa. Then the air pressure was reduced by 100 kPa (increasing p' to 200 kPa and reducing s to 100 kPa) and the sample left to equalize until the change in the water content had ceased. This test produced two data points on the normal compression hyper-line (but at two different values of suction). The sample was then sheared under constant water content, rising suction conditions (type D). In Test S2 the sample was equalized at a mean net stress of 100 kPa and a suction of 300 kPa and the air pressure was then reduced in two decrements of 100 kPa. This test produced 3 data points on the normal compression hyper-line, at three different values of suction. Test S3 produced 4 data points on the normal compression hyper-line with suction values of 400, 300, 200 and 100 kPa and mean net stress values of 100,200, 300 and 400 kPa respectively. Shearing was not

conducted in Tests S2 and S3.

The equalization curves produced from these step loading tests were used to evaluate the value of the consolidation coefficient c_v. The root time method was adopted to calculate the 90% consolidation time and hence a value for c_v, even though this method was strictly applicable only to saturated soil. The consolidation coefficient was calculated to be $7.2*10^{-8}$ m^2/sec.

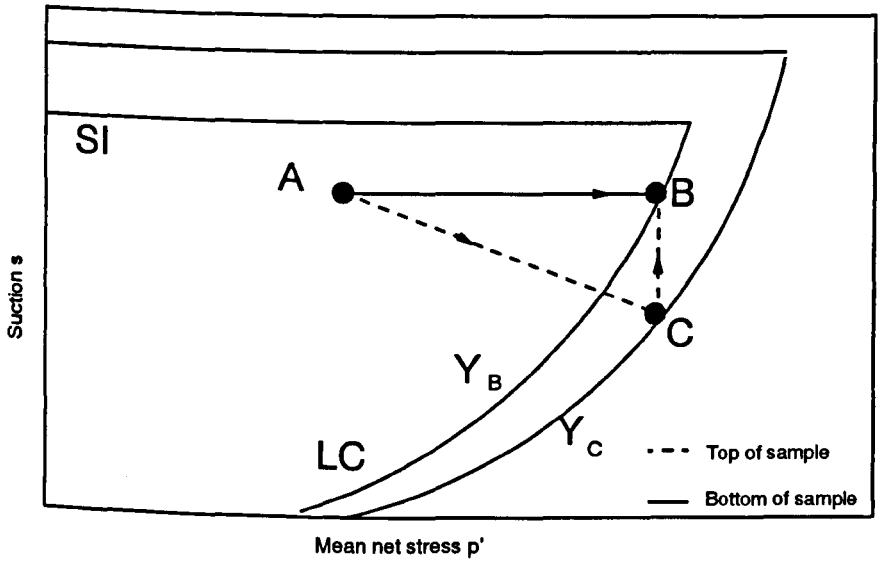

Fig (6.1) Stress paths for isotropic consolidation by step-increment of cell pressure

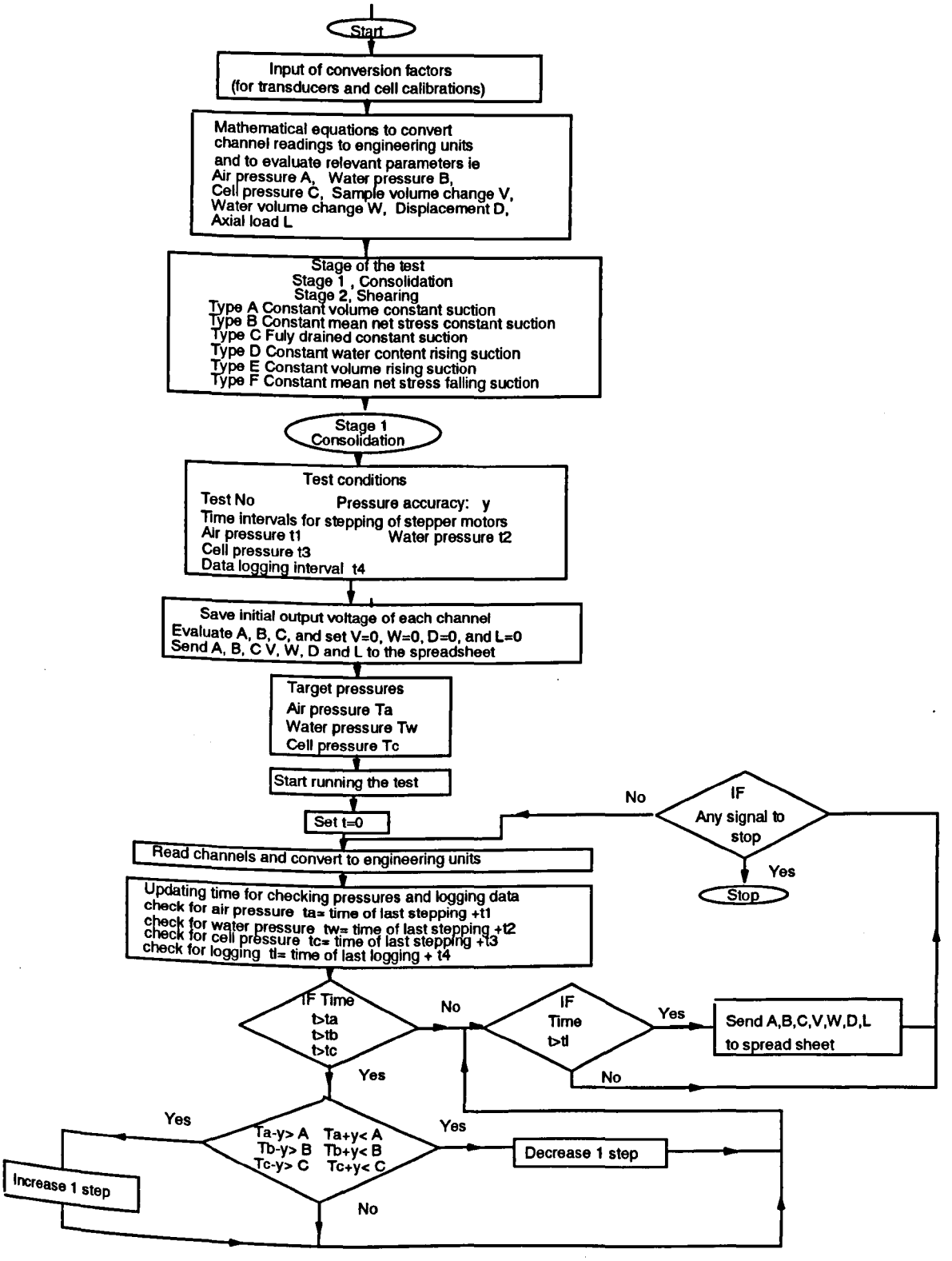

Fig (6.2) Flow chart for consolidation stage

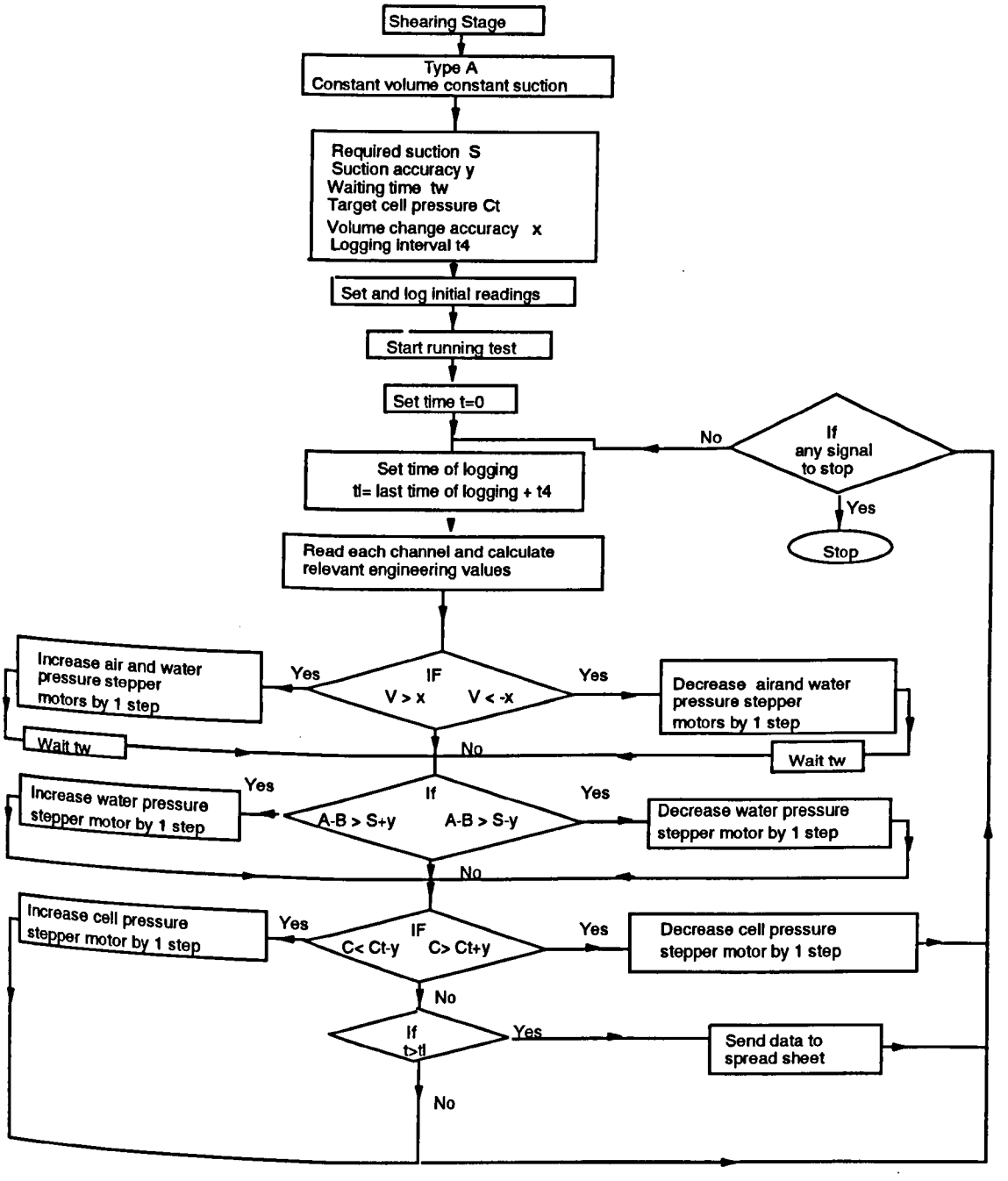

Fig (6.3) Flow chart for constant volume, constant suction shearing

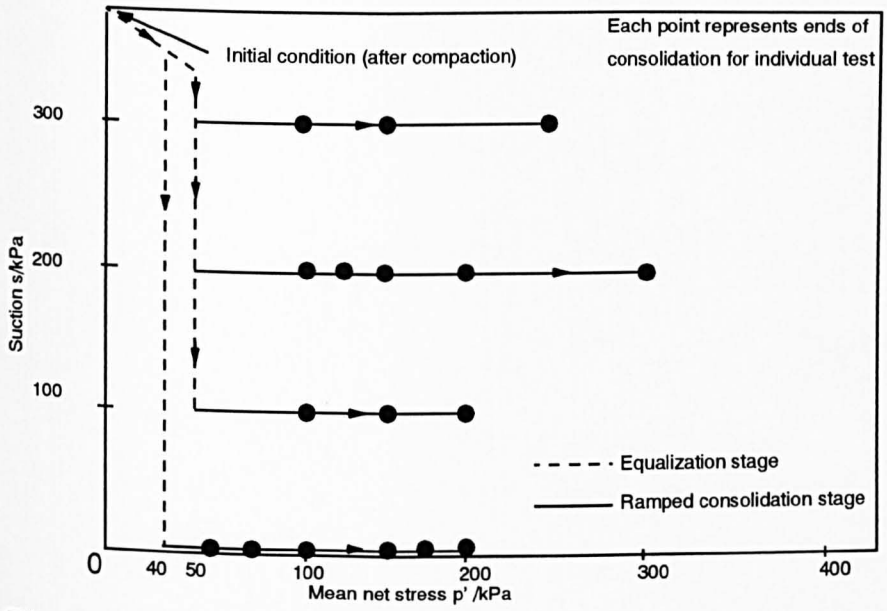

Fig (6.4) Stress paths during eqalization and consolidation stages

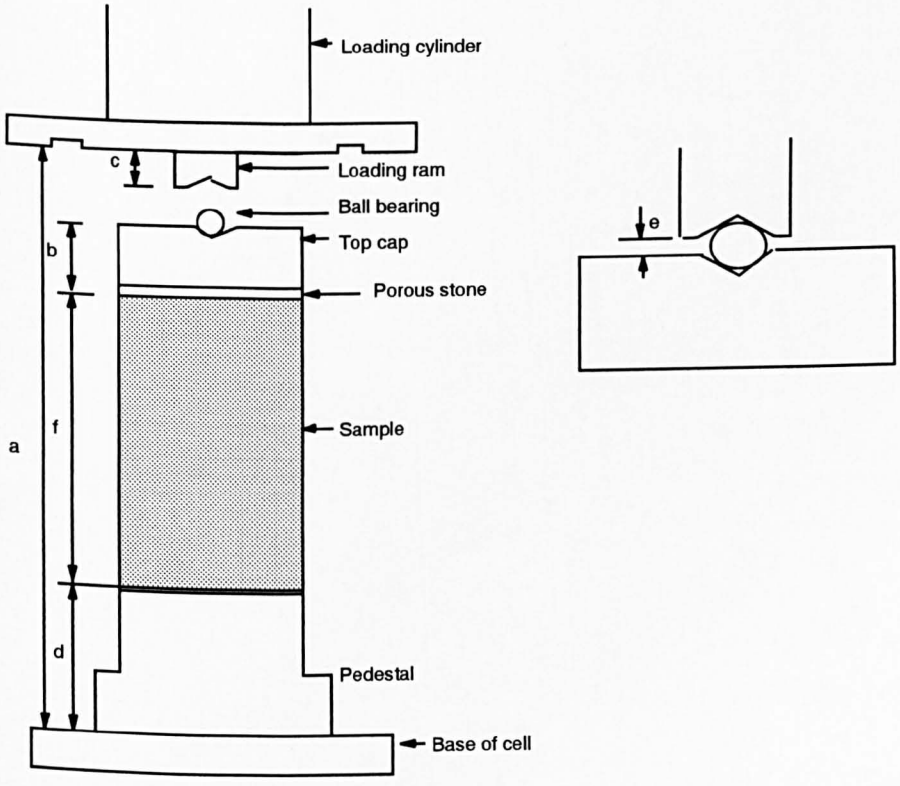

Fig (6.5) Measurement of sample height before shearing

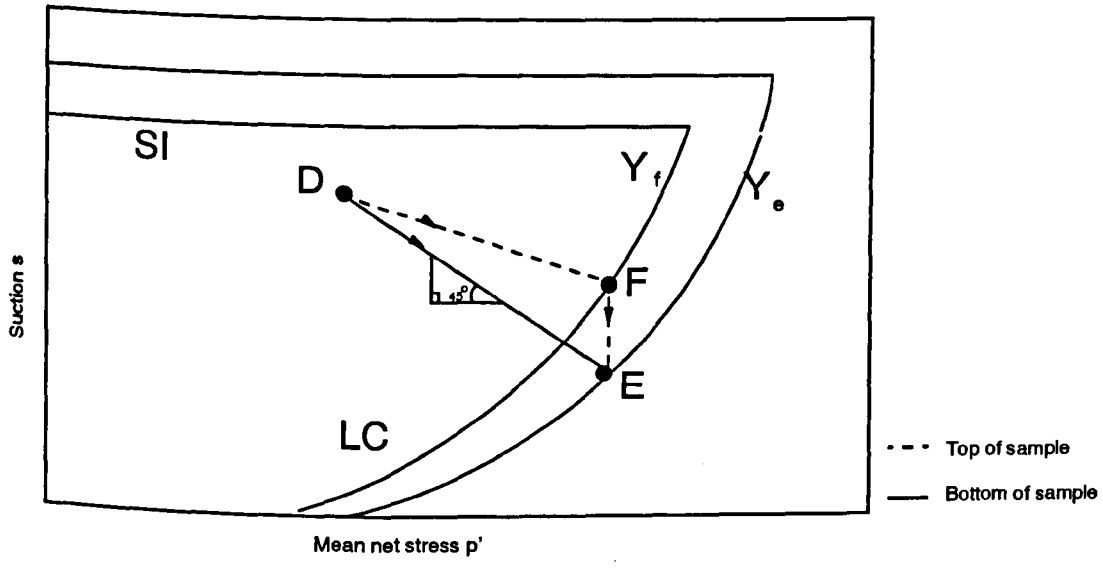

Fig (6.6) Stress paths for isotropic consolidation by step-decrement of pore air pressure

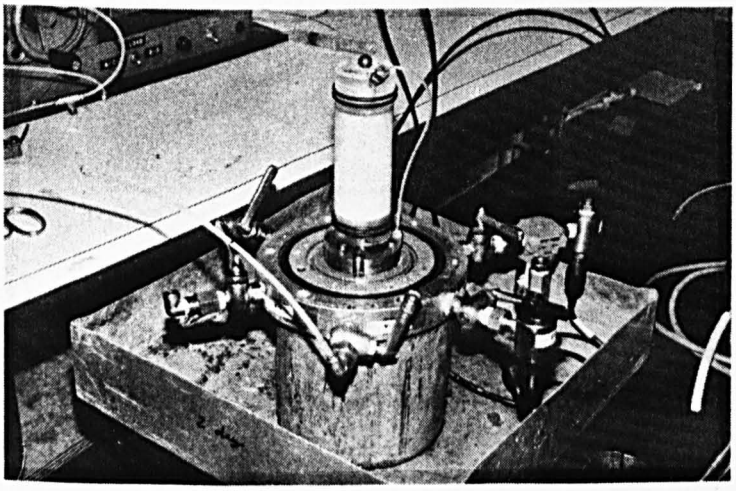

Photo (6.1) Mounting the sample on the pedestal

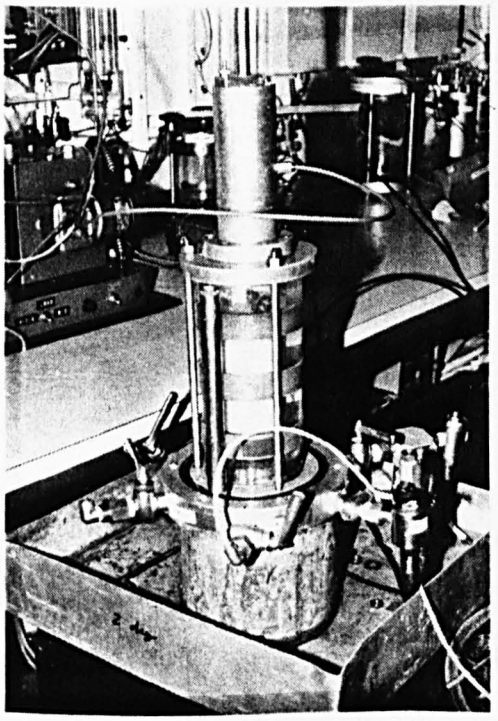

Photo (6.2) An assembled inner cell.

Test No. and type	EQUALIZATION		NORMAL COMPRESSION		TIME SPENT ON EACH TEST (weeks)
	s/ kPa	p'/ kPa	s/ kPa	p'/ kPa	
1A	200	50	200	150	2 *
2A	200	50	200	100	4
3A	200	50	200	200	4
4A	200	50	200	150	4
5A	200	50	200	300	6
6B	200	50	200	100	5
7B	200	50	200	200	4
8C	200	50	200	150	5
9C	200	50	200	100	5
10A	100	50	100	150	4
11B	100	50	100	100	5
12B	100	50	100	200	5
13C	100	50	100	150	5
14A	300	50	300	50	4 *
15A	300	50	300	250	4
16B	300	50	300	100	5
17C	300	50	300	100	5
18C	300	50	300	150	5
19A	0	35	0	175	4
20A	0	35	0	200	4
21B	0	35	0	55	4
22B	0	35	0	100	5
23B	0	35	0	200	5
24C	0	35	0	150	5
25C	0	35	0	150	5
26C	0	35	0	75	5
27D	100	50	100	100	5
28D	200	50	200	100	5
29E	100	50	100	150	4
30F	200	50	200	125	5

Types of shearing test
A: Constant volume, constant suction
B: Constant mean net stress, constant suction
C: Fully drained, constant suction
D: Constant water content, rising suction
E: Constant volume, rising suction
F: Constant mean net stress, falling suction

* Shearing stage not conducted

Table (6.1) Test numbers, stress conditions during equalization and compression and time taken for each test.

CHAPTER 7

EXPERIMENTAL RESULTS

CHAPTER 7

EXPERIMENTAL RESULTS

This chapter contains the experimental results obtained in the research, together with a brief initial discussion of the results.

7.1 EQUALIZATION

Before each sample was isotropically consolidated to a virgin state, it was allowed to equalize at a mean net stress of 50 kPa and the required value of suction (zero, 100, 200 or 300 kPa). The exception was the test series conducted at zero suction, where equalization took place at a mean net stress of 40 kPa (see Section 6.3.2).

Figs (7.1a) and (7.1b) show the changes in water content during the equalization stage plotted against the square root of time for all tests. In each case water flowed into the sample so that the water content of the sample increased during the equalization stage (suggesting that the suction present after compaction was greater than 300 kPa). As expected, the increase in water content was greatest for tests where the applied suction was lowest. The increase in water content was approximately 2.5% when the applied suction was 300 kPa and approximately 19% when

the applied suction was zero.

The shapes of the equalization curves shown in Fig (7.1) were very consistent for all tests. The initial part of each curve was almost linear (with the changes of water content plotted against square root of time) and the curve then flattened and approached an asymptotic value as equalization progressed. There was slight non-linearity in the very first part of most curves and this may have been due to improper contact between the sample and the high air entry filter as a result of the fuse wire technique (see Section 4.11.4). The variation of the water content with time during the equalization stage clearly fell into a narrow band for each value of suction, except for three tests at suction value of 200 kPa. In three of the tests conducted at a suction of 200 kPa there was a considerable lag in the flow of water into the sample, in the early part of the equalization stage. These three tests were all performed early in the test programme and the discrepancy may reflect unintentional variation in test procedure (for example, incomplete de-airation of the high air entry filter), before the procedure was perfected. However, even in these three anomalous tests, the final changes in water content (at the end of the equalization stage) were very repeatable and entirely consistent. This provides confidence that the sample preparation technique and the resultant soil fabric was repeatable.

In those tests where the applied suction was zero, it was difficult to estimate precisely the net volume of water that actually flowed into the sample, because a substantial amount of water flowed out into the air line connected to the top of the sample (starting to emerge approximately 6 days after the beginning of the equalization stage). To correct for this effect the amount of water collected from the air line was measured at the end of equalization and the assumption was then made that the rate of flow into the air line was constant from the time that water was first observed in the line. The amount of water collected from air line was proportionally deducted from the inflow of water recorded by the water volume change unit.

Figs (7.2a), (7.2b) and (7.2c) show the changes in the specific volume during the equalization stage for tests conducted at suction values of zero, 100, 200 and 300 kPa. The results have been presented in three separate plots in order to highlight the small variations in the behaviour of tests conducted at different values of suction.

Inspection of Fig 7.2 indicates that there appear to be at least two parts to each equalization stage: (a) "immediate" reduction in volume upon the initial application of mean net stress and (b) swelling during subsequent equalization, as the suction fell from its initial very high value (after compaction) to its final value. In the tests at zero suction (and to a lesser extent those at a suction of 100

kPa) there was a third stage, with a final reduction in volume (collapse) during the later part of equalization. In all tests, final equalization was reached within 5 to 6 days of starting the equalization stage.

The amount of initial compression that took place during the application of mean net stress was approximately the same in all tests (Δv= -0.01 to -0.015) , as would be expected. However the amount of subsequent swelling and (where applicable) collapse was, strongly dependent on the applied change of suction. When the applied suction was zero, the changes of specific volume during swelling was approximately Δv=+0.03. The amount of swelling reduced as the applied suction increased. When the applied suction was zero the final collapse of the samples was given by approximately Δv=-0.08. A much smaller amount of collapse (approximately Δv=-0.01) was observed when the applied suction was 100 kPa, and no sign of collapse behaviour was observed at applied suctions of 200 and 300 kPa.

The behaviour observed during the equalization stage can be explained by reference to the LC yield curve proposed by Alonso, Gens and Josa (1990). Fig(7.3) shows the position of the yield curve produced by the initial compaction process and the stress paths adopted during the equalization stage. Paths AB_oC_o, ABC_1, ABC_2 and ABC_3 were adopted during the equalization of samples at applied suctions of zero, 100, 200 and 300 kPa respectively. A

reduction in suction causes swelling of unsaturated soil when the stress path remains within the elastic region whereas collapse is caused when the yield curve is reached. Inspection of Fig7.2 suggests that the yield curve produced by the compaction process passed outside points C2 and C3 in Fig 7.3 (because no collapse occured in the tests with s= 200 kPa or s= 300 kPa), just inside point C1 (because a small amount of collapse was observed in tests with s= 100 kPa) and well inside point CO (because there was a larger amount of collapse in the tests with s = 0). Fig 7.3 also explains why the amount of swelling (in the early part of equalization) was greatest for the test series with zero applied suction (because these tests had the greatest length of (swelling) test path inside the yield curve). The shape of the yield curve produced by the compaction process is examined further in Section 7.2.1.

In the tests with applied suction of zero, it was difficult to monitor the changes of water content during the equalization stage, because of the outflow of water into the air pressure line. However, the degree of saturation was expected to be 100 % at the end of equalization. The degree of saturation calculated from the wet weight of the sample measured at the end of the test showed the sample reached full saturation at the end of shearing (measured values of S_r ranged from 99.5 and 100.5%) but there was no guarantee that the sample was fully saturated during the equalization stage. Nevertheless the assumption was made

that the degree of saturation was 100% from the end of the equalization stage onwards and the water content and the degree of saturation were calculated based on this assumption and the measured specific volume of the sample.

Table 7.1 shows, for each sample, the specific volume, degree of saturation and water content at the end of the equalization, together with the corresponding values after compaction (prior to equalization). After compaction the specific volume was approximately 2.204 with a maximum variation of ±0.012, the degree of saturation was approximately 53.8% with a variation of ± 1.3% and the water content was approximately 24.42% with a variation of ±0.47%. The small variations in v, S_r and w provided evidence of the uniformity of the kaolin, the repeatability of the sample compaction procedure and the accuracy of the various measurement techniques.

After equalization the specific volume varied from 2.147 (at zero suction) to 2.228 (at suction of 200 kPa), the degree of saturation varied from 60.2% (at suction of 300 kPa) to 100% (zero suction) and the water content varied from 26.90% (at suction of 300 kPa) to 43.76% (at zero suction). At the end of equalization, the variation in the specific volume was approximately ±0.008 (at 300 kPa suction), ±0.013 (200 kPa suction), ±0.010 (100 kPa suction) or ±0.012 (zero suction). The variation in water content was approximately ±0.25% (at 300 kPa suction),

±0.54% (200 kPa suction), ±0.24% (100 kPa suction) or ±0.45 (zero suction). These figures were very similar to the corresponding variations prior to equalization, suggesting that no major sources of additional variability were introduced during equalization. In fact the very slight improvement in variability may indicate a tendency for slight variations between samples produced by the compaction process to be partially eliminated during subsequent equalization.

One additional piece of information gathered from the tests at zero suction was the permeability of saturated compacted kaolin. The pore pressure at the top of the sample was maintained at 35 kPa while the pore water pressure at the bottom of the sample was maintained at 50 kPa. This caused a vertical hydraulic gradient of 15 and created a constant upward flow once the sample became fully saturated. The final (equilibrium) value of flow rate in at the base of the sample and out at the top via the air line, was approximately 3 cm^3 per day. The area of the sample was approximately 0.00196m^2 and the calculated permeability (based on the average of 5 tests) was therefore approximately $7.8*10^{-6}$ m/s (with a variation of ±10%).

As a check, the measured value of permeability k was used to calculate an independent value of coefficient of consolidation c_v:

$$c_v = \frac{k}{m_v \gamma_w} \qquad (7.1)$$

where m_v was the compressibility and γ_w was the unit weight of water. Two alternative values of m_v were calculated based on the slopes of the normal compression line $\lambda(o)$ and swelling line κ, because it was unclear whether it was appropriate to consider an elastic or a plastic value of compressibility. A value of 0.11 was taken (see Section 7.2.1) for $\lambda(o)$ and a value of 0.04 (equivalent to swelling gradient for saturated reconstituted kaolin) was taken for κ. The values of c_v calculated from Equation (7.1) was $3.7*10^{-8}m^2/s$ when considering $\lambda(o)= 0.11$ and $10.3*10^{-8}m^2/s$ when considering $\kappa = 0.04$. The c_v value calculated from the equalization stages of the step-loading tests was approximately $7.2*10^{-8}m^2/s$. This value fell between the two possible values calculated from Equation 7.1, suggesting that it was at least of the correct order of magnitude.

7.2 CONSOLIDATION

7.2.1 Main test series

Fig 7.4 shows the variation in specific volume v with mean net stress p' during ramped consolidation (with p' on a logarithmic scale). However the curves shown in Fig 7.4 are not quite perfect constant suction consolidation plots, because of non-equalization of pore water pressure u_w during ramped consolidation. This slight lack of

equalization is demonstrated by the small vertical step at the end of each curve, corresponding to complete equalization of pore water pressure to the water back pressure value during the 24 hour rest period at the end of ramped consolidation.

For each test shown in Fig 7.4, there was a clear indication that the soil started to yield as the mean net stress was increased. The yield point at a given value of suction was identified by a marked change in the slope of the continuous plot of specific volume against the logarithm of mean net stress. The value of the yield stress increased as suction increased.

The consolidation data for tests conducted at zero suction (shown in Fig 7.4) show a slightly different pattern, during the early part of consolidation because of the non-standard procedure that was employed during the equalization stage. During equalization the water back pressure applied at the base of the sample was 50 kPa, but in order to ensure full saturation, the air back pressure applied at the top of the sample was slightly lower at 35 kPa (see Section 6.3.2). During equalization water began flowing from the sample into the air drainage line, implying that the pore water pressure at the top of the sample was 35 kPa once the sample became fully saturated. Ramped consolidation was started immediately after closing the air drainage line at the end of the equalization stage

and no time was left between the end of equalization and the beginning of ramped consolidation. Therefore the pore water pressure in the upper part of the sample must have risen from 35 kPa to 50 kPa (the value of water back pressure applied at the base of the sample) during the early part of the ramped consolidation stage. The sample therefore swelled very slightly during the initial part of the ramped consolidation stage (see Fig 7.4) because the application of cell pressure was very slow compared to the rate at which the pore water pressure would have risen to 50 kPa at the top of the sample. This swelling and the non-uniform stress conditions throughout the sample meant that the value of yield stress indentified for tests at zero suction was possibily less accurate than for tests at higher values of suction.

Fig (7.5) shows the yield stress values taken from Fig(7.4) plotted against the suction. The values of yield stress were calculated by using Casagrande's graphical construction (Craig 1987). The values of yield stress calculated at a given suction showed very little variation (about ±5 kPa). This suggested that the compaction process produced very repeatable samples.

The yield points for suction values of 100, 200, and 300 kPa shown in Fig (7.5) have been joined to give the yield curve produced by the compaction process. The qualitative form of this yield curve is consistent with the model

proposed by Alonso, Gens and Josa (1990). The yield points from the tests at zero suction were probably on a different yield curve, because significant collapse occurred during the equalization stage (suggesting yielding and expansion of the LC yield curve).

Fig (7.6) shows the variation in water content during the ramped consolidation stage for some typical tests conducted at the 4 different values of suction (zero, 100, 200, and 300 kPa). For tests conducted at a suction of 200 or 300 kPa, a small amount of water flowed into the sample during ramped consolidation. For tests conducted at a suction of 100 kPa initially a small amount of water flowed into the sample , but the flow direction then reversed as the mean net stress increased. However, for all tests conducted at suctions of 100, 200, and 300 kPa, the total changes of water content during ramped consolidation were less than 0.5%. For tests conducted at zero suction (saturated conditions) the water would, of couse, be expected to flow out of the sample during consolidation. However Fig (7.6) shows a slight flow into the sample during the first part of the consolidation stage. This was presumably due to initial swelling of the upper part of the sample as the pore water pressure rose from 35 kPa to 50 kPa (see above).

In the tests conducted at zero suction (saturated conditions), the flow of water from the sample would be expected to equal the reduction of the sample volume.

However a difference between the sample volume change and the water volume change was noted (see Fig 7.7) (the water volume change was less than the sample volume change). This difference could have been caused either by incomplete saturation of the sample during the equalization stage or by air still trapped in the air line and the low air entry filter. Similar behaviour was noted during the ramped consolidation stage of each test conducted at zero suction.

Fig (7.8) shows the value of specific volume v at the end of consolidation (for all tests) plotted against the corresponding value of mean net stress p', with p' on a logarithmic scale. The values of specific volume and water content at the end of ramped consolidations are set out in Table 7.2. The maximum variation in the specific volume at a given combination of mean net stress and suction was approximately ±0.013. The variation in the specific volume therefore remained approximately unchanged from the start of the equalization stage to the end of the consolidation stage.

For each value of suction the data points in Fig 7.8 defined a normal compression line that can be represented by a linear equation:

$$v=N(s)-\lambda(s)\ln\left(\frac{p'}{p_a}\right) \qquad (7.2)$$

To make the expression dimensionally consistent, and also to minimise the error in the evaluation of N(s),

atmospheric pressure p_a (assumed as 100 kPa) has been introduced in Equation 7.2. If the intercept N(s) was evaluated at p'=1 kPa then the value of N(s) would be very susceptible to any small error in the slope $\lambda(s)$. Therefore the values of N(s) were calculated when p' was 100 kPa.

Both the slope $\lambda(s)$ and intercept N(s) of the normal compression hyper-line were found to be functions of suction, as shown in Fig (7.9) and Fig (7.10) respectively. N(s) increased with increasing suction whereas the slope $\lambda(s)$ decreased with increasing suction (for suction greater than 100 kPa). This behaviour was consistent with the model proposed by Alonso, Gens and Josa (1990). Unexpectedly, the slope $\lambda(s)$ appeared to decrease sharply as the suction was reduced to zero (see Fig 7.9). This behaviour was inconsistent with the proposals of Alonso, Gens and Josa (1990). It is possible that $\lambda(s)$ increased with decreasing suction right down to zero suction and there was then a discontinuity in the value of $\lambda(s)$ corresponding to the change from unsaturated to saturated conditions.

The normal compression line for zero suction fell considerably below the corresponding normal compression line for reconstituted saturated kaolin (see Fig 7.8). Also, the slope of the compression line for saturated compacted kaolin was considerably less than the slope of the compression line for saturated reconsituted kaolin.

Fig 7.11 shows, for all tests, the water content at the end of consolidation plotted against the mean net stress p' (with p' on a logarithmic scale). For the tests conducted at zero suction the water content was calculated from the sample volume change by assuming that the sample was fully saturated at the end of consolidation. This assumption was made because of the difficulty in estimating the volume of water that had flowed into the air drainage line and the top porous stone during equalization and consolidation. The maximum variation in the water content at any given combination of suction and mean net stress was approximately ±0.36% ie approximately the same as the variation found before and after the equalization stage.

For each value of suction the data points in Fig (7.11) defined a normal compression line that can be represented by a linear equation:

$$w=A(s)-\alpha(s)\ln\left(\frac{p'}{p_a}\right) \qquad (7.3)$$

Atmospheric pressure p_a has again been introduced to make the expression dimensionally consistent and to minimise the error involved in estimating the values of the intercept A(s). The variation of the slope $\alpha(s)$ and intercept A(s) with suction are plotted in Fig (7.12) and Fig (7.13) respectively. The intercept A(s) decreased steadily with increasing suction. The slope $\alpha(s)$ also decreased sharply as suction was increased from zero. The normal compression line became approximately horizontal ($\alpha(s) = 0$) as suction

reached 200 kPa and the slope was negative at a suction of 300 kPa.

7.2.2 Step-loading tests

The step-loading tests were conducted before the main test series by adopting a diagonal consolidation path with falling suction (see Section 6.5). The results from the three tests are presented in Figs (7.14) and (7.15).

Fig (7.14) shows the specific volume v plotted against the mean net stress p' (with p' on a logarithmic scale). The solid lines and the individual data points show the reduction in suction during each test. For example, Test S1 started at a mean net stress of 100 kPa and suction of 200 kPa and finished at a mean net stress of 200 kPa and suction of 100 kPa. Also shown , for comparison, as dashed lines in Fig 7.14 are the constant suction normal compression lines identified from the main test series.

At first sight values of specific volume obtained in the step-loading tests showed reasonable agreement with the corresponding normal compression lines established in the main test series (constant suction ramped consolidation). On closer inspection however the values of the slope $\lambda(s)$ of a constant suction normal compression line that would have been obtained by joining together the relevant data points from the step-loading tests were significantly lower than the values obtained from the main test series (see Fig

7.14). It was unclear whether this was due to measurement error, non-equalization of pore water pressure during consolidation or dependency of soil behaviour on consolidation method.

Fig 7.15 shows the water content w from the step loading consolidation tests plotted against the mean net stress p' (with p' on a logarithmic scale), together with the corresponding normal compression lines for constant suction from the main test series. Again values of water content from the step-loading tests appear on first inspection to agree reasonably well with the normal compression lines from the main test series, but closer inspection shows that the step-loading tests produced lower values of w than the main test series at suctions of 100 and 200 kPa.

7.3 SHEARING

7.3.1 Loading ram friction

Friction between the linear bearings and the loading ram caused difficulties during the shearing stage of several tests. This problem occurred only in System A and there was no indication of problems in System B. 4 of 18 tests conducted with System A were noticeably affected by friction on the loading ram (Tests 1A, 15A, 20A and 22B,)

Test 1A was aborted at the start of the shearing stage when it was realised while bringing the loading ram into contact

with the sample that there was substantial friction on the loading ram. The linear bearings were immediately removed and a visual inspection showed evidence of rust on the ball bearings . The linear bearings were therefore replaced.

In tests 15A, 20A and 22B (which were conducted much later in the test sequence) the shearing stages were completed, but the stress-strain curves showed marked fluctuations of measured deviator stress (see Fig 7.16), unlike the smooth stress-strain curve normally observed (see Section 7.3.3 below). In Test 20A substantial friction was also noted when bringing the loading ram into contact with the sample at the start of the shearing. After each of these tests, inspections indicated rust on the bearings and slight pitting of the loading ram surface (particularly after Test 20A) . The bearings were cleaned after Tests 15A and 22B and replaced for a second time after Test 20A (tests were not necessarily conducted according to the order of the test numbers). The loading ram surface was smoothed after Tests 20A and 22B. The problems with rust on the bearings were thought to occur because of the need to assemble the triaxial cell under water in order to achieve complete de-airing (see Section 4.3.1). Regular oiling of the bearings was performed in an attempt to minimise the difficulties.

Four criteria were considered when deciding whether or not to use the results of tests affected by ram friction: (a)

whether friction had been noticed before the start of the shearing stage (when the loading ram was brought into contact with the sample): (b) whether the stress-strain curve indicated the occurrence of ram friction throughout the shearing stage or only part of the stage; (c) the apparent magnitude of the friction (assessed from the fluctuation of the stress-strain curve) as a percentage of the deviator stress at failure; and (d) the degree of rusting and pitting observed in the final visual inspection of the linear bearings and the loading ram. The decision was taken to include the results from Test 15A in the analysis because there was no indication of friction when the shearing stage was started, the sample had almost reached a critical state before substantial fluctuations of the stress-strain curve were observed, the estimated friction was just 5% of the final deviator stress and there was very little indication of rust or pitting from the inspection of the bearings and loading ram. Tests 20A and 22B were considered to be more severely affected by ram friction and the results of the shearing stage of these tests were not included in subsequent analysis.

7.3.2 Quality of test control

In all 6 types of shearing stage described in Section 6.1.2 at least one state variable was externally controlled to maintain a constant value (except in test type D, where the water content was maintained constant just by closing the

drainage valve).

In test types A, B and C the suction applied to the sample was held constant throughout the shearing stage. The suction was maintained constant by increasing or decreasing the pore air pressure and pore water pressure by equal amounts. Fig (7.17) shows three typical test results (2A, 7B and 9C) obtained in tests where the suction was held constant. The fluctuation in the suction was approximately ±2 kPa. The trigger levels of ±0.5 kPa set in the control program (see Section 6.2.2) are also marked in Fig (7.17). The fact that the fluctuations were greater than the specified trigger levels was attributed to time lag in the stepper motors. However the level of control actually achieved (±2 kPa) was considered acceptable.

In test types A and E the volume of the sample was held constant throughout the shearing stage. The volume of the sample was maintained constant by increasing or decreasing the pore air pressure (and the pore water pressure by the same amount in test type A). Fig (7. 17) shows two typical test results (2A and 29E) obtained in tests where the volume of the sample was held constant. The fluctuation of specific volume was within the trigger limits of ±0.0003 specified in the control program.

In test types B and F the mean net stress was held constant. The mean net stress was held constant by

increasing or decreasing pore air pressure (while also controlling pore water pressure). Fig (7.17) shows typical test results (6B and 30F) where the value of the mean net stress was maintained constant. The trigger levels set in the control program were ±0.5 kPa, but the actual fluctuations were typically ±1 kPa.

In test type D the water content of the sample was maintained constant. There was no control software needed to maintain the water content of the sample constant because this particular test condition was achieved simply by closing the water drainage valve.

7.3.3 Stress-strain behaviour

All samples tended towards a critical state at the end of shearing with mean net stress p', deviator stress q, suction s, specific volume v and water content w all either constant or changing only very slowly. In the constant suction shear tests (types A, B, and C) and the constant mean net stress, falling suction shear test (type F) water content was still changing at a very slow rate at the end of each test. In the constant water content, rising suction shear tests (type D) the suction was still changing slightly at the end of each test. In the constant volume, rising suction shear tests (type E) both suction and water content were changing at a slow rate at the end of shearing. If the water content or the suction failed to

stabilise completely, the final recorded value of w or s was taken as the critical state value.

Fig (7.18) shows the stress and strain data for the constant volume, constant suction shear tests (type A). All state variables except water content w reached a critical state at an axial strain of about 12 to 14 % (although very little increase in the deviator stress was observed beyond a strain of 8%). Water content w continued to increase slowly until the tests were terminated, although it should be appreciated that the total changes of water content shown in Fig 7.18 are relatively small (1 to 2 %).

Fig (7.19) shows the stress-strain behaviour for a constant volume, constant suction shear test (type A) conducted at at zero suction (Test 19A). Unfortunately Test 19A, had to be terminated prematurely at an axial strain of 8% because of failure of the pressure supply. However the sample appeared to be close to a critical state when the pressure supply failed, and the final recorded values were therefore taken as representative of the critical state. Considerable differences in behaviour were noted compared with the remaining type A tests conducted at higher values of suction:

(a) the fluctuation of the pore water pressure was much higher than the fluctuation of pore water pressure and pore air pressure observed in the other

type A tests. This could be because the volume of the saturated sample showed much greater time lag in responding to applied pore pressure changes than the corresponding unsaturated samples (in which compression of the air phase allowed almost instantaneous response).

(b) Although Test 19A was a constant volume shear test conducted at zero suction (saturated conditions) a substantial amount of water (approximately 3 cm^3) flowed into the sample during shearing. This indicated the possibility of trapped air in the air line or in the top porous stone. However, as with all tests conducted at zero suction, the variation of water content during shearing was calculated from the measured volume change (zero for a constant volume test) and an assumption of 100% degree of saturation.

Fig (7.20) show the stress and strain data for constant p' constant suction tests conducted at suctions of 100, 200 and 300 kPa. In all tests the deviator stress q and specific volume v reached critical state values at an axial strain of about 25 to 30 % , but the water content w continued to change at a slow rate.

Fig (7.21) show the stress and strain data for 2 constant p' constant suction tests conducted at zero suction (Tests

21B and 23B), which showed noticeably different results from those conducted at higher suctions. Unfortunately Test 23B could not be completed due to failure of the pressure supply system. A peak deviator stress and dilation at the end of the shearing were clearly evident in Test 21B and there was some evidence of similar behaviour in the prematurely terminated Test 23B. The pore water pressure u_w also fell from a peak to a critical state value in Test 21B. The difference between the peak and critical state values of deviator stress in Test 21B was about 15 % of the peak deviator stress. There was no evidence of a shear plane at the end of shearing. It appeared that the highest rate of dilation occurred approximately when the peak deviator stress occurred.

Fig (7.22) show the stress and strain data from fully drained, constant suction tests (type C) conducted at suctions of 100, 200 and 300 kPa. The deviator stress q, mean net stress p' and specific volume v all reached a critical state at an axial strain of about 30-35%, although water content w was still increasing slowly when the tests were terminated.

Fig (7.23) shows the stress and strain data for 3 fully drained constant suction tests (type C) conducted at zero suction. A distinctly different stress-strain behaviour was observed to that seen in the equivalent tests conducted under higher values of suction. There was evidence of a

peak value of deviator stress followed by a small reduction to a critical state value. The volumetric strain showed a similar pattern. Unfortunately Test 24C was terminated soon after reaching the peak, because up to this point in the test programme all tests had approached the critical state condition without an earlier peak. However the error caused by this early termination of Test 24C was probably small, because the differences between peak and critical state values were small. Although the deviator stress in Test 25C and 26C was apparently falling towards a final steady state value, the sample failed on a distinct shear plane before the final critical state was achieved. However it appeared that the critical state deviator stress would not be substantially lower than the peak deviator stress. Therefore the critical state deviator stress was taken as the deviator stress just before the appearance of a shear plane. The volume of samples initially reduced (compressed) and then dilated toward the critical state. The critical state values of specific volume were again taken as the specific volume just before the appearance of a shear plane. The amount of post peak dilation was small compared to the earlier compression. Therefore the error in estimating critical state values of specific volume was again thought to be small.

Fig (7.24) show the stress and strain data for three tests conducted with constant water content, rising suction shearing (type D). The deviator stress q and specific

volume v reached critical state values at an axial strain of about 30-35 % (similar to the fully drained tests type C), but the pore water pressure continued to drop so that the suction was still increasing at a slow rate when the shearing stage was terminated. In one test (28D) there was evidence of a shear plane, and therefore the deviator stress and the specific volume just before the shear plane appeared were taken as critical state values.

Fig (7.25) shows the stress and strain data for a single constant volume, increasing suction shear test (type E). The observed behaviour was slightly different from the other constant volume tests conducted at constant suction (Type A). The deviator stress continued to increase at a slow rate, while the suction reached a peak value of about 235 kPa and then gradually fell. The water content of the sample initially reduced, as the suction increased rapidly, but later the water content started to increase. The critical state values of deviator stress or suction could not be identified. Also the water content continued to increase at a slow rate when the test was terminated.

Fig (7.26) show the stress and strain data for a single constant mean net stress, falling suction shear test (type F). The behaviour was very similar to the constant mean net stress tests conducted at constant suction (type B). The suction stopped falling when the deviator stress reached a critical state (because of the method of test

control, see Section 6.1.2). The deviator stress q, specific volume v and suction s all reached a critical state at an axial strain of about 25%, but the water content continued to fall at a slow rate when the test was terminated.

In all tests, the stresses changed very rapidly during the early part of the shearing stage. This was most marked in the constant volume, constant suction tests (type A), where the deviator stress increased to approximately 50% of its critical state value within the first 1% of axial strain. The increases of pore air pressure and pore water pressure within the first 1% of axial strain were also about 50% of the total changes to the critical state values. At the other extreme, in the fully drained tests and constant water content tests (type C and D) the deviator stress increased by about 15 % of its critical state value within the first 1% of axial strain. The rates of increase of the deviator stress, pore air pressure and pore water pressure were therefore excessively high during the early stages of shearing, particularly in the constant volume tests. This was because tests were conducted with strain control rather than stress control. This could have been avoided by selecting a much slower strain rate in the early part of the shearing stage and increasing the speed in the later part of the stage, but this was not feasible with the triaxial frame used in the testing programme.

The repeatability of stress-strain behaviour when conducting tests under similar stress conditions is very important when formulating any model of soil behaviour. The data from the consolidation stage suggested a high degree of repeatability under isotropic loading conditions (see Section 7.2.1 above). Only one repeat shearing test was conducted, under fully drained conditions at zero suction (Tests 24C and 25C). The stress-strain behaviour obtained in both tests was almost identical (see Fig 7.23) and the critical state deviator stress differed by only 3.5% in the two tests. The same behaviour was noted in the volume change of the two samples, where the maximum compression of the sample differed by only 2% in the two tests.

7.3.4 Test paths

Fig 7.27 shows the test paths for constant suction shear tests (type A, B and C) conducted at zero suction. Plots of q versus p', v versus p'(with p' on a logarithmic scale) and w versus p' (with p' on a logarithmic scale) are shown in Fig (7.27a) , Fig (7.27b) and Fig (7.27c) respectively. The plots include two fully drained tests, two constant mean net stress tests and one constant volume test. Similar test paths for the constant suction shear tests conducted at suctions of 100, 200 and 300 kPa are shown in Fig (7.28), Fig (7.29) and Fig (7.30) respectively.

In Fig (7.27) to Fig (7.30) the initial points on the

normal compression line are represented by open data points and the final critical state points are represented by closed data points. Inspection of Fig (7.27) to Fig (7.30) shows that the critical states for a given value of suction appear to lie on a unique critical state line that is independent of stress path adopted to reach the critical state.

Fig 7.31 shows the test paths for the shear tests in which suction varied (types D, E and F). The plots include three constant water content, rising suction shear tests (type D), one constant volume, rising suction shear test (type E) and one constant mean net stress, falling suction shear test (type F). The values of suction at the critical state are marked against the critical state data points for each test. Also shown in the same plots are the critical state lines and normal compression lines derived from the constant suction shear tests (taken from Fig 7.27 to 7.30).

Inspection of Fig (7.31a) to Fig (7.31c) shows that the critical state values of q, p', s, v and w in the variable suction shear tests of types D and F were entirely consistent with the critical state lines derived from the constant suction shear tests (types A, B and C). This provides further evidence of a unique critical state hyper-line for unsaturated soil, that is independent of the stress path followed to the critical state. However the critical state data from the constant volume, rising

suction test (Test 29E) were not consistent with the critical state lines derived from the other tests. In particular there was a large mis-match in the values of v, p' and suction (see Fig 7.31b). The reason for these discrepancies in Test 29E was that the stress path in this test moved inside the state boundary, and headed towards the equivalent of the Hvorslev surface (see Section 8.2.3 below). It is likely therefore that a true critical state was not reached (note that the deviator stress continued to rise, see Fig 7.25).

7.3.5 Critical state relationships.

Fig (7.32) shows critical state data of q plotted against p' for a total of 24 constant suction shear tests conducted at 4 different values of suction (zero, 100, 200 and 300 kPa). The critical state values of q for each value of suction appear to fall on a straight line given by the following equation:

$$q=M(s)p'+\mu(s) \qquad (7.4)$$

Where M(s) is the slope of the critical state hyper-line at a given value of suction and $\mu(s)$ is the intercept or the apparent cohesion caused by suction.

Fig (7.33a) shows the value of M(s) plotted against suction. It appears that the value of M(s) remained approximately constant and equal to about 0.93 for suction values of 100 kPa and over. M(s) reduced to about 0.81 as

the suction was decreased to zero. Escario and Juca (1989) reported a similar pattern of behaviour, with Φ' in Equation 2.16 increasing slightly with suction. There is the possibility of a discontinuity in the value of M(s) at s = 0 (corresponding to the transition from unsaturated to saturated conditions). The value of M for saturated reconstituted kaolin is approximately 0.95 (Richardson, 1988). Therefore the value of M(s) when suction was zero (saturated conditions) was significantly lower than the value for reconstituted kaolin. This suggests that the soil fabric produced by the compaction process continued to have a significant influence on soil behaviour, even after shearing to critical states.

Fig (7.33b) shows the value of the intercept $\mu(s)$ plotted against suction. $\mu(s)$ increased monotonically as the suction was increased, although not at a linear rate. This was consistent with the behaviour reported by Escario and Saez (1986), Gan, Fredlund and Rahardjo (1988) and Escario and Juca (1989), who reported that the value of Φ^b in Equation 2.16 decreased with increasing suction. These previous authors also reported that Φ^b was equal to Φ' when suction was zero (see Section 2.6). This means that the gradient $d\mu(s)/ds$ should be equal to M(s) when the suction falls to zero. Inspection of Fig (7.33b) shows that $d\mu(s)/ds$ was approximately equal to 0.8 when suction was zero and this was consistent with the value of 0.81 obtained for M(s) in tests conducted at zero suction.

Fig (7.34) shows critical state values of v plotted against p' (with p' on a logarithmic scale) for 24 constant suction shear tests conducted at 4 different values of suction (zero, 100, 200 and 300 kPa). The critical state values of v appear to fall on a unique critical state hyper-line (ie a unique line for each value of suction). The critical state lines for higher value of suction are curved and therefore cannot be parallel to the corresponding normal compression line at the same value of suction (see Fig 7.8). Critical state lines for different values of suction all appeared to merge into a single line at values of p' in excess of 200 kPa.

At zero suction, the critical state plot of v versus ln(p') was a straight line with a slope of 0.11, roughly equal to the slope $\lambda(s)$ of the normal compression line at zero suction (see Fig 7.8 and 7.9). This is consistent with the behaviour of reconstituted saturated soils. However the slope and position of the critical state line at zero suction were very different to those of the critical state line for saturated reconstituted kaolin (see Fig 7.34). This provides further confirmation of the significant influence of the soil fabric produced by compaction (even after shearing to critical states).

Inspection of Fig (7.34) suggests the existence of a unique critical state hyper-line relationship of the form postulated in Equation 3.16:

$$v=f(p',s) \qquad (7.5)$$

However, given the curvature of the lines in Fig 7.34 and the fact that the positions of the lines do not progress in a smooth sequence with increasing suction, the best form of the relationship is not immediately obvious. This question is discussed further in Section 8.1.2.

Fig (7.35) shows critical states values of w plotted against p' (with p' on a logarithmic scale) for 24 constant suction shearing tests conducted at 4 different values of suction (zero, 100, 200 and 300 kPa). It is interesting to compare Fig (7.35) with Fig (7.11) and to note that the critical state hyper-line lies above the normal compression hyper-line at suctions of 100, 200 and 300 kPa whereas, of course, the critical state hyper-line lies below the normal compression hyper-line at zero suction.

The critical state values of w appear to fall on a unique critical state hyper-line, that can be fitted by the following equation:

$$w=B(s)-\beta(s)\ln\left(\frac{p'}{p_a}\right) \qquad (7.6)$$

To make the expression dimensionally consistent and to minimise the error in the evaluation of the intercept B(s), atmospheric pressure p_a (assumed as 100 kPa) has been introduced in Equation 7.6. Both the intercept B(s) and the

slope $\beta(s)$ of the critical state hyper-line are functions of suction, as shown in Fig (7.36a) and Fig (7.36b). Both $B(s)$ and $\beta(s)$ decrease with increasing suction.

Equations 7.4 and 7.6 (derived from the constant suction shear tests were used to predict the critical state values of deviator stress and suction for the variable suction shear tests type D and critical state deviator stress and water content for the shear test type F. This involved combining the critical state relationships (Equations 7.4 and 7.6) with the relevant test conditions and the initial state of the sample at the start of shearing. Unfortunately it was not possible, at this point, to predict the corresponding critical state values of specific volume v, because the critical state relationship for specific volume (Equation 7.5) had yet to be fitted by a mathematical expression. For the same reason, it was impossible (at this stage) to predict any details of the critical state for the single type E test (Test 29E), because one of the test conditions in this variable suction test was that the specific volume was held constant. In any case, it was considered unlikely that Test 29E reached a critical state, because the stress path headed inside the state boundary hyper-surface (see Section 7.3.4).

Fig (7.37a) shows predicted versus measured values of deviator stress q at the critical state for Tests 27D, 28D, 1SD and 30F. Fig (7.37b) shows predicted versus measured

values of suction s for Tests 27D, 28D and 1SD. The predicted values of q are all within 90 to 105% of measured values and the predicted values of s are within 85 to 100% of measured values. In Test 29F the water content of the sample at the end of compression (just before shearing) was about 29.1% and it reached a critical state at a water content of about 33.3%. The predicted critical state water content of the sample in this test was 32.7%. This was a pleasing level of agreement and provided further support for the existence of a unique critical state hyper-line.

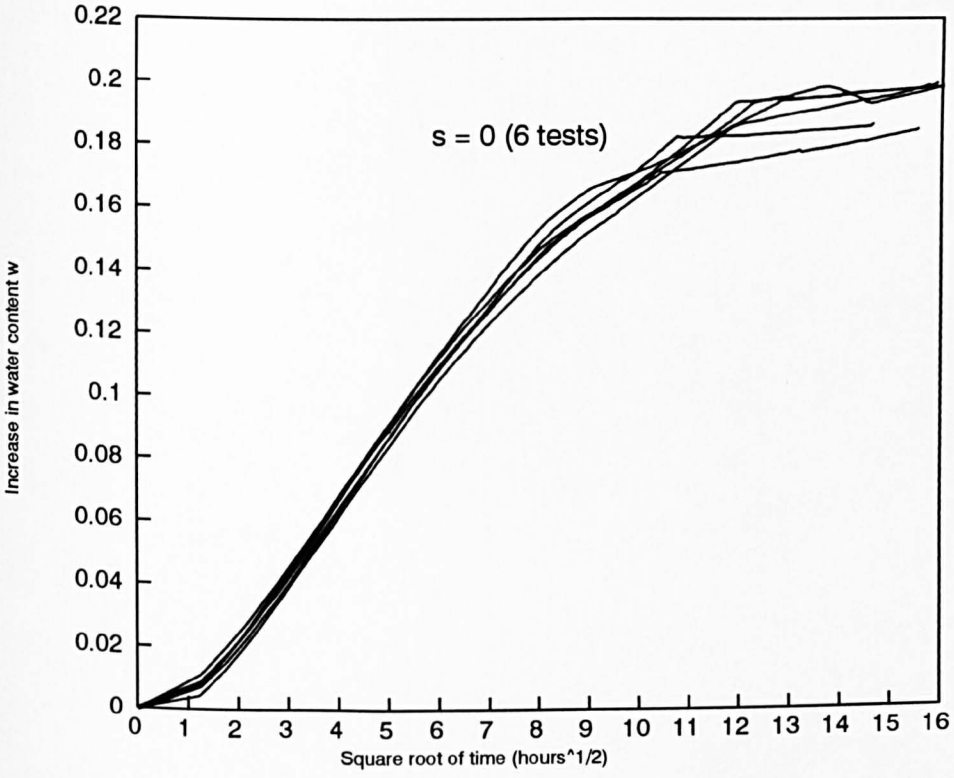

Fig (7.1a) Increase in water content during equalization stage
(Tests at zero suction)

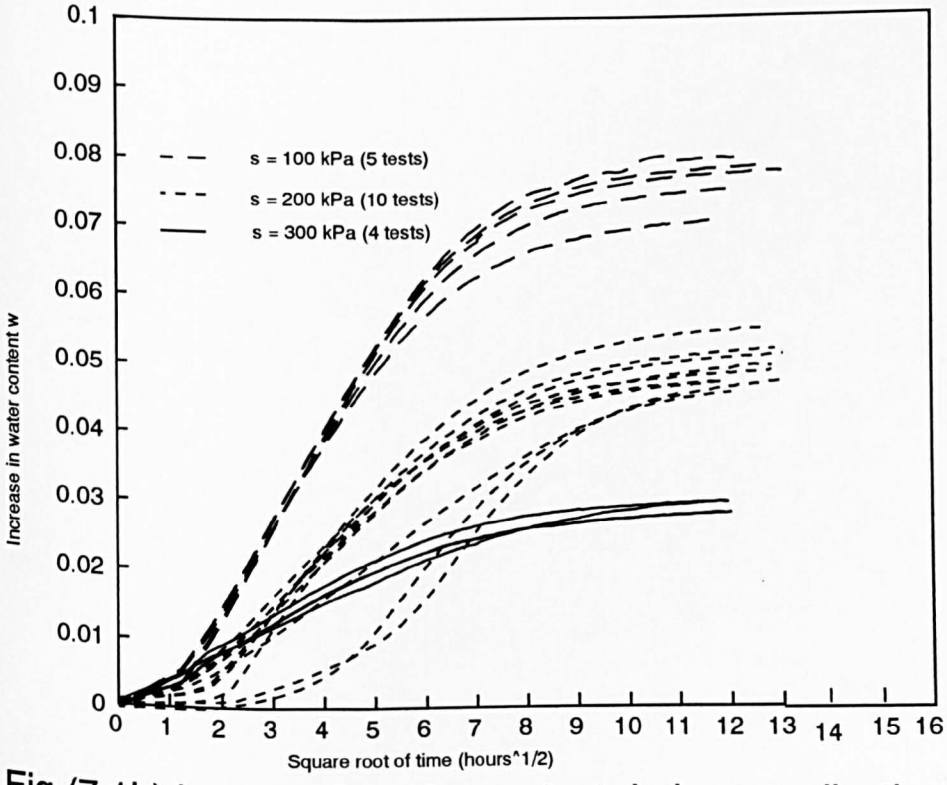

Fig (7.1b) Increase in water content during equalization stage
(Tests with s > 0)

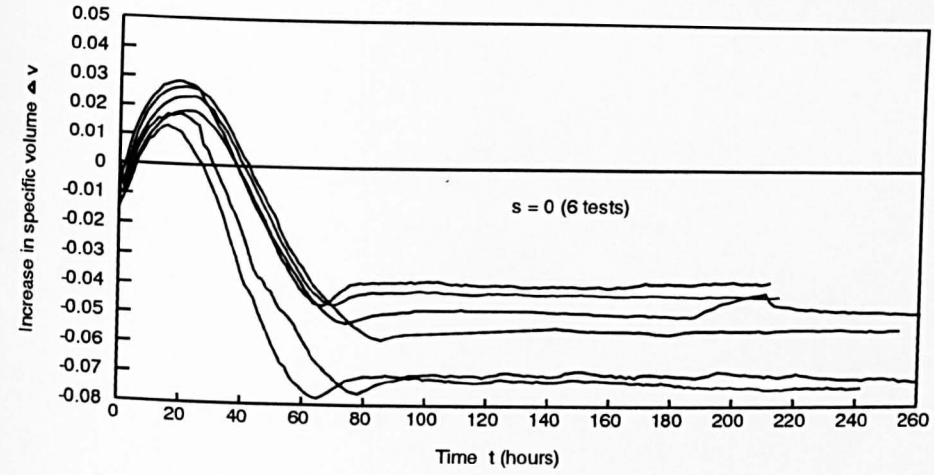

(a)

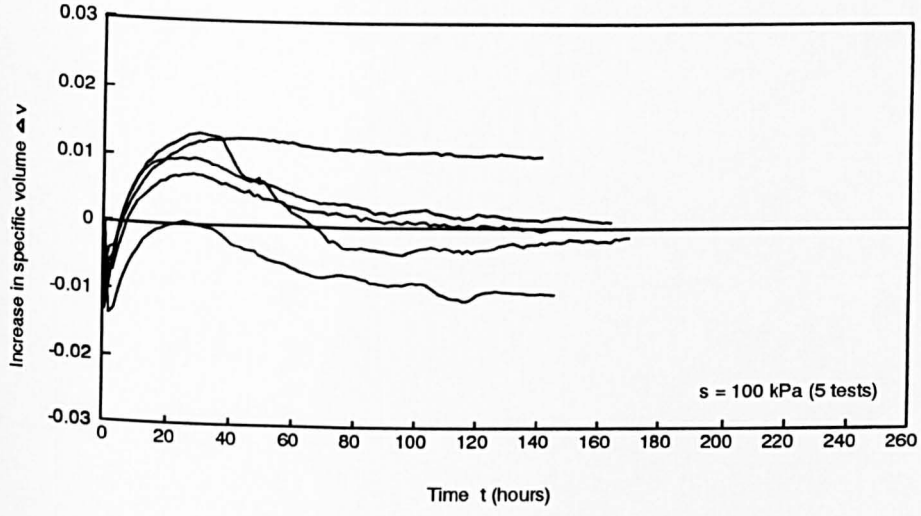

(b)

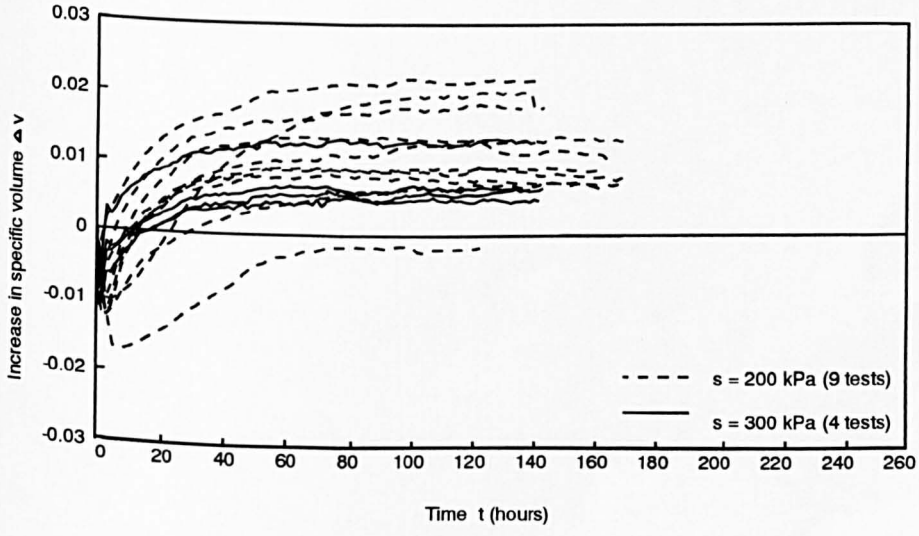

(c)

Fig (7.2) Change in specific volume during equalization

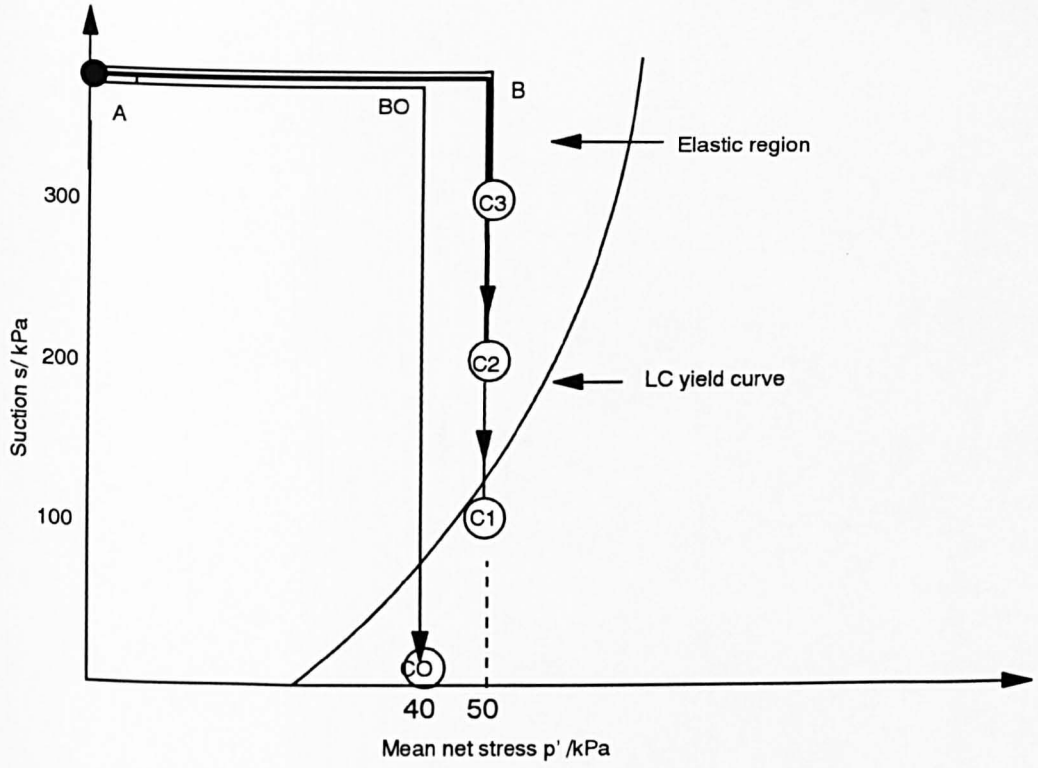

Fig (7.3) Stress paths during equalization

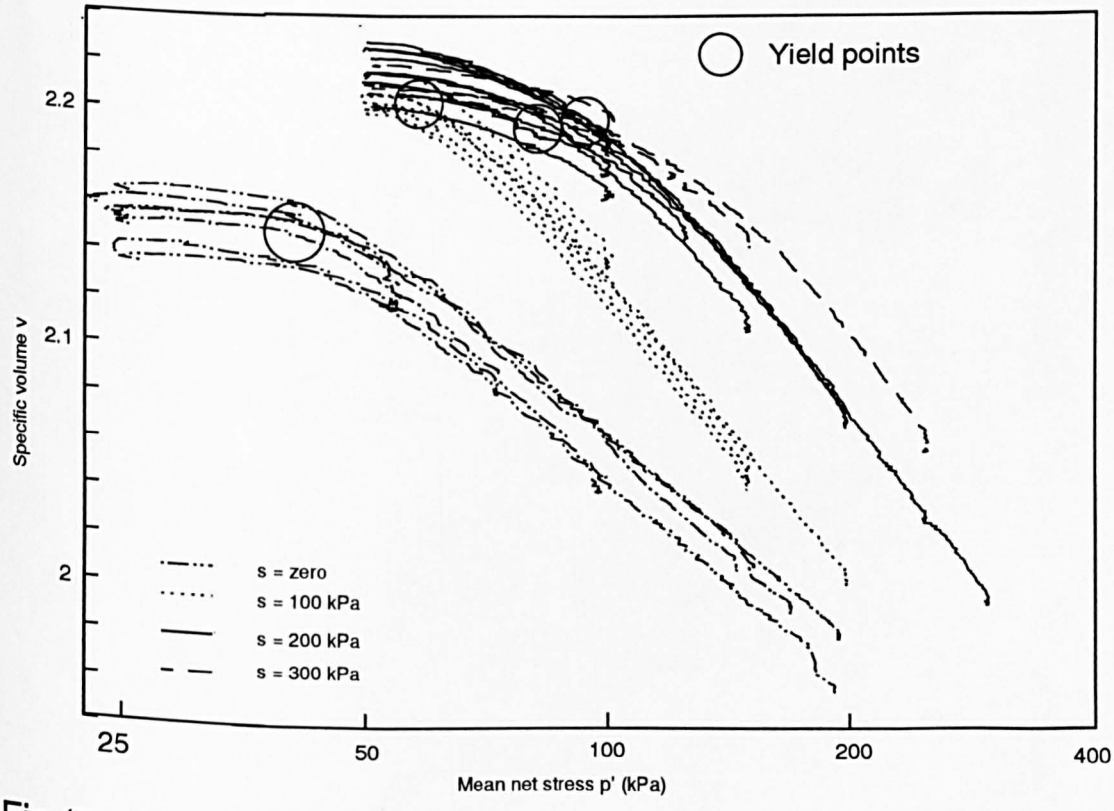

Fig (7.4) Variation in specific volume during ramped consolidation

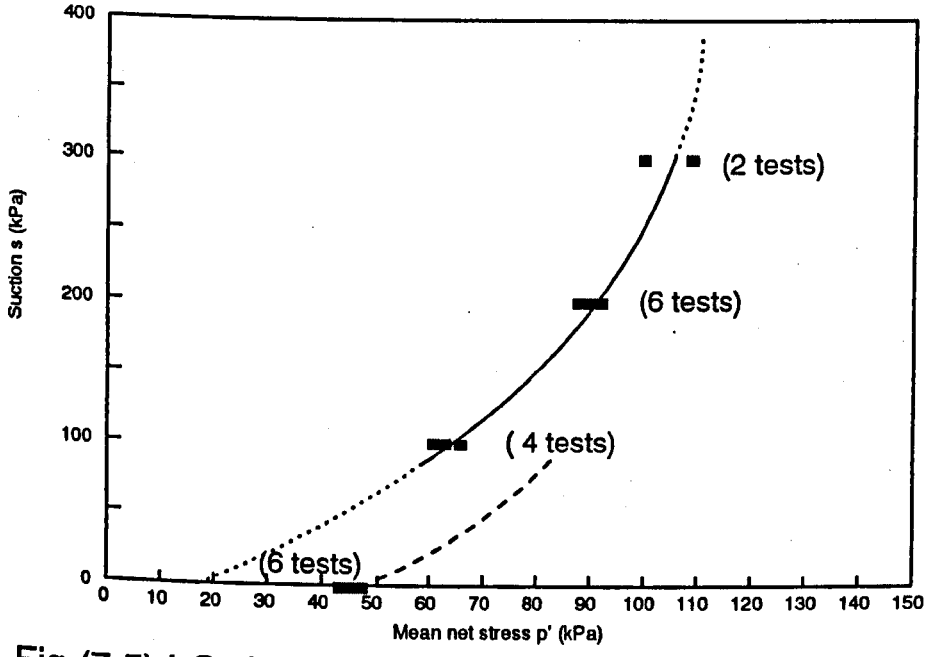

Fig (7.5) LC yield curve produced by initial compaction

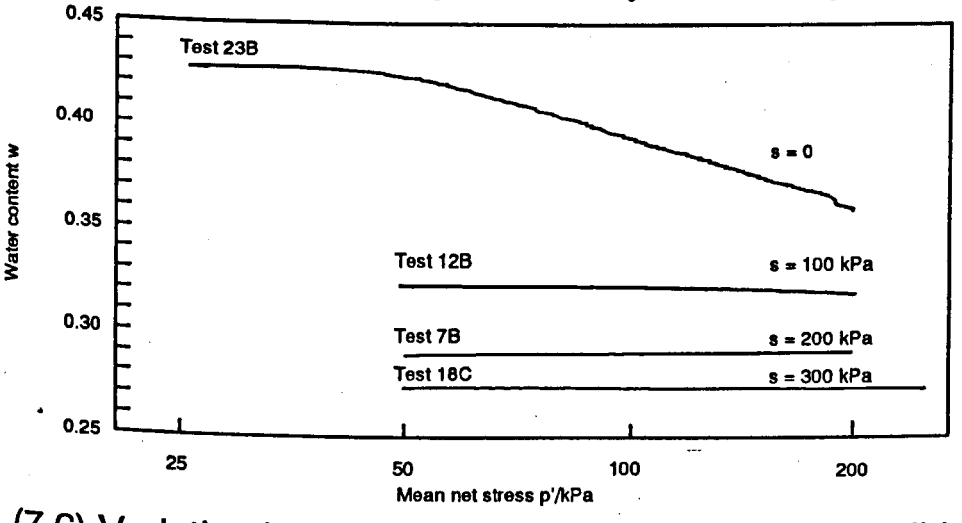

Fig (7.6) Variation in water content during ramped consolidation

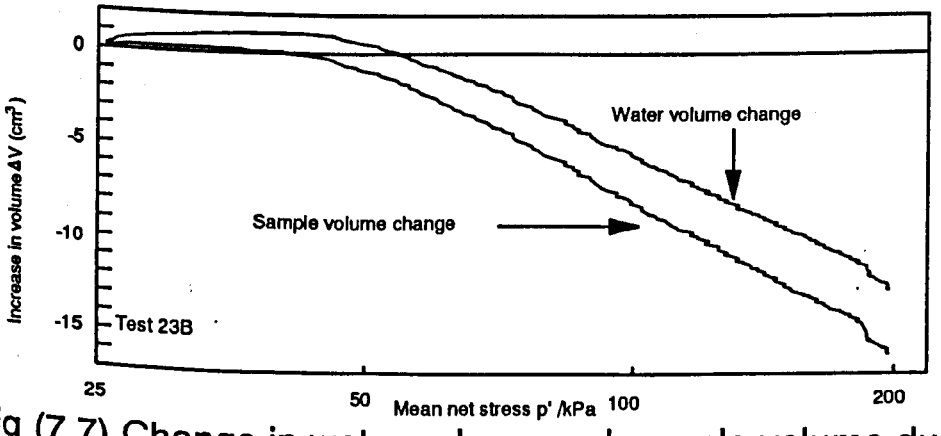

Fig (7.7) Change in water volume and sample volume during ramped consolidation at zero suction

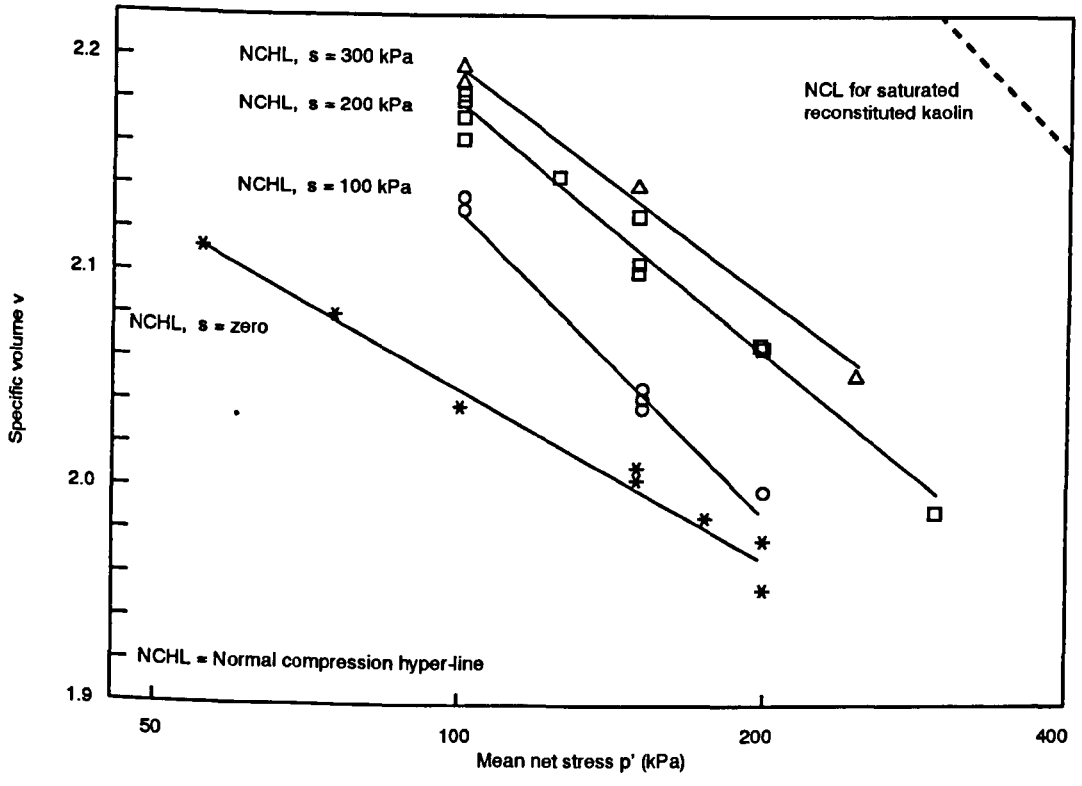

Fig (7.8) Specific volume versus mean net stress on isotropic normal compression hyper-line

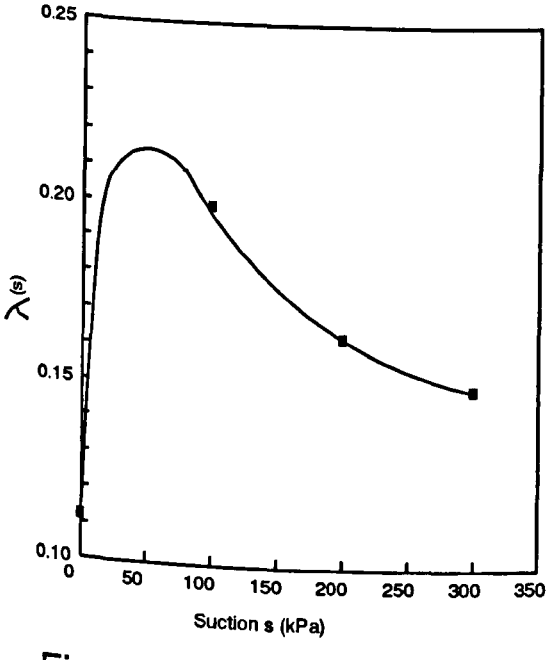

Fig (7.9) λ (s) versus suction

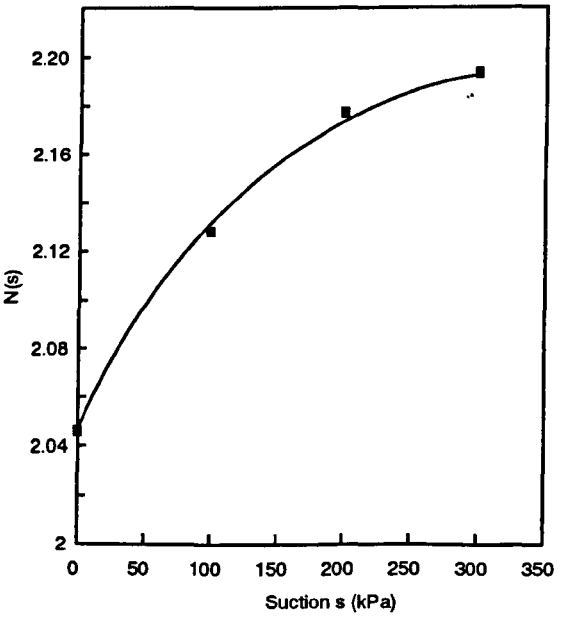

Fig (7.10) N(s) versus suction

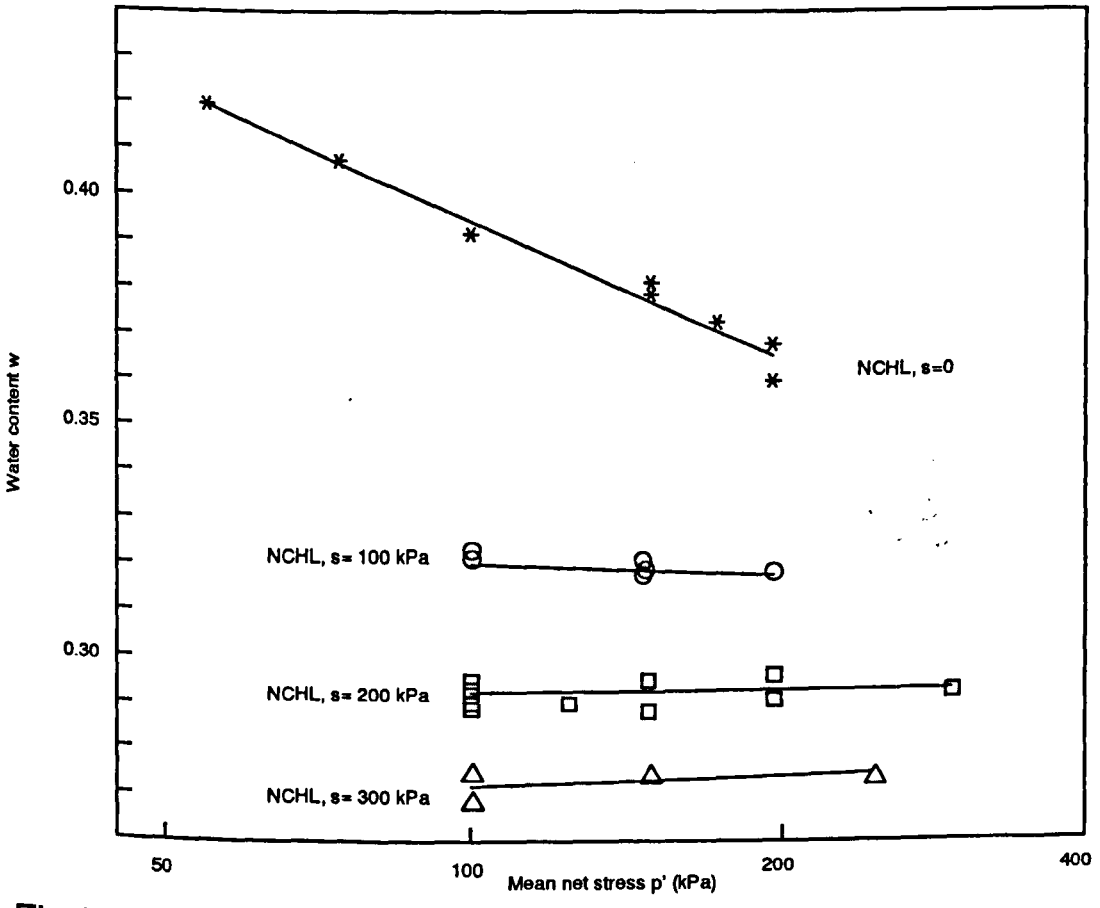

Fig (7.11) Water content versus mean net stress on isotropic normal compression hyper-line

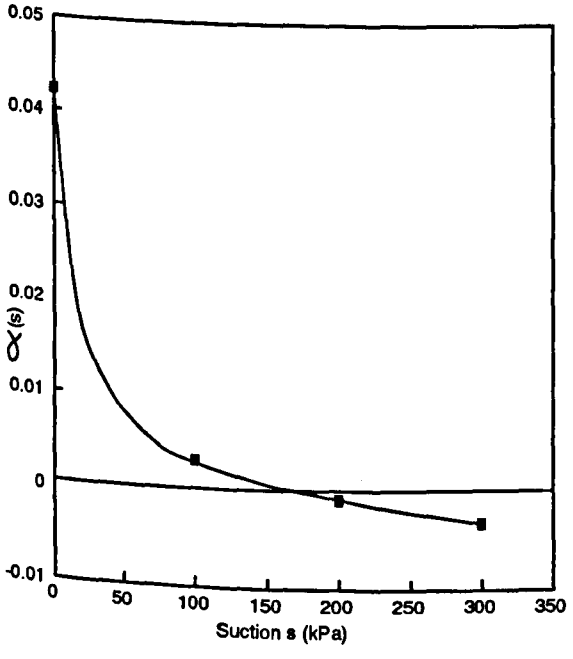

Fig (7.12) $\propto$ (s) versus suction

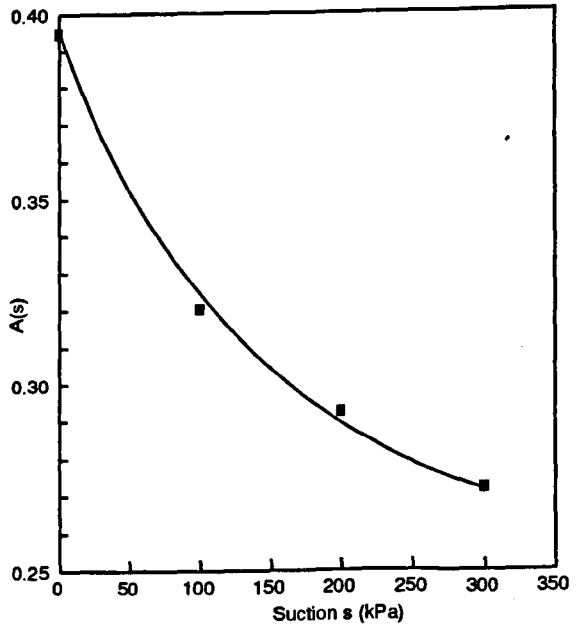

Fig (7.13) A(s) versus suction

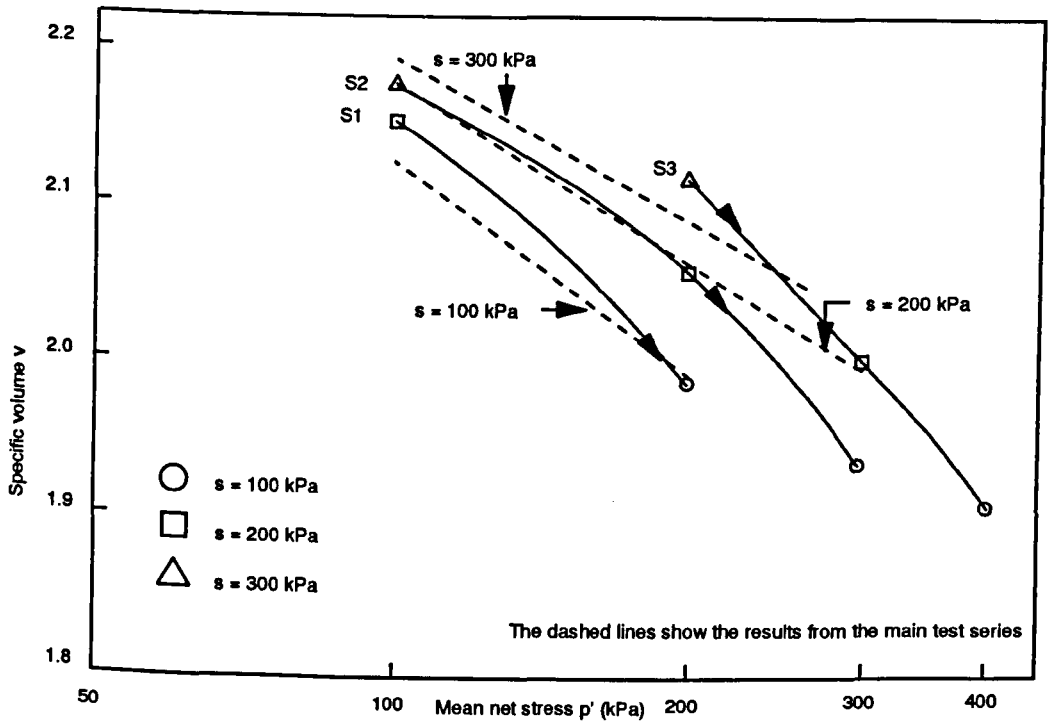

Fig (7.14) Specific volume plotted against mean net stress for step-loading compression tests

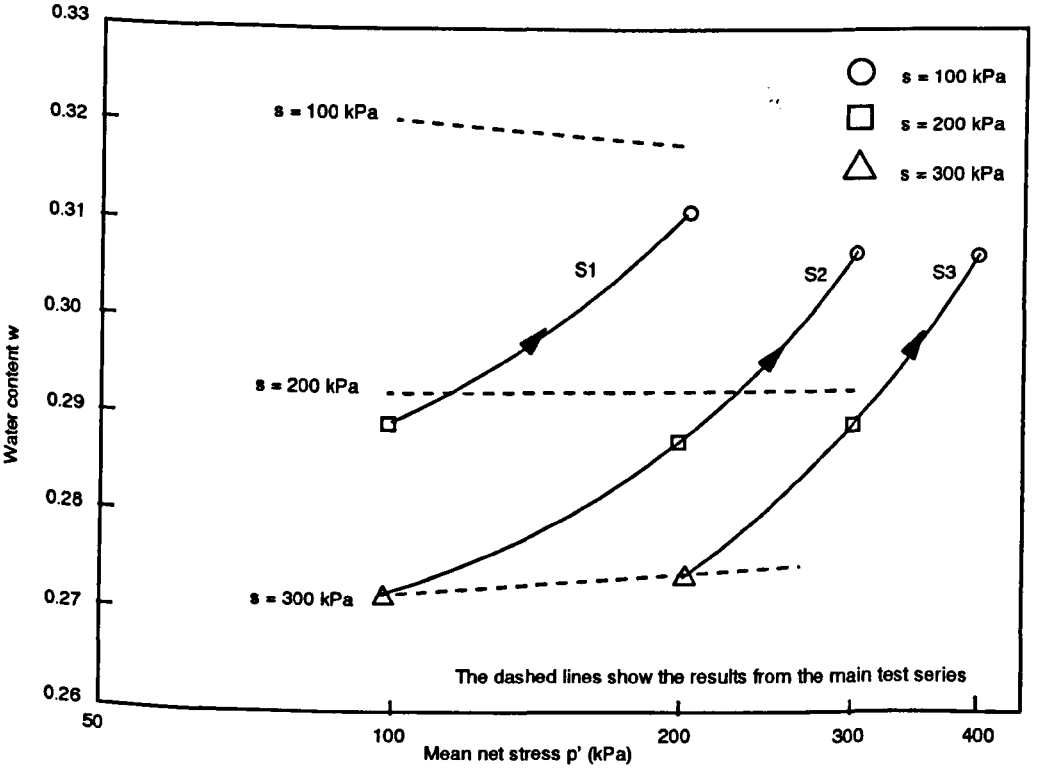

Fig (7.15) Water content plotted against mean net stress for step-loading compression tests

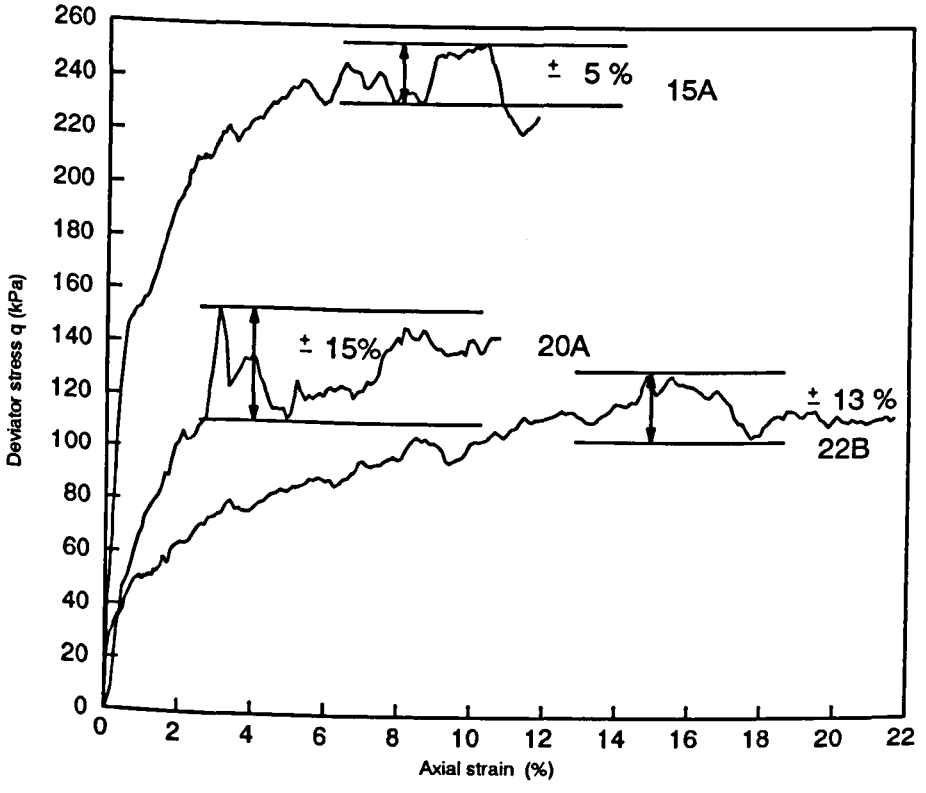

Fig (7.16) Loading ram friction in Tests 15A, 20A and 22B

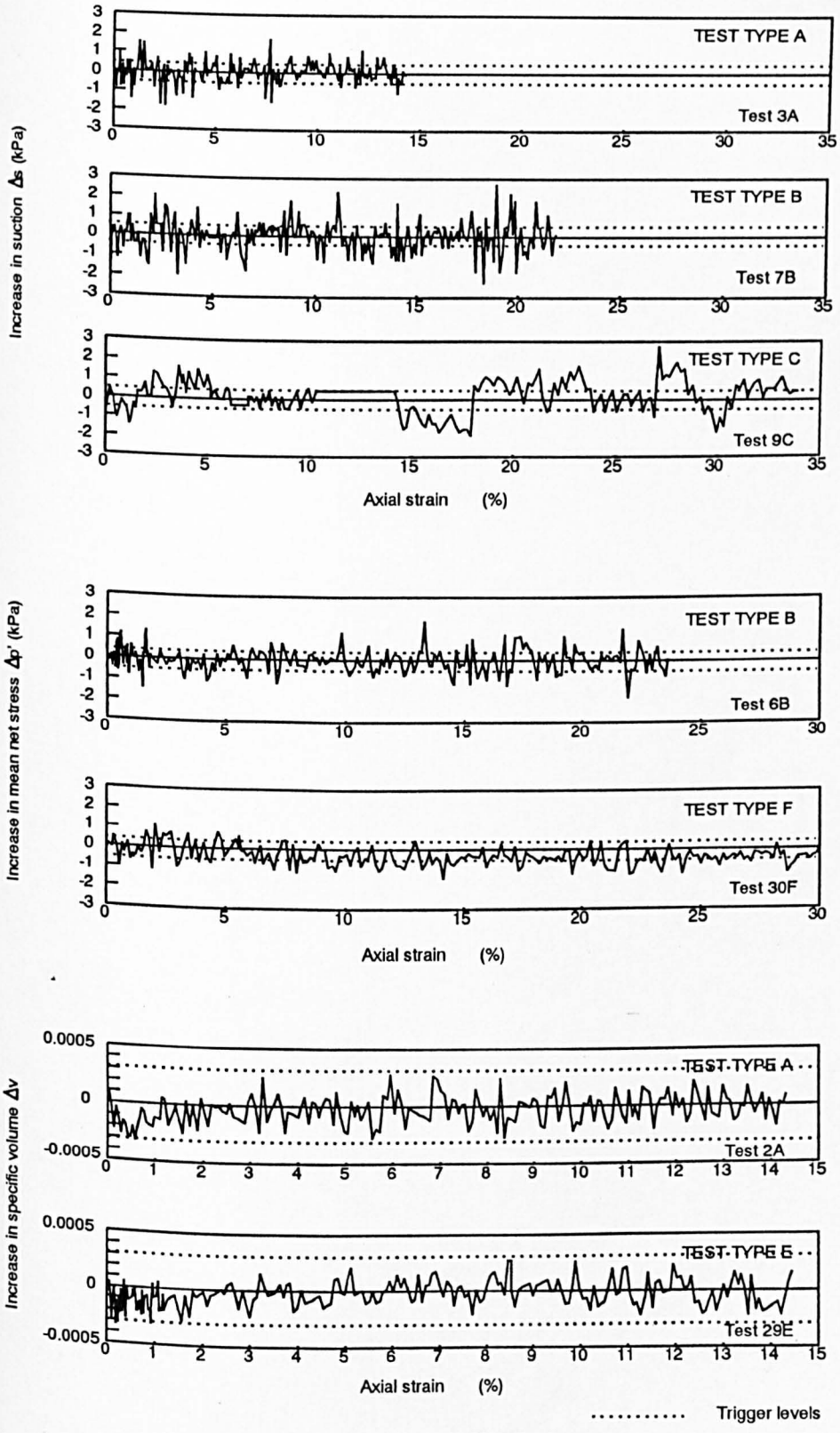

Fig (7.17) Quality of test control

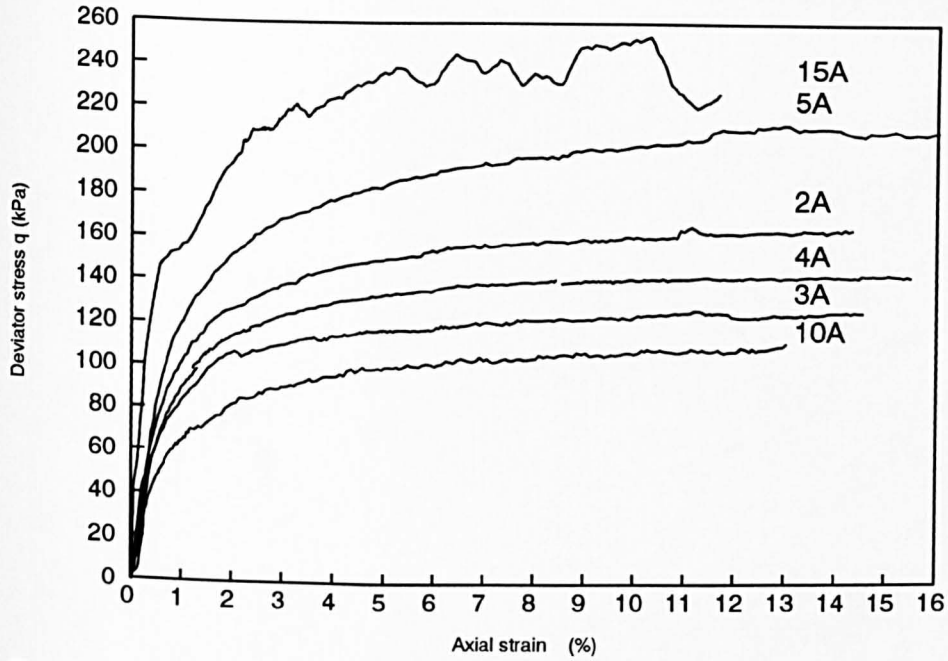

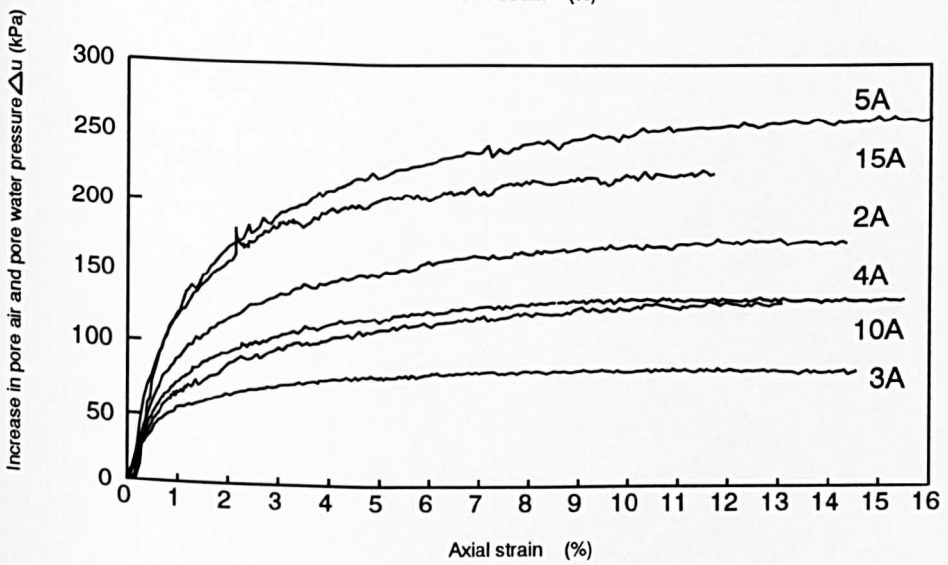

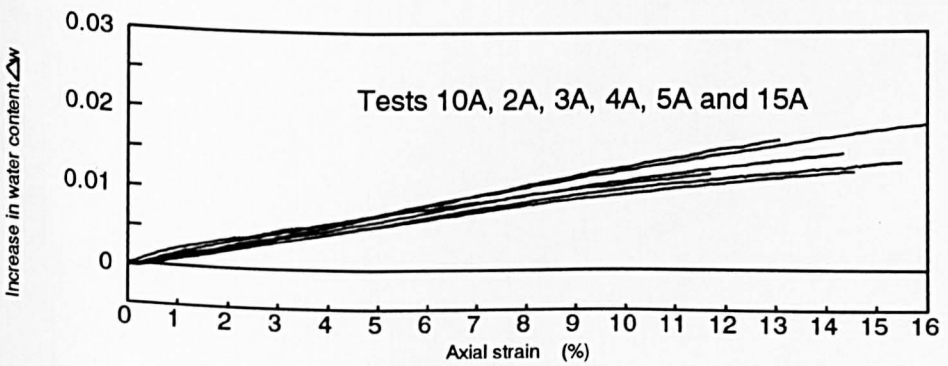

Fig (7.18) Stress-strain behaviour for constant volume, constant suction shear tests (type A)

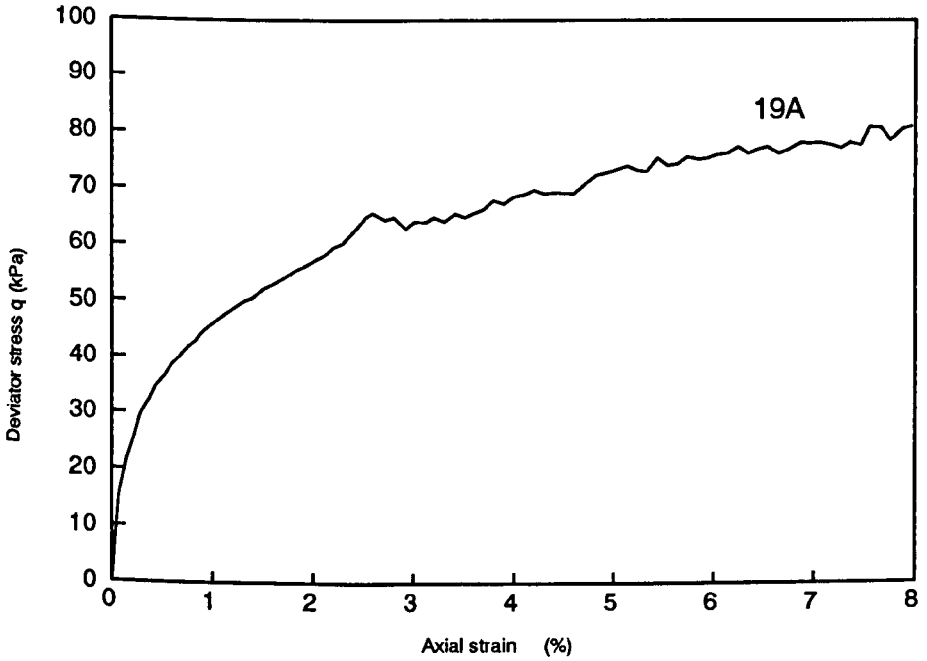

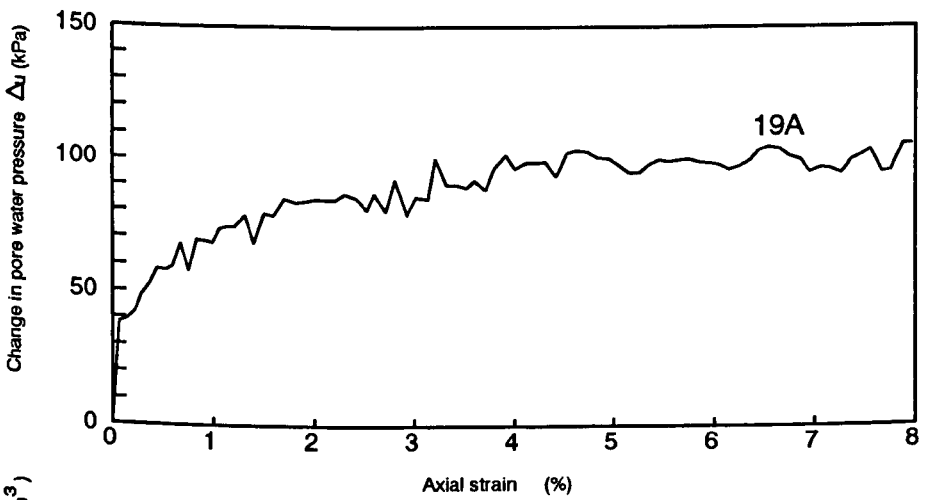

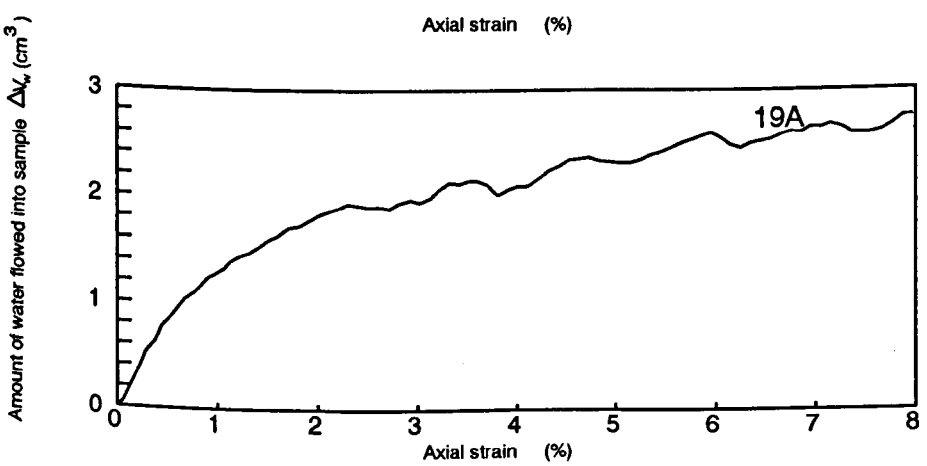

Fig (7.19) Stress-strain behaviour for constant volume, constant suction shear test (type A) at zero suction

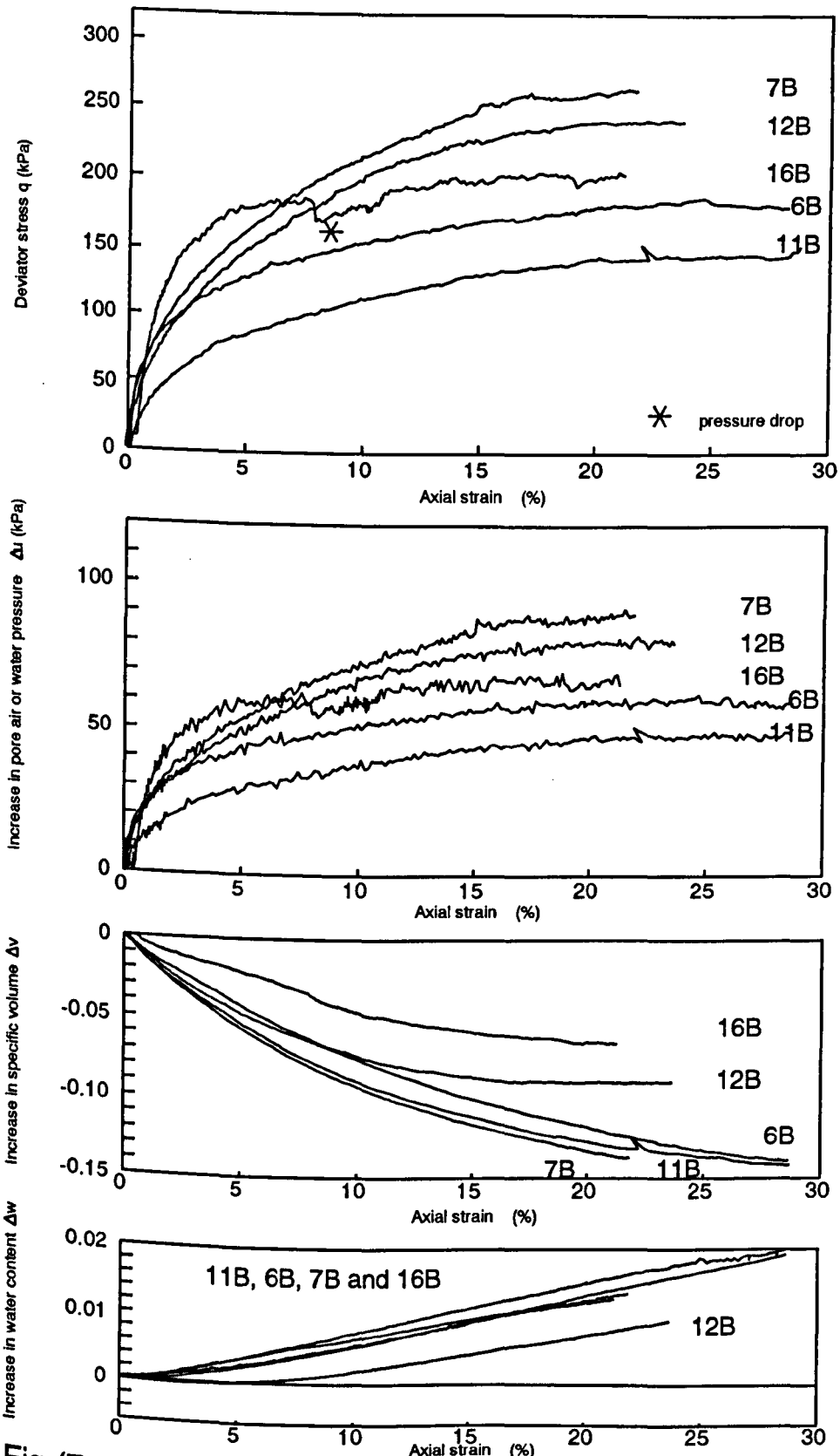

Fig (7.20) Stress-strain behaviour for constant mean net stress, constant suction tests (type B)

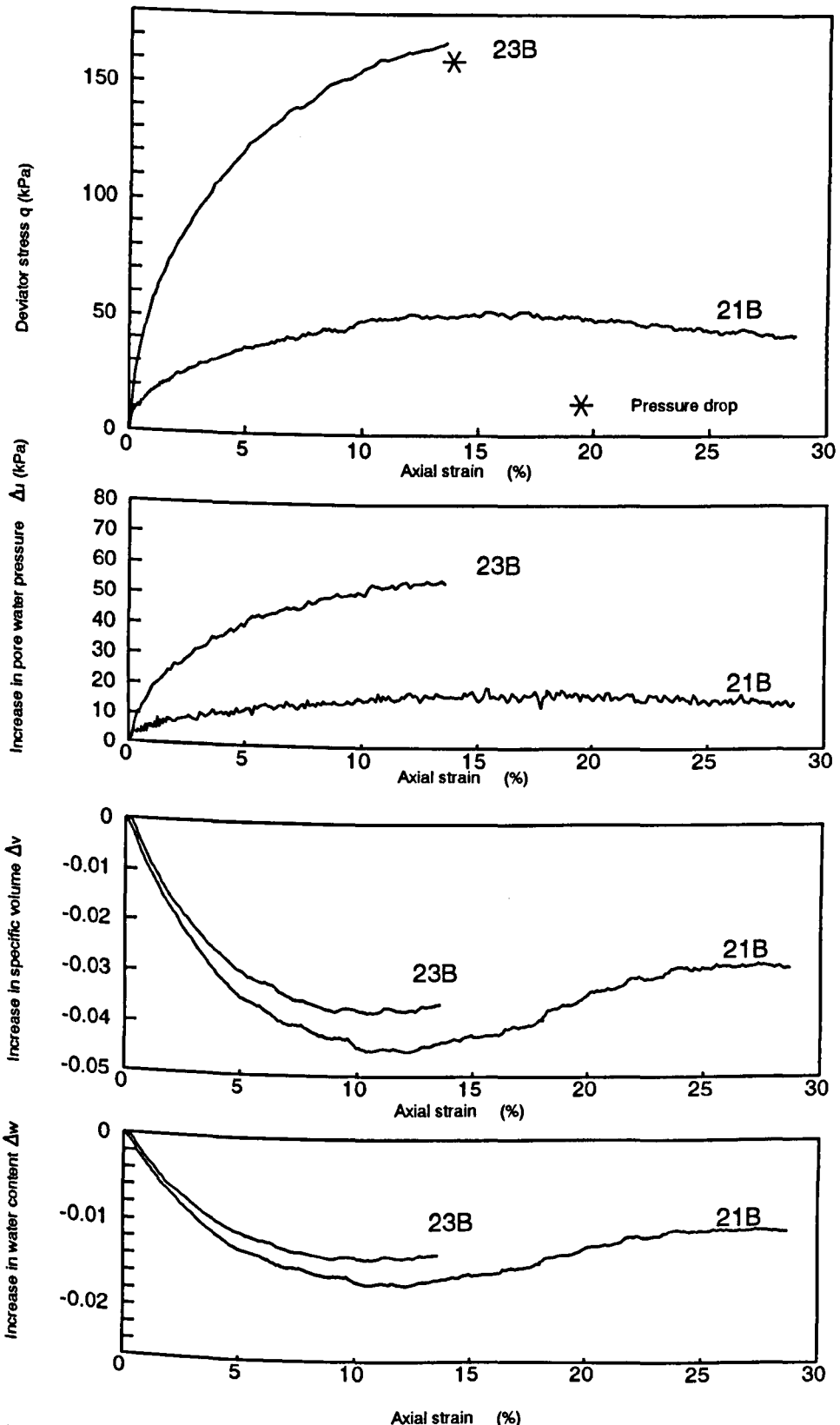

Fig (7.21) Stress-strain behaviour for constant mean net stress, constant suction tests (type B) at zero suction

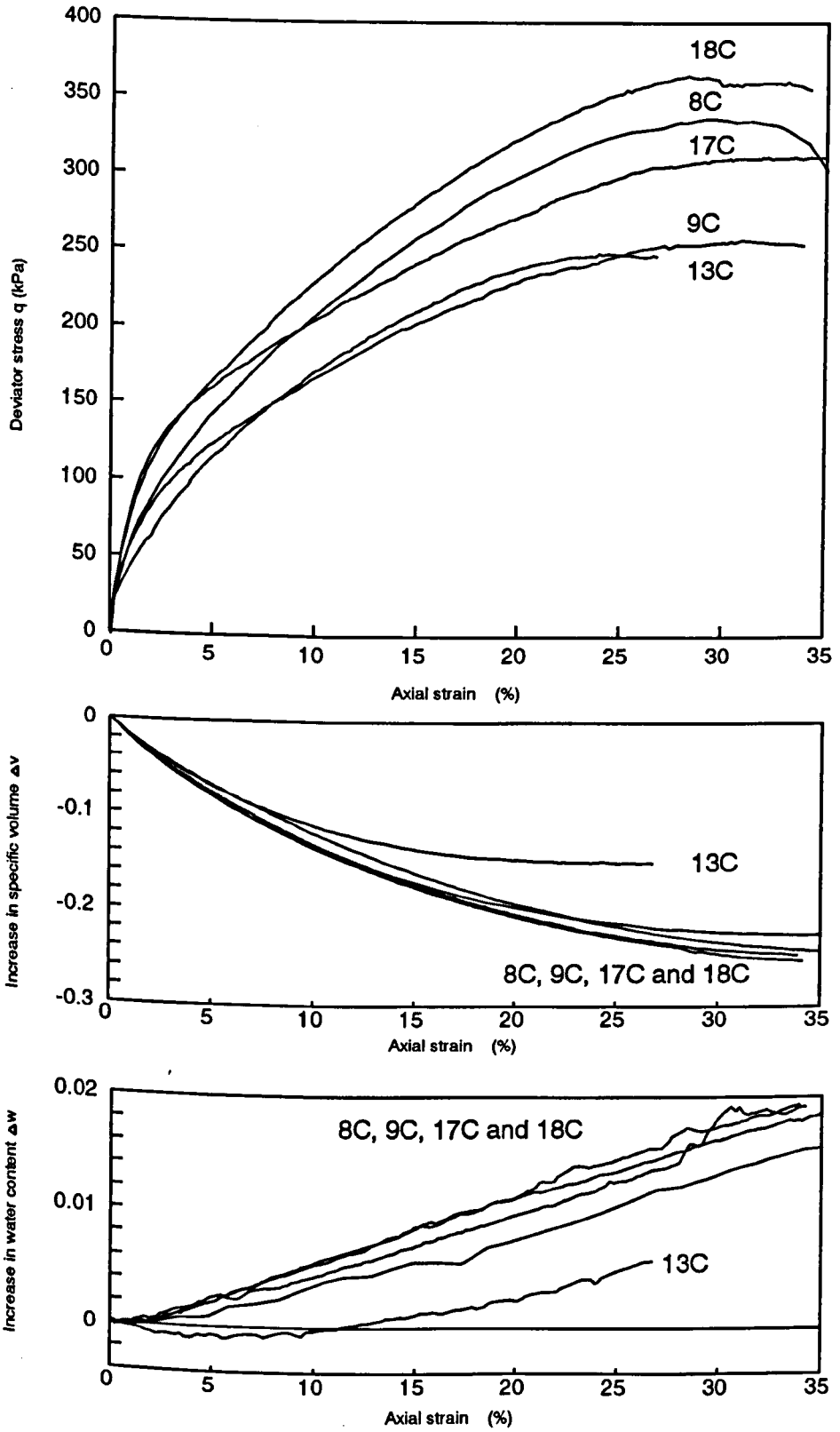

Fig (7.22) Stress-strain behaviour for fully drained, constant suction tests (type C)

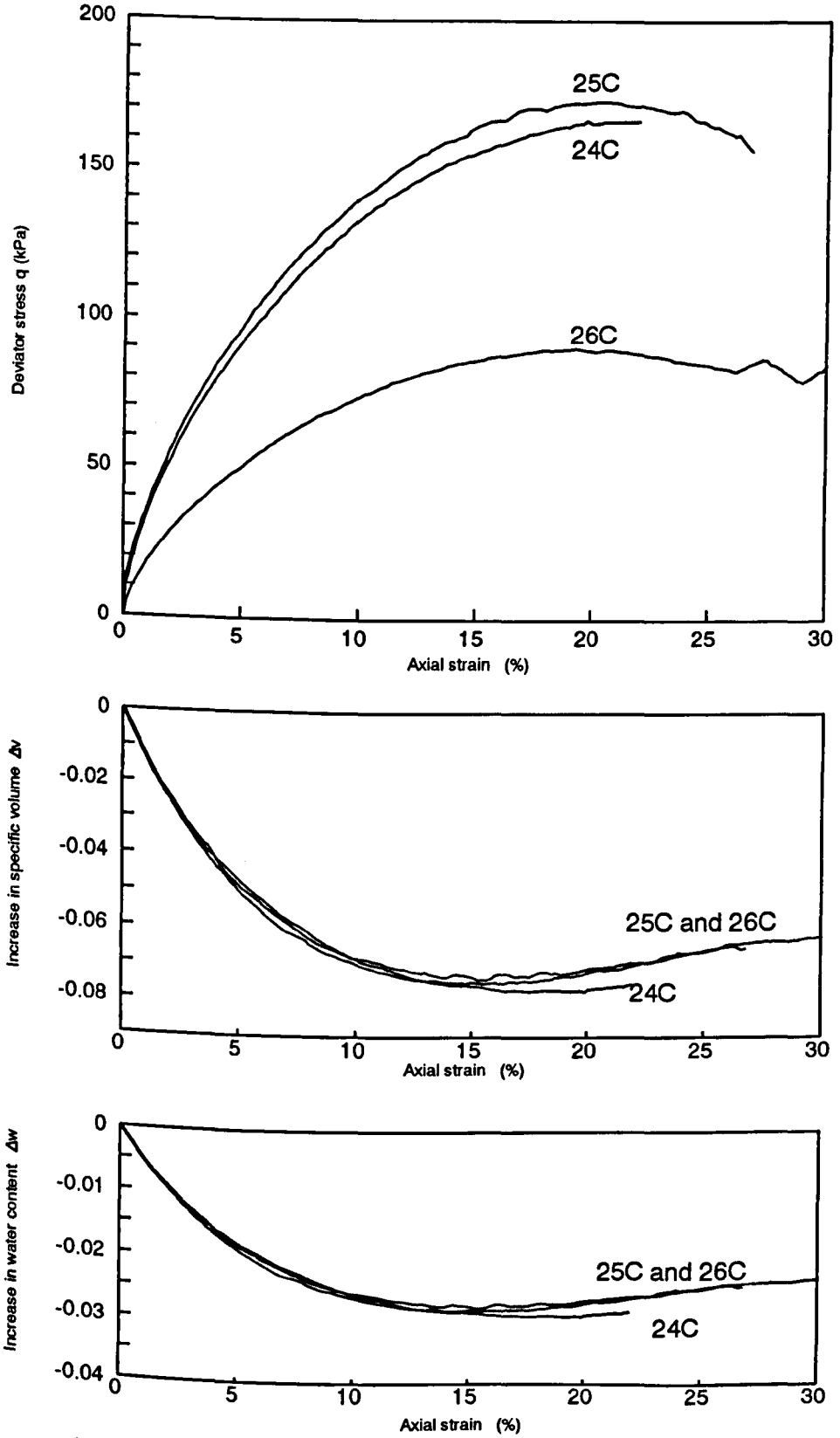

Fig (7.23) Stress-strain behaviour for fully drained, constant suction tests (type C) at zero suction

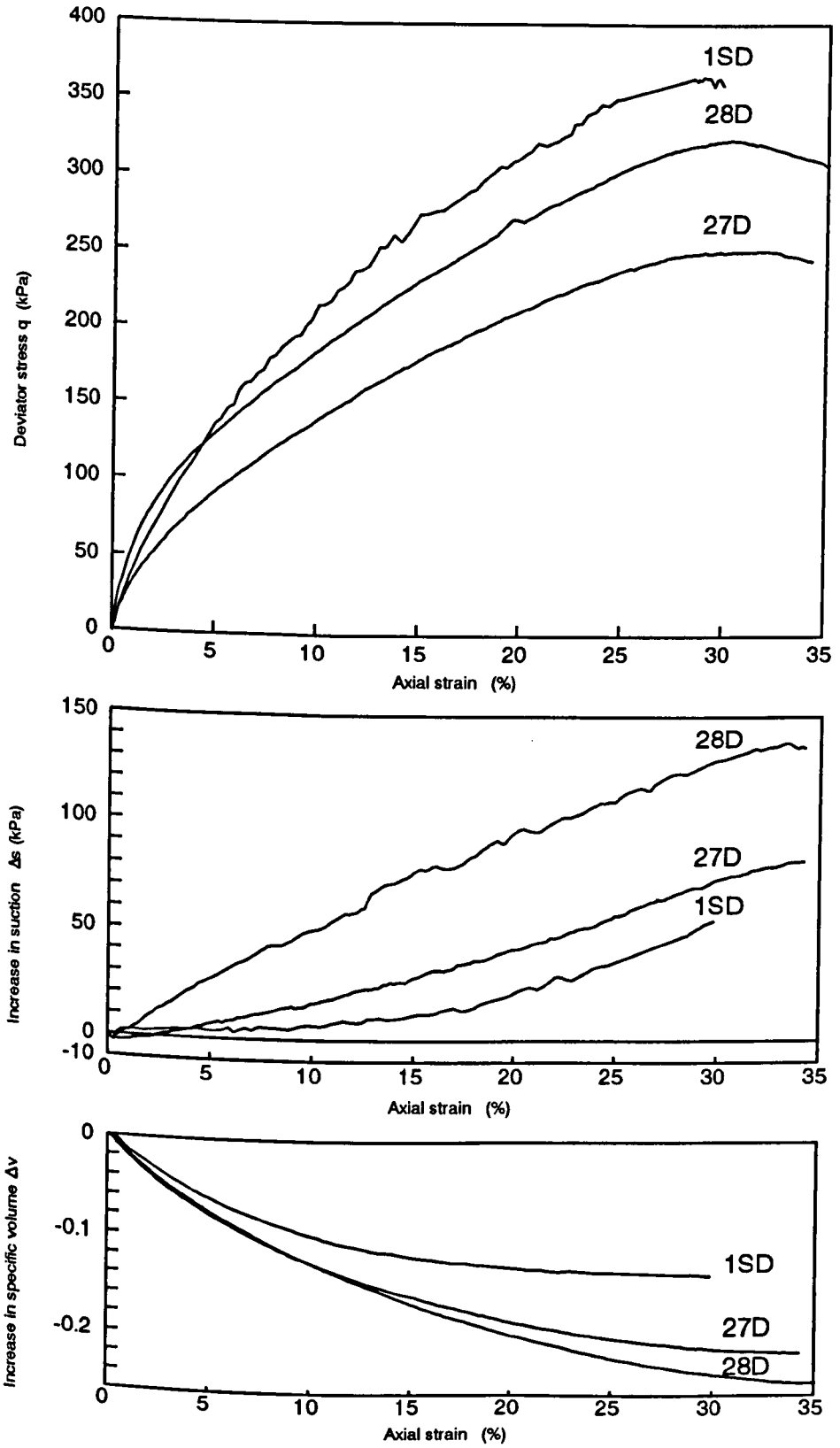

Fig (7.24) Stress-strain behaviour for constant water content, rising suction shear tests (type D)

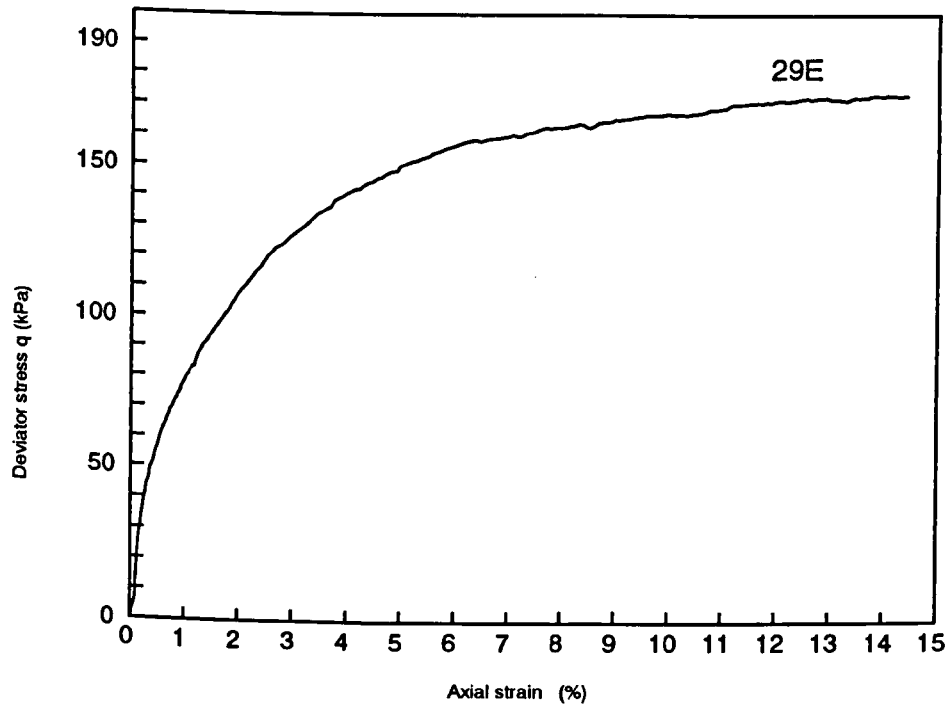

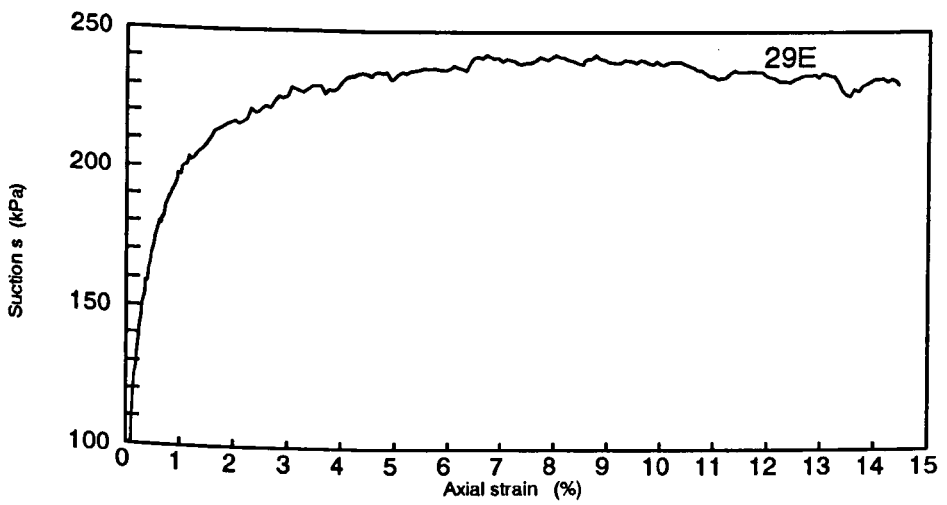

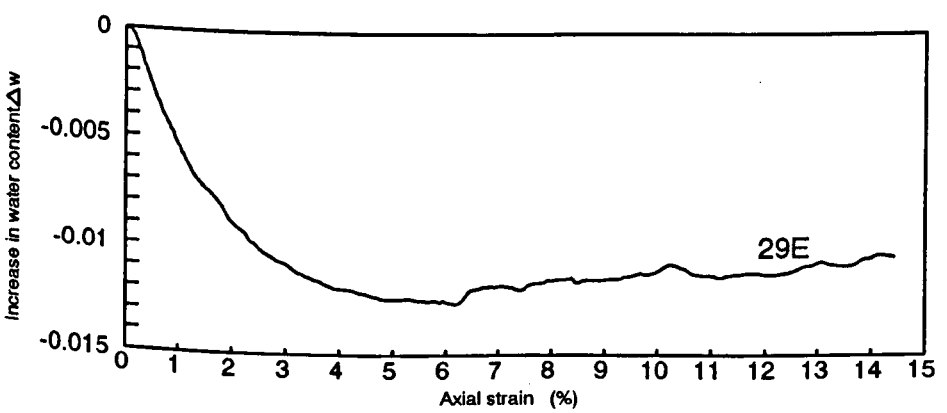

Fig (7.25) Stress-strain behaviour for constant volume, increasing suction test (type E)

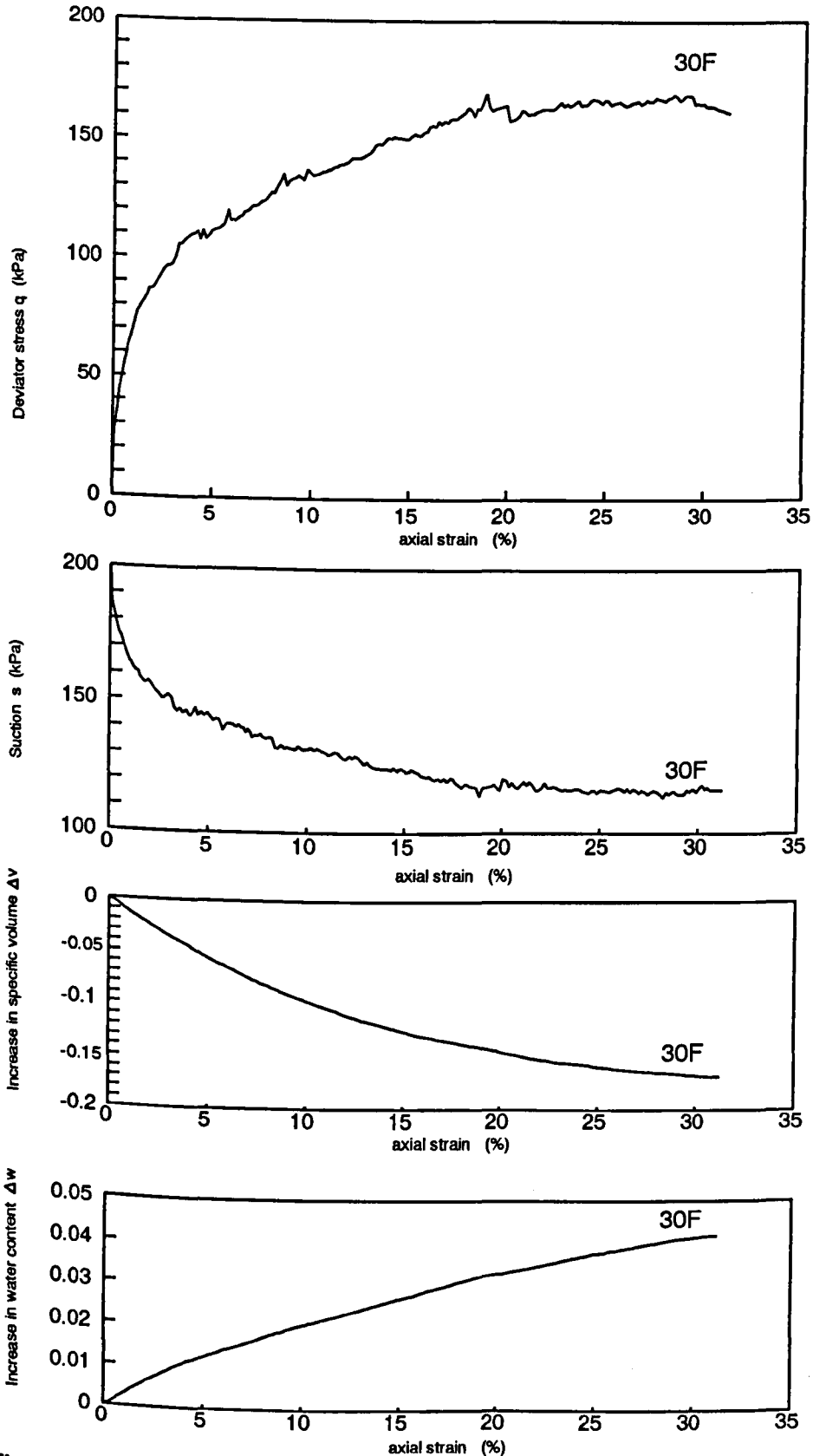

Fig (7.26) Stress-strain behaviour for constant mean net stress, falling suction shear test (type F)

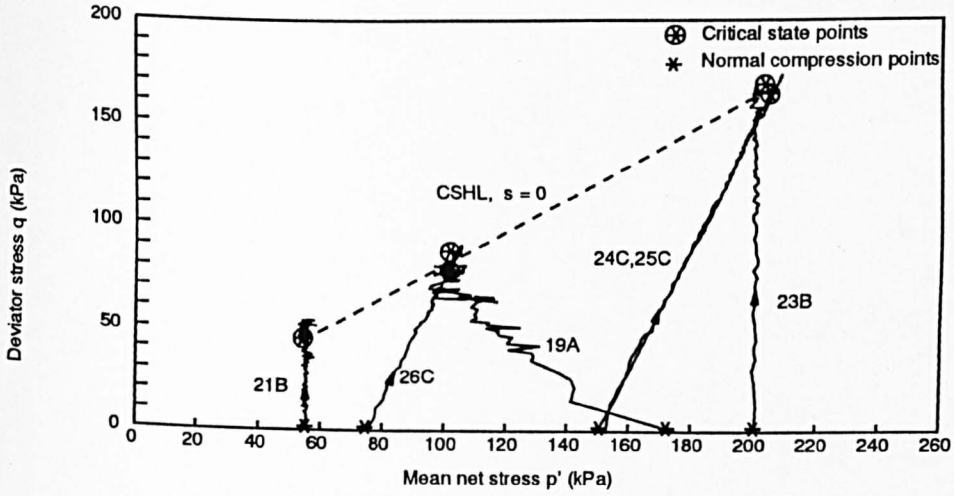

(a) Deviator stress plotted against mean net stress

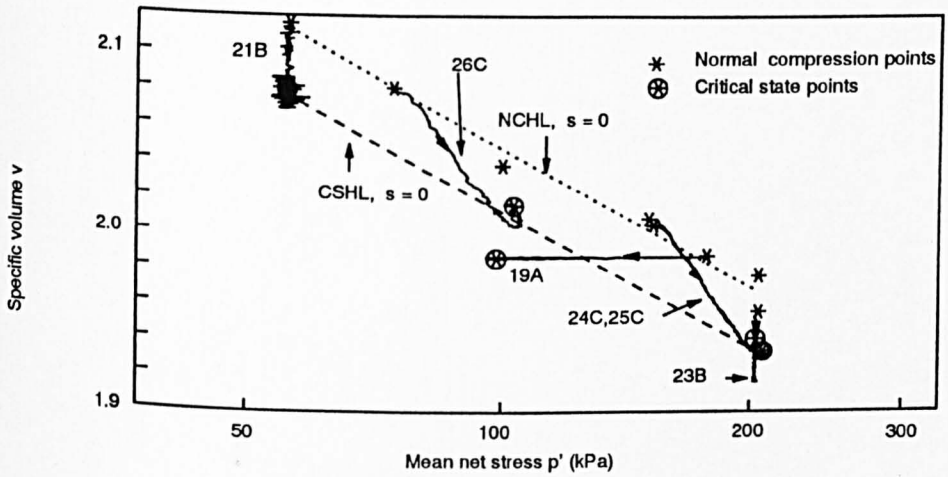

(b) Specific volume plotted against mean net stress

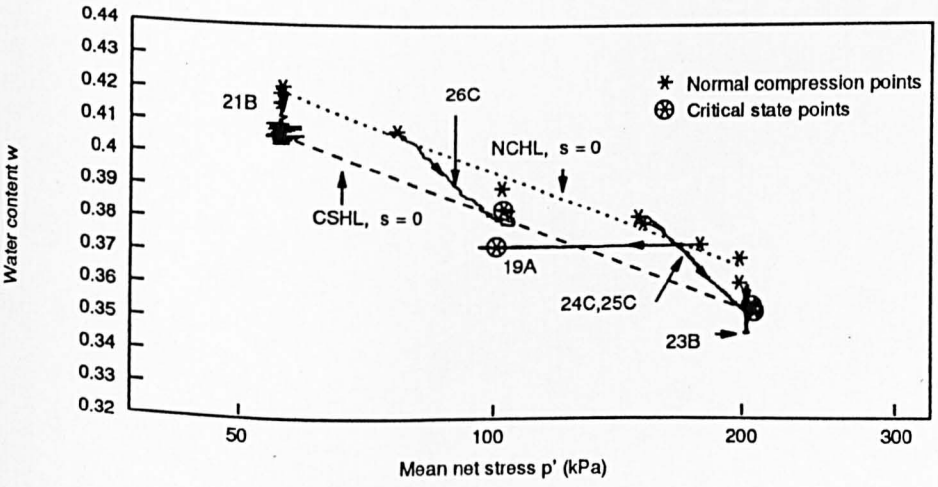

(c) Water content plotted against mean net stress

Fig (7.27) Test paths of shear tests conducted at zero suction

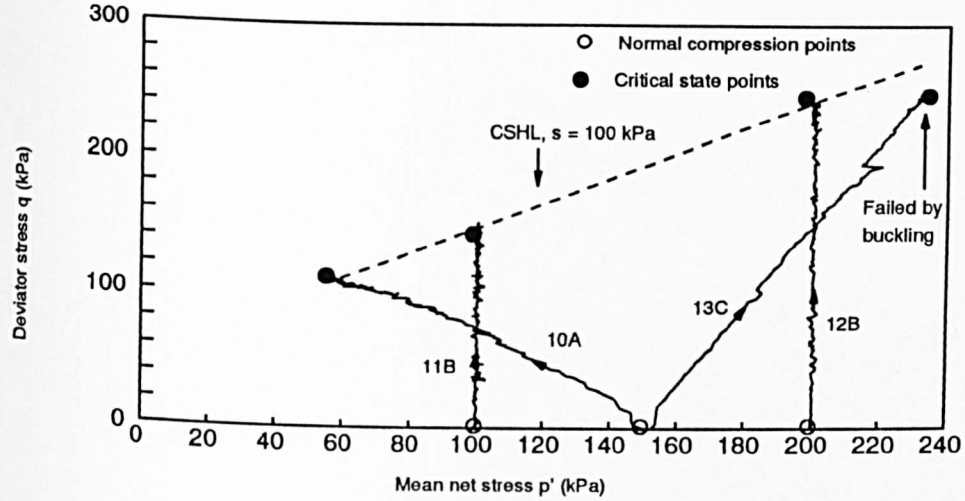

(a) Deviator stress plotted against mean net stress

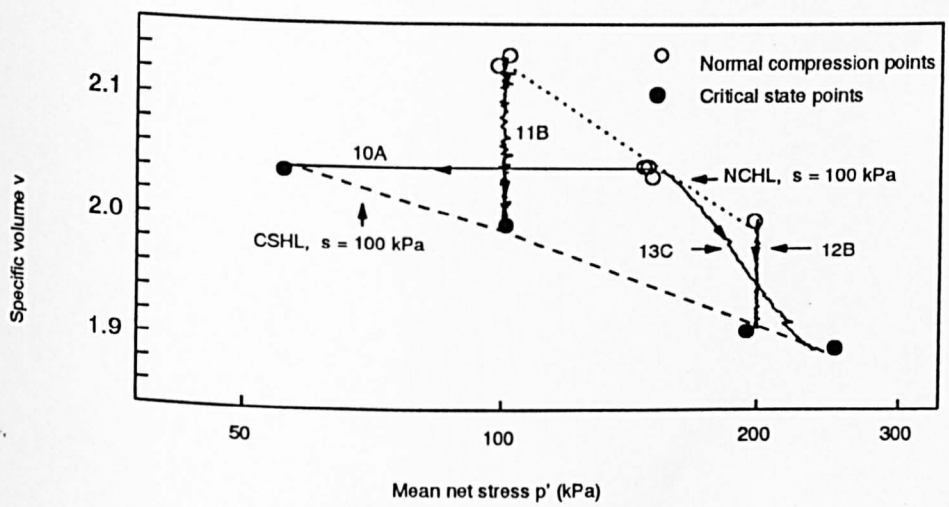

(b) Specific volume plotted against mean net stress

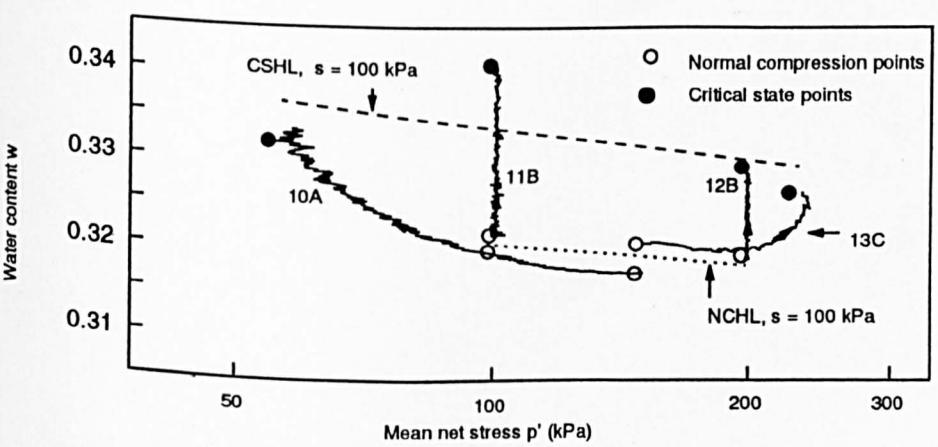

(c) Water content plotted against mean net stress

Fig (7.28) Test paths for shear tests conducted at suction of 100 kPa

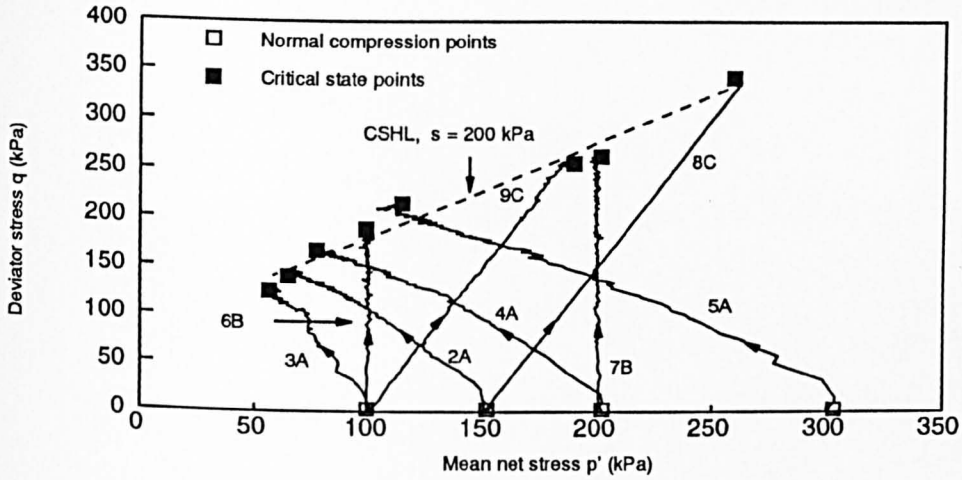

(a) Deviator stress plotted against mean net stress

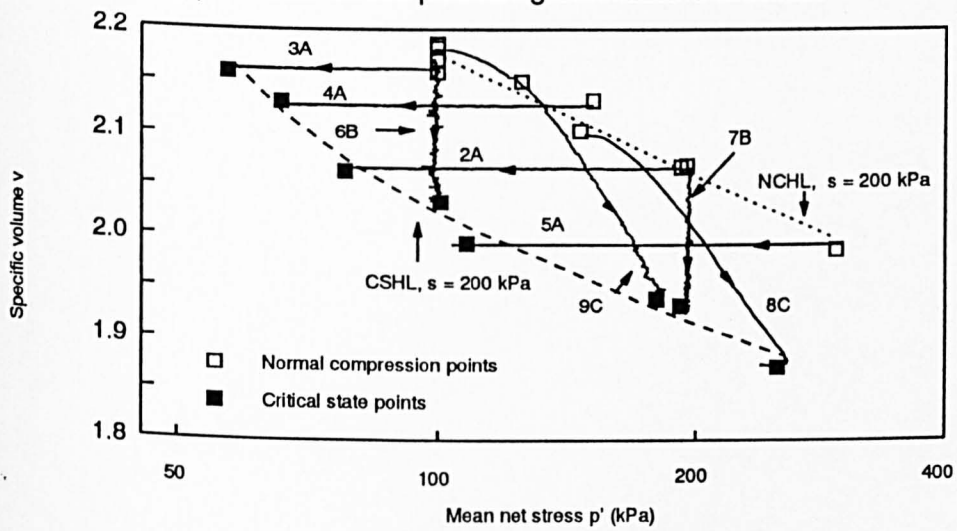

(b) Specific volume plotted against mean net stress

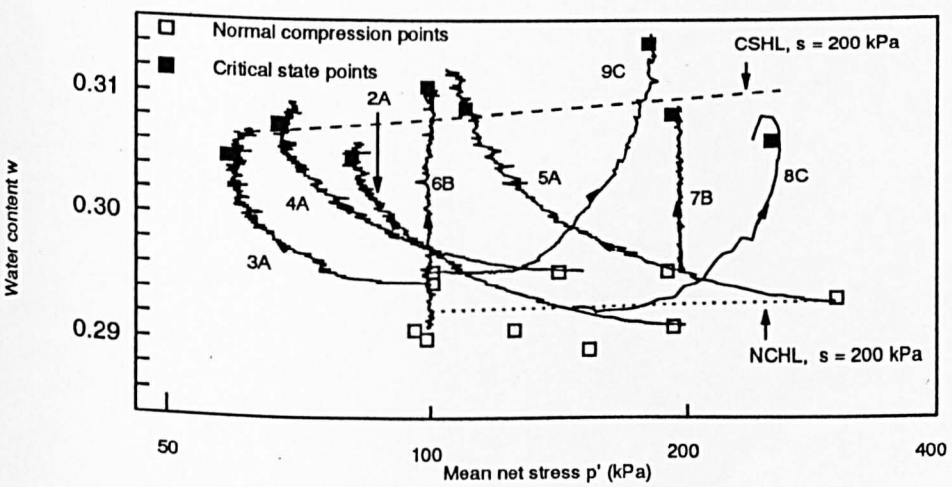

(c) Water content plotted against mean net stress

Fig (7.29) Test paths for shear tests conducted at suction of 200 kPa

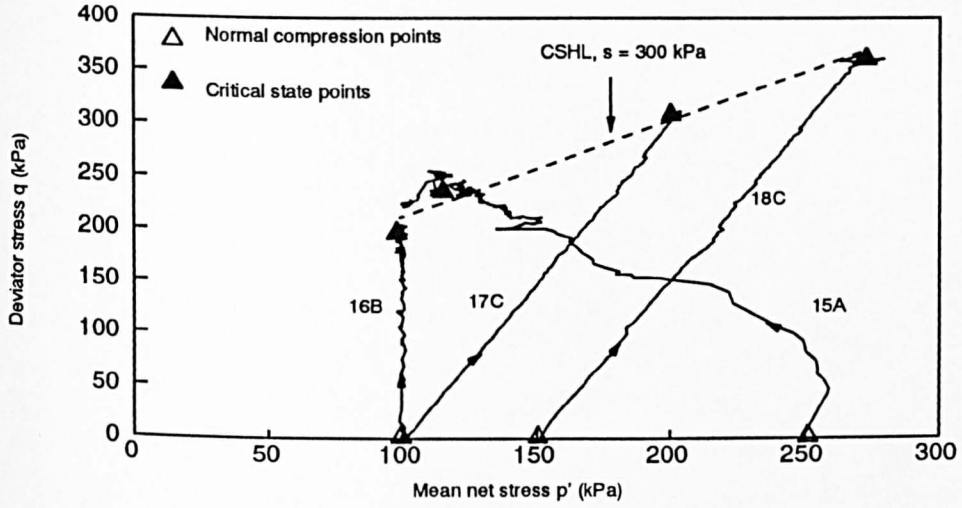

(a) Deviator stress q plotted against mean net stress

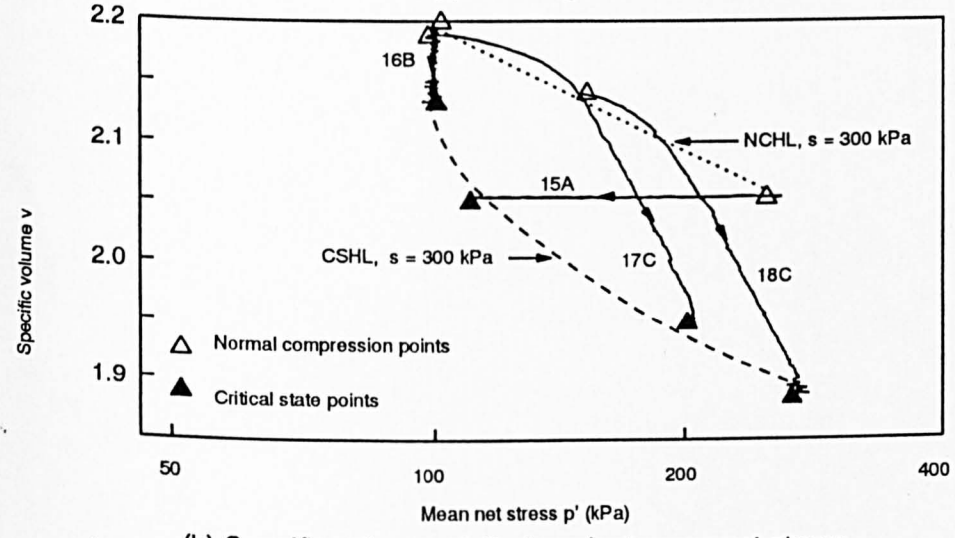

(b) Specific volume plotted against mean net stress

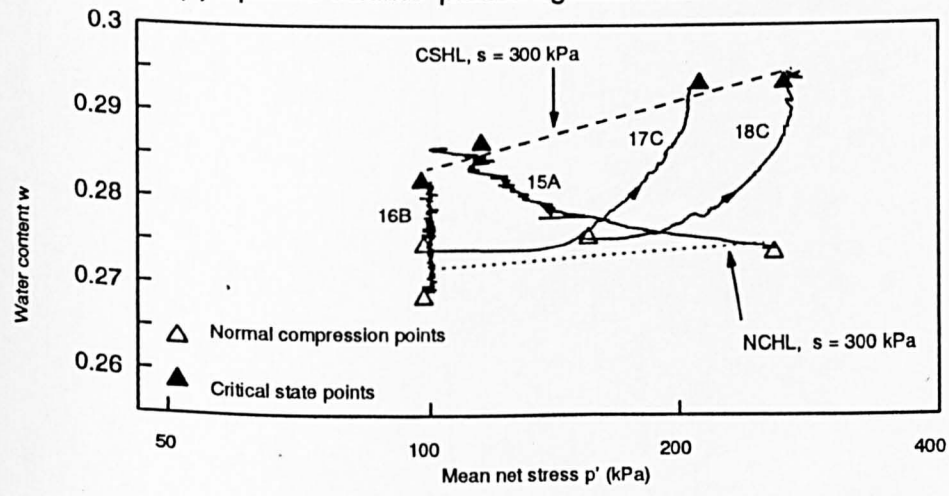

(c) Water content plotted against mean net stress

Fig (7.30) Test paths for shear tests conducted at suction of 300 kPa

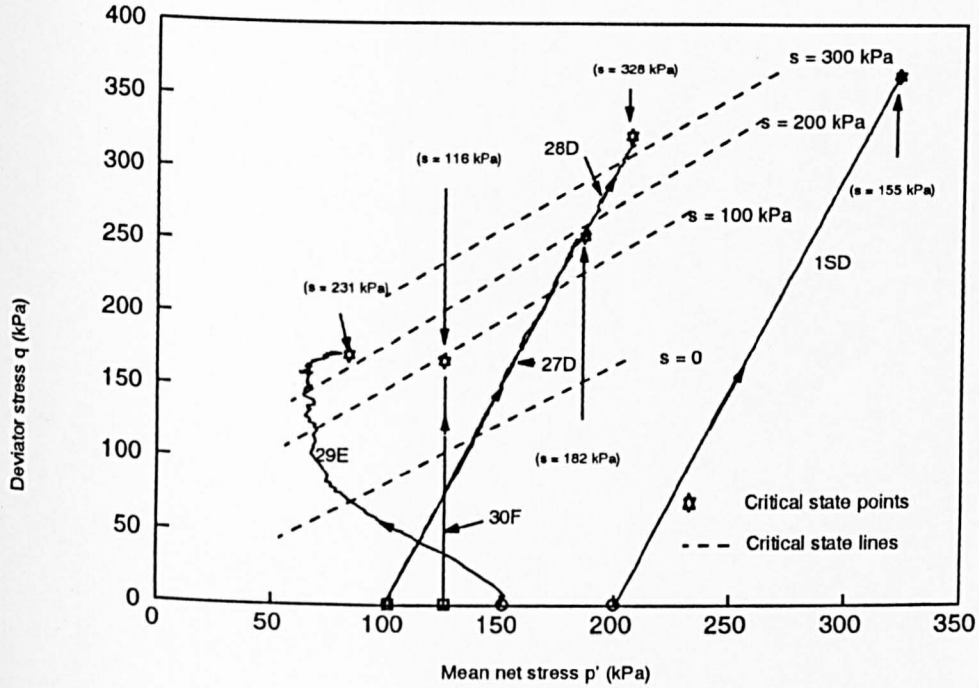

(a) Deviator stress q plotted against mean net stress

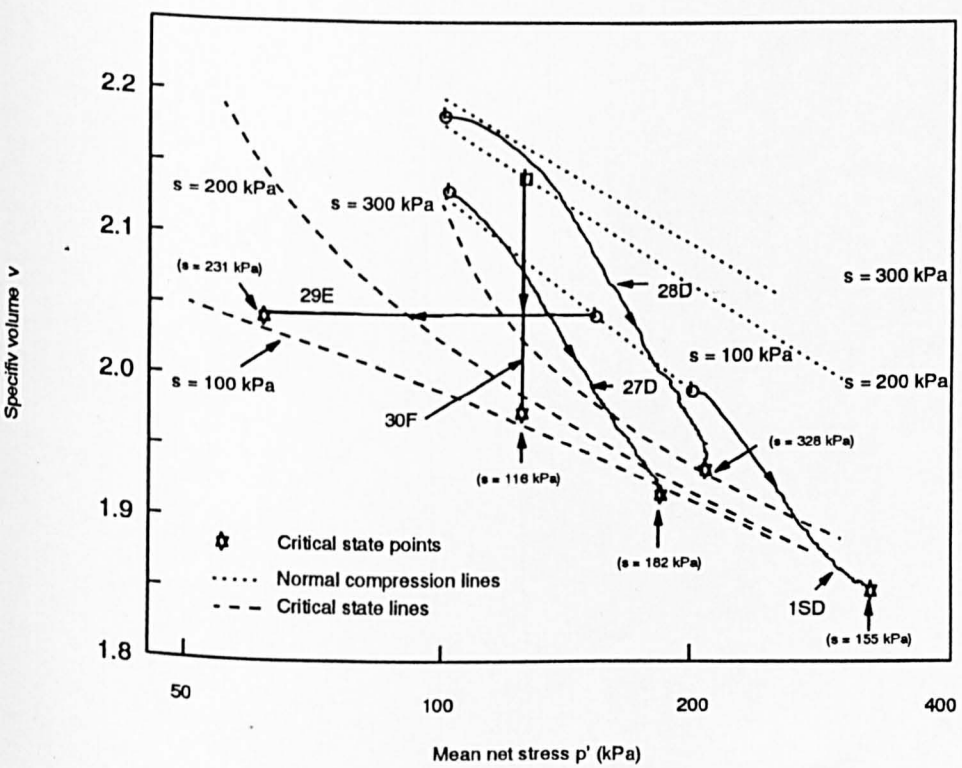

(b) Specific volume plotted against mean net stress

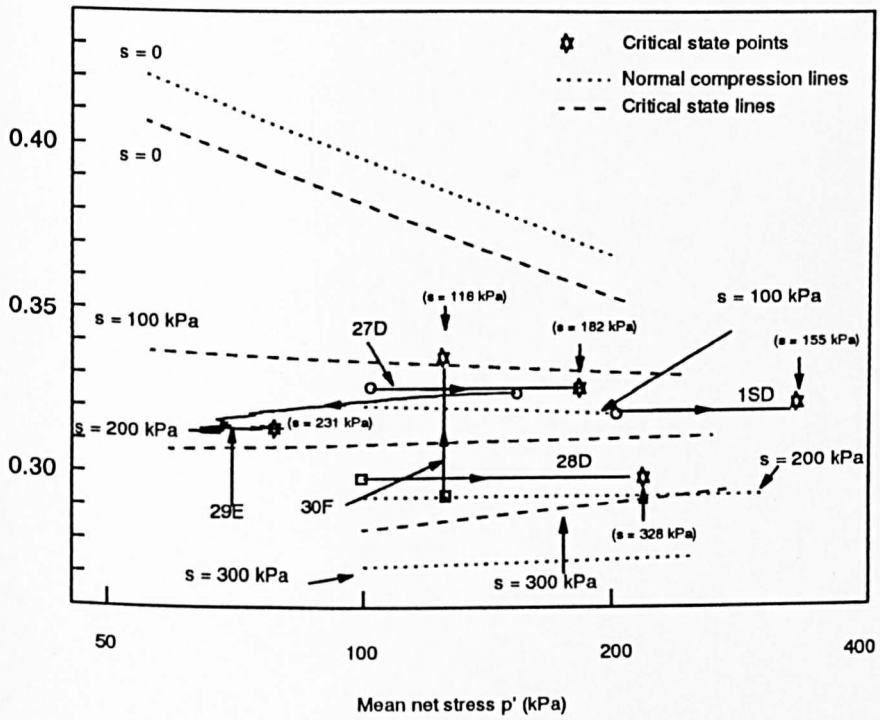

(c) Water content plotted against mean net stress

Fig (7.31) Test paths for variable suction shear tests (types D, E and F)

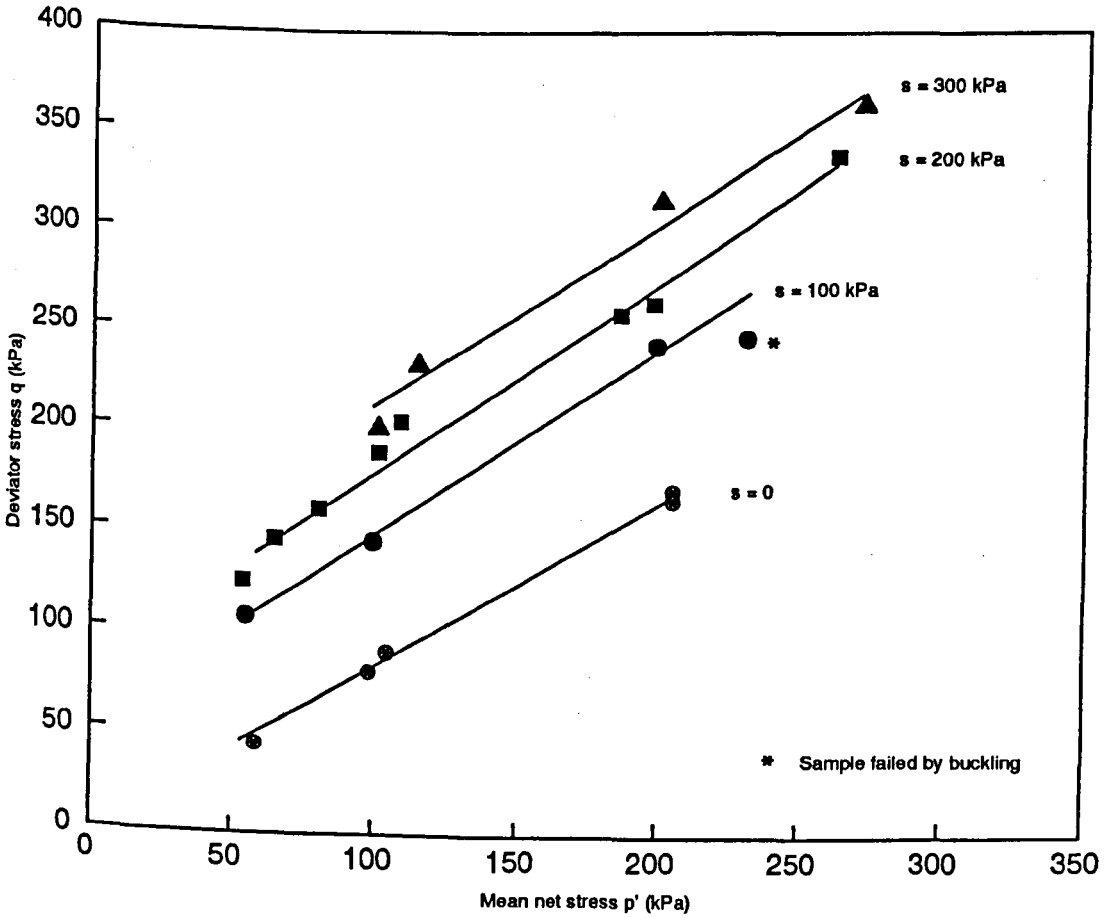

Fig (7.32) Deviator stress versus mean net stress at critical states

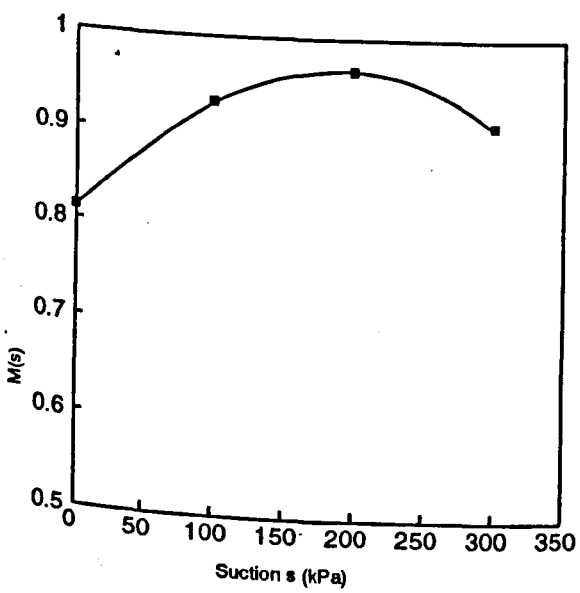

Fig (7.33a) M(s) versus suction

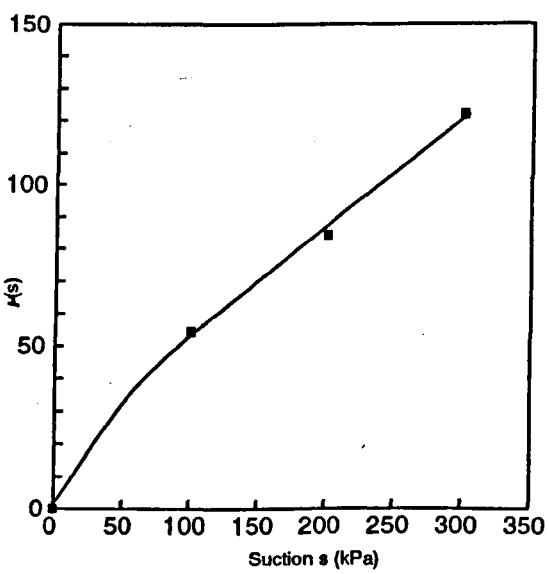

Fig (7.33b) $\mu(s)$ versus suction

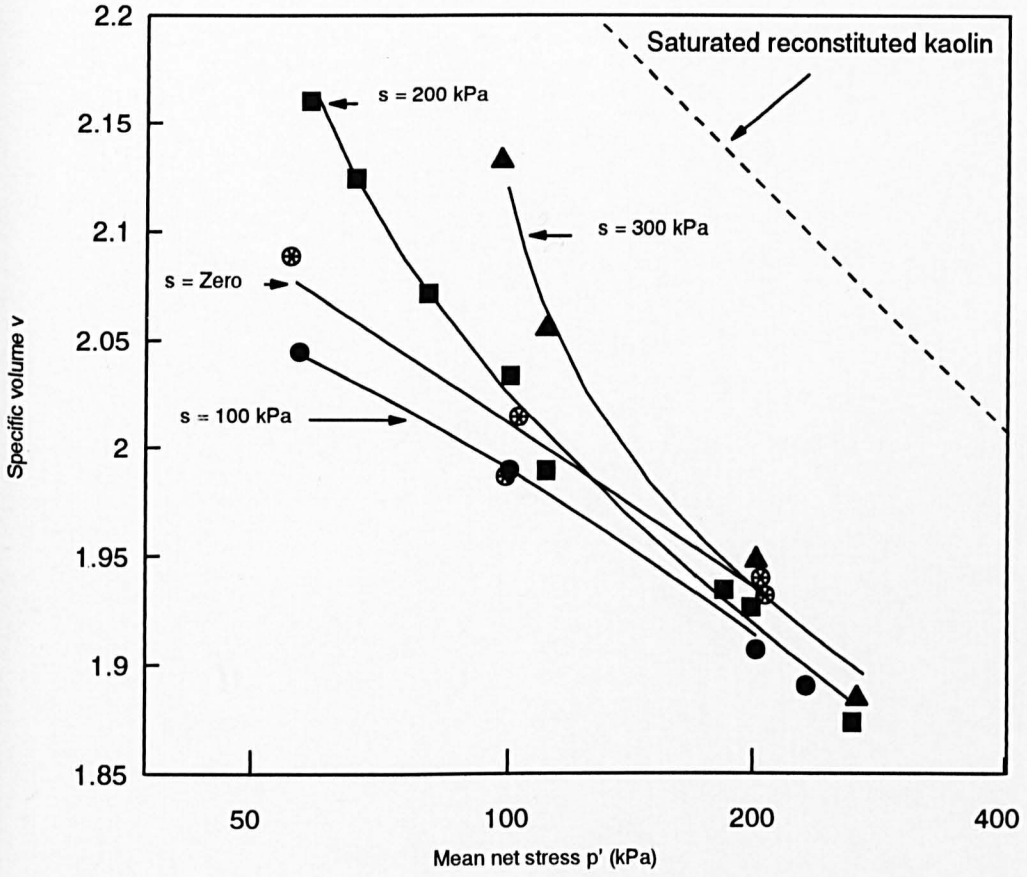

Fig (7.34) Specific volume versus mean net stress at critical states

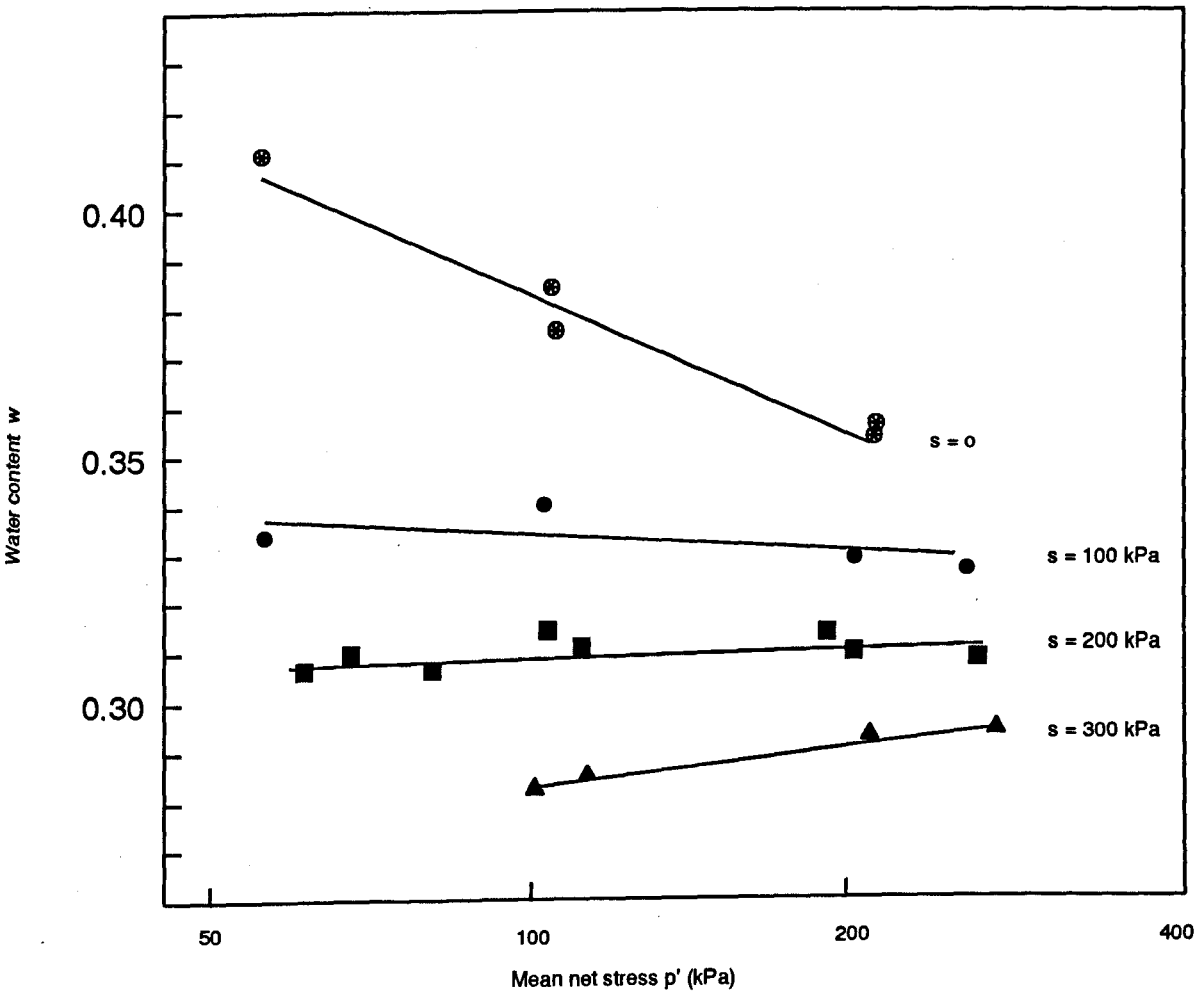

Fig (7.35) Water content versus mean net stress at critical states

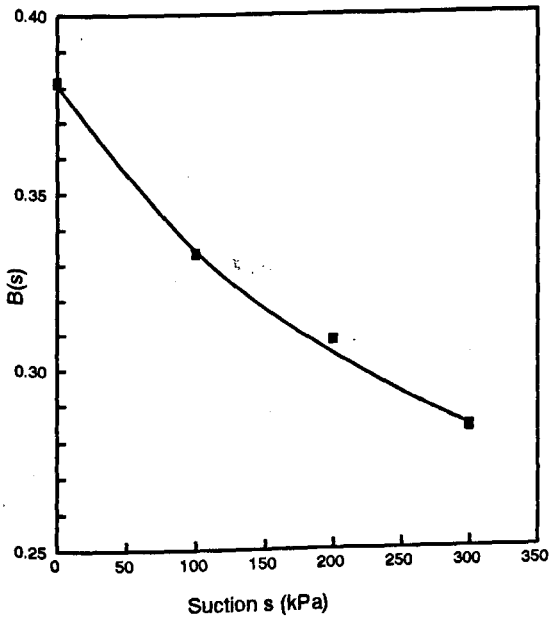

Fig (7.36a) B(s) versus suction

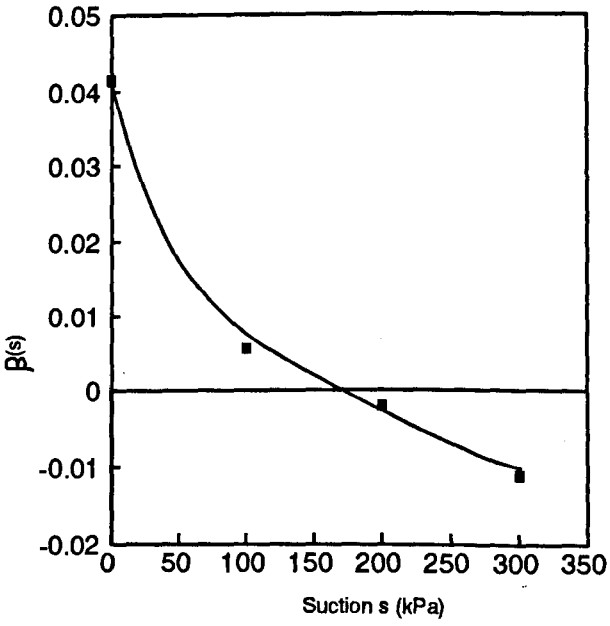

Fig (7.36b) β(s) versus suction

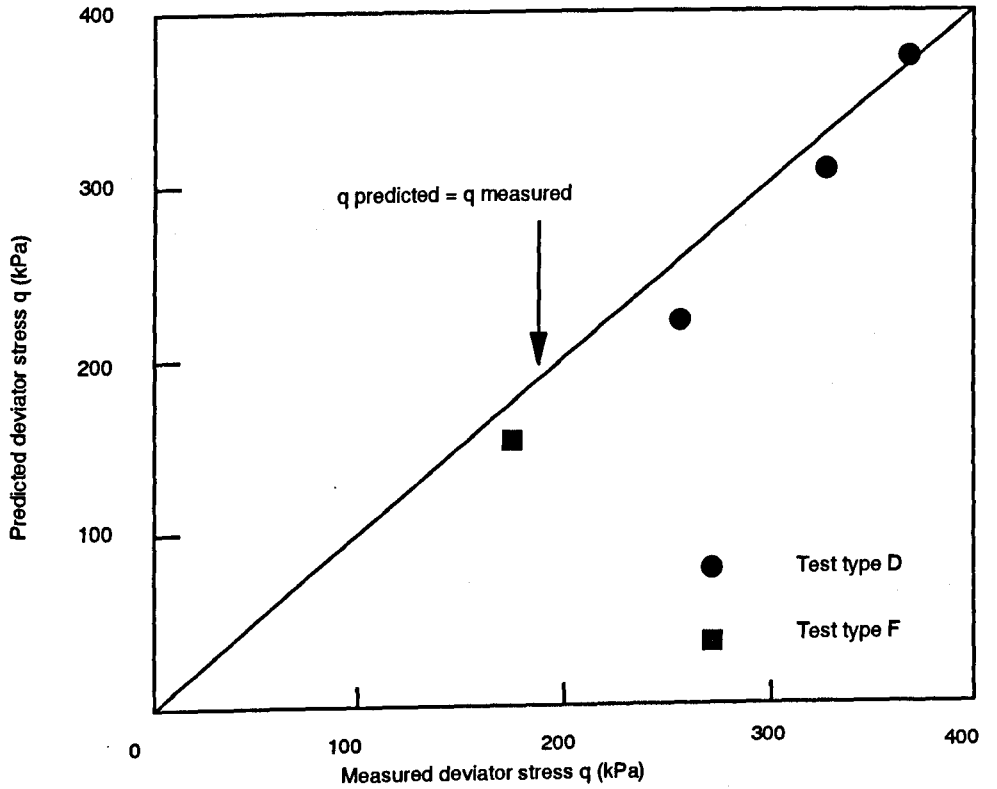

Fig (7.37a) Predicted versus measured deviator stress at crtical states for variable suction tests

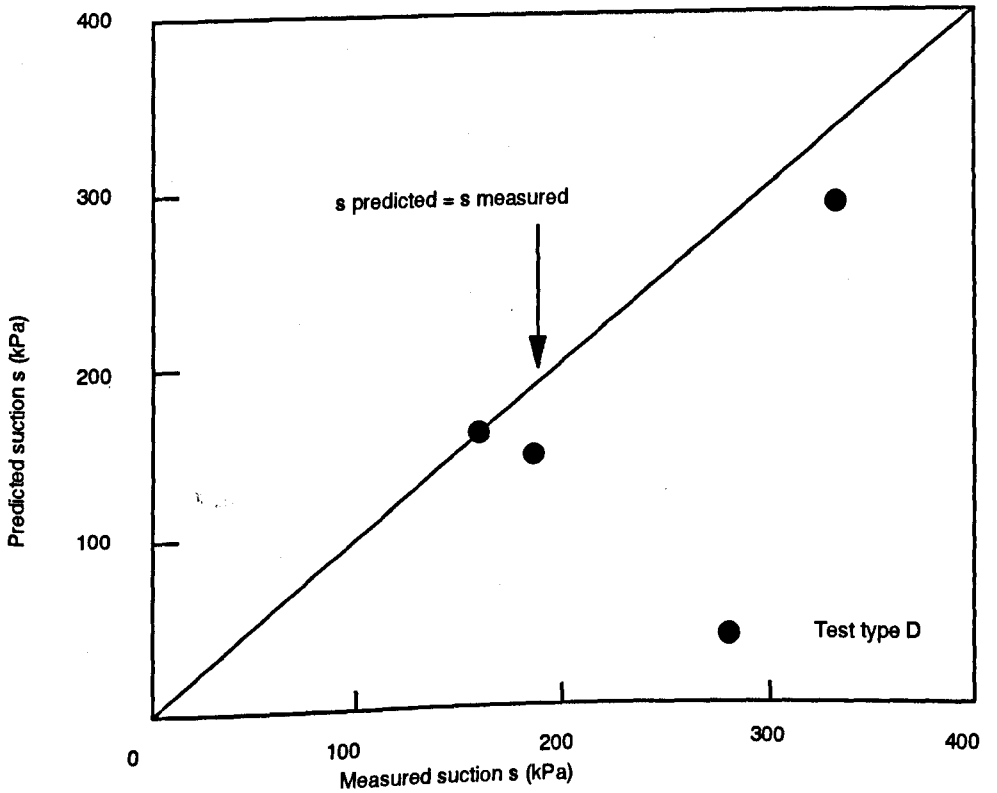

Fig (7.37b) Predicted versus measured suction at critical states for variable suction tests

	TEST NO.	AFTER COMPACTION			AFTER EQUALIZATION				
		v	S_r (%)	w (%)	p' (kPa)	s (kPa)	v	S_r(%)	w (%)
Suction zero test series	19A	2.2042	53.62	24.37	40	0	2.1500	100	43.39
	20A	2.1972	54.30	24.53	40	0	2.1599	100	43.76
	21B	2.2086	53.91	24.58	40	0	2.1562	100	43.63
	22B	2.2081	54.86	25.01	40	0	2.1361	100	42.87
	23B	2.2068	53.34	24.28	40	0	2.1331	100	42.75
	24C	2.2003	54.14	24.52	40	0	2.1153	100	42.08
	25C	2.1999	54.34	24.61	40	0	2.1511	100	43.43
	26C	2.1909	54.54	24.5	40	0	2.1478	100	43.31
Suction 100 kPa test series	10A	2.1998	53.73	24.32	50	100	2.1999	70.25	31.81
	11B	2.2127	53.12	24.30	50	100	2.2135	70.21	32.15
	12B	2.2028	54.14	24.57	50	100	2.2015	71.21	32.28
	13C	2.2071	52.99	24.14	50	100	2.1975	70.98	32.07
	27D	2.1947	55.12	24.85	50	100	2.2054	70.14	31.91
	29E	2.2092	52.94	24.08	50	100	2.2052	69.86	31.77
Suction 200 kPa test series	1A	2.2129	53.41	24.46	50	200	2.2112	63.30	28.93
	2A	2.1947	54.31	24.50	50	200	2.2128	63.44	29.04
	3A	2.2083	54.15	24.69	50	200	2.1988	65.00	29.40
	4A	2.2096	53.54	24.40	50	200	2.2202	64.08	29.74
	5A	2.2167	52.98	24.32	50	200	2.2245	63.56	29.36
	6B	2.2085	53.21	24.26	50	200	2.2155	63.37	29.06
	7B	2.2148	52.48	24.05	50	200	2.2283	63.57	29.46
	8C	2.2067	53.44	24.33	50	200	2.2023	64.01	29.03
	8C	2.2122	53.79	24.60	50	200	2.2214	63.92	29.46
	28D	2.2031	53.42	24.25	50	200	2.2254	62.60	28.94
	30F	2.1884	53.99	24.21	50	200	2.2065	63.35	28.83
Suction 300 kPa test series	14A	2.2035	53.85	24.45	50	300	Discontinued	Discontinued	Discontinued
	15A	2.2051	52.68	23.95	50	300	2.2183	58.53	26.90
	16B	2.2023	54.40	24.68	50	300	2.2088	60.18	27.45
	17C	2.2004	54.08	24.45	50	300	2.2053	60.23	27.39
	18C	2.2014	54.26	24.60	50	300	2.2087	60.04	27.38

Table (7.1) Values of state parameters before and after equalization

TEST No	NORMAL COMPRESSION				CRITICAL STATE					COMMENT
	p'(kPa)	s (kPa)	v	w (%)	p'(kPa)	q (kPa)	s (kPa)	v	w (%)	
1A	150	200	2.1054	28.88						FRICTION ON RAM
3A	100	200	2.1617	29.46	58.5	125.9	200	2.1617	30.48	
2A	200	200	2.0669	29.54	80.0	162.8	200	2.0669	30.50	
4A	150	200	2.1267	29.57	66.5	142.7	200	2.1267	30.77	
5A	300	200	1.9903	29.29	111.4	211.8	200	1.9903	30.91	
6B	100	200	2.1718	29.08	100.6	185.9	200	2.0326	31.07	
7B	200	200	2.0649	29.14	198.6	264.6	200	1.9286	30.89	
8C	150	200	2.0989	29.39	262.5	337.5	200	1.8749	30.60	
9C	100	200	2.1804	29.54	185.5	257.4	200	1.9349	31.47	
10A	150	100	2.0423	31.70	55.7	107.9	100	2.0423	33.17	
11B	100	100	2.1329	32.15	100.0	145.0	100	1.9917	34.07	
12B	200	100	1.9981	31.89	200.0	241.5	100	1.9092	32.92	
13C	150	100	2.0384	32.03	247.4	231.8	100	1.8889	32.59	BUCKLING FAILURE
14A	50	300								FILTER FAILURE
15A	250	300	2.0534	27.36	112.7	232.0	300	2.0534	28.58	
16B	100	300	2.1951	26.85	99.0	203.1	300	2.1298	28.18	
17C	100	300	2.1880	27.40	203.1	312.5	300	1.9453	29.26	
18C	150	300	2.1402	27.51	271.0	364.8	300	1.8874	29.35	
19A	175	0	1.9865	37.22	100	80.9	0	1.9865	37.22	
20A	200	0	1.9750	36.79						FRICTION ON RAM
21B	55	0	2.1145	42.05	55	43.0	0	2.0862	40.98	
22B	100	0	2.0377	39.15						FRICTION ON RAM
23B	200	0	1.9539	35.99						PRESSURE DROP
24C	150	0	2.0084	38.05	205.6	166.8	0	1.9328	35.20	
25C	150	0	2.0046	37.90	206.0	168.2	0	1.9377	35.38	
26C	75	0	2.0789	40.71	103.5	85.6	0	2.0146	37.22	
27D	100	100	2.1294	31.97	183.6	252.8	182.7	1.9127	31.97	
28D	100	200	2.1842	29.04	206.8	323.0	328.5	1.9353	29.04	
29E	150	100	2.0463	31.72	76.3	172.9	231	2.0463	30.67	
30F	125	200	2.1450	29.08	125.0	169	116	1.9768	33.33	
1SD	100	200	2.1526	28.89						
	200	100	1.9868	31.10	321	364	155	1.8500	31.10	
2S	100	300	2.1750	27.18						
	200	200	2.0566	28.71						
	300	100	1.9345	30.68						
3S	100	400	2.2035	26.22						
	200	300	2.1158	27.34						
	300	200	1.9992	28.87						
	400	100	1.9104	30.61						

Table (7.2) Values of state parameters before and after shearing

CHAPTER 8

FURTHER DEVELOPMENT OF CRITICAL STATE FRAMEWORK

CHAPTER 8

FURTHER DEVELOPMENT OF CRITICAL STATE FRAMEWORK

In this Chapter an attempt is made to provide a more complete formulation of a critical state framework for unsaturated soil behaviour.

8.1 NORMAL COMPRESSION AND CRITICAL STATE HYPER-LINES

The proposed unsaturated critical state model was defined in terms of 5 state variables: mean net stress p', deviator stress q, suction s, specific volume v and water content w (see Chapter 3). Normal compression and critical state hyper-lines were each defined by 3 equations. The experimental data arising from this research project supports the existence of these proposed relationships.

8.1.1 Normal compression relationships

Three normal compression relationships, defining a normal compression hyper-line, are proposed as follows:

$$q=0 \qquad (8.1)$$

$$v=N(s)-\lambda(s)\ln\left(\frac{p'}{p_a}\right) \tag{8.2}$$

$$w=A(s)-\alpha(s)\ln\left(\frac{p'}{p_a}\right) \tag{8.3}$$

Equation (8.1) is true by definition for isotropic stress states, while the linear relationships (with p′ on a logarithmic scale) of Equations 8.2 and 8.3 are supported by the experimental data presented in Section 7.2.1. The intercepts and slopes N(s), λ(s), A(s) and α(s) in Equations 8.2 and 8.3 are all functions of suction (see Figs 7.9, 7.10, 7.12 and 7.13). Equations 8.1, 8.2 and 8.3 are entirely consistent with the form of the normal compression relationships proposed in Chapter 3 (Equations 3.12, 3.13 and 3.14).

8.1.2 Critical state relationships

Three critical state relationships, defining a critical state hyper-line, are proposed as follows:

$$q=M(s)p'+\mu(s) \tag{8.4}$$

$$v=\Gamma(s)-\psi(s)\ln\left(\frac{p'-C(s)}{p_a}\right) \tag{8.5}$$

$$w=B(s)-\beta(s)\ln\left(\frac{p'}{p_a}\right) \tag{8.6}$$

Equations 8.4 and 8.6 have already been shown to fit the critical state data presented in Section 7.3.5, with the intercepts and slopes M(s), $\mu(s)$, B(s) and $\beta(s)$ all functions of suction (see Figs 7.33 and 7.36). Equation 8.5 was selected as a suitable form for the third critical state equation relating specific volume v to mean net stress p' and suction s. A factor C(s) was introduced in Equation 8.5 in order to model the curvature of the critical state lines shown in Fig 7.34. A limitation to the use of Equation 8.5 is that it is only applicable for values of p' higher than the value of C(s), otherwise the term ln(p'-C(s)) becomes indeterminate.

Values of $\Gamma(s)$, $\Psi(s)$ and C(s), calculated by regression analysis of the constant suction shear test data, are shown in Fig (8.1a), (8.1b) and (8.1c) respectively. The parameter C(s), shown in Fig (8.1c), is positive for suctions of zero, 200 and 300 kPa (giving a critical state line that is concave upwards) and negative for s=100 kPa (giving a line that is concave downwards). The parameter $\Psi(s)$, shown Fig (8.1b), can be thought of as the asymptotic slope of the critical state hyper-line at high values of p', and the variation of $\Psi(s)$ with suction is very similar to the variation of the slope $\lambda(s)$ of the normal compression hyper-line (see Fig 7.9). However $\Gamma(s)$, shown in Fig (8.1a), displays a very different variation with suction to that of N(s), the intercept of the normal compression line (see Fig 7.10). All three plots in Fig

(8.1) indicate the distinct possibility of discontinuities in the values of $\Gamma(s)$, $\Psi(s)$ and $C(s)$ at $s=0$ (corresponding to the transition from unsaturated to saturated conditions).

Fig (8.1d) shows predicted versus measured values of specific volume at critical states for Tests 27D, 28D, 1SD and 30F. The agreement shown in Fig (8.1d) is excellent and further support for the existence of unique critical state hyper-line.

Equations 8.4, 8.5 and 8.6 are entirely consistent with the form of the critical state relationships proposed in Chapter 3 (Equations 3.15, 3.16 and 3.17).

8.2 STATE BOUNDARY HYPER-SURFACE AND YIELD CURVES

A state boundary hyper-surface was proposed in Chapter 3, linking the normal compression hyper-line to the critical state hyper-line. Having established normal compression relationships and critical state relationships that are independent of stress path to the critical state then the existence of a state boundary hyper-surface appears more probable.

8.2.1 Existence of state boundary hyper-surface

Fig (8.2) shows the stress paths (q versus p') for constant

suction shear tests (type A, B and C) conducted at a suction of 200 kPa. Values of v are shown against the constant volume stress paths, but also the changing values of v are shown on the constant p′ and fully drained test paths (at intervals of $\Delta v = 0.03$). Inspection of the figure shows that the values of v from the three different types of shear test are reasonably consistent throughout the shearing process. The discrepancies are greatest during the middle part of the stress paths, when there was likely to be significant non-equalization of pore water pressure.

Fig (8.3), (8.4) and (8.5) show corresponding plots for the constant suction shear tests conducted at suctions of zero, 100 and 300 kPa respectively. The data in Figs 8.2 to 8.5 showed reasonable consistency. The difference in the specific volume at a point where two stress paths intersected was typically less than 0.03. This was very pleasing, given that the variation of specific volume between identical samples was ±0.012 prior to shearing (see section 7.1) and the subsequent accuracy of the measurement of changes of specific volume was approximately ±0.011 (see Section 4.2.3).

The fact that contours of specific volume (applicable to all test conditions) can be drawn on a plot of q versus p′ (for a given value of suction) suggests that the existence of a unique state boundary relationship of the form proposed in the Equation 3.20:

$$v=f(p',q,s) \tag{8.7}$$

By plotting values of water content w, instead of specific volume, it might have been possible to demonstrate the existence of a second unique state boundary relationship of the form proposed in Equation 3.21:

$$w=f(p',q,s) \tag{8.8}$$

However, instead of this, it was decided to investigate further a possible form for the first state boundary relationship described in Equation 8.7.

8.2.3 Development of first state boundary relationship from elliptical yield curves

If the soil behaviour inside the state boundary hyper-surface is assumed to be elastic, then any point on the state boundary is also on a yield surface in q,p',s space. Fig (8.6a) shows a constant suction cross-section of such a yield surface ie a yield curve in the q, p' plane. The yield curve forms the top of a constant suction elastic wall extending upwards from a constant suction swelling line in the v,p' plane (Fig 8.6b). The yield curve must therefore pass through points A and B, corresponding to the intersection of the elastic wall with the normal compression line for the relevant value of suction and the critical state line for the relevant value of suction.

If the elastic swelling index κ is assumed to be independent of suction, as assumed by Alonso, Gens and Josa (1990) and as supported by the experimental data of Vicol (1990), then the equation of a given elastic wall is:

$$v=N(s)-\lambda(s)\ln\left(\frac{p_o'}{p_a}\right)+\kappa\ln\left(\frac{p_o'}{p'}\right) \tag{8.9}$$

where the isotropic yield stress p_o' defines the particular elastic wall. The value p_c' of the mean net stress at point B (where the yield curve meets the critical state line) is then given by the intersection of the elastic wall and the critical state line in the v,p′ plane:

$$v_c=N(s)-\lambda(s)\ln\left(\frac{p_o'}{p_a}\right)+\kappa\ln\left(\frac{p_o'}{p_c'}\right)=\Gamma(s)-\psi(s)\ln\left(\frac{p_c'-C(s)}{p_a}\right) \tag{8.10}$$

By rearranging Equation (8.10):

$$p_c'=C(s)+p_a\exp\left(\frac{\Gamma(s)-N(s)+\lambda(s)\ln\left(\frac{p_o'}{p_a}\right)-\kappa\ln\left(\frac{p_o'}{p_c'}\right)}{\psi(s)}\right) \tag{8.11}$$

p_c' occurs on both sides of Equation (8.11), but an iterative procedure can be used to calculate a value for p_c' for a given value of p_o' (and the relevant value of suction).

A shape must be now selected for the yield curve passing through point A (with coordinates $p' = p_o'$, $q = 0$) and

point B (with coordinates $p' = p_c'$ (given by the Equation 8.11) and $q = M(s)\, p_c' + \mu(s)$). The most obvious choice is an elliptical yield curve, equivalent to the Modified Cam clay model for saturated soil (Roscoe and Burland, 1968). If the flow rule is associated (at least at critical states), then the apex of the ellipse must be at point B (the intersection with the critical state line). If the ellipse is extended beyond B it will not pass through the origin in the q, p' plane (see Fig 8.6), and the aspect ratio M^* of the ellipse (which is a function of s and p_o') can be related to the slope M(s) and intercept $\mu(s)$ of the critical state line:

$$M^* = \left(\frac{M(s) p_c' + \mu(s)}{p_o' - p_c'} \right) \tag{8.12}$$

The equation of the elliptical yield curve passing through points A and B is then given by the following equation:

$$q^2 = M^{*2} (p_o' - p')(p' + p_o' - 2p_c') \tag{8.13}$$

where the isotropic yield stress p_o' can be related to the current value of p' and v at a general point x on the elastic wall (Fig 8.6) by rearranging Equation (8.9):

$$p_o' = \exp\left(\frac{N(S) - v - \kappa \ln p' + \lambda(s) \ln p_a}{\lambda(s) - \kappa} \right) \tag{8.14}$$

and p_c' and M^* are then given by Equations 8.11 and 8.12 respectively. Equation 8.13, in combination with Equations 8.14, 8.11 and 8.12, forms a state boundary relationship

of the type presented in Equation 8.7.

8.2.4 Prediction of test paths

Using the state boundary relationship of Equations 8.13, 8.14, 8.11 and 8.12, together with the test conditions and the initial state of the sample it was possible to predict complete test paths (in q, p',v space) for the constant suction shear tests (type A, B and C).

Test paths were not predicted for the variable suction shear tests (types D, E and F) because this would have required a lengthy interpolation procedure. In addition, it would have been impossible to predict test paths for test type D without the second state boundary relationship (linking water content to the other variables), because this test type included constant water content control. The lack of the second state boundary relationship also meant that it was not possible to predict the variation of water content during the constant suction shear tests (only the initial and final values of w on the normal compression hyper-line and the critical state hyper-line could be calculated).

The soil constants used in predicting the various test paths are listed in Table 8.1. The first 5 columns in Table 8.2 shows how the test path was predicted for the first few increments of a typical constant volume, constant

suction shear test (Test 4A). An initial value of v was calculated from the known value of p′ after consolidation and the equation of the relevant normal compression line. v then remained constant at this value throughout the shearing process (see column 1 of Table 8.2). Fixed increments of p′ (in this case $\Delta p'$ = -7 kPa) were then considered (see column 2). For each value of p′, and the fixed value of v, it was possible to calculate a value for the isotropic yield stress p_o' from Equation 8.14 (see column 3). The value of mean net stress at the intersection of the yield curve with the critical state line p_c' was then calculated from Equation 8.11, using an iterative procedure (see column 4). Finally, the deviator stress q was calculated by using Equation 8.13, with M^* given by Equation 8.12 (see column 5 in Table 8.2).

The first 5 columns of Table 8.3 shows the prediction of the first few increments of a typical constant p′, constant suction shear test (Test 6B). Column 1 gives the constant value of p′. The easiest way to proceed was then to consider increments in the isotropic yield stress p_o', corresponding to a given expansion of the yield curve (see column 2). For each value of p_o', v could be calculated from Equation 8.14 (column 3) and p_c' from Equation 8.11 (column 4). Finally the deviator stress q was calculated from Equation 8.13, with M^* given by the Equation 8.12 (see column 5). Fully drained, constant suction shear tests (type C) were predicted in a similar fashion, by

considering fixed expansions of the yield curve.

To predict a test path it was necessary to calculate values for p_o' and p_c' for all points in the test. Strictly this meant that the values of p_o' and p_c' should remain throughout within the range of values for which experimental data were available to define the normal compression line and critical state line respectively. Unfortunately, if this restriction had been applied rigorously then no test paths would have been predicted. Therefore, it was decided to predict those test paths which did not involve too much extrapolation beyond the range of experimental data to calculate p_o' and p_c'. Test paths were therefore predicted for three constant volume, constant suction tests (2A, 4A, and 19A), one constant p', constant suction test (6B) and three fully drained, constant suction tests (9C, 17C and 26C). Two other tests (15A and 13C) could have been included, but they were omitted because the experimental data were considered to be of lower quality (there was some evidence of loading ram friction in Test 15 A and the sample in Test 13 C failed at an unusually low strain due to buckling).

To predict the various test paths, an assumption had to be made for the value of the swelling gradient κ. A value of 0.035 was selected as being approximately $0.2\lambda(s)$, where $\lambda(s)$ was taken as an average value over the relevant range of suction from zero to 300 kPa. Although this was a

relatively arbitrary assumption, the influence of the value of κ was checked by investigating the effect on the predicted test path of a typical fully drained test (Test 9C) of assuming 3 different values of κ. Fig (8.7) shows the predicted test path for Test 9C with κ equal to 0.025, 0.035 and 0.045. The three test paths are virtually indistinguishable and it therefore appeared that the influence of κ was minimal. A value of 0.035 therefore was assumed in predicting all remaining test paths.

Fig (8.8) shows the predicted test paths and the experimental tests paths for two constant volume tests (2A, 4A) conducted at a suction of 200 kPa. It appears that the predicted test path for each test lies slightly above the experimental test path. This is consistent with the slight discrepancies noted between the constant volume test paths and the values of v from other test types (see Fig 8.2). The discrepancy could be due to non-uniqueness of the state boundary, but could equally well be due to non-equalization of pore water pressure throughout the sample (bearing in mind that the tests were strain controlled, at a rate that was selected to give virtually complete equalization only at failure).

Fig (8.9) shows the predicted and experimental test paths for a constant volume test (19A) conducted at zero suction. The agreement is rather poor, although this may be partly due to the fact that the experimental data were considered

to be of relatively poor quality in this test. The quality of the test was hampered by considerable "spikiness" in the feedback control (this only happened in constant volume tests conducted at zero suction).

Fig (8.10) shows predicted and experimental test paths for a constant mean net stress test (6B) conducted at a suction of 200 kPa. The test path is plotted in q, v space, because p' remained constant during shearing. The agreement between predicted and experimental test paths is excellent.

Fig (8.11), Fig (8.12) and Fig (8.13) show predicted and experimental stress paths for fully drained tests (26C, 9C and 7C) conducted at suctions of zero, 200 and 300 kPa respectively. The agreement between predicted and experimental stress paths is excellent. All the important features observed in the experimental paths have been revealed in the predicted test paths.

In general, therefore, inspection of Figs (8.8) to (8.13) indicates a pleasing level of success in the prediction of test paths for constant suction shear tests (bearing in mind that the experimental tests were designed to provide high quality critical state data but were conducted too fast to provide high quality test paths).

A qualitative explanation can be put forward at this stage, of why Test 29E (a constant volume, increasing suction

shear test) did not reach a critical state. Fig (8.14) shows qualitative predictions of constant suction cross-sections of the same yield surface plotted in q,p′ space. The experimental test path obtained in Test 29E is also plotted in Fig (8.14). Bearing in mind the significant increase in suction during shearing, it appears that the test path went well inside the yield surface and headed towards a Hvorslev type surface.

8.3 FLOW RULE AND PREDICTION OF SHEAR STRAIN

An associated flow rule was adopted to predict the development of shear strain during constant suction shear tests. The ratio of plastic volumetric strain increment $d\varepsilon_v^p$ to plastic shear strain increment $d\varepsilon_s^p$ was therefore given by:

$$\frac{d\varepsilon_v^p}{d\varepsilon_s^p} = -\frac{dq}{dp'} \tag{8.15}$$

where q and p′ were values of deviator stress and mean net stress on the current yield curve (ie with s and p_o' held constant).

By differentiating Equation 8.13 with respect to p′ (while holding M^*, p_o' and p_c' constant):

$$\frac{dq}{dp'} = -M^{*2}\frac{(p'-p_c')}{q} \tag{8.16}$$

Inserting this in Equation 8.15:

$$d\varepsilon_s^p = q\frac{d\varepsilon_v^p}{M^{*2}(p'-p_c')} \qquad (8.17)$$

By knowing the plastic volumetric strain increment the value of the plastic shear strain increment can be therefore calculated. Elastic shear strains were neglected, so Equation (8.17) provided the total shear strain increment.

The shear strain predicted from Equation (8.17) was the true shear strain of the sample. This predicted true shear strain should be compared with the true shear strain measured in the experimental tests. The following equations were used to transform the measured nominal values of axial strain ε_a and volumetric strain ε_v to true values of axial strain ε_{at}, volumetric strain ε_{vt} and shear strain ε_{st}:

$$\varepsilon_{at} = -\ln(1-\varepsilon_a) \qquad (8.18)$$

$$\varepsilon_{vt} = -\ln(1-\varepsilon_v) \qquad (8.19)$$

$$\varepsilon_{st} = \varepsilon_{at} - \frac{1}{3}\varepsilon_{vt} \qquad (8.20)$$

Predictions of shear strains were made for the same tests for which the predictions of test path were made (Tests 2A, 4A, 19A, 6B, 9C, 17C and 26C). Columns 6 to 11 of Tables 8.2 and 8.3 show the incremental procedure used to evaluate shear strain for the first few increments of two typical tests.

The influence of the swelling gradient κ on the prediction of shear strain was investigated for a typical fully drained test (Test 9C). Three different values of κ were considered (0.025, 0.035 and 0.045). Fig (8.15) shows how the value of κ influences the predicted development of shear strain in the sample. Greater shear strains were predicted for higher values of κ. The value of κ was assumed to be 0.035 for all remaining predictions (to be consistent with the test path predictions).

Fig (8.16) shows deviator stress-true shear strain curves for constant volume, constant suction tests (2A and 4A) conducted at a suction of 200 kPa. Fig (8. 17) shows a similar plot for a constant volume test conducted at zero suction (Test 19A). The comparison between predicted and measured shear strains was very poor in constant volume tests. The model drastically under-estimated the shear strain during the early stage of each test.

Fig (8.18) shows the predicted and experimental stress-strain curves for a constant mean net stress, constant suction test (6B) conducted at a suction of 200 kPa. Again, the prediction was not particularly good, with the shear strain under-estimated during the early part of the test and over-estimated during the later part.

Figs (8.19), (8.20) and (8.21) show the predicted and experimental stress-strain curves for fully drained tests,

conducted at suctions of zero, 200 and 300 kPa respectively. Predicted shear strains again under-estimated the measured values during the early part of each test and over-estimated the measured values later in the test.

Overall the agreement between predicted and experimental values of shear strain was not particularly good. Possible reasons for the inconsistencies included:

(a) The flow rule for unsaturated soil may well be non-associated.

(b) Elastic components of shear strain were neglected in the prediction of shear strain. In reality there may well be significant elastic shear strains.

(c) The experimental measurements of shear strain were not very accurate in the early part of shearing (because the test procedure was designed primarily to provide high quality critical state data). In particular, the axial strain of the sample was measured externally, leading to significant over-estimation of strain at small strains (Burland and Symes, 1982).

(d) The experimental values of strain may well have been affected by significant non-equalization of

pore water pressure in the samples during shearing.

Modification to the prediction method could have been included to account for points (a) and (b) above in an attempt to produce better agreement with the experimental measurements of shear strain. However this was considered to be unjustified, given the weaknesses in the experimental data outlined in points (c) and (d).

8.4. COMPARISON WITH BARCELONA MODEL.

Alonso,Gens and Josa (1990) proposed an elasto-plastic critical state model for unsaturated soils, described in Sections 2.7 and 3.3. The constitutive model (refered to as the "Barcelona" model hereafter) was defined in terms of 4 state variables: mean net stress p', deviator stress q, suction s and specific volume v. Water content w was not considered as a fifth variable in their analysis. It is worth examining how well the Barcelona model performs in predicting the experimental behaviour observed in this project.

The shape of the yield curve produced by the compaction process and observed during the consolidation stage (Fig 7.5) was qualitatively consistent with the loading collapse (LC) yield curve proposed in the Barcelona model (see Equation 2.25 and Fig 2.27). Similarly, the pattern of swelling and collapse observed during the equalization

stage (Section 7.1) was consistent with the shape of LC yield curve in the Barcelona model.

In the Barcelona model the slope of the isotropic normal compression line for constant suction loading $\lambda(s)$ was assumed to decrease monotonically with increasing suction from the saturated value $\lambda(o)$, becoming asymptotic to a value $r\lambda(o)$ at high suction (see Equation 2.24):

$$\lambda(s)=\lambda(o)[(1-r)\exp(-\beta s)+r] \qquad (8.21)$$

Comparison with the experimental results presented in Fig (7.9) suggests that the Barcelona model can adequately represent the variation of $\lambda(s)$ for suctions greater than 100 kPa, but cannot model the sharp drop in the value of $\lambda(s)$ as suction tends to zero (as mentioned previously, there may well be a discontinuity in the soil behaviour at s=0).

The shear strength behaviour of unsaturated soil was modelled by the following equation in the Barcelona model (see Equation 2.26):

$$q=Mp'+Mks \qquad (8.22)$$

The slope M of the critical state line at constant suction was considered to be unaffected by the value of suction, while the apparent cohesion due to suction (Mks) was assumed to increase linearly with suction. Comparison with Equation (7.4) and the data presented in Fig (7.33) suggests that the slope M(s) varied slightly with suction

and the "apparent cohesion" $\mu(s)$ did not vary quite linearly with suction. However, over the stress range examined in this research, the simple relationship of Equation 8.22 assumed in the Barcelona model was a reasonably good first approximation.

The Barcelona model includes a yield surface in q, p', s space. Constant suction cross-sections of this yield surface are elliptical in shape (see Fig 8.22), as proposed in the development of the state boundary relationship in Section 8.2.3. However in the Barcelona model the aspect ratio of the ellipse is constant (and equal to the slope of the critical state line M) and the ellipse intersects the negative p' axis at a point C, the coordinate of which varied only with suction. In contrast, for the elliptical yield curve suggested in Section 8.2.3 the aspect ratio M^* varies with both suction and the current isotropic yield stress p_o', (see Fig 8.6 and Equation 8.12) and the position of point C is also a function of p_o' as well as suction. This flexibility was found to be necessary in order to correctly model the position of the critical state hyper-line in both the q, p' plane and the v, p' plane. The equation of the elliptical yield curve in the Barcelona model is given by:

$$q^2 = M^2 (p_o' - p')(p' + ks) \qquad (8.23)$$

Where p_o' is given by Equation 8.14. This is significantly simpler than the elliptical yield curve presented in

Section 8.2.3 (see Equations 8.13, 8.14, 8.11 and 8.12).

A consequence of the form of the elliptical yield curve proposed in the Barcelona model is that the projection of the critical state hyper-line in the v, p' plane is given by Equation 2.27:

$$v=N(s)-[\lambda(s)-\kappa]\ln\left(2+\frac{ks}{p'}\right)-\lambda(s)\ln p' \qquad (8.24)$$

The critical state line for a constant value of suction is therefore concave downwards for all values of suction, becoming parallel to the corresponding normal compression line at high values of p' (see Fig 8.22). This does not fit well with the observed experimental data (see Fig 7.34). Therefore, the price to pay for the relatively simple form of elliptical yield curve is a poor representation of the volumetric response.

As the Barcelona model does not represent well the position of the critical state hyper-line in the v, p' plane, the test paths predicted by the model are likely to show significant errors, unless the predicted position of the relevant part of the critical state hyper-line coincidentally happens to fit the true position reasonably well for the particular test. Despite this fact, the Barcelona model must be considered a major step forward, as it is qualitatively consistent with virtually all the major features observed in the experimental data.

8.5 PHYSICAL INTERPRETATION OF OBSERVED BEHAVIOUR

The structure of unsaturated soils plays a major role in their mechanical behaviour. The influence of the structure of the unsaturated compacted soil was noted in various places during this research project.

Compacted unsaturated soil is formed by number of packets or lumps and each packet is formed by individual particles. The packets are considered to be saturated and held together by negative pore water pressures whereas the larger pore spaces between the packets are unsaturated (probably filled with a mixture of water and air). Two levels of soil structure can therefore be identified: the saturated "microstructure" within an individual packet and the unsaturated "macrostructure" formed by the arrangement of many packets.

Within the research project, many aspects of the observed soil behaviour were explained by the concept of yielding. Various pieces of experimental evidence suggest that this was yielding of the "macrostructure", whereas the saturated "microstructure" of each individual packet remained heavily over-consolidated and therefore essentially elastic in behaviour.

The initial water content of all samples was approximately 25 %. Therefore, if the microstructure of the packets was

saturated and all the soil particles were within the packets the local water content of this microstructure could not be greater than 25% (which would correspond to no water in the large inter-packet macrostructural voids). Assuming λ= 0.19 and N=3.30 for saturated kaolin (Schofield and Wroth, 1968), at this water content the saturated microstructure would be normally consolidated only at a stress of almost 6000 kPa. This is far larger than the stresses imposed at any time during the test programme. Therefore it is likely that the individual saturated packets remained heavily over-consolidated throughout.

The "elastic" swelling of samples during the equalization stage could be explained as the microstructure of individual heavily over-consolidated packets taking up water as the suction was reduced. The major compression (collapse) that occurred in the later part of the equalization stage in some tests could be explained as the collapse of the macrostructural arrangement of packets, due to the loss of strength at the inter-packet contacts (friction at the inter-packet contacts would become less when suction falls). This collapse was associated with movement of the LC yield curve, which therefore represents yielding of the macrostructure (and not the microstructure).

During the consolidation stage, samples were brought to

"virgin" states on the normal compression hyper-line. It can now postulated that this normal compression hyper-line corresponded to normal compression of the macrostructure, whereas the microstructure was still heavily over-consolidated. This is consistent with the fact that the normal compression lines for all values of suction (including zero) fell considerably below the normal compression line for saturated reconstituted kaolin (see Fig 8.23) and had a slope that was between the elastic swelling index κ and the plastic compression index λ for saturated reconstituted kaolin. The normal compression lines for compacted kaolin would intersect the normal compression line for reconstituted kaolin at a very high value of stress, and this could correspond to yielding of the saturated microstructure of individual packets.

During shear tests where the water content was allowed to vary (test types A, B, C, E and F), the water content continued to increase slowly even at very large strains when all other state variables had reached a critical state and the tests were terminated. Similarly in constant water content tests (type D) the pore water pressure continued to rise slowly after all other parameters had stabilised. This pattern of behaviour could be attributed to the fact that the microstructure of heavily over-consolidated packets never reached a true critical state on shearing and continued to dilate, even though the macrostructure had been sheared to a critical state.

This explanation of the observed soil behaviour in terms of a normally consolidated macrostructure and a heavily over-consolidated microstructure suggests that a complete critical state framework for unsaturated soil should allow for the possibility of a second level of yielding (of the microstructure) at very high stresses. However the stress levels required to cause this microstructural yielding would often be so great that they would have no practical relevance.

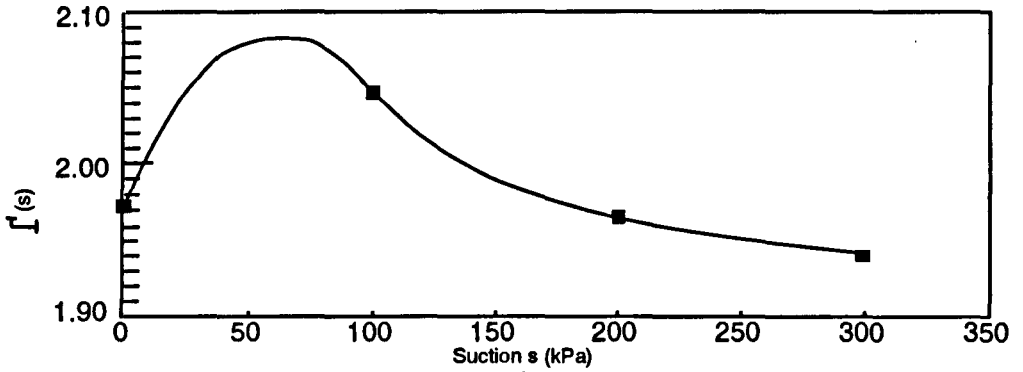

Fig (8.1a) Γ(s) versus suction

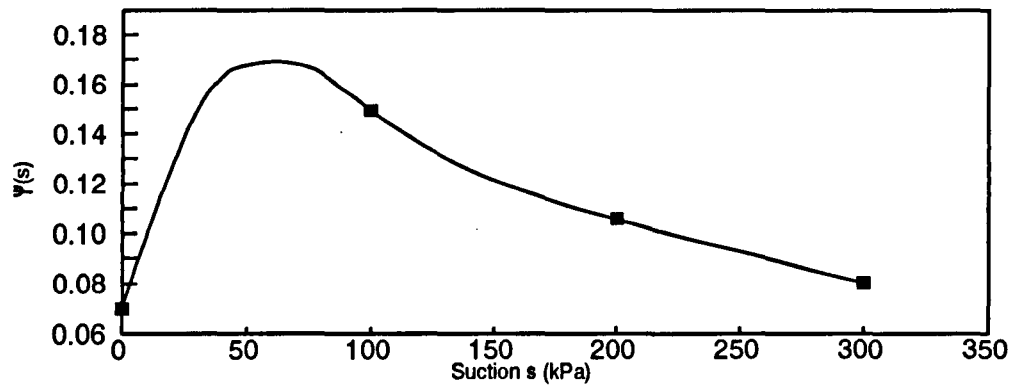

Fig (8.1b) Ψ(s) versus suction

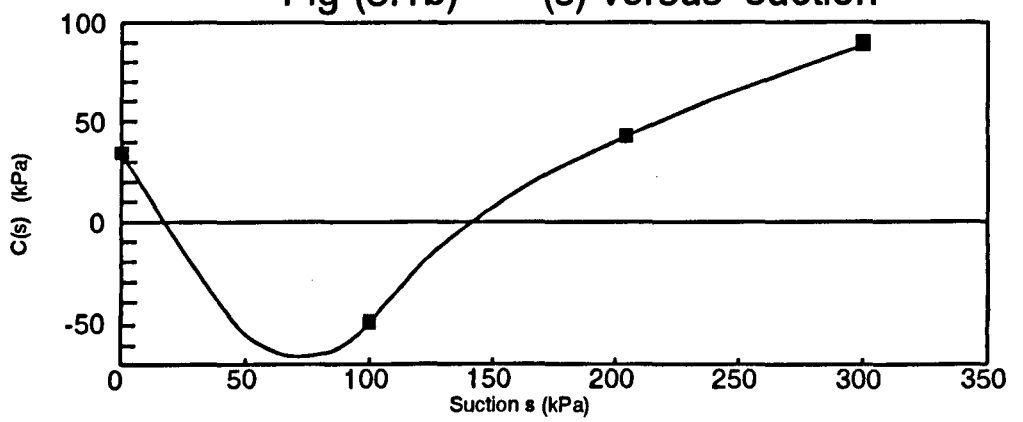

Fig (8.1c) C(s) versus suction

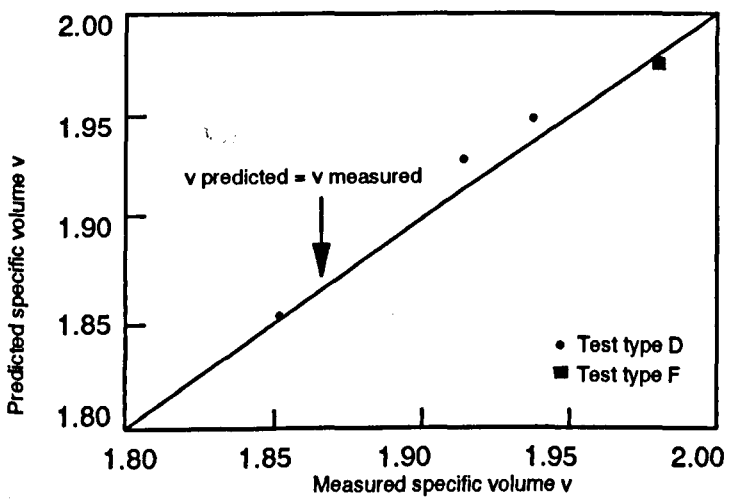

Fig (8.1d) Predicted versus measured specific volume at critical states for variable suction tests

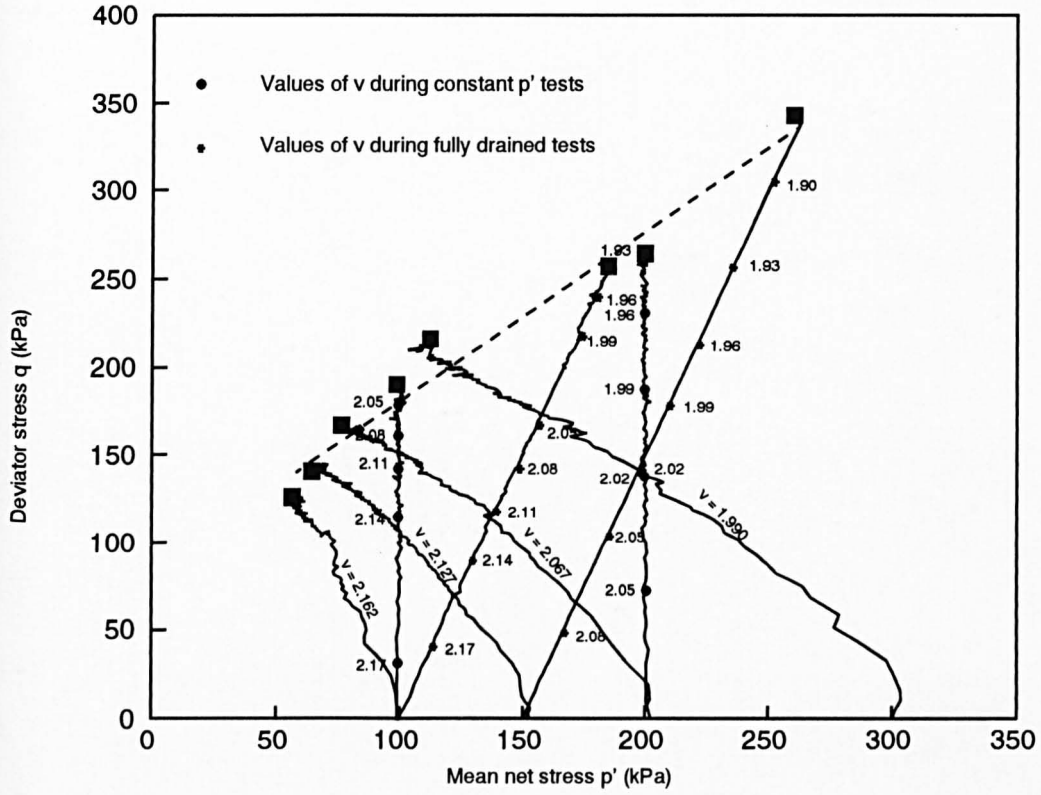

Fig (8.2) Specific volume data at a suction of 200 kPa

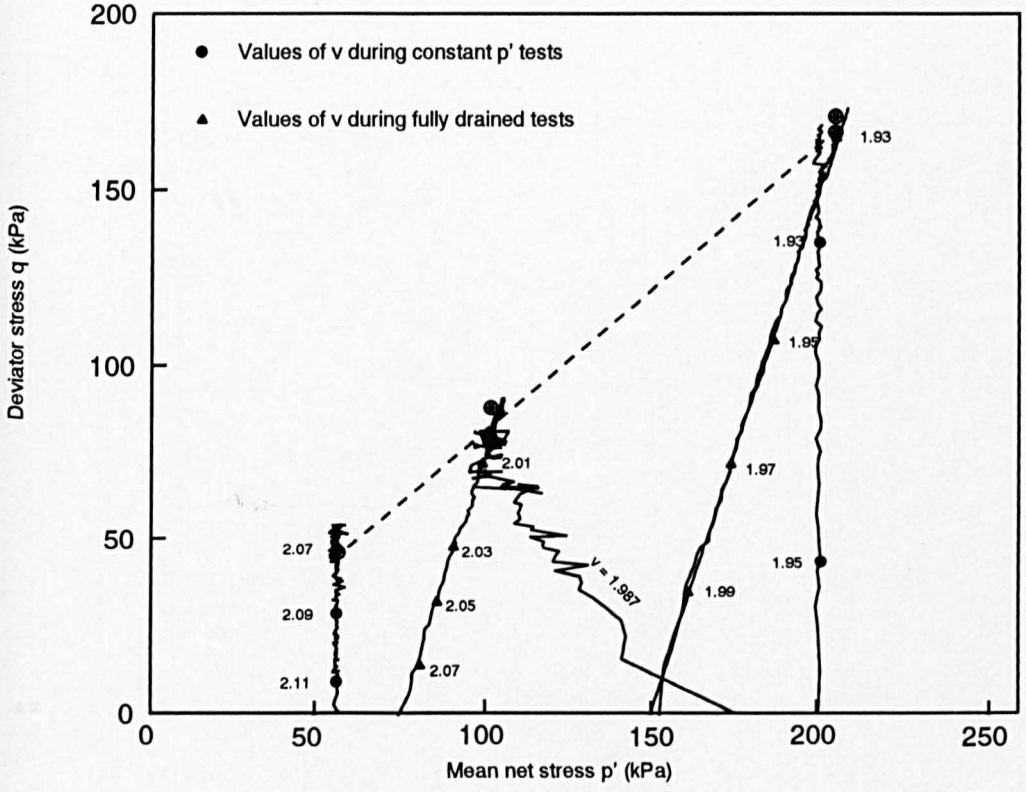

Fig (8.3) Specific volume data at zero suction

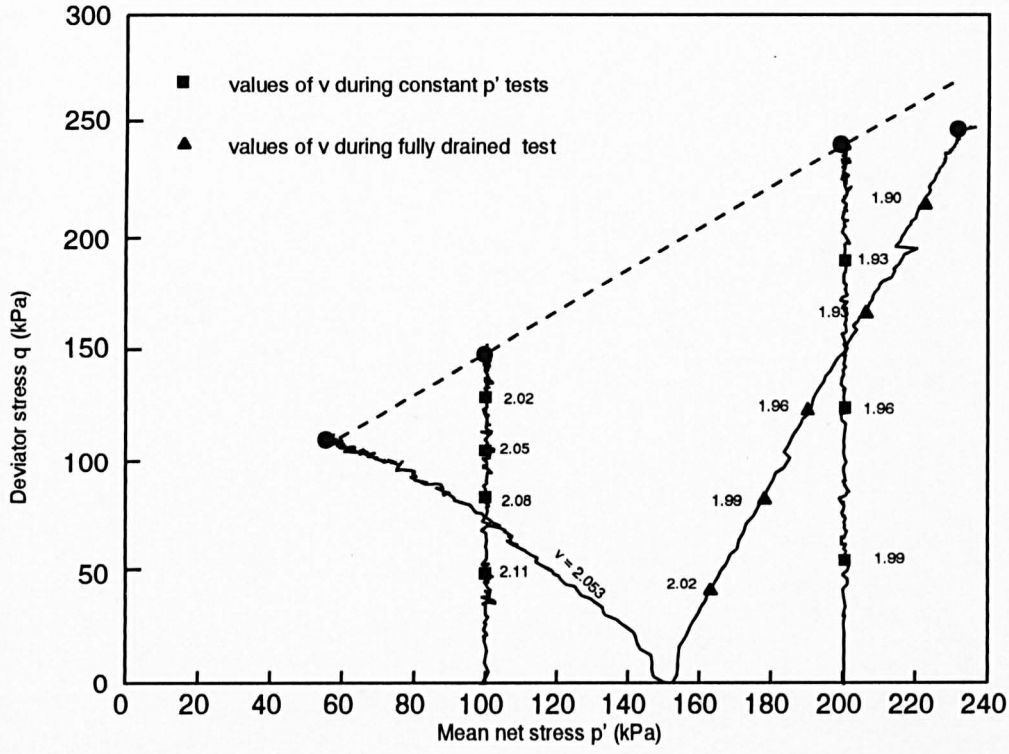

Fig (8.4) Specific volume data at suction of 100 kPa

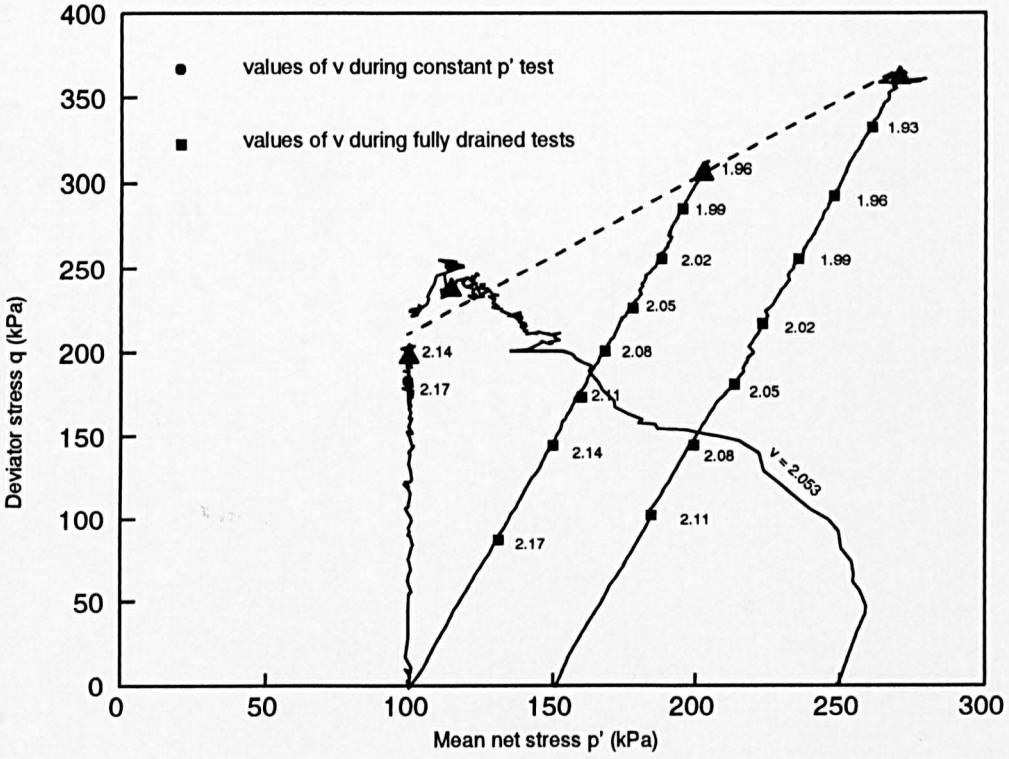

Fig (8.5) Specific volume data at suction of 300 kPa

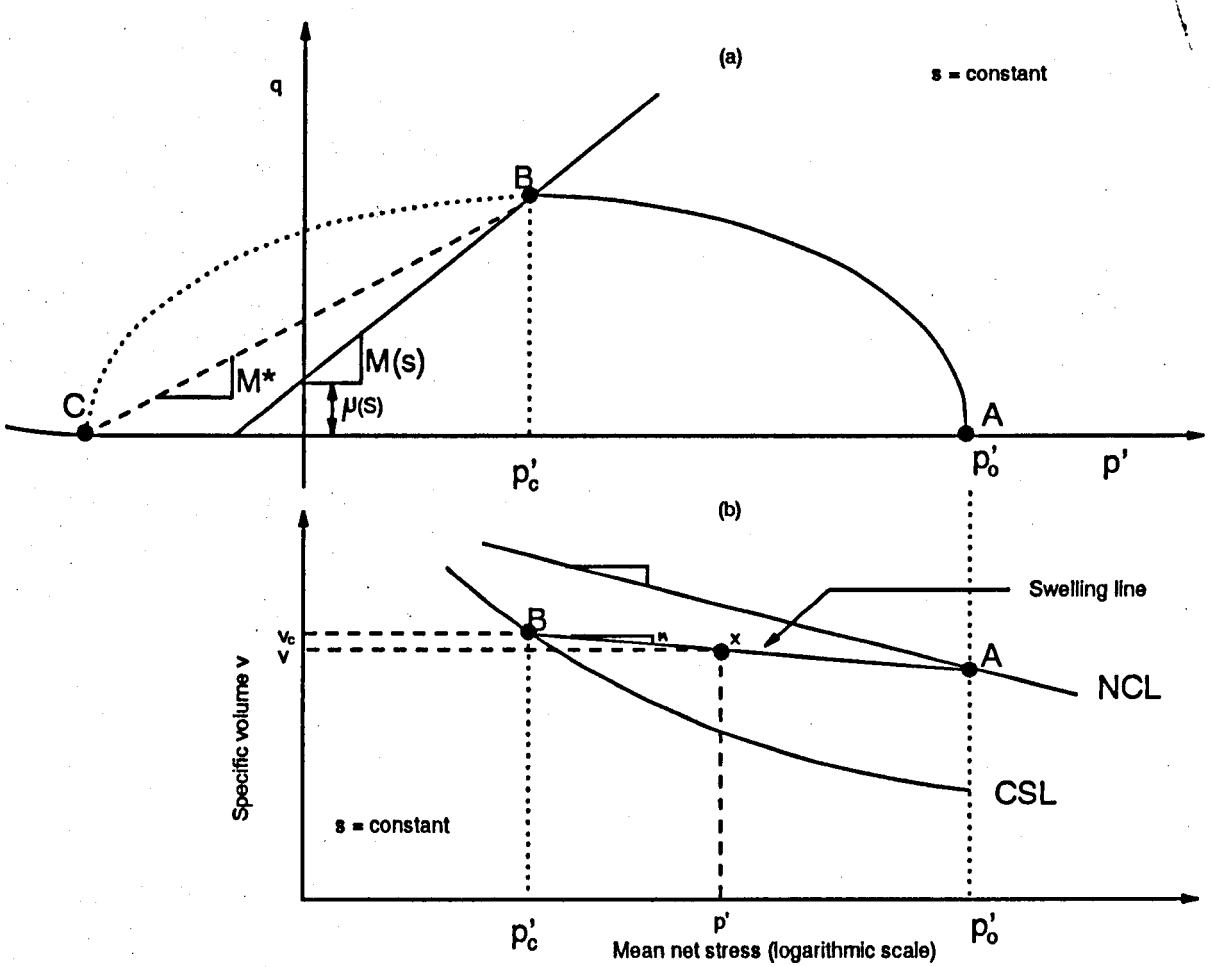

Fig (8.6) Proposed elliptical yield curve for constant suction

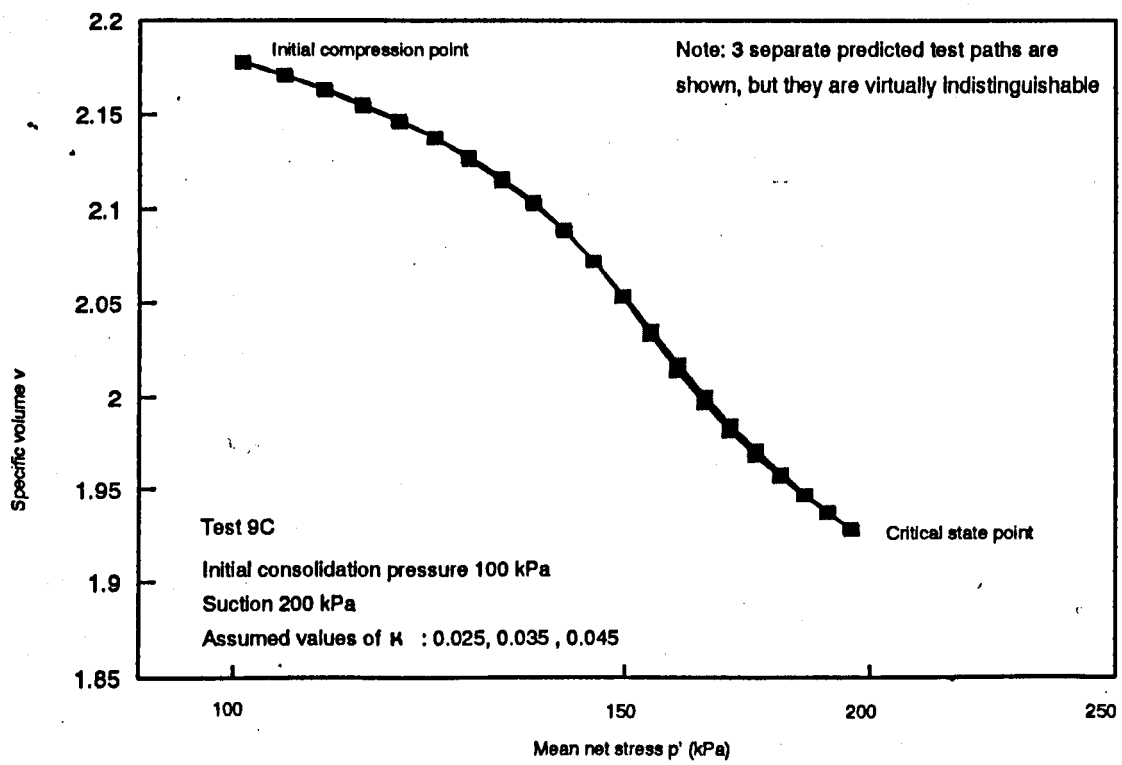

Fig (8.7) Influence of swelling gradient κ on the predicted test path for Test 9C

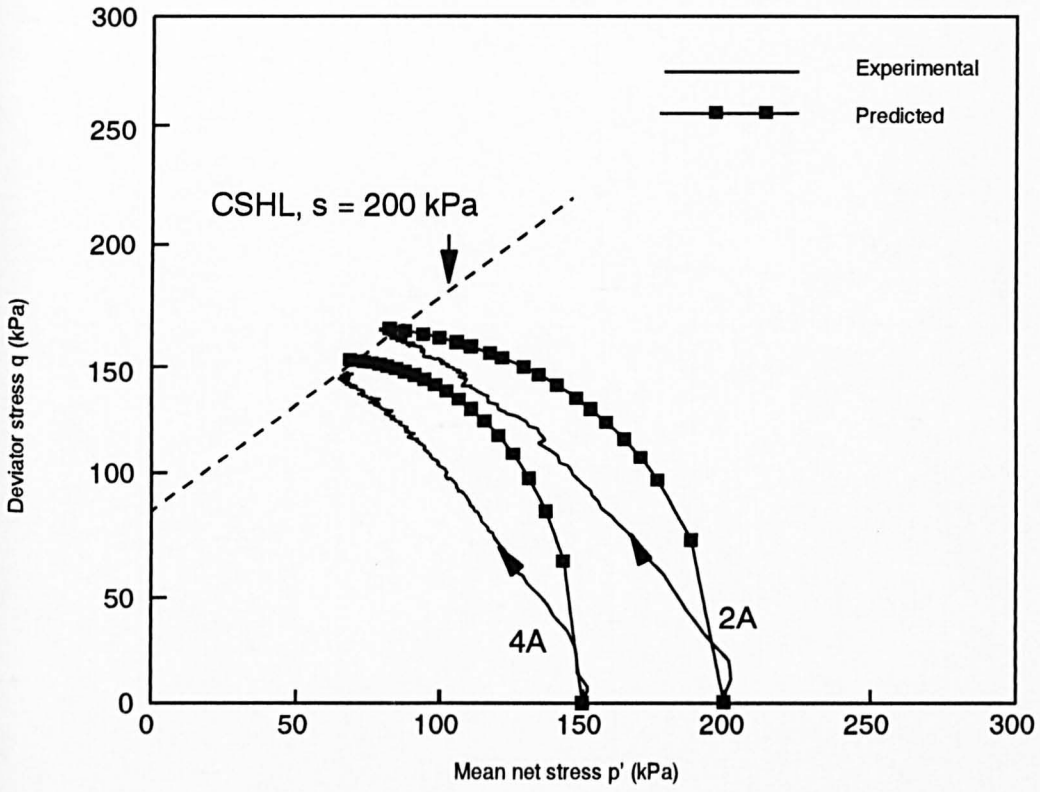

Fig (8.8) Comparison of predicted and experimental test paths for constant volume, constant suction tests at a suction of 200 kPa

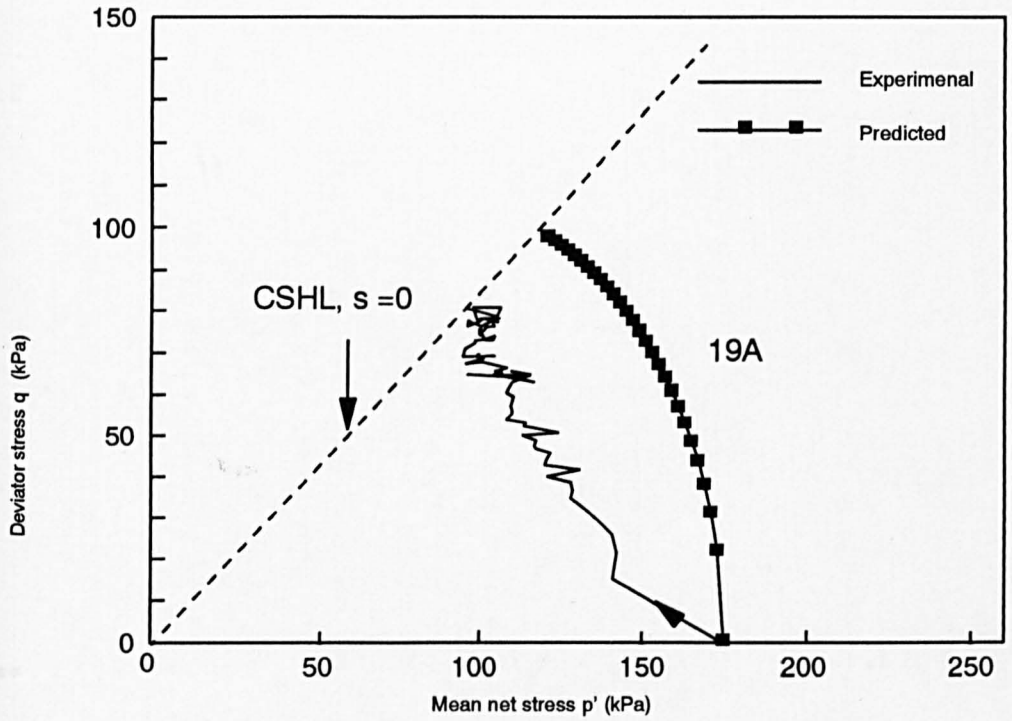

Fig (8.9) Comparison of predicted and experimental test paths for a constant volume, constant suction test at zero suction

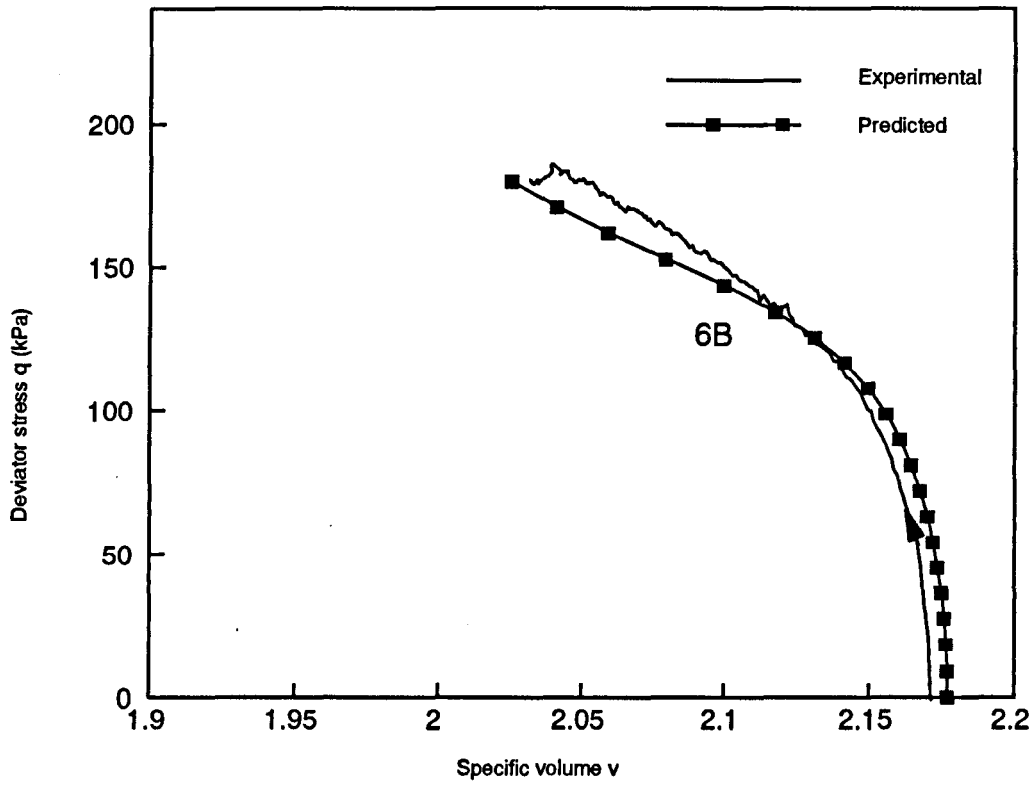

Fig (8.10) Comparison of predicted and experimental test paths for a constant mean net stress, constant suction test at a suction of 200 kPa

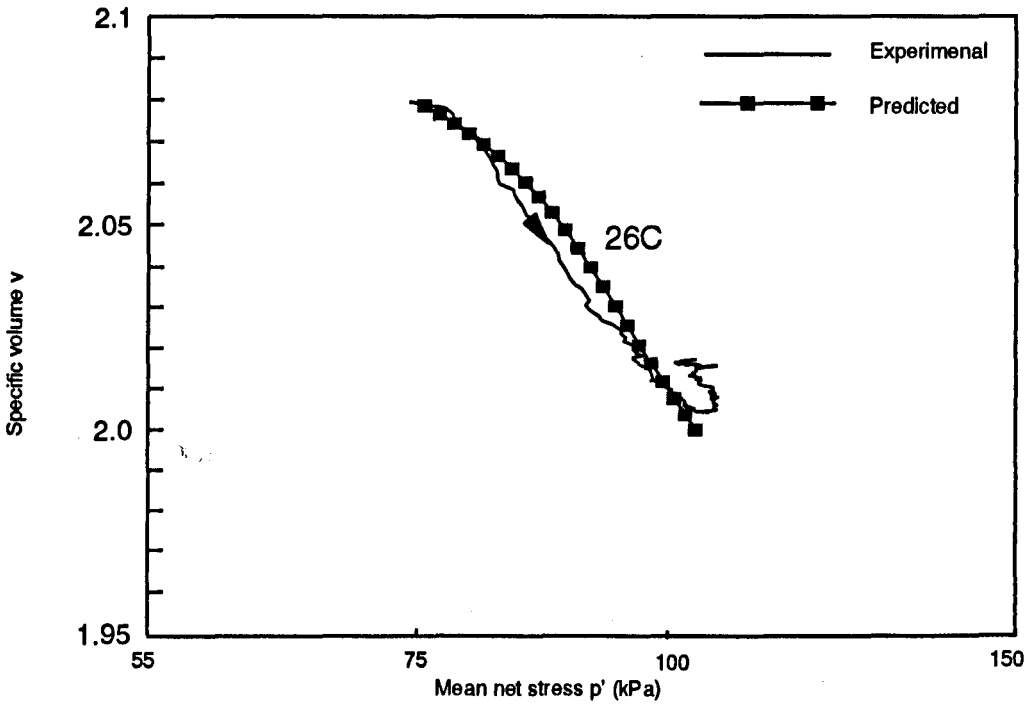

Fig (8.11) Comparison of predicted and experimental test paths for a fully drained, constant suction test at zero suction

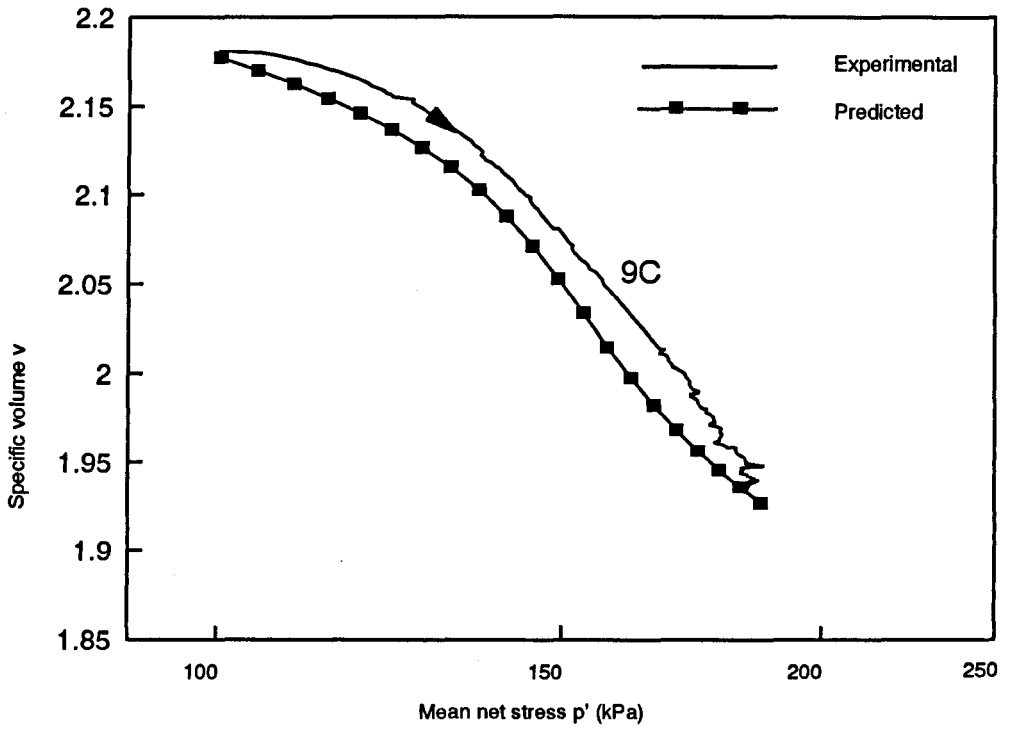

Fig (8.12) Comparison of predicted and experimental test paths for a fully drained, constant suction test at a suction of 200 kPa

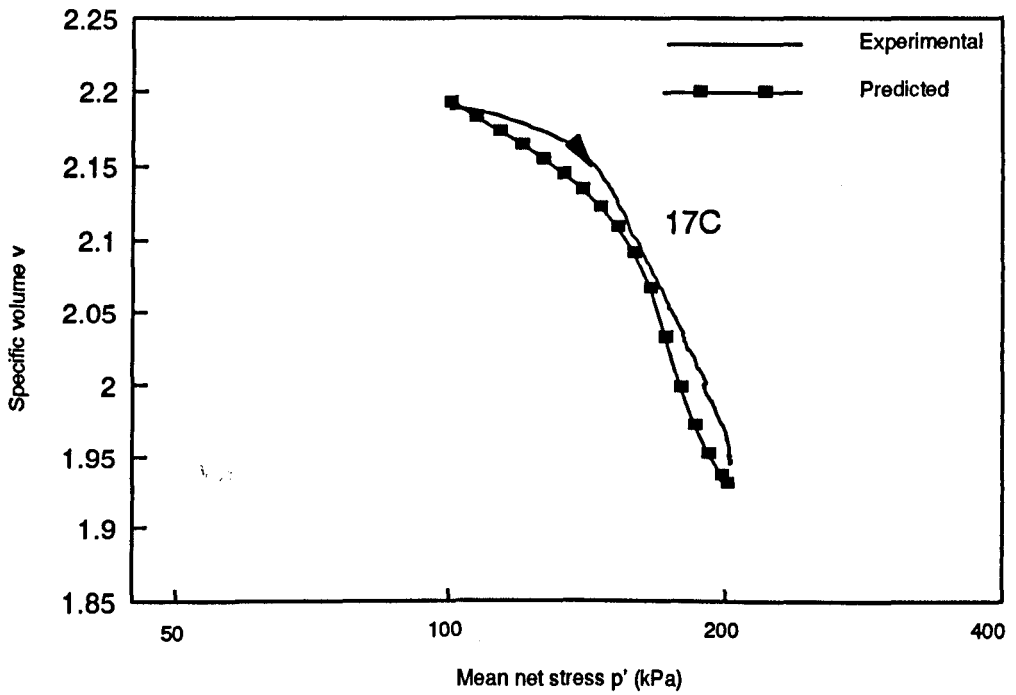

Fig (8.13) Comparison of predicted and experimental test paths for a fully drained, constant suction test at a suction of 300 kPa

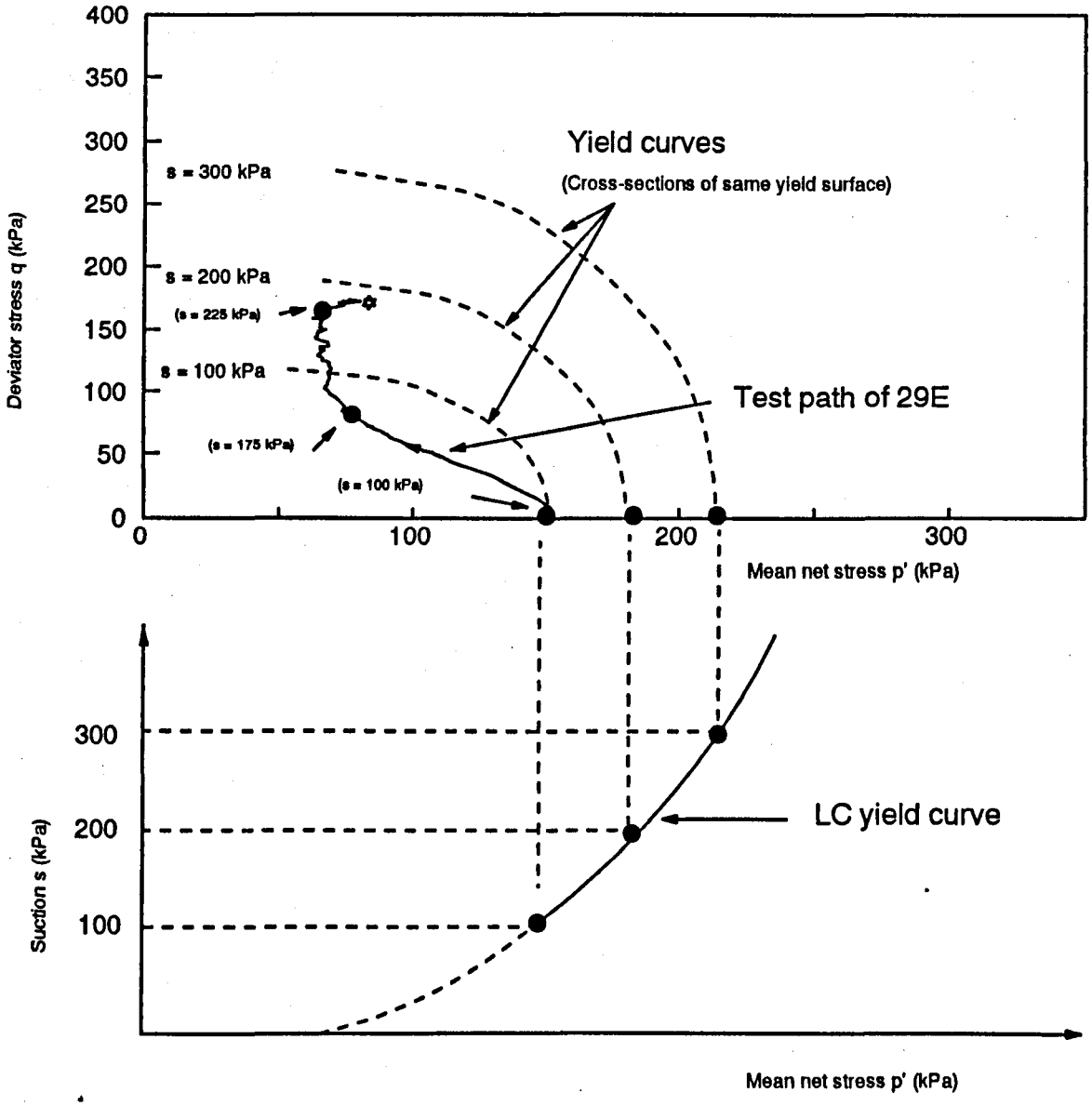

Fig (8.14) Test path for variable suction shear test, 29E

(A qualitative explanation for why test 29E did not reach critical state)

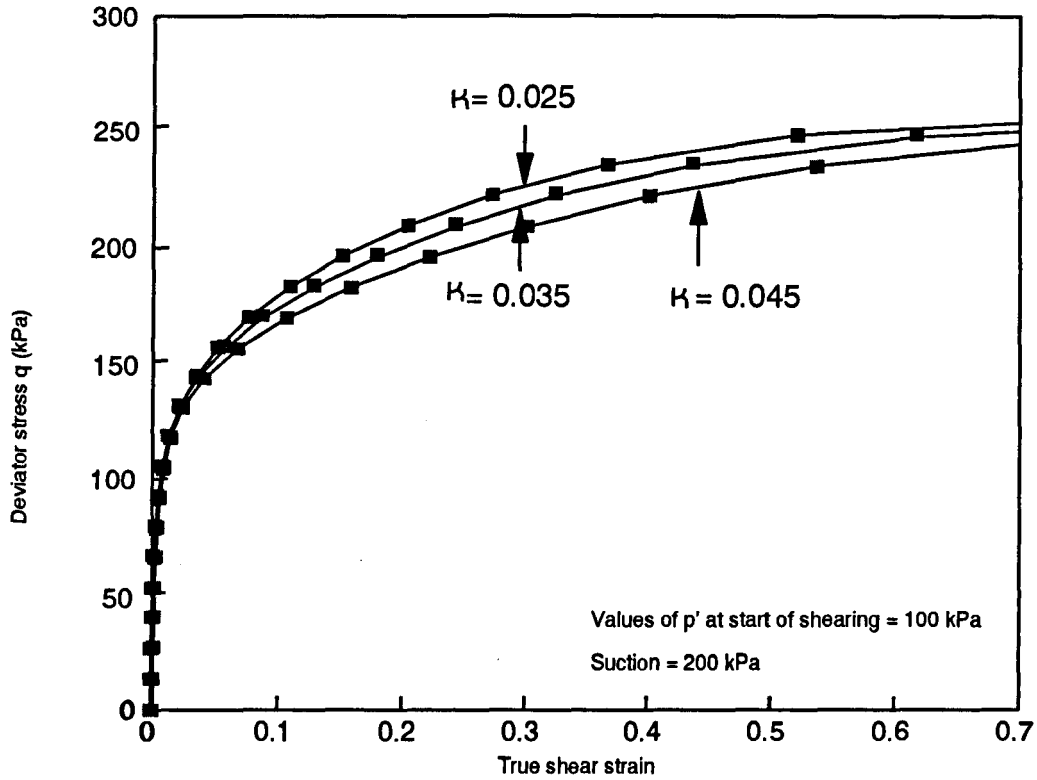

Fig (8.15) Influence of swelling gradient κ on prediction of shear strain (Test 9C)

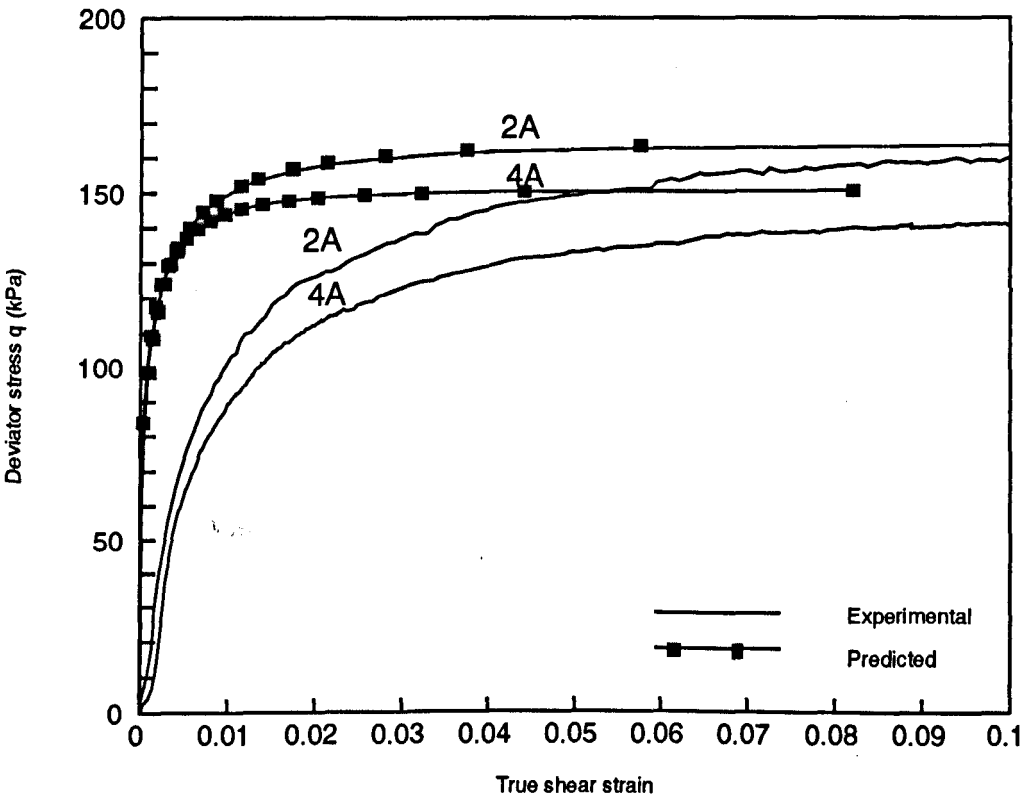

Fig (8.16) Comparison of predicted and experimental shear strain for constant volume, constant suction tests at a suction of 200 kPa

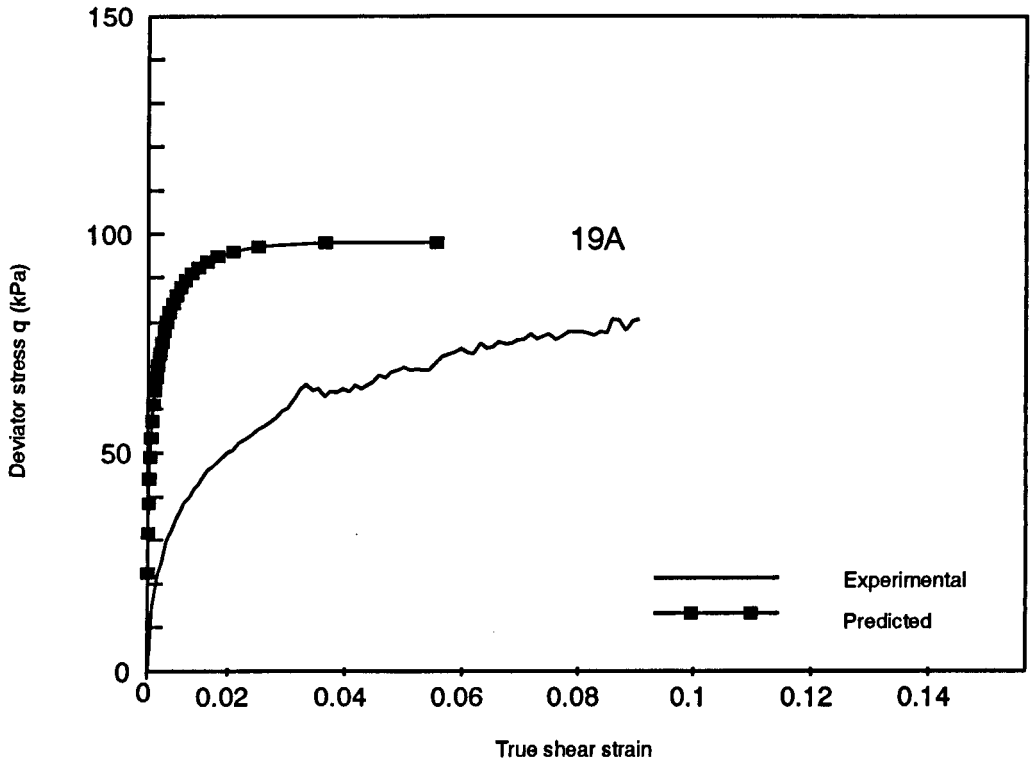

Fig (8.17) Comparison of predicted and experimental shear strain for a constant volume, constant suction test at zero suction

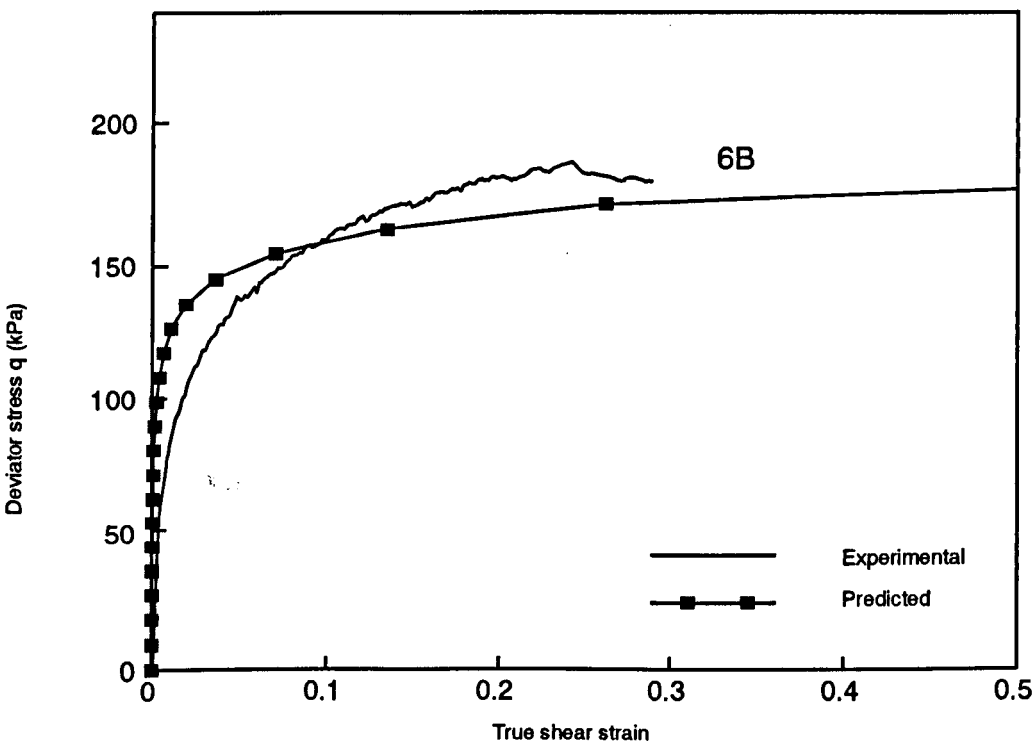

Fig (8.18) Comparison of predicted and experimental shear strain for a constant mean net stress, constant suction test at a suction of 200 kPa

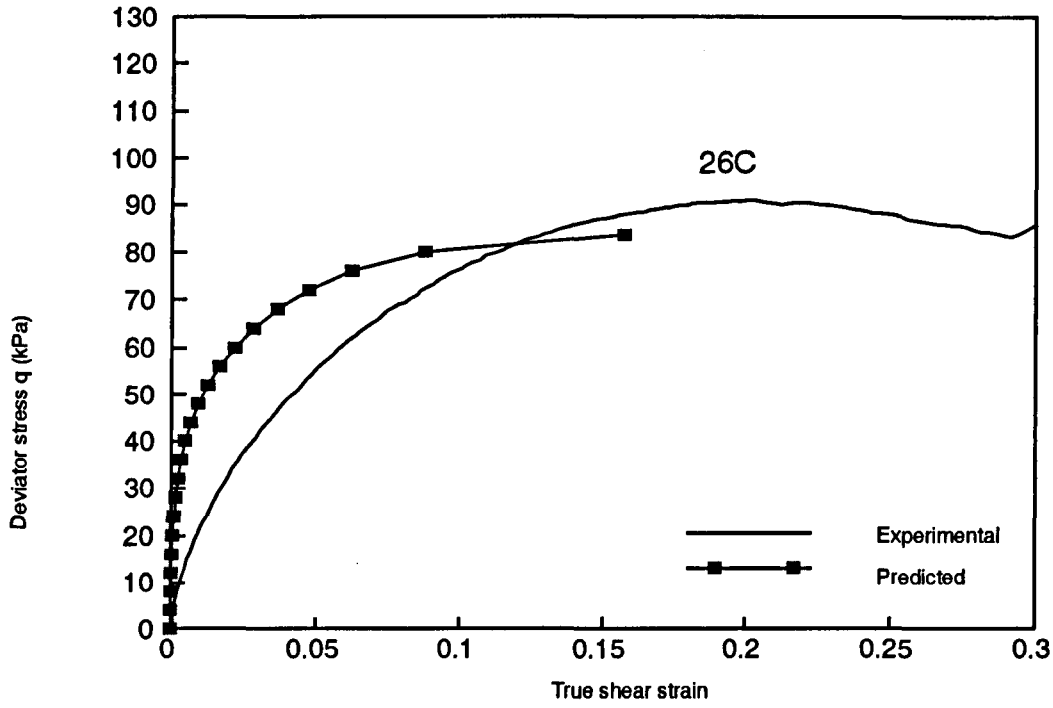

Fig (8.19) Comparison of predicted and experimental shear strain for a fully drained, constant suction test at zero suction

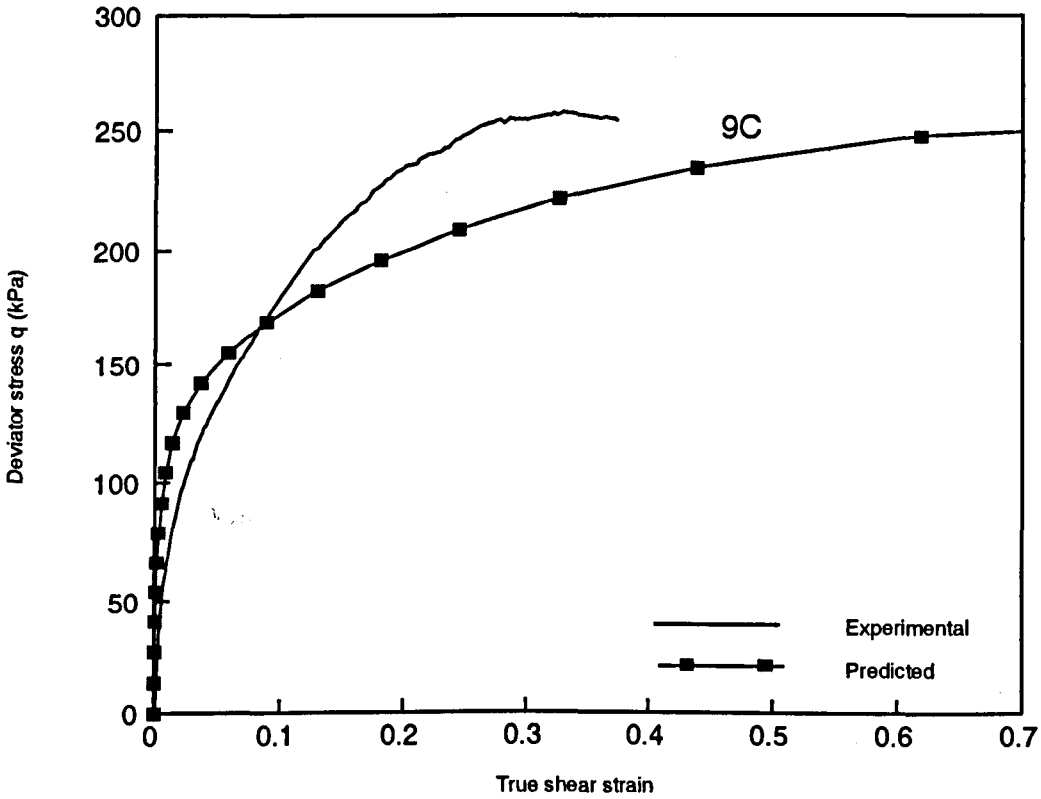

Fig (8.20) Comparison of predicted and experimental shear strain for a fully drained, constant suction test at a suction of 200 kPa

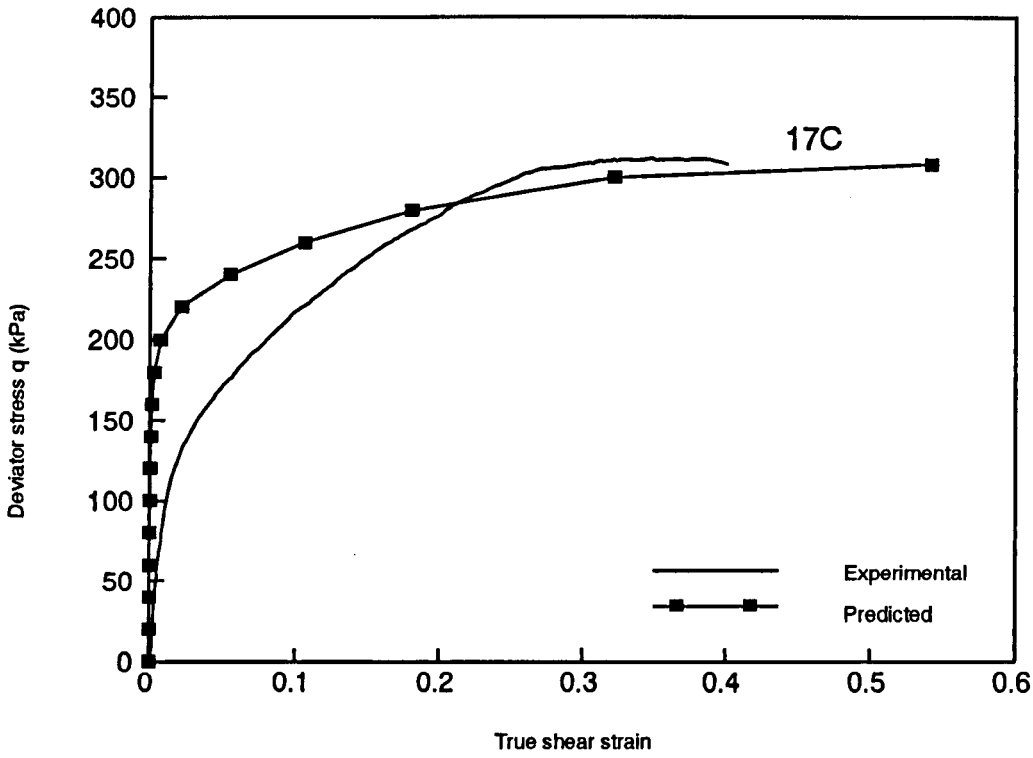

Fig (8.21) Comparison of predicted and experimental shear strain for a fully drained, constant suction test at a suction of 300 kPa

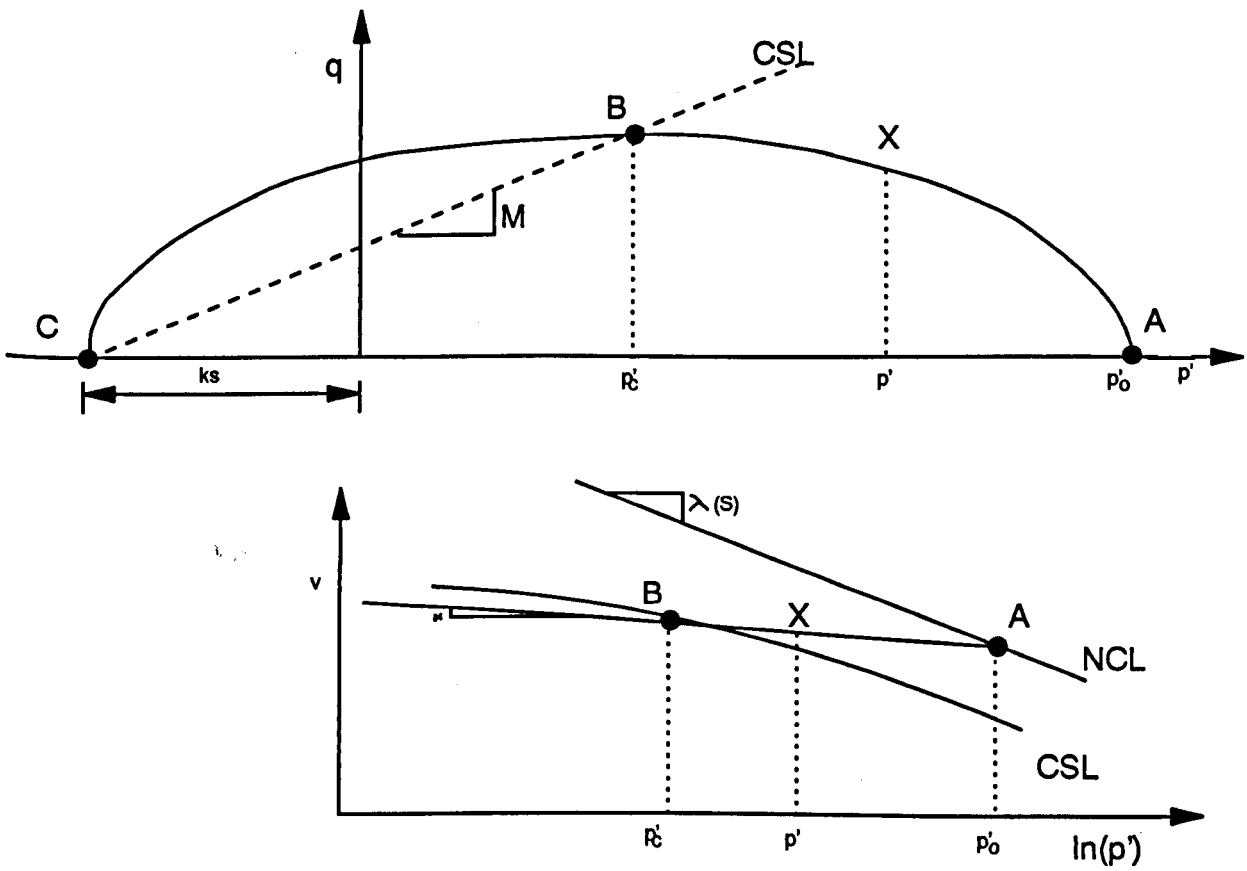

Fig (8.22) Elliptical yield curve in Barcelona model

(After Alonso, Gens and Josa, 1990)

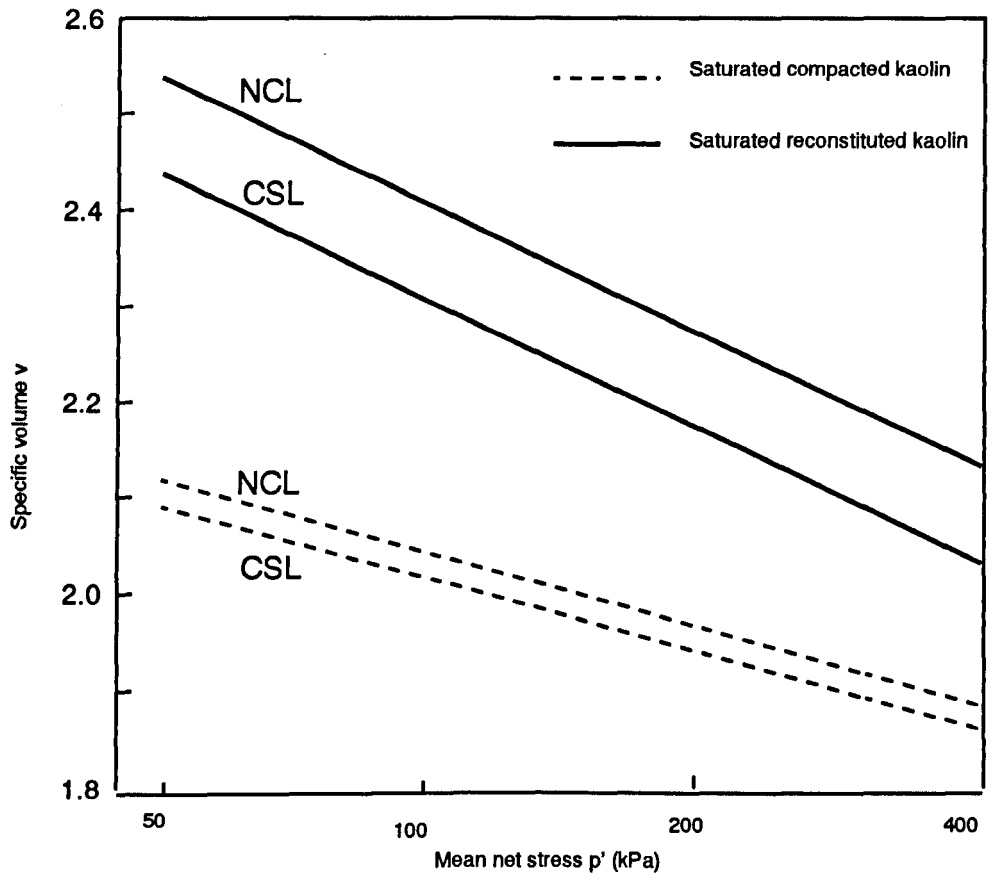

Fig (8.23) Positions of normal compression and critical state lines for compacted and reconstituted kaolin

Suction/kPa	λ (s)	N (s)	M (s)	μ (s) (kPa)	Ψ (s)	Γ (s)	C (s) (kPa)
0	0.1121	2.0463	0.8130	0	0.0700	1.9727	35
100	0.1997	2.1281	0.9325	54.2	0.1493	2.0483	-48
200	0.1637	2.1772	0.9593	83.5	0.1060	1.9661	43
300	0.1495	2.1927	0.9102	122.0	0.0800	1.9437	89

Table (8.1) Soil constants at given values of suction

v (1)	p' (kPa) (2)	p'_0 (kPa) (4)	p'_c (kPa) (3)	q (kPa) (5)	$\frac{d\varepsilon_v^p}{d\varepsilon_s^p}$ (6)	$\Delta\varepsilon_v = \frac{-\Delta v}{v}$ (7)	$\Delta\varepsilon_v^e = \frac{\kappa^*}{v}\Delta p'/p'$ (8)	$\Delta\varepsilon_v^p$ = (7)-(8) (9)	$\Delta\varepsilon_s^p$=(9)/(6) (10)	$\varepsilon_s^p = \Sigma$(10)
2.1109	150.0	150.0	62.00	0						0.0
					7.68	0.0	-0.000792	0.000792	0.000111	
2.1109	143.0	151.9	62.38	63						0.000111
					2.64	0.0	-0.000832	0.000832	0.000315	
2.1109	136.0	154.0	62.76	87						0.000427
					1.82	0.0	-0.000875	0.000875	0.000481	
2.1109	129.0	156.2	63.15	102						0.000908
					1.36	0.0	-0.000924	0.000924	0.000678	
2.1109	122.0	158.7	63.55	114						0.001587

Table (8.2) Prediction of test path and shear strain for a constant volume, constant suction shear test (Test 4A)

p' (kPa) (1)	p'_0 (kPa) (2)	v (3)	p'_c (kPa) (4)	q (kPa) (5)	$\frac{d\varepsilon_v^p}{d\varepsilon_s^p}$ (6)	$\Delta\varepsilon_v = \frac{-\Delta v}{v}$ (7)	$\Delta\varepsilon_v^e = \frac{\kappa^*}{v}\Delta p'/p'$ (8)	$\Delta\varepsilon_v^p$ = (7)-(8) (9)	$\Delta\varepsilon_s^p$=(9)/(6) (10)	$\varepsilon_s^p = \Sigma$(10)
100	100.0	2.1772	54.13	0						0
					32.95	0.000437	0	0.000437	0.000013	
100	100.75	2.1763	54.25	24.5						0.000013
					13.29	0.000453	0	0.000453	0.000034	
100	101.50	2.1752	54.36	34.5						0.000047
					9.96	0.000441	0	0.000441	0.000044	
100	102.25	2.1743	54.47	42.0						0.000091
					8.29	0.000409	0	0.000409	0.000049	
100	103.00	2.1734	54.57	47.5						0.000141

Table (8.3) Prediction of test path and shear strain for a constant mean net stress, constant suction shear test (Test 6B).

CHAPTER 9

CONCLUSIONS AND RECOMMENDATIONS

CHAPTER 9

CONCLUSIONS AND RECOMMENDATIONS

In the earliest research on unsaturated soils, attempts were made to employ the principle of a single effective stress in order to understand the mechanical behaviour of unsaturated soil (Bishop, 1959). The principle of a single effective stress was however later shown, by practical evidence, to be inapplicable to unsaturated soil and researchers subsequently proposed using two independent stress state variables to model unsaturated soil behaviour (see Sections 2.4 and 2.5). The use of two independent stress state variables is now widely accepted, but until recently the shear strength and volume change of unsaturated soil were treated completely separately. In the most recent research on unsaturated soil behaviour, in the U.K and Spain, researchers have been focusing on the development of a generalised constitutive framework, linking shear strength to volume change behaviour of unsaturated soil. The research described in this thesis, forms a significant contribution in this attempt to develop a generalised constitutive framework for unsaturated soil behaviour.

A critical state framework involving 5 state variables (p', q, s, v and w, see Chapter 3) has been proposed. Evidence

supporting the proposed critical state framework was provided by data generated from series of triaxial tests conducted on unsaturated compacted kaolin.

In this final Chapter, conclusions are drawn on the progress made in the development of the critical state framework, on the suitability of the experimental apparatus the procedures adopted in the project and on possible applications of the critical state framework. Recommendations are then made for further research that could be done on unsaturated soils.

9.1 EXPERIMENTAL APPARATUS AND PROCEDURES

50 mm diameter triaxial samples of unsaturated compacted speswhite kaolin were prepared by static compaction in a mould at a moisture content of about 25% (4% dry of optimum). Each sample was compacted in 9 layers and each layer was compacted to a pressure of 400 kPa by applying a constant displacement rate of 1.5mm/min (see Section 5.3). This sample preparation method, outlined in Chapter 5, produced samples of excellent uniformity, and repeatability. The measured variation in the initial specific volume was approximately ±0.012, the variation in water content was approximately ±0.47% and the variation in the degree of saturation was approximately ±1.3%. Although this static compaction method produced suitable samples for testing, one practical drawback of the method

was that the soil structure produced by the static compaction may not have been representative of the soil structures developed during compaction in the field.

Two independent experimental systems (Systems A, and B) were developed to conduct the testing programme. Each system consisted of a double-walled triaxial cell, a compression frame, 7 transducers (3 pressure transducers, 2 volume change units, one LVDT and one load cell) and a logging and control system. Software was written in Quick Basic to log the output of each transducer and to control the cell pressure, pore air pressure and pore water pressure (via stepper motors operating regulators) in order to provide the desired test conditions. The volume change of the sample was measured by measuring the flow of water in or out of the inner cell. In System A cell volume change and water volume change were measured by differential pressure transducers connected to burette systems, whereas in System B cell volume change and water volume change were measured by Imperial College type volume change devices.

Using the calibration and experimental procedures outlined in Chapters 4 and 6, the specific volume of each sample was monitored to an accuracy of ±0.011 and the water content was monitored to an accuracy of ±0.09% (see Section 4.3).

The measurement of sample volume change has often been a source of difficulty in the testing of unsaturated soils.

Double-walled triaxial cells have been successfully used in the past to measure sample volume change in unsaturated soils (Wheeler 1986, Sham 1989) and this approach was successfully employed in the research described in this thesis. Although the double-walled cell proved to be ideal for the measurement of sample volume change there was some difficulty in accurately measuring deviator load with the particular design of double-walled cell employed, because the load cell was positioned external to the triaxial cell. The loading ram moved within two linear bearings, and friction between the loading ram and the linear bearings (arising from corrosion of the bearings) caused difficulties in some tests (see Section 7.3.2). For future research, it is planned to improve the design by measuring the deviator load with an internal load cell. Placing the load cell inside the inner cell does however mean that there will be one more calibration in the apparent volume change of the cell, arising from the volume change caused by the deformation of the load cell with axial load. Appropriate corrections will also have to be made to the measurement of axial displacement of the sample (for the compliance of the load cell), if the axial displacement is measured externally.

Before each sample was isotropically consolidated to a virgin state, it was allowed to equalize at a mean net stress of 50 kPa and the required value of suction (zero, 100, 200 or 300 kPa) (see Section 6.3.2). The sample was

then consolidated by increasing the cell pressure at a rate of 0.6 kPa/hour while holding pore air pressure and pore water pressure constant. Each sample was taken to a mean net stress p' higher than the yield stress caused by initial compaction.

Six different types of shear test were conducted (see Section 6.1.2). Among them, three types of shear test were conducted at constant suction and the rest of them were conducted with variable suction.

The shearing stage was conducted sufficiently slowly to achieve almost complete equalization of pore water pressure throughout the sample at failure, but too fast to allow for equalization of pore water pressure during the early stages of shearing. This was particularly true in constant volume, constant suction tests (type A), where deviator stress, pore air pressure and pore water pressure increased by about 50% of the total change to a critical state value within the first 1% axial strain (see Section 7.3.3). This lack of equalization during the early part of shearing may have caused significant errors in the apparent test paths and made it difficult accurately to identify the shape of the state boundary.

Apart from the slight problems caused by the choice of external load cells and the non-equalization of pore water pressure during the early part of shearing, the

experimental apparatus and procedures proved to be highly successful in meeting the needs of the experimental test programme.

9.2 CRITICAL STATE FRAMEWORK

Unsaturated compacted soil samples were isotropically consolidated at given values of suction. Each sample was taken to a stress level higher than the yield stress caused by initial compaction. The yield stress caused by the compaction process was identified by a rapid change in the slope of the continuous plot of v versus ln(p'). The yield stress increased as suction increased (see Section 7.2).

Data generated from consolidation and shearing were used to establish a critical state framework for unsaturated soil. Three equations defining a normal compression hyperline were proposed:

$$q=0 \tag{9.1}$$

$$v=N(s)-\lambda(s)\ln\left(\frac{p'}{p_a}\right) \tag{9.2}$$

$$w=A(s)-\alpha(s)\ln\left(\frac{p'}{p_a}\right) \tag{9.3}$$

Equation 9.1 was true by definition for isotropic stress states. Equation 9.2 and Equation 9.3 were well supported by the experimental data generated from the triaxial test

programme. The slopes ($\lambda(s)$ and $\alpha(s)$) and intercepts (N(s) and A(s)) of the normal compression hyper-line were all functions of suction.

Three equations defining a critical state hyper-line were proposed:

$$q=M(s)p'+\mu(s) \tag{9.4}$$

$$v=\Gamma(s)-\psi(s)\ln\left(\frac{p'-C(s)}{p_a}\right) \tag{9.5}$$

$$w=B(s)-\beta(s)\ln\left(\frac{p'}{p_a}\right) \tag{9.6}$$

where M(s), $\mu(s)$, $\Gamma(s)$, $\Psi(s)$, C(s), B(s) and $\beta(s)$ were all functions of suction. Support for the existence of Equations 9.4 to 9.6 was provided by the data generated from the experimental programme (see Section 7.3). The value of M(s) was approximately constant when suction was higher than 100 kPa and M(s) fell sharply when suction fell to zero. The value of $\mu(s)$ changed with suction in a non-linear fashion. This was consistent with previous results reported by Escario and Saez (1986), Gan, Fredlund and Rahardjo (1988) and Escario and Juca (1989). Equations (9.5) and (9.6) had not been proposed by any previous researchers, and the demonstration of the existence of such relationships was an important achievement of the research presented in this thesis.

Two equations defining a state boundary hyper-surface were proposed:

$$v=f(p',q,s) \tag{9.7}$$

$$w=f(p',q,s) \tag{9.8}$$

The existence of a relationship of the form shown in Equation 9.7 was supported by data from the experimental research programme (see Section 8.2.1). The data have not yet been analysed to show whether there was evidence of the existence of a second state boundary relationship of the form shown in Equation 9.8.

A possible form for the first state boundary relationship proposed in Equation 9.7 was derived by assuming that constant suction cross-sections of the yield surface in q, p' s space were elliptical in shape. On this basis various shear test paths were predicted (in q, p', s, v space) and compared with the experimental test paths. The agreement between predicted and experimental test paths was very pleasing indeed. It was not possible to predict the variation of water content w throughout a shear stage, because of the lack of the second state boundary relationship (Equation 9.8). For the same reason it was impossible to predict test paths for any constant water content tests.

An associated flow rule was used to predict the shear

strain during shearing (see Section 8.3). The agreement between predicted and observed shear strain was very poor. The discrepancies were probably due to a combination of weaknesses in the theoretical predictions (the assumption of an associated flow rule and the omission of elastic shear strain) and errors in the experimental measurements in the early stages of shearing (due to non-equalization of pore water pressures and inaccuracies in the measurements of small strains).

8.3 INFLUENCE OF SOIL STRUCTURE

Unsaturated compacted clay soils consist of saturated packets separated by larger inter-packet voids that are not filled entirely with water. The arrangement of packets forms an unsaturated "macrostructure" whereas the structure within a packet forms a saturated "microstructure". The microstructure of the saturated packets is usually heavily overconsolidated, whereas the macrostructural arrangement may well be normally consolidated or only lightly overconsolidated. This suggests that there will be two yield stresses corresponding to a given initial structure, the yield stress of the macrostructure and a second, much higher, yield stress of each packet (see Section 8.4).

The influence of soil structure was noticed at each stage of the triaxial tests on unsaturated compacted kaolin samples. During the initial equalization stage samples

swelled, suggesting that each saturated packet was taking up water as the suction was reduced. However, for those samples taken to lower values of suction (zero or 100 kPa) the samples compressed (collapsed) during the later phase of the equalization stage. This was thought to be due to yielding of the macrostructure. The yield curve produced by the compaction process, and identified in the subsequent consolidation stage of each triaxial test, was also thought to represent yielding of the macrostructure. On shearing, the water content of samples continued to increase in test types A, B, C, E and F (where the drainage line was open) even though all other state variables had reached a critical state. Similarly the suction continued to increase during shearing in test type D (where the drainage line was closed to maintain constant water content during shearing) even though other state variables had reached a critical state. This pattern of behaviour indicated that each heavily over-consolidated saturated packet was continuing to dilate during shearing. This suggested that the saturated soil within each packet never reached a critical state, even when the unsaturated macrostructure was at a critical state.

The positions of the normal compression hyper-line, critical state hyper-line and state boundary hyper-surface within the critical state framework developed in this research are likely to depend upon the initial structure of the unsaturated soil. The proposed framework has been

validated for only one initial structure of compacted kaolin, but the hope is that the framework would be equally valid for other initial soil structures (produced by different compaction processes or different moulding water contents) provided that the relevant soil constants were suitably adjusted. Development of a model that could be used independent of initial structure would be desirable, however such a model would be more complex. In any case, the framework currently proposed could be applied in most field situations, because the initial structure of compacted soil would normally be identical throughout a given layer of fill because the same compaction process would be used throughout.

9.4 APPLICATION OF THE MODEL

Unsaturated soils are found all over the world. Unsaturated conditions exists in natural soil above the water table, when soils are compacted for construction purposes and when gas is generated within the soil by biological activity. The proposed critical state framework is a powerful tool in attempting to understand unsaturated soil behaviour and in providing qualitative and quantitative predictions of soil behaviour.

A critical state framework for unsaturated soil would have applications at three different levels:

(a) A critical state framework could be used to provide a qualitative assessment of unsaturated soil behaviour under any loading or drainage conditions. For example, reduction of suction (wetting) would produce swelling if the soil state were inside the state boundary, but plastic collapse if the soil state were on the state boundary. Reduction in suction also would produce a decrease in shear strength. Increases of suction would produce elastic compression if the soil was within elastic region but plastic compression if the soil state were on the SI yield surface.

(b) A critical state framework could be used as guidance when selecting drained and undrained strength parameters to be used in conventional limit equilibrium or plasticity calculations. Such calculations are widely used, in saturated and unsaturated soils, to predict the bearing capacity of foundations, the stability of slopes or the active and passive earth pressures on retaining structures. In limit equilibrium and plasticity calculations the soil is idealised as a rigid-perfectly plastic material, with cohesion c and friction angle ϕ, and the critical state framework can be used to suggest appropriate values of c and ϕ under drained or undrained conditions.

For loading under drained conditions of the water phase (where the value of pore air pressure is zero, the value of pore water pressure is known and therefore the value of suction is known) the shear strength τ can be calculated

from Equation 9.4. Equation (9.4) can be converted to a more conventional form of Mohr-Coulomb equation as follows

$$\tau=c'+\sigma'\tan\phi' \tag{9.9}$$

where σ' is the net normal stress ($\sigma-u_a$) on a failure plane, and ϕ' and c' are given by:

$$\phi'=\sin^{-1}\left(\frac{3M(s)}{6+M(s)}\right) \tag{9.10}$$

$$c'=\frac{(3-\sin\phi')\mu(s)}{6\cos\phi'} \tag{9.11}$$

Equations (9.9) to (9.11) indicate that, under drained conditions, unsaturated soil failing at a critical state can be treated as a Mohr-Coulomb material with a friction angle ϕ' that varies slightly with suction (although the variation of M(s) with suction is relatively small, and it will often be acceptable to simply take a saturated value of ϕ') and an apparent cohesion intercept c' that is strongly dependent on suction (via the term $\mu(s)$). In many practical situations suction will vary with depth, and this means that the value of $\mu(s)$ will change with depth and therefore c' will change with depth. The variation of c' with depth must therefore be included in any drained limit equilibrium or plasticity calculations (perhaps by treating the soil as a layered deposit).

For rapid loading (under undrained conditions) the water content of the unsaturated soil will remain constant, but

the value of the suction is initially unknown. However the value of the shear strength can be calculated by combining Equations (9.4) and (9.6). Eliminating suction from both equations:

$$q=f(p,w) \tag{9.12}$$

Equation 9.12 indicates that the undrained strength of unsaturated soil is a function of water content and mean net stress (whereas in saturated soil, it is only a function of water content). In practice, this means that the undrained friction angle with respect to total stress ϕ_u is non-zero. Wheeler and Sivakumar (1992b) show how the critical state framework can be used to estimate appropriate values for c_u and ϕ_u.

(c) A formalised constitutive model based on the proposed critical state framework could be incorporated within a finite element program for the solution of boundary value problems including unsaturated soil. The unsaturated elasto-plastic critical state model proposed by Alonso, Gens and Josa (1990) (the "Barcelona" model) is currently being implemented within the finite element program CRISP at Sheffield University (Nesnas, in preparation). Once implemented and validated, the modified version of CRISP should be capable of analysing many boundary value problems involving drained conditions, where the value of suction is known. As the Barcelona model does not include water content as a fifth state variable, the finite element program will not be applicable to undrained problems.

9.5 RECOMMENDATIONS FOR FURTHER WORK

The research presented in this thesis has provided a possible framework enabling unsaturated soil behaviour to be understood and predicted. However the proposed model, as it now stands, is incomplete, because there are many questions unanswered eg the existence and form of the second state boundary relationship (for water content) and the influence of the initial soil structure on the various relationships within the proposed model. The following recommendations are therefore made for future research into unsaturated soil behaviour and the further development of the critical state model.

(a) Further analysis of the data generated from this research is necessary to establish whether a second state boundary relationship (linking water content w to two other state variables) exists, and if so to establish the form of this relationship.

(b) It is very clear that the structure of unsaturated soil plays a major role in the mechanical behaviour, and therefore an experimental programme of research is required to explore the influence of the initial structure on the various relationships within the critical state framework. A research project on this topic has just started at Oxford University.

(c) The "elastic" behaviour of unsaturated soils, inside the state boundary, was not examined in any detail in the present research project (where all samples were consolidated to virgin states, so that the test paths during shearing all traversed the state boundary). A research project currently in progress at Sheffield University (Zakaria, in preparation) is investigating the behaviour of unsaturated compacted kaolin inside the state boundary. The project will also provide further information on the shape of the yield surface and on whether the flow rule is associated.

(d) The existence of the SI yield curve, proposed by Alonso, Gens and Josa (1990), was not examined in the present research project, because the initial suction caused by the compaction process was higher than the suction values subsequently applied in the various triaxial tests (zero to 300 kPa). Therefore an experimental programme of research is required to explore the existence of the SI yield curve and its influence within the critical state framework.

(e) Further work could be done on the implementation of the proposed critical state model within finite element programs. As already stated, Nesnas (in preparation) is implementing the Barcelona model within the finite element program CRISP, but this version will not be capable of analysing undrained problems, because of the omission of

water content as a fifth state variable in the Barcelona model. The implementation of a model based on the critical state framework proposed in this thesis (including water content as a variable) would allow drained and undrained problems to be analysed. It would also be possible subsequently to use such a program to analyse time-dependent processes (such as consolidation or inundation) using a coupled analysis involving the relevant flow and continuity expressions.

(f) The model developed in this research project basically consisted of 3 equations to define the normal compression hyper-line and 3 equations to define the critical state hyper-line. However, within these 6 equations there were 11 separate parameters that were functions of suction ($N(s)$, $\lambda(s)$, $A(s)$, $\alpha(s)$, $M(s)$, $\mu(s)$, $\Gamma(s)$, $\Psi(s)$, $C(s)$, $B(s)$ and $\beta(s)$). It would therefore be very difficult to apply this model in practical situations as it now stands, because a test programme similar to that presented in this thesis would be required to define the variations of these 11 parameters with suction for the particular soil being considered. Therefore it will be necessary in the future to simplify the model as much as possible and to devise a suitable testing programme to measure the relevant soil parameters.

(g) Most of the research on unsaturated soil behaviour conducted in recent years has concentrated on compacted

unsaturated soils. However unsaturated natural soils are also very widespread throughout the world, and the behaviour of these natural soils may be very different to that of compacted fills (because of the different soil structure). Therefore experimental research should be carried out to establish whether the proposed critical state framework can also be applied to natural soils.

REFERENCES

Aitchison, G.D.,1960. Relationships of moisture stress and effective stress functions in unsaturated soils. Proc. Conf. Pore pressure and suction in soils. Butterworths, London, pp 47-52.

Alonso, E.E., Gens, A. and Josa, A., 1990. A constitutive model for partially saturated soils. Geotechnique, Vol 40, No.3, pp 405-430.

Alonso, E.E., Gens, A. and Hight, D.W.,1987. General report , Special problems soils. 9th ECSMFE, Dublin, Vol.3, pp 1087-1146.

Barden, L., Madedor, A.O. and Sides, G.R., 1969. Volume change characteristics of unsaturated clay. J.SMFE, ASCE, 95, SM1, pp 33-51.

Barden, L. and Sides, G.R., 1970. Engineering behaviour and structure of compacted clay. J.SMFE, ASCE, 96, SM4, pp 1171-1201.

Bishop, A.W., 1959. The principle of effective stress. Teknisk Ukeblad, Vol 39, pp 859-863.

Bishop, A.W.,1960. The measurement of pore pressure in the triaxial test. Proc. Conf. on pore pressure and suction in soils. Butterworths, London, pp36-46.

Bishop, A.W. and Donald, I.B., 1961. The experimental study of partially saturated soils in the triaxial apparatus. Proc 5 th ICSMFE, Paris. Vol.1, pp 13-21.

Bishop, A.W., and Blight, E.,1963. Some aspects of

effective stress in saturated and partly saturated soils. Geotechnique, Vol 13, No.3, pp177-197.

Booth, A.R., 1975. The factors influencing collapse in compacted soils. 6th Reg. Conf. for Africa on SMFE, Durban,Vol. 1, pp 57-63.

Brackley, I.J.A., 1975. A model of unsaturated clay structure and its application to swell behaviour. 6th Reg. Conf. for Africa on SMFE, Durban, Vol. 1, pp 71-78.

Burland, J.B., 1964. Effective stress in partially saturated soils. Geotechnique, Vol 14, pp 64-68.

Burland, J.B. and Symes, M.J. 1982. A simple axial displacement gauge for use in the triaxial apparatus. Geotechnique, Vol. 32, No. 1, pp 62-65.

Casagrande, A., 1936. The determination of the preconsolidation load and its practical significance. Proc. 1st ICSMFE, Cambridge (Mass), Vol. 3, pp 60.

Chandler, R.J. and Gutierrez, C.I., 1986. The filter paper method of suction measurement. Geotechnique, Vol. 36, No. 2, pp 265-268.

Clayton, C.R.I. and Khatrush, S.A., 1987. A new device for measuring local axial strain on triaxial specimen. Geotechnique, Vol. 30, No. 4, pp 593-597.

Costa Filho, L.M., 1980. A laboratory inverstigation of the small strain behaviour of London clay. Phd thesis, University of London.

Craig,R.F., 1987. Soil Mechanics, 4th edition. Published by Van Nostrand Reinhold (UK) Co.Ltd, England.

Croney,D. and Colemam, J.D.,1960. Pore pressure and suction

in soil. Proc. Conf. on pore pressure and suction in soils. Butterworths, London, p 31.

Donald, I.B., 1960. Discussion. Conf. on pore pressure and suction in soils. Butterworths. pp 69-70.

Donald, I.B., 1963. Effective stress parameters in unsaturated soils. Proc. 4th Australian and New zealand Conf. on SMFE. Vol 1, pp 41-46.

Edil, T.B., Motan, S.E. and Toha, F.X., 1981. Mechanical behaviour of unsaturated soils. Laboratory shear strength of soils, ASTM, STP 740.

Escario, V., 1980. Suction controlled penetration and shear tests. Proc. 4th Int. Conf. Expansive soils, Vol. 2, pp 781-797.

Escario, V. and Juca, J.F.T., 1989. Strength and deformation of partly saturated soils. Proc. 12th ICSMFE, Rio de Janeiro, Vol. 1 , pp 43-46.

Escario, V. and Saez, J., 1986. The shear strength of partially saturated soils. Proc. 12th ICSMFE, Vol. 1, pp 43-46.

Fredlund, D.G., 1975. A diffused air volume indicator for unsaturated soils. Canadian Geotechnical J., Vol 12, pp 533-539.

Fredlund, D.G. 1979. Appropriate concepts and technology for unsaturated soils. Canadian Geotechnical J., Vol. 16, 121-139.

Fredlund, D.G., 1985. Soil mechanics principles that embrace unsaturated soils. Proc. 11th ICSMFE., San Francisco, Vol. 2, pp 465-472.

Fredlund, D.G. and Morgenstern, N.R.,1976. Constitutive relationships for volume change in unsaturated soils. Canadian Geotechnical J. Vol. 13, pp 261-276.

Fredlund, D.G. and Morgenstern, N.R., 1977. Stress state variables for unsaturated soils. Proc. ASCE, Vol. 103, No. SM5, pp 447-466.

Fredlund, D.G., Morgenstern, N.R. and Widger, R.A., 1978. The shear strength of unsaturated soils. Canadian Geotechnical J. , Vol. 15, pp 313-321.

Fredlund, D.G., Rahardjo, H. and Gan, J.K.M., 1987. Non-linearity of strength envelope for unsaturated soils. Pro. 6 th Int. Conf. on Expansive soils, New Delhi, India, pp 1-4.

Fredlund, D.G. and Wonk, D.K.H. , 1989. Calibration of thermal conductivity sensor for measuring soil suction. Geotechnical testing J., GTJODJ, Vol. 12, No. 3, pp 188-194.

Gan, J.K.M, Fredlund, D.G., and Rahardjo., 1988. Determination of shear strength parameters of an unsaturated soil using direct shear test. Canadian Geotechnical J., Vol. 25, pp 500-510.

Gardner, T.N., 1988. The acoustic properties of gassy soil. D.Phil thesis, University of Oxford.

Gens, A., Alonso, E.E. and Josa, A.,1989. Elasto-plastic modelling of partially saturated soils. Proc. of NUMOG III, Edited by Pietruszczak, S. and Pande, G.N. pp 163-170.

Gulhati, S.K. and Satiya, B.S., 1987. Shear strength of partly saturated soils. 10th ICSMFE, Stockholm. Vol. 1, pp

609-612.

Hilf, J.N., 1956. An investigation of pore water pressure in compacted cohesive soils. Technical Memorandom 654. U.S. Department of the Interior Bureau of Reclamation, Denver.

Jennings, J.E.B., 1960. Pore pressure and suction . A revised effective stress law for use in the prediction of behaviour of unsaturated soils. Pore pressure ans suction in soils. Butterworths, London, pp 26-30.

Jennings, J.E.B. and Burland, J.B. , 1962. Limitations to the use of effective stress in partially saturated soils. Geotechnique, Vol. 12, No. 2, pp 125-144.

Jardine, R.J., Symes, M.J. and Burland, J.B., 1984. Measurement of soil stiffness in the triaxial apparatus. Geotechnique 34, No. 3, pp 323- 340.

Josa, A., Alonso, E.E., Lloret, A. and Gens, A., 1987. Stress-strain behaviour of partially saturated soils. Proc. 9th ECSMFE, Dublin, Vol. 2, pp 561-564.

Karube, D. and Kato, S., 1989. Yield function of unsaturated soils. Proc. 12th ICSMFE, Rio de Janeiro, Vol. 1, pp 615-618.

Krahn, J., Fredlund, D.G. and Klassen, M.J., 1989. Effect of suction on slope stability at Notchhill. Canadian Geotechnical J., Vol. 26, No.2, pp 269-278.

Lade, P.V., 1988. Automatic volume change and pressure measurement devices for triaxial testing of soils. Geotechnical Testing Journal , Vol. 11, No. 4, pp 263-268.

Lloret, A. and Alonso, E.E., 1985. State surfaces for partly saturated soils. Proc 11th ICSMFE, San Francisco,

Vol. 2, pp557-562.

Matyas, E.L and Radhakrishna, H.S., 1968. Volume change characteritstics of partly saturated soils. Geotechnique, Vol. 18, pp 432-448.

Maswoswe, J., 1985. Stress path for a compacted soil during collapse due to wetting. PhD Thesis. Imperial College, London.

Nageswaran, S., 1983. Effect of gas bubbles on seabed behaviour. D.Phil thesis, University of Oxford.

Nesnas, K. (in preparation). Numerical formulation of a critical state model for unsaturated soil. Phd thesis, to be submitted to University of Sheffield.

Pradhan, T.B.S., Tatsuoka, F. and Molenkamp,F., 1986. Accuracy of automated volume change measurement by means of differential pressure transducer. Soils and Foundations, Vol. 26, No. 4, pp 150-158.

Rendulic, L., 1936. Discussion on relationship between void ratio and effective principle stress for a remoulded silty clay. Proc. 1st ICSMFE, Cambridge (Mass), Vol. 3, pp 48-51.

Richardson, D., 1988. Investigation of threshold effect in soil deformation. Phd thesis, City university.

Roscoe, K.H. and Burland, J.B., 1968. The generalised stress-strain behaviour of wet clay. Engineering plasticity. Cambridge University Press, pp 536-607.

Roscoe,K.H. and Poorooshasb, H.B., 1963. A theoretical and experimental study of strains in triaxial tests on normally consolidated clays. Geotechnique, Vol. 13, No. 1, pp 12-38.

Seed, H.B. and Chan, C.K., 1959. Structure and strength

characteristics of compacted clays. Proc. ASCE, No.SM5, pp 87-127.

Schofield, A.N., 1935. The pF of the water in soil. Trans. 3rd Int. Cong. Soil Sience, Vol. 2, pp 37-48.

Schofield, A.N. and Wroth, C.P., 1968. Critical state soil mechanics. McGraw-hill, London.

Sham, W.K., 1989. The undrained shear strength of soil containing large gas bubbles. Phd thesis, Queen's University of Belfast.

Shridharan, A., Venkatappa, G. and Samudra, P., 1973. Volume change characteristics of parly saturated clays during soaking and the role of effective stress. JSSMFE, Vol. 13, No. 3, pp 1-15.

Sills,G.C., Wheeler,S.J., Thomas,S.D. and Gardner, T.N., 1991. Behaviour of offshore soils containing gas bubbles. Geotechnique, Vol.41, No.2, pp 227-241.

Sivakumar, V. and Wheeler, S.J., (in preparation). A critical state framework for unsaturated soils. To be submitted to Geotechnique.

Thomas, S.D., 1987. The consolidation behaviour of gassy soils. DPhil thesis, University of Oxford.

Toll, D.G., 1990. A framework for unsaturated soil behaviour . Geotechnique, Vol. 40, No.1, pp 31-44.

Toll, D.G. and Hight, D.W., 1990. Desaturation of soils. Geotechnique, Vol.40, No.1, pp 44-50.

Vicol, P.T., 1990. Comportement hydraulique et mecanique dun sol fin non sature application a la modelisation. Phd thesis, L' Ecole, National des Ponts et Chaussees.

Vaughan, p., 1987. Private conversation, Imperial College of Science, Technology and Medicine.

Wheeler, S.J., 1986. The stress-strain behaviour of soils containing gas bubbles. D.Phil thesis, University of Oxford.

Wheeler,S.J., 1988a. A conceptual model for soils containing large gas bubbles. Geotechnique, Vol. 38, No. 3, pp 389-397.

Wheeler, S.J., 1988b. The undrained shear strength of soils containing large gas bubbles. Geotechnique, Vol . 38, No. 3, pp 399-413.

Wheeler, S.J. 1991. An alternative framework for unsaturated soil behaviour. Geotechnique, Vol. 41, No. 2, pp 257-261.

Wheeler, S.J. and Sivakumar, V, 1992a. Critical state concept for unsaturated soil. Proc. 7th International Conf. on Expansive Soils, Dallas, August 1992, pp 167-172.

Wheeler, S.J. and Sivakumar, V, 1992b. Development and application of a critical state model for unsaturated soil. Wroth Memorial Conf. on Predictive Soil Mechanics, Oxford, July 1992.

Wheeler, S.J., (in press). Constitutive modelling for unsaturated soils. In constitutive modelling in geotechnical engineering by Wroth, C.P, Houlsby, G.T. and Burd, H., SERC report.

Wonk, K.H. and Ho, A., 1987. An evaluation of a thermal conductivity sensor for measurment of soil matric suction. Internal Report, Dept of Civil Engineering, University of

Saskatchewan. Canada.

Wood, D.M., 1979. The behaviour of partly saturated soils. A review. University of Cambridge, CUED/D-soils/TR 69.

Wroth, C.P. and Houlsby, G.T., 1985. Soil Mechanics: Property characterization and analysis procedure. Proc. 11th ICSMFE, San Francisco, Vol. 1, pp 1-55.

Zakaria, I. (in preparation). Yielding of unsaturated soil. Phd thesis, to be submitted to University of Sheffield.